INTRACELLULAR PATTERNING ALONG THE ANTERIOR-POSTERIOR AND CIRCUMFERENTIAL POLARITY AXES IN *TETRAHYMENA THERMOPHILA*

by

CHINKYU LEE

(Under the Direction of Jacek Gaertig)

ABSTRACT

Not much has been revealed about how organelles are assembled into patterns inside cells. Ciliates are good models to study intracellular pattern formation due to the complex cortical pattern on the cell surface that is accurately replicated during cell division. For example, in *Tetrahymena thermophila*, the feeding organelle oral apparatus is located near the anterior cell end, and the oral primordium (new oral apparatus) is formed at ciliary row posterior to the old oral apparatus. The contractile vacuole pores, organelles required for osmoregulation, are located near the posterior cell end and on the cell's right side (cell's perspective). The goal of my doctoral research was to characterize gene products implicated in intracellular pattern formation in *T. thermophila*. In my first project, I characterized the *cdaH-1* mutant that displays a pleiotropic phenotype with multiple defects in anterior-posterior patterning. We found that CdaH is a *Tetrahymena* ortholog of conserved Fused/Stk36 kinases. CdaH plays multiple roles in patterning on both global and local scale. The global function of CdaH is in maintaining the subequatorial position of the oral primordium. The local functions of CdaH include induction of the division boundary, generation of new cell ends, cytokinesis and stability of the oral primordium. CdaH prominently colocalized with the contractile ring, implying a possibility that its ancestral function is associated with actin. In my second project, I characterized the *hpo1* mutants that

are affected in patterning on the circumferential axis. Loss-of-function of Hpo1 caused displacement and excessive number of oral primordia. We discovered that Hpo1 is an Armc9-like protein that accumulates on the cell's right side, as a bidirectional gradient with drop-offs in concentration on the ventral and dorsal side. Our data indicate that Hpo1 functions as a bilateral repressor that spatially excludes oral development from its domain. That Hpo1 marks the position for extra oral apparatus formed on the dorsal side of *janus* mutant reflects the role of Hpo1 as the bilateral repressor. Double mutants lacking Hpo1 and Bcd1 display diverse patterning defects, including elongated cell morphology. Overall, we conclude that circumferential patterning in *Tetrahymena* involves multiple factors that are localized as gradients.

Index : CdaH, Fused, Hpo1, Armc9, Oral apparatus, Oral primordium, Contractile vacuole pore, Division boundary, Anterior-Posterior, Circumferential

INTRACELLULAR PATTERNING ALONG THE ANTERIOR-POSTERIOR AND CIRCUMFERENTIAL POLARITY AXES IN *TETRAHYMENA THERMOPHILA*

by

CHINKYU LEE

B.S. Pusan National University, South Korea, 2015

M.S. Yonsei University, South Korea, 2018

A Dissertation Submitted to the Graduate Faculty of The University of Georgia in Partial Fulfillment of the Requirements for the Degree

DOCTOR OF PHILOSOPHY

ATHENS, GEORGIA

2025

INTRACELLULAR PATTERNING ALONG THE ANTERIOR-POSTERIOR AND CIRCUMFERENTIAL POLARITY AXES IN *TETRAHYMENA THERMOPHILA*

by

Chinkyu Lee

Major Professor: Jacek Gaertig

Committee: Edward Kipreos

Jonathan Eggenschwiler

Karl Lechtreck

Scott Dougan

Electronic Version Approved:
Ron Walcott
Dean of the Graduate School
The University of Georgia
May 2025

DEDICATION

Dedicated to all the scientists who laid the foundation that made my work possible.

ACKNOWLEDGEMENTS

I would like to express how much grateful I am to my mentor Dr. Jacek Gaertig, remembering his persistent effort and care for my progression not only as a scientist, but also as a human being. His curiosity and passion in science has always been the best guideline on becoming a scientist. It was a great honor to work as his mentee throughout my PhD years. I am also grateful to my committee professors: Dr. Karl Lechtreck, Dr. Edward Kipreos, Dr. Jonathan Eggenschwiler, and Dr. Scott Dougan. Their constructive and insightful feedback and suggestions provided during annual committee meetings have also helped me to make progress.

In addition, I express my gratitude to our collaborators. Dr. Wolfgang Maier applied bioinformatics approach that enabled us to study patterning at the molecular level. Dr. Yu-yang Jiang greatly helped me by sharing his protocols I used as reference for my experiments. I thank Dr. Kentaro Nakano for sharing his strategy of labeling actin protein, one of the hardest experiments I have experienced during my PhD years. Dr. Eric Cole provided us with insightful working model explaining complicated phenotype of the strains. I was also lucky to be able to take advantage of using *Tetrahymena* strains and plasmids generated by Dr. Ewa Joachimiak and Dr. Dorota Wloga. I thank Dr. Khanh Huy Bui for including me as a collaborator in his research project. Throughout my PhD years, my research outcome is primarily composed of microscope images, and I must thank Dr. Muthugapatti Kandasamy and Dr. Peter Kner for providing me with pieces of advice for decent microscopy. I will also remember amazing assistance I received from Ms. Mary Ard in my electron microscopy. I also would like to thank my parents and sister who have always helped me with wise or encouraging words. Their care and support have been so helpful in maintaining my confidence and overcoming some difficulties, such as loneliness international students often encounter when studying abroad.

I also thank my brother-in-law for being an amazing husband for my sister and father for my nephew. I also thank my cute and adorable nephew who has made me smile and given much more meaning to my life.

TABLE OF CONTENTS

CHAPTER 1

INTRODUCTION AND LITERATURE REVIEW

1. Definition and importance of cell polarity

Cell polarity is an asymmetrical placement of cellular structures or non-uniform distribution of molecules across the cell. For example, cilia on the apical side of epithelial cells exhibit important functions in our body, such as preventing entry of dust into our respiratory system. Neuron is a highly polarized cell with specialized structures, such as signal-receiving dendrites and signal-sending synapses at the axon's terminal. Cell polarity can also play a role as an inhibitor against tumor development by maintenance of cell-cell junctions by apical and basal factors (reviewed in (Cole and Gaertig, 2022)). Unicellular organisms can help understanding the principles of cell polarity without complications of the multicellular environment and may unfold ancestral mechanisms underlying cell polarity. Among unicellular models, ciliates display strikingly elaborate cell polarity characterized by invariable placement of cortical organelles forming the cortical pattern.

Throughout my PhD years, my research focused on principles underlying intracellular pattern formation in the small ciliate *Tetrahymena thermophila* and explored where such mechanisms stand during the evolutionary history of establishment of cell polarity. The broad question is whether the pathways implicated in intracellular patterning of *T. thermophila* are conserved or lineage-specific. This is an important question because ciliates have diverged from other eukaryotes over 1,000 million years ago (Frankel, 2008). Below I reviewed the cell polarity mechanisms in a range of organisms, including *T. thermophila*.

2. Cell polarities in well-studied model organisms

Cell polarity is established along a variety of directional axes (anterior-posterior, proximal-distal, apical-basal, dorsal-ventral, left-right). For example, wing cells of *Drosophila* display alignment of hair projections pointing in the same direction, revealing what is known as the Planar Cell Polarity (PCP) (Adler, 2012; Wang et al., 2014). The one cell stage of *C. elegans* is a well-studied example for establishment of cell polarity characterized by asymmetrical distribution of polarity factors along the anterior-posterior axis. Left-right asymmetry is manifested in diverse evolution lineages by either unidirectional rotation of cilia that carry left-right asymmetry determinants during vertebrate development (Sung et al., 2016) (reviewed in (Hamada, 2020)) or left-right bias in cell migration (Gros et al., 2009; Mendes et al., 2014) (reviewed in (Ferreira and Vermot, 2017)). In this subchapter, I reviewed diverse examples of cell polarities in several organisms that have been widely adopted as model organisms in the biology laboratories.

2.1. *Saccharomyces cerevisiae*

The budding yeast *S. cerevisiae* divides unequally by forming a bud. Budding occurs just once per cell cycle (Bi and Park, 2012; Hartwell, 1971) and the budding site is not random but rather determined by the position of the bud scar where budding occurred in the previous generation. Cdc42, originally characterized as a protein that displays a domain similar to the regions of *Ras* proteins implicated in GTP binding (Johnson and Pringle, 1990), plays a critical role in budding and consequently is a key cell polarity factor. Cdc42, a regulator of diverse downstream effectors, is one of the most highly conserved GTPases that regulate cell polarity in diverse organisms, including yeast (reviewed in (Chiou et al., 2017)). *S. cerevisiae* initially displays multiple sites enriched by Cdc42 but after apparent competition, only one Cdc42 zone is selected as a site for bud growth (Witte et al., 2017; Wu et al., 2015) (reviewed in (Chiou et al., 2017)). Hyperactive (gain-of-function) Cdc42 confers production of multiple buds during a single cell cycle even in the absence of activator GEF (Bi and Park,

2012; Caviston et al., 2002), while a loss-of-function mutation in Cdc42 confers failure in bud formation (Adams et al., 1990; Miller and Johnson, 1997). Thus, Cdc42 activity is essential for bud emergence and its regulation important for bud singularity. From its initial homogenous distribution, active Cdc42-GTP localizes to the bud site before the actual bud emergence (Brauns et al., 2023), and Cdc42 enrichment at the future bud site is enhanced by a positive feedback loop, consisting of GEF-containing complex (serving as binding partner of active Cdc42) that activates additional adjacent Cdc42 that subsequently binds to additional complex and the following amplification of cluster (Kozubowski et al., 2008). Among the effectors of Cdc42 there is Formin, whose localized activation leads to increased assembly of microfilaments growing out toward the site of budding (Evangelista et al., 1997; Evangelista et al., 2002; Sagot et al., 2002) (reviewed in (Chiou et al., 2017)). The microfilament network serves as a track for vesicles that support plasma membrane expansion and cell wall assembly (Adams and Pringle, 1984; Novick and Botstein, 1985) and transfer of parental components to the daughter cell (Hill et al., 1996; Simon et al., 1997; Takizawa et al., 1997; Yang and Pon, 2002). For cytokinesis, Cdc42 and its effector Gic(s) (GTPase-interacting components) regulate assembly of septin, a cytoskeletal GTP-binding protein that forms a ring at the bud neck (Bi and Park, 2012; Sadian et al., 2013). Septins are assembled into a ring shape that is eventually expanded into an hourglass shape that is split into two cortical rings that confines cytokinesis machine in-between at the beginning of cytokinesis (Bi and Park, 2012). Septins play a role as a scaffold for the actomyosin ring that drives cytokinesis (reviewed in ((Meitinger and Palani, 2016)). The bud eventually grows in size, and given its enlargement of domain covered by Cdc42 along the enlarged plasma membrane of bud (Tong et al., 2007), Cdc42 is thought to exhibit defining role for final dimension of polarized growth (reviewed in (Martin and Arkowitz, 2014)).

2.2. *Caenorhabditis elegans*

The roundworm *C. elegans* is often employed as a good model for those who are

interested in cell polarity. The first cell cycle of *C. elegans* embryo has been a fundamental model in unfolding mechanisms leading to asymmetrical division (reviewed in (Pacquelet, 2017)). The one-cell *C. elegans* undergoes rounds of asymmetric cell divisions that generate six founder cells followed by cell type specification (Sulston et al., 1983) (reviewed in (Rose and Gonczy, 2014)). Decades ago, six *par* (partitioning defective) genes were discovered in genetic screens for cytoplasmic partitioning factors in the early stage embryo of *C. elegans* (reviewed in (Goldstein and Macara, 2007)). The PAR proteins are required for establishment of asymmetry that define the anterior-posterior body axis of *C. elegans* (reviewed in (Gomes and Bowerman, 2002)). The first cell division in the zygote is asymmetric, producing a larger anterior and a smaller posterior domain, respectively. *par* mutations disturb the ability of the embryo to undergo an asymmetric cell division. For example, *par-5* mutant displays similarly sized anterior and posterior cell (smaller than anterior cell in wild type) at the two-cell embryo stage (Morton et al., 2002). To properly understand the entire process of cell polarity exhibited in *C. elegans*, one has to start from understanding what happens during the early zygotic stage. Upon fertilization, *C. elegans* goes through completion of meiosis followed by formation of the maternal and paternal pronucleus (Goldstein and Hird, 1996). Only the paternal pronucleus is associated with microtubule-nucleating centrosome, due to the removal of centrosome from oocyte before fertilization. PAR proteins are initially distributed evenly either in the cortex or cytoplasm but after receiving unknown signals from the centrosome, the zygote undergoes ‘symmetry breaking’, a process where the contractile actomyosin network and cortical Par proteins are polarized in anterior pole by cortical flow, while cytoplasmic Par proteins are translocated to posterior pole (reviewed in (Gan and Motegi, 2020)). The finding that ablation of centrosome by laser treatment affects Par distribution while depletion of microtubules does not affect suggests that the centrosome (not the microtubules that it nucleates) is a critical factor for polarity establishment (Cowan and Hyman, 2004) (reviewed in (Rose and Gonczy, 2014)). The anterior factors are PAR-3, PAR-6, and PKC-3, whereas the posterior factors are PAR-

2, and PAR-1. Anterior Par proteins (aPAR) and posterior Par proteins (pPAR) exclude each other via phosphorylation inhibiting their plasma membrane association, maintaining their biased distribution (reviewed in (Lang and Munro, 2017)). In recent studies, requirement of Aurora A kinase (AIR-1 in *C. elegans*) has been demonstrated by RNAi-mediated knockdown of AIR-1 that resulted in disrupted distribution of PAR proteins, such as bipolar or lacking PAR-2 in cortex (Kapoor and Kotak, 2019; Klinkert et al., 2019; Manzi et al., 2024; Reich et al., 2019). For cortical accumulation of PAR-2, AIR-1 may possibly serve as upstream kinase or indirect regulator by antagonizing aPAR proteins (Manzi et al., 2024). Polarity factor CDC42 is known to regulate anterior polarization of PAR proteins (Gotta et al., 2001; Kay and Hunter, 2001). The polarization of Par proteins is essential for cell fate determination. The posterior PAR-1 phosphorylates MEX-5, a factor required for polarized localization of cell fate determinants, resulting in disassociation of MEX-5 from RNA-containing complex and its diffusion to anterior side due to increased mobility (reviewed in (Rose and Gonczy, 2014)). Anteriorly-enriched MEX-5 functions to inhibit expression of germline-specific proteins (Schubert et al., 2000) and thus the anterior domain of the one-cell stage embryo is destined to become somatic blastomere. MEX-5 restricts germline factors such as PIE-1 to the posterior domain through increased degradation (reviewed in (Rose and Gonczy, 2014)). Cortical Par proteins are also implicated in the promotion of cytokinesis by confining inhibitors of F-ACTIN of the contractile ring to anterior side (Jordan et al., 2016). The principle of mutual antagonism between kinases along A/P axis is highly conserved during evolution. In *Tetrahymena*, there is an anterior-posterior antagonism (involving anterior Hippo signaling and posterior cyclin E) that drives induction and positioning of division boundary (Jiang et al., 2020) (reviewed in (Cole and Gaertig, 2022)), suggesting that the link between mutual inhibition of polarized cortical factors and cytokinesis may possibly be highly conserved and could have evolved before the emergence of Metazoa among the ancestral eukaryotes.

In addition to such elaborate molecular polarity along A/P axis, *C. elegans* can also be a

reference model in studying establishment of the apicobasal polarity in epithelial cells. In the growing intestine of *C. elegans*, the well-conserved Hippo pathway consisting of a cascade of kinases, is required for maintenance of apicobasal polarity by inhibiting nuclear transport of transcription co-factor YAP-1 and expression of its target genes whose misregulated expression may lead to basolateral trafficking of new apical proteins (Lee et al., 2019). Involvement of the Hippo pathway in the apicobasal polarity is also reported in studies on renal epithelia (reviewed in (Michgehl et al., 2017)) and epithelium of *Drosophila* (Genevet et al., 2009) (reviewed in (Genevet and Tapon, 2011)), indicative of conserved functionality of the Hippo components in cell polarization. Importantly, our lab has documented an essential role of the Hippo pathway in patterning on the anterior-posterior axis in *Tetrahymena* (see below).

2.3. *Drosophila melanogaster*

In *D. melanogaster*, the embryo undergoes segmentation as a result of differential gene expression that depends on the segment location in the embryo. The initial polarity of the embryo is established by opposite gradients of anterior-enriched Bicoid and posterior-enriched Nanos (reviewed in (Snustad and Simmons, 2009)). The *Bicoid* and *Nanos* mRNAs are transported along microtubules and become enriched in the anterior and posterior region, respectively. Consequently, upon fertilization the high point of Bicoid gradient forms at the anterior end (Ali-Murthy and Kornberg, 2016), whereas Nanos is high at the posterior end of embryo (Wang et al., 1994). The gradients of these proteins control patterning of body structures along the anterior-posterior axis. For example, *bicoid* mutants lack the head and have the duplicated telson (Driever and Nusslein-Volhard, 1988). Nanos is required for establishment of the germ-line lineage (Hayashi et al., 2004; Kobayashi et al., 1996) (reviewed in (De Keuckelaere et al., 2018)). Both Bicoid and Nanos regulate gene expression: Bicoid is a transcription factor and Nanos is a repressor of translation. The insect embryo undergoes multiple rounds of the cell cycle and becomes multinucleated with

nuclei anchored to the cortex. The concentration gradients of Bicoid and Nanos lead to different patterns of gene expression between individual nuclei along the anterior-posterior axis. The opposing gradients of polarity factors in *Drosophila* and the resulting cell specification are reminiscent of the asymmetrical distributions of polarity factors in *C. elegans* where the anterior and posterior factors specify the somatic and germ-line blastomere, respectively. Thus, the principles underlying embryo polarization at one-cell stage are conserved (despite the differences in the nature of early polarity factors between *C. elegans* and *Drosophila*). The egg polarity gene products (including Bicoid and Nanos) regulate the levels of expression of genes whose products create body segments. Among them the activities of gap gene products, transcriptional regulators: Hunchback (a transcriptional regulator) and Caudal, are required. Nanos represses translation of Hunchback mRNA in the posterior region, while Bicoid increases Hunchback gene transcription in the anterior region (Dearden and Akam, 1999). Domain of posteriorly-enriched Caudal is defined by gradient of anteriorly-enriched Hunchback by exclusion from its domain (Schulz and Tautz, 1995). As the term ‘gap’ indicates, the mutations from these genes cause body gaps in the embryos (e.g. embryos lacking thoracic and anterior abdomen segments (Rosenberg et al., 1986)). The gap gene products play a critical role in establishing stripes of gene expression of pair-rule genes (Kraut and Levine, 1991) acting in the below hierarchy. Two pair-rule genes *Fushi Tarazu* and *Even Skipped* (Driever and Nusslein-Volhard) control pattern of transcription factor Engrailed and Wingless, the factors defined as “segment polarity” gene products, resulting in their distinct molecular organization within each segment (Ingham et al., 1988). Mutual signaling between Wingless and Engrailed/Hedgehog signaling occurs at the border of parasegment (Gritzan et al., 1999). Mutations in segment polarity genes disturb fate specification of body segments (Nusslein-Volhard and Wieschaus, 1980), such as a lack of a wing and duplicated thorax displayed in the *wg* mutant (Bejsovec, 2018). At the lowest hierarchy, the homeotic gene activities are required for specification of distinctive, development of each segment (metamere) (reviewed

in (Morata, 1993)). For instance, the formation of the *Drosophila* gonad necessitates functionality of a specific homeotic gene *abdominal-A* (*abd-A*) (Greig and Akam, 1995). Most of the homeotic genes of *Drosophila* are placed in the form of two large gene clusters consisting the Antennapedia complex (required for specification of the identity of the head, and thoracic segments) and Bithorax complex (required for determining the rest of thoracic segments and abdominal segments), respectively (reviewed in (Lepesant, 1990)).

Drosophila has been used extensively to study a type of cell polarity called the planar cell polarity (PCP). PCP refers to a uniform alignment of individual cells within a sheet of cells. In *Drosophila* wing cell, PCP is manifested in uniform positions of actin hairs on the apical cell surface. The core PCP components are asymmetrically distributed along the cell's proximal-distal axis. The PCP factors induces downstream effectors to initiate formation of the actin hair that point to the distal direction (reviewed in ((Singh and Mlodzik, 2012)). Along the epithelial plane, PCP is also displayed in the sensory organ precursor cells whose PCP factors, polarized either anteriorly or posteriorly, bias cortical recruitment of dynein motors, which results in linking astral microtubules to cell cortex, and asymmetric spindle orientation (Se´galen et al., 2010) (reviewed in (Devenport, 2014)).

Neuroblast (NB) can be referred to as an example of a cell displaying apicobasal polarity in *Drosophila*. NB serves as a progenitor cell for neurons and glia. In the NB delaminated from epithelium, proteins are asymmetrically distributed (apical proteins required for orientation of spindle that undergoes rotation during metaphase for alignment with epithelial layer in perpendicular/ basal proteins serving as cell-fate determinants essential for differentiation of neuron (reviewed in (Yu et al., 2006))). It is to some extent reminiscent of asymmetrical cell division of *C. elegans* embryo whose underlying process places cell-fate determinants asymmetrically along polarity axis. To sum up, *Drosophila* uses a range of cell polarities for sophisticated pattern formation of its body parts or cell differentiation and represents one of the most powerful model organisms for understanding cell polarity.

3. Cell polarities in ciliates

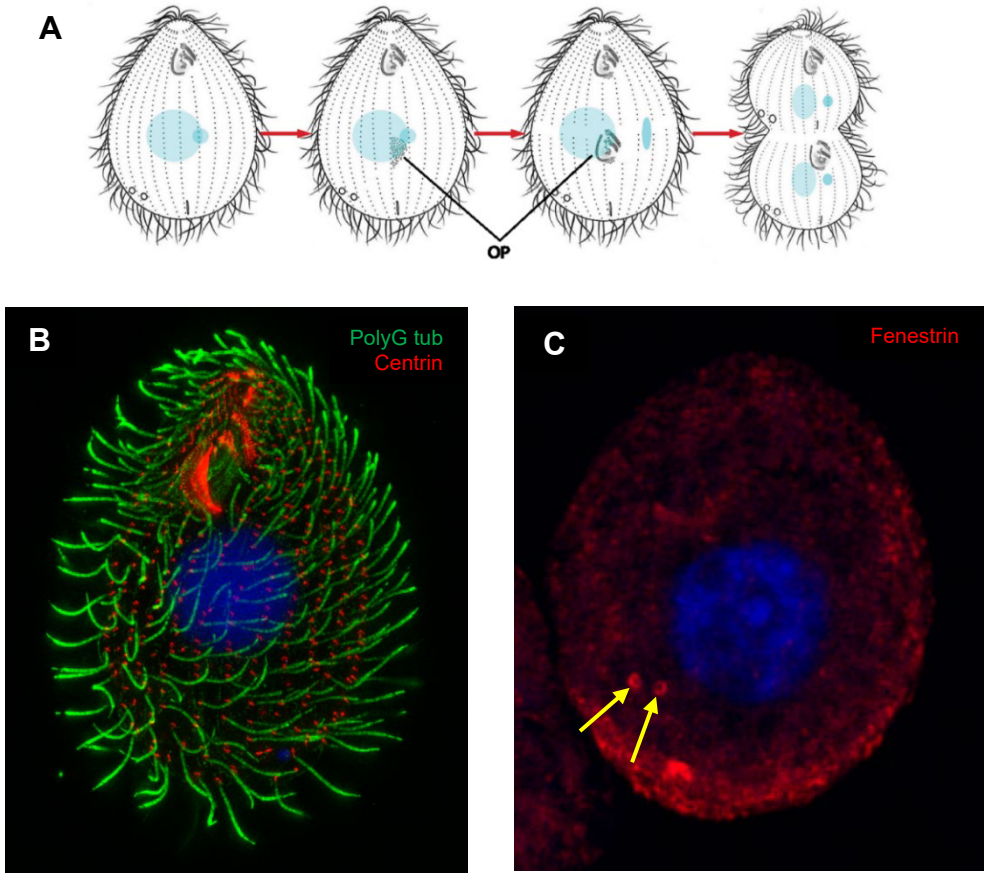

Figure 1.1. Depiction and microscope images showing cortical organelles of *T. thermophila*. (A) Picture (the courtesy of Eric Cole (Saint Olaf University, USA)) describing a course of cell division of *T. thermophila*. Note that new organelles labeled in the illustration are assembled at the same longitude as old organelles. (B) SR-SIM image of the wild type cell labeled by anti-polyG tubulin antibody (green), anti-centrin antibody (red), and DAPI (blue). Note array of cilia along rows of basal bodies and oral apparatus shown near the anterior end of cell. (C) Confocal image of the wild type cell labeled by anti-fenestrin antibody (red), and DAPI (blue). Note the two CVPs (indicated by the yellow arrows) in the proximity of posterior end of cell. Abbreviation: OP; Oral primordium

Ciliates have on their surface numerous cilia and other types of microtubule-rich organelles that are positioned at specific locations along the cell-wide polarity axis. In general, ciliates have two polarity axes: anterior-posterior (A/P) and circumferential (C). The A/P polarity axis could also be described as a “front-rear” axis as ciliates most of the time swim in the forward direction with their anterior end leading. The C polarity describes the placement of organelles around the cell circumference. *Tetrahymena thermophila* is a small

ciliate whose cilia are nucleated from basal bodies (BBs) most of which are aligned as longitudinal rows spanning the length of the cell. A subset of cilia are organized as 4 short oral rows within the oral apparatus (Fig. 1.1A,B). A large number of cilia and the availability of methods for isolating cilia renders *T. thermophila* to be an excellent organism to explore characteristics and functions of ciliary proteins (Gaertig et al., 2013). *T. thermophila* has also been used extensively in exploring intracellular pattern formation of cortical organelles thanks to the pioneering work of Joseph Frankel and colleagues (University of Iow in isolating and characterizing cortical mutants (reviewed in (Frankel, 1989; Frankel, 2008)). I will now review the cell polarity features and some underlying mechanisms in ciliates.

3.1. Intracellular pattern formation of organelles

In *Tetrahymena*, the feeding organelle called oral apparatus (OA) is located very close to the anterior cell end. In contrast, the osmoregulator contractile vacuole pores (CVP) and the cytoproct (CYP) are located near the posterior cell end. The circumferential polarity axis is unusual because ciliates lack symmetry in the lateral placement of cortical organelles. The cell circumference is organized around ~ 20 rows of somatic locomotory cilia that are equally spaced apart. A good analogy of the circumferential polarity would be a clock dial with 20 ″hour positions″ that correspond to each of the longitudinal ciliary rows (we define each row on the basis of numerical position: 0 is assigned to the row along which OA is aligned. On the cell's perspective, the adjacent right and left row is defined as +1 and -1, each. The following adjacent right and left row is defined as +2 and -2, each, and so on.). There is only a single OA and its cortical side is by definition called ventral. The CYP, organelle that function as ejector of spent content of food vacuoles, is located at about the same circumferential position as the oral apparatus, in the posterior/ventral region. In contrast the CVPs are located near usually two somatic rows located on the right side of the cell. *T. thermophila* divides by ″tandem duplication″, a transverse binary fission whose core step is

formation of equatorial division boundary (DB) that produces a tandem of daughters whose regions adjacent to DB are remodeled into new cell ends. Oral primordium (new oral apparatus) is assembled at the ciliary row along which old OA is positioned (the right postoral row). New CVPs and CYP are assembled at the same longitudes as the old CVPs and CYP respectively near the posterior end of the anterior daughter cell as depicted in the Fig. 1.1A.

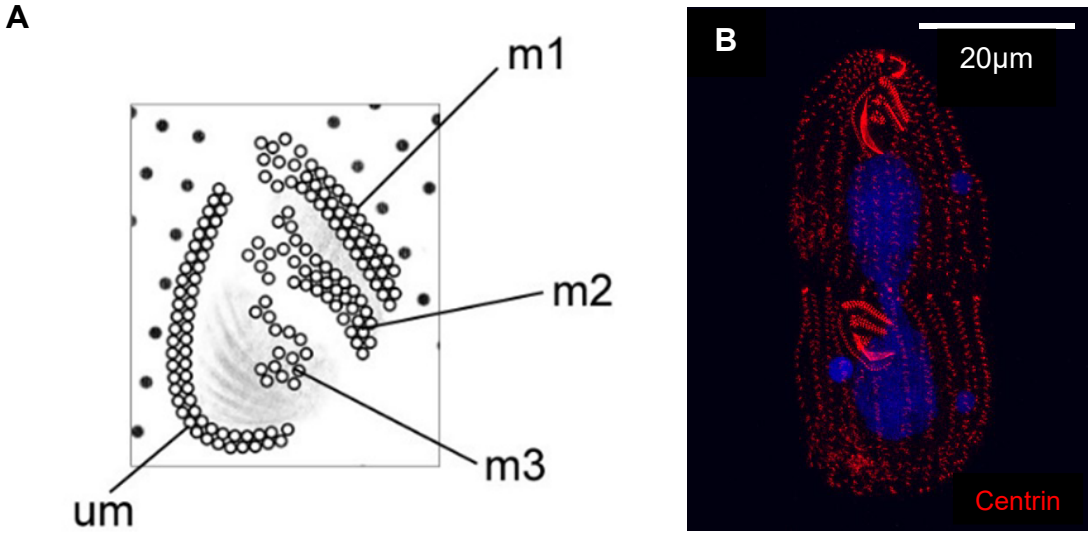

Figure 1.2. Oral apparatus of *T. thermophila* consists of four oral rows. Illustration (A) and SR-SIM image of wild type cell showing oral apparatus displaying one undulating membrane (um) and three membranelles (m1, m2, and m3) (B). The cells were labeled by anti-centrin antibody (red), and DAPI (blue).

In addition to the cell polarization at whole cell scale, sophisticated cell polarity is also established within organelles. The oral apparatus (OA) of *T. thermophila* is a perfect example for such internal organelle-level polarity, given its asymmetrical shape formed by cilia that are aligned into 4 oral rows: the so called “undulating membrane” (UM) on the right side, and 3 so called “membranelle” rows (M1, M2 and M3) on the left side (Fig. 1.2). Several gene products regulate the internal pattern of the OA. For example, certain mutations either increase (*mpD-1*) or decrease (*mpH-1* and *mpG*-1) the number of oral M rows (reviewed in (Frankel, 2008)). Our laboratory has recently identified the MpD gene product as Importin-9 that forms a gradient within the oral apparatus with the high point at row M1 (Deraniyagala et al JCB In

Press 2025). Such consistent pattern formation (either at global or local scale) established in wild type *T. thermophila* and relatively a short cell cycle enable ease of recognizing patterning defects in a large population of cortical mutants. When investigating other ciliated organisms, polarity of specific cortical organelle is either variable or invariable, depending on the species. Importantly, ciliates are an extremely diverse group and even relatively closely related ciliates can differ greatly in their cortical patterns. For example in *Paramecium*, the OA is positioned around midbody while CVPs and CYP are assembled at both of the cell ends (reviewed in (Cole and Gaertig, 2022)). Possibly, the patterning factors that place organelles at each of assigned position may be differently distributed or regulated, depending on the ciliate species. In contrast, among *Tetrahymena* species the CVP is generally placed on the right side of cell within a narrow range of cell circumference (Nanney et al., 1980). Another interesting variation is in the organization of the circumferential polarity axis is the case of *Stentor*. *Stentor* is a very large ciliate whose OA is placed at the anterior cell end whereas the holdfast (a part that attaches the cell to the substrate) is placed at posterior end. The OA is very large, occupies most of the cell circumference.

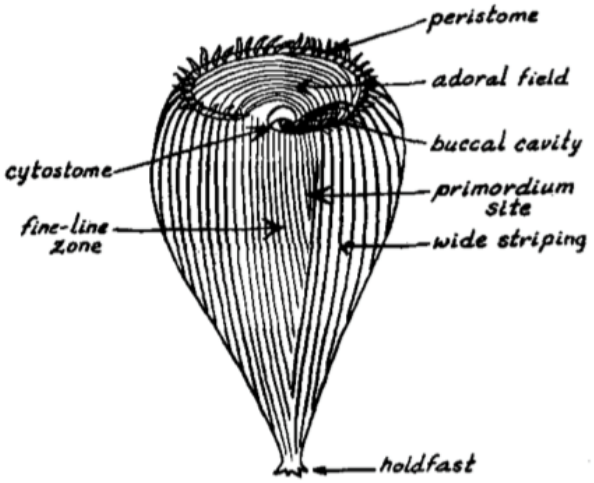

Figure 1.3. Illustration of large ciliate *Stentor*. The picture of *stentor* borrowed from (Tartar, 1956b). Note the L-R decreasing gradient in the stipe width along the cell circumference.

Strikingly, in *Stentor* the spacing between adjacent longitudinal (somatic) ciliary rows

depends on their circumferential position. The inter-row spaces are called “stripes” as they are filled with green pigment. The stripe width decreases from the cell’s left to right side. In other words, there is a circumferential L-R decreasing gradient in the stripe width (Uhlig, 1960) (Fig. 1.3). On the ventral side, the narrowest stripe meets the widest stripe forming the so called “locus of stripe contrast (LSC)” (Tartar, 1956a; Uhlig, 1960). Strikingly, the new oral apparatus forms at the LSC (Paulin and Bussey, 1971; Pelvat and Dehaller, 1979; Uhlig, 1960). We will discuss the lessons about pattern formation mechanisms that come from the experiments done on *Stentors* further. Taken together, patterning of ciliate organelles may be more complicated than the conventional perspective, and it would be promising to investigate if discrepancies in pattern formation among diverse ciliates is due to diverse mechanisms or species-specific modifications of common mechanisms (e.g. changes in the cortical distributions of conserved pattern regulators).

3.2. Cortex of ciliate, a center of the intracellular pattern formation

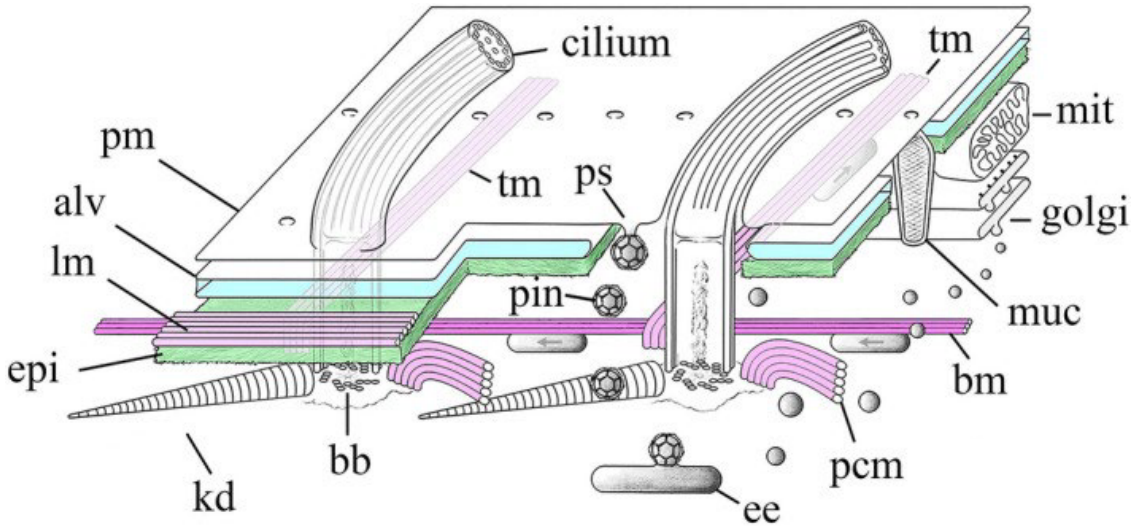

Figure 1.4. Cortex of *T. thermophila*. Depiction of organization of cotex in *T. thermophila* (borrowed from (Cole and Gaertig, 2022)). Note that the cortex is composed of layers, starting from the outermost layer plasma membrane (pm).

My doctorate research projects were mainly focused on the cortical development of *T. thermophila*. The cortex of *Tetrahymena* is composed of multiple layers starting from the plasma membrane (pm) on cell surface. Beneath the pm lie alveolar sacs that may serve as

calcium storage organelles (Hardt and Plattner, 2000; Lange et al., 1995; Plattner and Klauke, 2001; Plattner et al., 2012; Stelly et al., 1995; Stelly et al., 1991) (reviewed in (Cole and Gaertig, 2022)) (Fig. 1.4). Below the alveolar sacs, there are basal bodies (bb(s)) that nucleate cilia and adjacent parasomal sacs (ps) serving as a site for endocytosis of cortical components (Cole et al., 1987; Cole et al., 2023). A recent study suggests that parasomal sacs also function in exocytosis (Jiang et al., 2024). The third layer of cortex is occupied by a sheet of the nonmicrotubule cytoskeleton called “epiplasm (epi)”. The proteins that form the epiplasm are required for proper cell shape and organization of basal bodies (Honts and Williams, 2003; Williams, 2004). The upper and lower region of epiplasm is occupied by microtubule networks that extend across the cell (reviewed in (Cole and Gaertig, 2022)). Importantly, the longitudinal microtubule bundles (LMs) run along each ciliary row spanning the anterior-posterior polarity axis. On the other hand, the transverse microtubules align with the circumferential polarity axis. The microtubule-associated motor proteins may transport cortical regulator proteins along the microtubule networks as cargo to form the gradient of patterning factors. Taken together, ciliates display multiple-layered cortex exerting diverse roles, including intracellular pattern formation. In ciliates, the cortex also exhibits astonishing ability of developmental plasticity (reviewed in (Frankel, 1989)). It was revealed in the past that cellular fragment of *Stentor coeruleus* created by surgery regenerates its lost structures but such impressive regenerating capability is exerted only when at least a small patch of cortex is still retained after the surgery (Tartar, 1956c; Tartar, 1961). Therefore, it is logical to expect

that cues for how cortical organelles are organized into pattern are released from components of the cell cortex. For instance, given enrichment of microtubule networks and epiplasm within cortex, the cytoskeleton somehow may be associated with cues for intracellular pattern

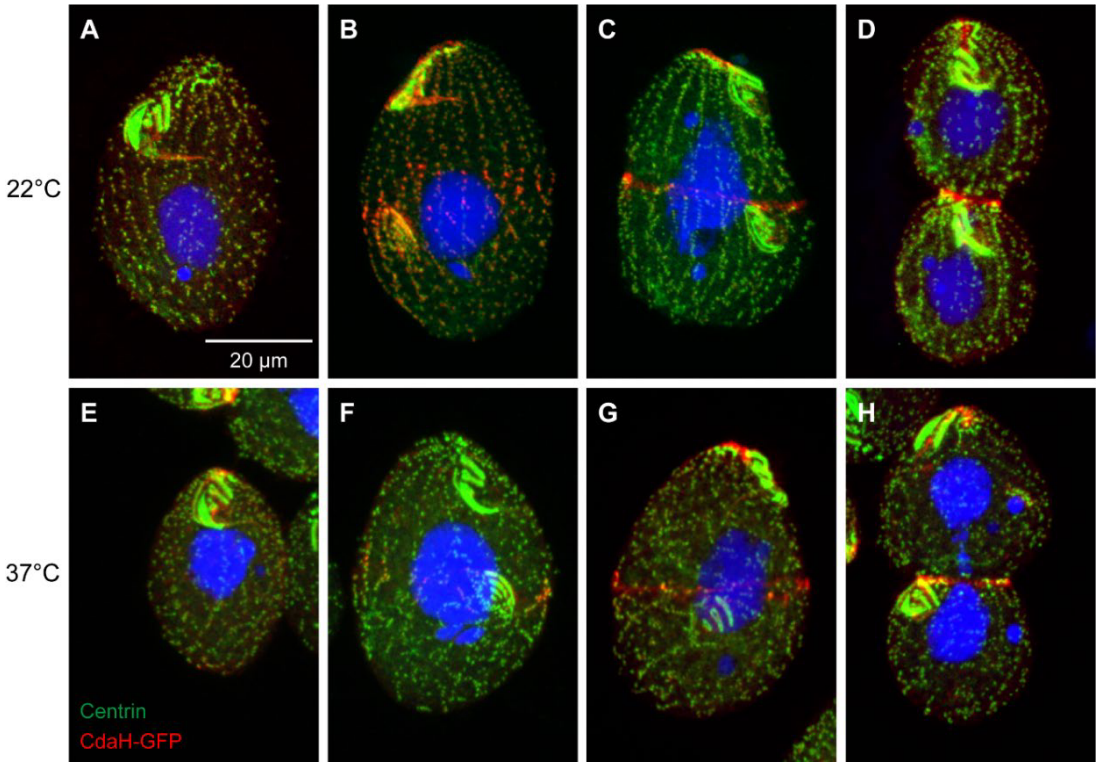

Figure 1.5. Disorganized basal bodies doesn't critically affect cortical patterning and division of *T. thermophila*. (A-H) Confocal images of temperature-sensitive *disA-1* mutants during interphase stage (A,E)and cell division stage (B-D;F-H). After incubated either at room temperature for overnight, the cells were labeled by anti-centrin antibody (green), anti-GFP antibody (red), and DAPI (blue). Note that in spite of disorganized basal bodies (the degree of disorganization appears as more prominent at 37°C) characterized by disrupted orientation of ciliary rows, division boundary and oral apparatus are intact.

formation. One can also deem the basal body as a promising contributor for intracellular pattern formation, given its enrichment on cortex. However, the basal bodies of hypotrich ciliates are resorbed at unfavorable condition such as stress or starvation (during the process of cyst formation) but the cortical pattern reforms correctly at favorable conditions (Fryd-Versavel et al., 2010; Grimes, 1973a; Grimes, 1973b). On the other hand, even in the absence of basal bodies, the submembraneous microtubules are retained in a highly organized form and the cell polarity features remains present on the cell surface (Fryd-Versavel et al., 2010). Moreover, in the *disA-1* mutant displaying highly disorganized BBs, the positions of major

organelles and the cell division course are not grossly affected (Galati et al., 2014; Jerka-Dziadosz et al., 1995) (Fig. 1.5), suggesting that BBs are not the important factors for intracellular pattern formation or if they are, they do not need to be organized into proper longitudinal rows. Intracellular pattern formation of ciliates also appears to reflect communication between the cortex and the endocytoplasm. For example, the division of micronucleus and macronucleus coincides with the time of cortical subdivision and cytokinesis, respectively (Jerka-Dziadosz et al., 2001; Kirk et al., 2008).

Importantly, there is evidence for mechanisms based on mutual antagonism of polarity factors in *Tetrahymena* (Jiang et al., 2020). In *C. elegans*, the anterior and posterior cortical Par proteins exclude each other from their domains by inhibiting their respective ability to bind to the plasma membrane. *In Tetrahymena*, a mutual antagonism occurs between the anteriorly located component of Hippo signaling (CdaI/Mst) and the posteriorly located CdaA/cyclin E and this interaction induces and positions the division plane along the cell's equator (Jiang et al., 2020).

Interestingly, ciliates also appear to possess the ability to adjust normally consistent cortical pattern in response to change in cell size. For instance, in *Stentor* excision of posterior end of cell induces anterior migration of originally determined equatorial fission line, resulting in equal cell division (Tartar, 1968). This seems to be an implication that the cortical pattern is adjusted in agreement with cell size (scaling). With all these, cortex of ciliates exerts powerful capability of reproducible patterning of organelle and its adjustment to the cell size. In the recent decades, there has been endeavor for exploring intracellular pattern formation at molecular level by application of forward genetics (Galati et al., 2014) to cortical mutants (Frankel, 2008). Below I introduce several patterning factors governing placement of organelles along the polarity axes of *T. thermophila*.

3.3. Molecular factors essential for intracellular pattern formation along polarity axes of *T. thermophila*

Cortical mutants can be classified on the basis of the scale of pattern formation. Global defects indicate mispositioning of cortical organelles along either the anterior-posterior (A/P) or the circumferential (C) polarity axis, whereas local defects indicate abnormal property of a particular cell structure. The examples are presented below. Over the decades, multiple gene products have been identified as patterning factors required for correct geometry of cortical organelles along the polarity axes or in internal patterning of organelle.

3.3.1 A/P patterning factors

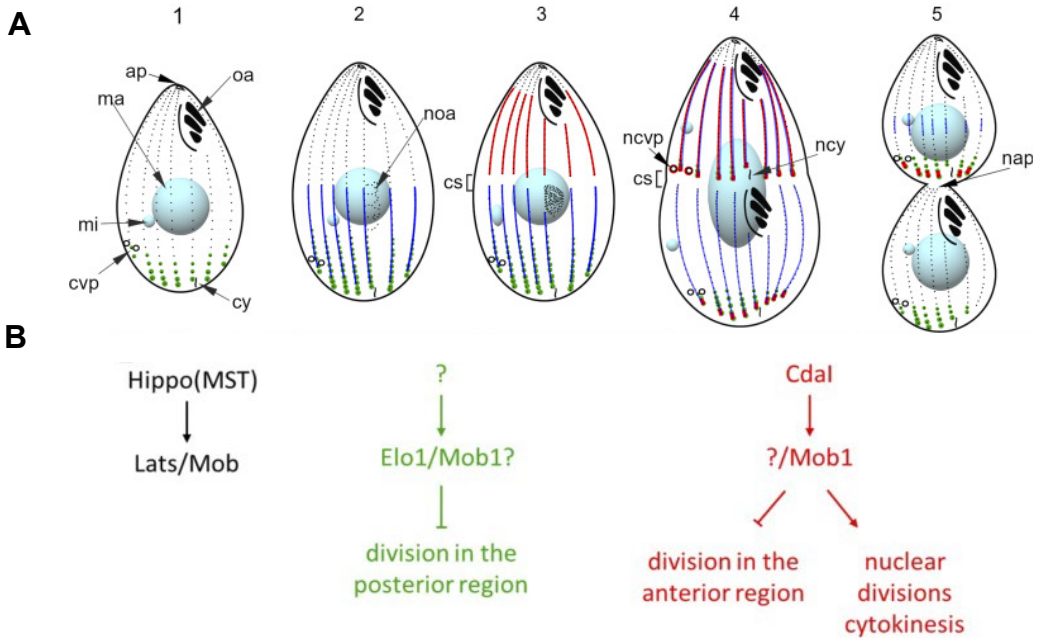

Figure 1.6. Molecular factors and involved pathways implicated in A/P patterning. (A) The illustration (borrowed from (Jiang et al., 2020)) depicting cortical localization of A/P patterning factors (Elo1 (green), CdaI (Red), and CdaA (Blue)) in dividing *T. thermophila.* (B) The summary (borrowed from (Jiang et al., 2019)) of Hippo components working in two circuits during cell division phase of *T. thermophila*.

3.3.1.1. Mob1 (The first Hippo factor defined as A/P patterning factor)

In the recent years, several genes required for intracellular pattern in *T. thermophila* have been identified by the application of forward genetics (Galati et al., 2014). This approach led to discoveries that link intracellular pattern formation of organelles to Hippo pathway, a kinase

cascade preserved well throughout the history of evolution. Initially discovered in *Drosophila*, Hippo pathway is required for a wide range of cellular phenomena such as proliferation, death, morphogenesis, and cell fate determination, and has been described as the 'jack of all trades' (Davis and Tapon, 2019). The Hippo pathway consists of cascade of kinases where Mst/Hippo kinase regulates activity of Lats kinase-Mob1 complex that controls activity of downstream effectors required for a variety of cellular processes. In the budding yeast, activation of Hippo pathway is required for exit from mitosis and subsequent initiation of G1 phase of cell cycle (Rock et al., 2013). In *C. elegans*, Hippo pathway contributes to the establishment of apicobasal cell polarity in a growing intestine by regulating the activity of transcription regulator Yap by cytoplasmic sequestration, preventing dysregulated target gene expression that may possibly affect identities of membrane domains (no clear border between apical and basal domain) (Lee et al., 2019). In *Drosophila,* Hippo pathway is involved in diverse activities such as the apico-basal polarity (reviewed in (Genevet and Tapon, 2011)), proliferation, apoptosis, and cell fate control (reviewed in (Varelas, 2014)). In the mammalian embryo, cells display different levels of Hippo activity that result in proper tissue specification and organ development (reviewed in ((Wu and Guan, 2021)). Recently, studies have revealed that Hippo pathway is required for intracellular pattern formation of ciliates. In *Stentor*, phenotypes conferred by knockdown of Mob1 (a Hippo pathway component that stimulates kinase activity of its binding partner Lats/Ndr), such as abnormal morphology characterized by excessive elongation or loss of wine-glass shape, and a failure of growth of anterior part from posterior fragment (during regeneration), revealing that Mob1 is implicated in proper morphogenesis and regeneration (Slabodnick et al., 2014). In dividing *Tetrahymena*, depletion of Mob1 (enriched at the posterior end of cell) resulted in wrong placement of the division plane, arrest in cytokinesis, and delayed ciliogenesis, indicating multiple roles in cortical development plan (Tavares et al., 2012). Mob1 localizes to the posterior region in both *Tetrahymena* and *Stentor,* two ciliate species separated by a very long period of evolution, indicating that the involvement of Hippo signaling in cortical patterning and cell division predates the emergence of diverse

lineages of ciliates (Slabodnick et al., 2014; Tavares et al., 2012).

3.3.1.2. Elo1

In the *elo1-1* mutant, OP and division plane are shifted posteriorly causing an asymmetrical cell division producing a large anterior daughter and a small posterior daughter cell (Frankel, 2008; Jiang et al., 2019). *elo1-1* was mapped to the *TTHERM_0035550* gene that encodes a Lats/NDR kinase (Jiang et al., 2019), a conserved component of Hippo kinase cascade (reviewed in (Hergovich, 2013)). The localization pattern of Elo1 is similar to that of Mob1 which is not unexpected as in other organisms the two proteins form a complex in which Mob1 activates the Lats kinase. At the posterior end of cell, Elo1 forms a decreasing gradient toward the anterior cell end. During early stage of division phase when OP starts to form o as “an anarchic field” (an early stage of oral development characterized by random orientation of BBs), Elo1-GFP formed gradient whose anterior end (Elo1-GFP lowest) was directly posterior to the anarchic field (Jiang et al., 2019). During later stages when the division boundary is induced, Elo1-GFP forms a tandem of shorter gradients at posterior end of each hemi-cell (reviewed in (Cole and Gaertig, 2022)). Taken together, Elo1 likely acts by preventing oral development from occurring too close to the posterior cell end. There are other possible examples of patterning factors acting by “cortical exclusion” (see below). This gradient-mediated placement of cortical organelles is also observed along the C axis where bidirectional gradient of Hpo1-3xHA appears to exclude oral apparatus and results in its correct circumferential localization (see the Chapter 3). Thus, we suggest that in *T. thermophila*, intracellular pattern formation of oral apparatus encompasses requirement of molecular gradients along the A/P and C polarity axis. Elo1 and Hpo1 are similar in that the weak point of each gradient borders the OA, indicating that they may share similarities in overall mechanism that demarcates location of oral apparatus.

3.3.1.3. Cdal

A temperature-sensitive *cdal-1* mutation confers anterior migration of OP and division

plane (Frankel, 2008; Jiang et al., 2017), leading to unequal cell division producing a small anterior daughter cell and large posterior daughter cell. But *cdaI-1* likely doesn't play a critical role in localization of cvp, indicating that posterior cell end patterning is relatively less dependent on CdaI (Jiang et al., 2017). *cdaI-1* was mapped to the *TTHERM_00971920* gene encoding a Hippo/Mst Kinase (Jiang et al., 2017). This suggests that the Hippo pathway controls correct anterior-posterior cell polarity in *Tetrahymena* possibly by activating downstream effectors or interaction with other molecular pathways required for intracellular pattern formation. CdaI accumulates at anterior cell half during division phase of *T. thermophila* (Fig. 1.6A). These results are intriguing in the light of data about Elo1/Lats and Mob1. Both CdaI/Mst and Elo1/Lats are orthologs of components of the kinase cascade of Hippo signaling so it is unexpected that the properties of these two proteins are so dramatically different. Namely, 1) Elo1 is posterior and CdaI is anterior, 2) loss-of-function mutations results in different outcomes: a loss of CdaI causes an anterior shift in the OP and division boundary (DB) position and exactly opposite effect is observed in the *elo1-1* mutant, 3) the gradients have different temporal patterns: the Elo1 posterior gradient is permanent (present even in interphase) while the anterior gradient of CdaI forms during cell division (before the emergence of the division boundary). Interestingly, dividing double mutants bearing loss of functional Elo1 and CdaI (hypomorphic) initially display a phenotype similar to that of the *elo1-1* single mutant (division plane posteriorly migrated) but later display a phenotype characteristic of hypomorphic CdaI (migration of the OP and division plane in the anterior direction) (Jiang et al., 2019). These results suggest that Elo1 and CdaI act as components of two separate Hippo signaling circuits (Elo1 may be a component of the "early Hippo circuit" and CdaI may be a component of the late Hippo circuit.) to control the position of the OP and the division plane (Jiang et al., 2019) (Fig. 1.6B). Along with CdaI, Mob1 may also be a part of late Hippo circuit given the similarity of defect conferred by downregulated Mob1 compared to defect conferred by *cdaI-1*, not *elo1-1* (Jiang et al., 2019). On the other side, Mob1 colocalizes with Elo1 so it is also likely a component of the early Hippo circuit. Given that there

is also a presence of TTHERM_001262898 (not yet been studied) similar to Mob4 (a subtype of Mob1) in animal lineages (Trammell et al., 2008; Ye et al., 2009), functionality of Mob4 may be involved in the early Hippo circuit instead of Mob1 (Jiang et al., 2019) (reviewed in (Cole and Gaertig, 2022)).

Recently, it has been revealed that CdaI (Mst/Hippo kinase) and CdaA (cyclin E) engage in a mutual antagonism for induction and equatorial localization of division boundary (DB) (Jiang et al., 2020). Posteriorly enriched CdaA and anteriorly enriched CdaI (Fig. 1.6A) exclude each other from each of their domains. While single *cdaA-1* mutants do not develop the division boundary, double mutants *cdaA-1;cdaI-1* do and regain the ability to proliferate, implying significance of balancing between CdaA and CdaI activity (Jiang et al., 2020). This discovery implicates cyclin E in cortical patterning in *T. thermophila*. On the other hand, there are a few reports linking cyclin E to cell polarity in *C. elegans* (Cowan and Hyman, 2006) and *Drosophila* (Berger et al., 2010; Berger et al., 2005; Bhat and Apsel, 2004). The relationship between CdaA and CdaI is reminiscent of mutual exclusion of anterior and posterior Par proteins of *C. elegans* for cell polarization and conservation of establishment of cortical antagonism (Adl et al., 2012; Jiang et al., 2020). In addition to such global scale pattern formation, extra oral M rows (more than 3) are frequently observed in the OP of *cdaI-1* single mutants. Thus, we propose that CdaI (Mst/Hippo kinase) also controls the size of oral apparatus. That one mutation (*cdaI-1*) causes defects in patterning at two scales (global and local) can be explained in two ways. One is that there is a functional connection between the global and local patterning. Specifically, the same mechanism that positions the op could also control the op internal organization. The second explanation is simpler: the protein CdaI functions in two or more pathways that control the global and local patterning. This explanation seems more likely as CdaI is a kinase and kinases are known to typically phosphorylate many substrates and localize at multiple places in the cell. In fact, CdaI whose loss affects the position of OP and DB division boundary localizes to both the vicinity of the division boundary and the OP. Thus, the same kinase could be influencing both the global and local patterning simply by

phosphorylating two or more substrates that act at multiple levels of patterning. As described in Chapter 2, I performed a study of another “multifunctional” kinase whose loss produces a combination of local and global patterning defects, CdaH, an ortholog of Fused/Stk36 kinases. In this case we again detected CdaH at multiple places that correlate with the multitude of patterning defects in the *cdaH-1* mutant (Lee et al., 2024).

3.3.2. C patterning factors

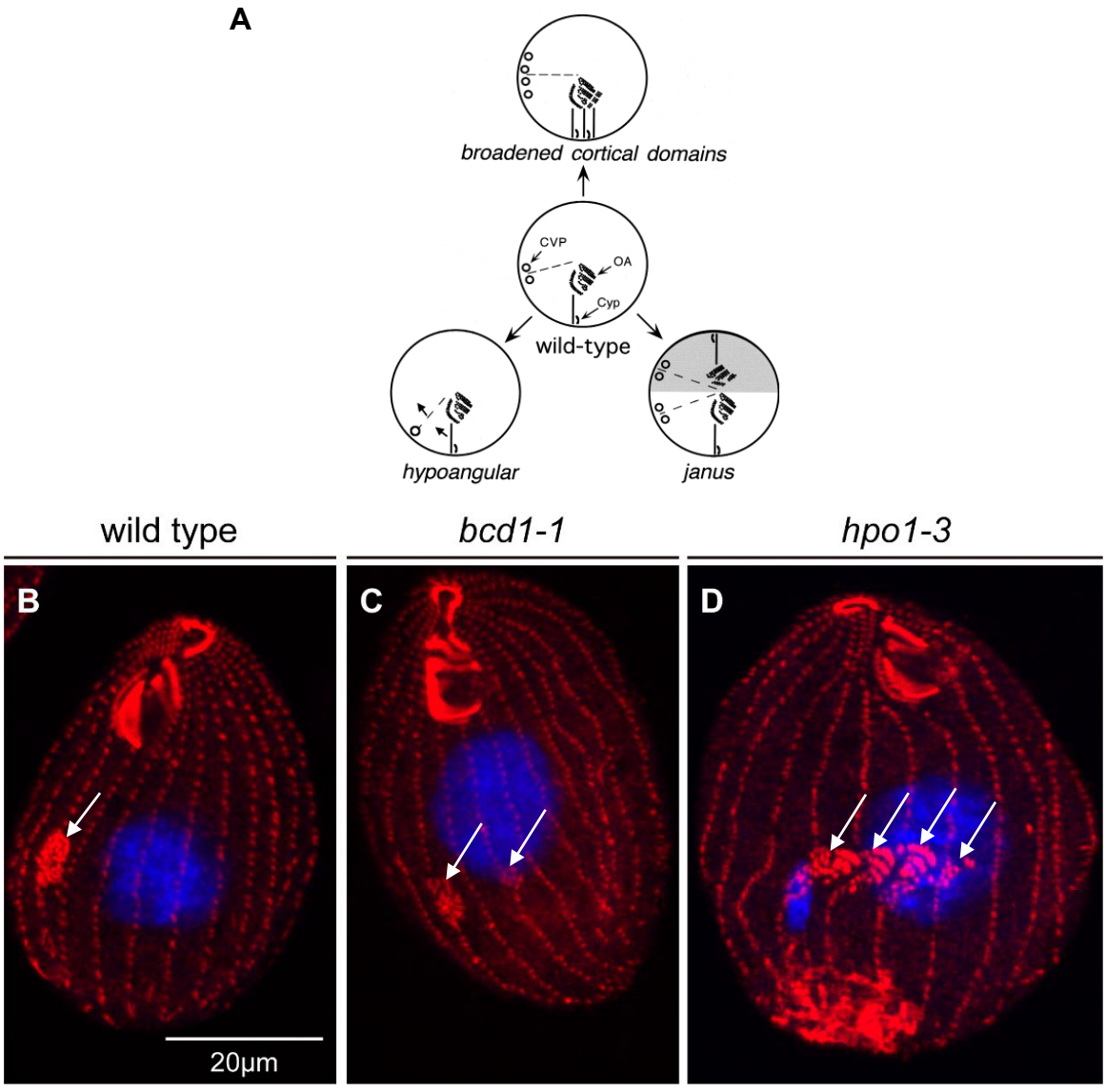

Figure 1.7. Mutants that confer C patterning defects. Illustration (borrowed from (Frankel, 2008)) (A) and confocal images that show C patterning mutants (C,D compare to B) displaying extra oral primordiums (OPs) (pointed by the white arrows) along cell circumference. Note two OPs and four OPs from *bcd1-1* (C) and *hpo1-3* mutant, respectively. The cells were labeled by anti-centrin antibody (red), and DAPI (blue).

C patterning is defined as correct placement of cortical organelle along the circumferential (left-right) polarity axis. For example, the OP is formed along the same longitude as the old OA, whereas CVPs are formed on the right side of wild type *T. thermophila.* Namely, proper patterning of cortical organelle also requires correct localization along the C axis, in addition to correct localization along the A/P axis. The C patterning mutants display incorrect geometry of cortical organelles, including examples of OP formed at different longitudes (either on the left or right side) as the old OA or formation of extra OPs along the cell circumference. The significance of investigating mechanisms underlying the C patterning may be conceived from multiple perspectives: How the C pattern forms without landmarks that are available on the A/P axis, such as cells ends? For example, the OP forms near a single specific ciliary row 0 that in every way seems to be identical structurally to any other ciliary rows; Row 0 is one of the two postoral rows that end near the mature OA and thus one possibility is the shorter length of row 0 may send cues for determination of The OP location. However, there are two short postoral rows and thus another mechanism must exist that distinguishes between row 0 and row +1 (left postoral row) that is not active in oral development. Another question is about how position-specific features are generated around the cell circumference. The most extreme example is how the circumferential gradient in the row spacing observed in *Stentor* (Fig. 1.3). However, C position specific row features are also observed in *Tetrahymena*. For example, a subset of anterior rows on the left-dorsal side end with BB pairs forming the so-called apical crown (Jerka-Dziadosz, 1981; McCoy, 1974). There is strong evidence for the existence of distinct circumferential regions that interact laterally to control pattern formation. For example, in *Stentor*, important interaction occurs along the longitude where the narrowly-spaced ciliary rows meet the widely-spaced ciliary rows(locus of stripe contrast or LSC). The OP forms at the LSC. Furthermore, cortical grafting experiments showed that extra OPs formed when artificial LSCs are created by grafts that place a portion of cortex with narrow stripes next to wide stripes (Tartar, 1956b; Uhlig, 1960) (reviewed in (Frankel, 1989))). Another question is whether the AP and C patterning mechanisms interact, for example by sharing some

components (I will present evidence in Chapter 4 that this could be the case.). Below I will review the C patterning mutants investigated so far and some known properties behind the C patterning in *T. thermophila*.

3.3.2.1. Hpo1

To fully understand intracellular pattern formation of *T. thermophila*, relatively unstudied C (left-right) patterning must not be overlooked. *hpo1-3* confers excessive op generally displaced either to left or right direction (Chapter 3; Fig. 1.7A,D compare to B) along the cell circumference and reduced # of CVPs on right side of cortex (Frankel et al., 1993) (see Fig. 3.S1 of Chapter 3). In the wild type, only one OP forms along a postoral row defined as 'position 0' (right (cell's perspective) row from two postoral rows; middle row is defined as position 0 when three postoral rows that occasionally appear especially in mutants) (Fig. 1..7B), and in *hpo1-3* strain, such cortical development plan is disrupted as reflected from excess of OPs along cell circumference (Fig. 1.7D). Temperature-sensitive *hpo1-3* also displays posterior migration of OPs when incubated at restrictive temperature for a prolonged time (Frankel et al., 1993), indicating that molecular pathways implicated in A/P and C patterning are not completely separated.

3.3.2.2. Bcd1

Bcd1 (Broadened cortical domain1), recently identified as BEACH domain protein, is another left-right patterning factor that regulates cortical dimension occupied by organelles by controlling membrane trafficking that remodels the cortex (Cole et al., 1987; Cole et al., 2023). *bcd1* alleles confer increased number of OPs along cell circumference (Cole et al., 1987) (reviewed in (Frankel, 2008)) (Fig. 1.7A, C compare to B) and CVPs. The pinosomes (labeled by FM 1-43 dye) deliver surface membrane and extracellular materials by dynamin-mediated endocytosis (Elde et al., 2005), and the significant reduction in pinocytotic activity reflected by FM labeling was displayed in *bcd1-2* mutant, indicating that Bcd1 regulates the cortical pattern by activating pinocytosis (Cole et al., 2023). *bcd* alleles also display

excessive number of CVPs (Cole et al., 1987) (reviewed in (Frankel, 2008)), and the recent observation that both *hpo1* and *bcd1* cause excess of op but respectively exerts contrasting impact on # of cvp (see Fig. 3.S1 of the C

hapter 3) implies that op and cvp are organized into pattern independently at the molecular level. In addition to implication in cortical patterning along cell circumference, it was revealed from the lethal double mutant expressing *hpo1 ko* and *bcd1-2* that either Hpo1 and Bcd1 or required for cell viability (synthetic lethality). This double mutant displays gross defects in cortical development characterized by abnormal shape of cell and oral apparatus (See Fig. 3.9 of the Chapter 3). This may indicate requirement of interaction between Hpo1 as a right factor and Bcd1 as a left factor, respectively, similar to the case of grafting experiment of *Stentor* revealing that oral development is delayed until the weak stripe contrast (created by juxtaposition of left and right cortex) is remodeled into stronger stripe contrast by branching of stripes for oral development (Tartar, 1956b; Uhlig, 1960) (reviewed in (Frankel, 1989)).

3.3.2.3. Janus

janus alleles confer duplicated pattern of ventral side on dorsal side (Frankel and Nelsen, 1986; Frankel and Nelsen, 1987). The phenotype of the mutant is represented by extra oral apparatus on dorsal side (Fig. 1.7A; Fig. 1.8B compare A), similar to mythical image of Janus possessing two heads. As the principle behind the formation of extra OA in the *janu*s strain, the intercalation model that positional values (assigned to each individual ciliary row) undergoes duplication and reversal of positional values (intercalation) was proposed (Frankel and Nelsen, 1987). Hpo1 precisely accumulates in a form of bidirectional gradient between primary and secondary OA in the *janus* mutant (see Fig. 3.5 of the Chapter 3). This suggests that on dorsal side, Hpo1 marks cryptic position for extra OA expressed in the *janus* mutants. We suggest that Janus may serve as dorsal inhibitor against OA rather than regulator of maintenance in positional values. Recently, Jan A has been identified as a Polo kinase of *T.*

thermophila and shown accumulated on left side of cortex (Cole et al., 2024) (Fig. 1.8C-C'''). Other Polo-like kinases mark cortical domains with distinctive pattern, such as enrichment of Plk2 on the right side (opposite polarization against Jan A) and enrichment of Plk3 around the ciliary rows along which cvp(s) are aligned, indicative of involvement of Plks in cortical pattern formation in each of enriched domain (Cole et al., 2024). For instance, opposite polarity of Plk2 and Jan A may act as right and left cortical factor along C axis, possibly in a manner that Hpo1 and Bcd1 interact or other kinases interacting by mutual antagonism along A/P axis (Jiang et al., 2020).

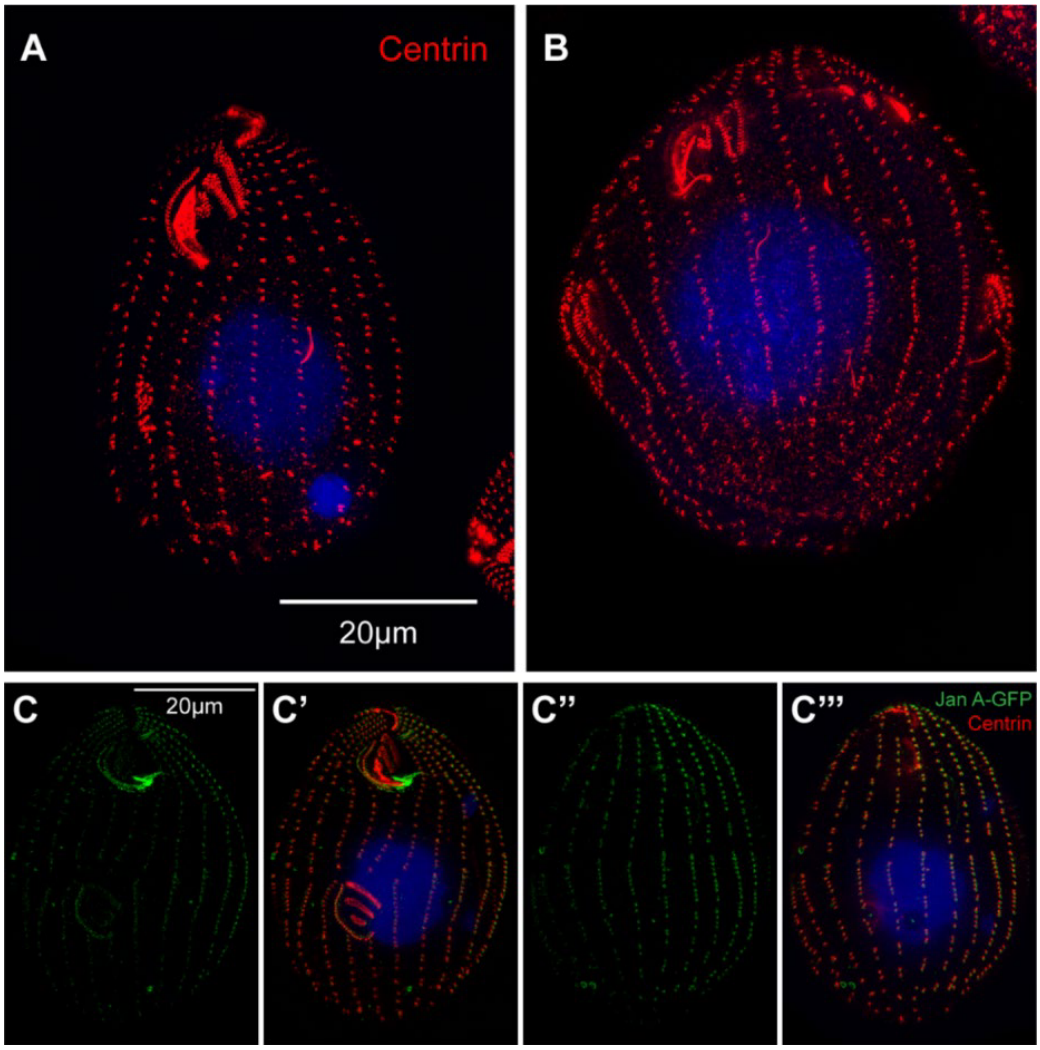

Figure 1.8. Left factor Janus is required for inhibition of extra oral induction along cell circumference. (A,B) SR-SIM images of wild type (also displayed in the Fig. 3.2 of the Chapter3) (A) and *janC-1* strain (B). After incubated at 38°C, the cells were labeled by anti-centrin antibody (red), and DAPI (blue). Note the extra oral apparatus and extra oral primordium in *janC-1* strain. (C-C''') SR-SIM images of two sides (ventral side displayed in the panel C,C' and dorsal side displayed in the panel C'',C''') of the cell expressing JanA-GFP. The cells were labeled by anti-GFP antibody (green), anti-centrin antibody (red), and DAPI (blue). Note the enrichment of JanA-GFP on dorsal/left side (cell's perspective) of the cell and oral apparatus and new oral apparatus exclusively formed on ventral side (C,C') and their absence on dorsal side (C'',C''').

Reference

Adams, A.E., D.I. Johnson, R.M. Longnecker, B.F. Sloat, and J.R. Pringle. 1990. CDC42 and CDC43, two additional genes involved in budding and the establishment of cell polarity in the yeast Saccharomyces cerevisiae. *J Cell Biol*. 111:131-142.

Adams, A.E., and J.R. Pringle. 1984. Relationship of actin and tubulin distribution to bud growth in wild-type and morphogenetic-mutant *Saccharomyces cerevisiae*. *J Cell Biol*. 98:934-945.

Adl, S.M., A.G. Simpson, C.E. Lane, J. Lukes, D. Bass, S.S. Bowser, M.W. Brown, F. Burki, M. Dunthorn, V. Hampl, A. Heiss, M. Hoppenrath, E. Lara, L. Le Gall, D.H. Lynn, H. McManus, E.A. Mitchell, S.E. Mozley-Stanridge, L.W. Parfrey, J. Pawlowski, S. Rueckert, L. Shadwick, C.L. Schoch, A. Smirnov, and F.W. Spiegel. 2012. The revised classification of eukaryotes. *J Eukaryot Microbiol*. 59:429-493.

Adler, P.N. 2012. The frizzled/stan pathway and planar cell polarity in the *Drosophila* wing. *Curr Top Dev Biol*. 101:1-31.

Ali-Murthy, Z., and T.B. Kornberg. 2016. Bicoid gradient formation and function in the *Drosophila* pre-syncytial blastoderm. *Elife*. 5.

Bejsovec, A. 2018. Wingless Signaling: A Genetic Journey from Morphogenesis to Metastasis. *Genetics*. 208:1311-1336.

Berger, C., R. Kannan, S. Myneni, S. Renner, L.S. Shashidhara, and G.M. Technau. 2010. Cell cycle independent role of Cyclin E during neural cell fate specification in *Drosophila* is mediated by its regulation of Prospero function. *Dev Biol*. 337:415-424.

Berger, C., S.K. Pallavi, M. Prasad, L.S. Shashidhara, and G.M. Technau. 2005. A critical role for cyclin E in cell fate determination in the central nervous system of *Drosophila melanogaster*. *Nat Cell Biol*. 7:56-62.

Bhat, K.M., and N. Apsel. 2004. Upregulation of Mitimere and Nubbin acts through cyclin E to confer self-renewing asymmetric division potential to neural precursor cells. *Development*. 131:1123-1134.

Bi, E., and H.O. Park. 2012. Cell polarization and cytokinesis in budding yeast. *Genetics*. 191:347-387.

Brauns, F., L. Inigo de la Cruz, W.K. Daalman, I. de Bruin, J. Halatek, L. Laan, and E. Frey. 2023. Redundancy and the role of protein copy numbers in the cell polarization machinery of budding yeast. *Nat Commun*. 14:6504.

Caviston, J.P., S.E. Tcheperegine, and E. Bi. 2002. Singularity in budding: a role for the evolutionarily conserved small GTPase Cdc42p. *Proc Natl Acad Sci U S A*. 99:12185-12190.

Chiou, J.G., M.K. Balasubramanian, and D.J. Lew. 2017. Cell Polarity in Yeast. *Annu Rev Cell Dev Biol*. 33:77-101.

Cole, E., and J. Gaertig. 2022. Anterior-posterior pattern formation in ciliates. *J Eukaryot Microbiol*:e12890.

Cole, E.S., P.C. Anderson, R.B. Fulton, M.E. Majerus, M.G. Rooney, J.M. Savage, D. Chalker, J. Honts, M.E. Welch, A.L. Wentland, E. Zweifel, and D.J. Beussman. 2008. A proteomics approach to cloning fenestrin from the nuclear exchange junction of *tetrahymena*. *J Eukaryot Microbiol*. 55:245-256.

Cole, E.S., J. Frankel, and L.M. Jenkins. 1987. *bcd*: A mutation affecting the width of organelle domains in the cortex of *Tetrahymena thermophila*. *Rouxs Arch Dev Biol*. 196:421-433.

Cole, E.S., W. Maier, H.V. Huynh, B. Reister, D.O. Sowunmi, U. Chukka, C. Lee, and J. Gaertig. 2024. The Janus A gene encodes a polo-kinase whose loss creates a dorsal/ventral intracellular homeosis in the ciliate, Tetrahymena. *bioRxiv*:2024.2012.2019.629484.

Cole, E.S., W. Maier, E. Joachimiak, Y.Y. Jiang, C. Lee, E. Collet, C. Chmelik, D.P. Romero, D. Chalker, N.K. Alli, T.M. Ruedlin, C. Ozzello, and J. Gaertig. 2023. The *Tetrahymena bcd1* mutant implicates endosome trafficking in ciliate, cortical pattern formation. *Mol Biol Cell*. 34:ar82.

Cowan, C.R., and A.A. Hyman. 2004. Centrosomes direct cell polarity independently of microtubule assembly in *C. elegans* embryos. *Nature*. 431:92-96.

Cowan, C.R., and A.A. Hyman. 2006. Cyclin E-Cdk2 temporally regulates centrosome assembly and establishment of polarity in *Caenorhabditis elegans* embryos. *Nat Cell Biol*. 8:1441-1447.

Davis, J.R., and N. Tapon. 2019. Hippo signalling during development. *Development*. 146.

De Keuckelaere, E., P. Hulpiau, Y. Saeys, G. Berx, and F. van Roy. 2018. Nanos genes and their role in development and beyond. *Cell Mol Life Sci*. 75:1929-1946.

Dearden, P., and M. Akam. 1999. Developmental evolution: Axial patterning in insects. *Curr Biol*. 9:R591-594.

Devenport, D. 2014. The cell biology of planar cell polarity. *J Cell Biol*. 207:171-179.

Driever, W., and C. Nusslein-Volhard. 1988. A gradient of bicoid protein in Drosophila embryos. *Cell*. 54:83-93.

Elde, N.C., G. Morgan, M. Winey, L. Sperling, and A.P. Turkewitz. 2005. Elucidation of clathrin-mediated endocytosis in *tetrahymena* reveals an evolutionarily convergent recruitment of dynamin. *PLoS Genet*. 1:e52.

Evangelista, M., K. Blundell, M.S. Longtine, C.J. Chow, N. Adames, J.R. Pringle, M. Peter, and C. Boone. 1997. Bni1p, a yeast formin linking cdc42p and the actin cytoskeleton during polarized morphogenesis. *Science*. 276:118-122.

Evangelista, M., D. Pruyne, D.C. Amberg, C. Boone, and A. Bretscher. 2002. Formins direct Arp2/3-independent actin filament assembly to polarize cell growth in yeast. *Nat Cell Biol*. 4:260-269.

Ferreira, R.R., and J. Vermot. 2017. The balancing roles of mechanical forces during left-right patterning and asymmetric morphogenesis. *Mech Dev*. 144:71-80.

Frankel, J. 1989. Pattern formation : ciliate studies and models. Oxford University Press, New York. xvii, 314 pages : illustrations pp.

Frankel, J. 2008. What do genic mutations tell us about the structural patterning of a complex single-celled organism? *Eukaryot Cell*. 7:1617-1639.

Frankel, J., L.M. Jenkins, E.M. Nelsen, and C.A. Stoltzman. 1993. Hypoangular: a gene potentially involved in specifying positional information in a ciliate, *Tetrahymena thermophila*. *Dev Biol*. 160:333-354.

Frankel, J., and E.M. Nelsen. 1986. How the mirror-image pattern specified by a janus mutation of Tetrahymena thermophila comes to expression. *Dev Genet*. 6:213-238.

Frankel, J., and E.M. Nelsen. 1987. Positional reorganization in compound *janus* cells of *Tetrahymena thermophila*. *Development*. 99:51-68.

Fryd-Versavel, G., M. Lemullois, and A. Aubusson-Fleury. 2010. Maintaining cell polarity through vegetative cell pattern dedifferentiation: cytoskeleton and morphogenesis in the hypotrich ciliate *Sterkiella histriomuscorum*. *Protist*. 161:222-236.

Gaertig, J., D. Wloga, K.K. Vasudevan, M. Guha, and W. Dentler. 2013. Discovery and functional evaluation of ciliary proteins in *Tetrahymena thermophila*. *Methods Enzymol*. 525:265-284.

Galati, D.F., S. Bonney, Z. Kronenberg, C. Clarissa, M. Yandell, N.C. Elde, M. Jerka-Dziadosz, T.H. Giddings, J. Frankel, and C.G. Pearson. 2014. DisAp-dependent striated fiber elongation is required to organize ciliary arrays. *J Cell Biol*. 207:705-715.

Gan, W.J., and F. Motegi. 2020. Mechanochemical Control of Symmetry Breaking in the Caenorhabditis elegans Zygote. *Front Cell Dev Biol*. 8:619869.

Gao, B., H. Song, K. Bishop, G. Elliot, L. Garrett, M.A. English, P. Andre, J. Robinson, R. Sood, Y. Minami, A.N. Economides, and Y. Yang. 2011. Wnt signaling gradients establish planar cell polarity by inducing Vangl2 phosphorylation through Ror2. *Dev Cell*. 20:163-176.

Genevet, A., C. Polesello, K. Blight, F. Robertson, L.M. Collinson, F. Pichaud, and N. Tapon. 2009. The Hippo pathway regulates apical-domain size independently of its growth-control function. *J Cell Sci*. 122:2360-2370.

Genevet, A., and N. Tapon. 2011. The Hippo pathway and apico-basal cell polarity. *Biochem J*. 436:213-224.

Goldstein, B., and S.N. Hird. 1996. Specification of the anteroposterior axis in *Caenorhabditis elegans*. *Development*. 122:1467-1474.

Goldstein, B., and I.G. Macara. 2007. The PAR proteins: fundamental players in animal cell polarization. *Dev Cell*. 13:609-622.

Gomes, J.E., and B. Bowerman. 2002. Caenorhabditis elegans par genes. *Curr Biol*. 12:R444.

Gotta, M., M.C. Abraham, and J. Ahringer. 2001. CDC-42 controls early cell polarity and spindle orientation in *C. elegans*. *Curr Biol*. 11:482-488.

Greig, S., and M. Akam. 1995. The role of homeotic genes in the specification of the *Drosophila* gonad. *Curr Biol*. 5:1057-1062.

Grimes, G.W. 1973a. Differentiation during encystment and excystment in Oxytricha fallax. *J Protozool*. 20:92-104.

Grimes, G.W. 1973b. Morphological discontinuity of kinetosomes during the life cycle of Oxytricha fallax. *J Cell Biol*. 57:229-232.

Gritzan, U., V. Hatini, and S. DiNardo. 1999. Mutual antagonism between signals secreted by adjacent wingless and engrailed cells leads to specification of complementary regions of the *Drosophila* parasegment. *Development*. 126:4107-4115.

Gros, J., K. Feistel, C. Viebahn, M. Blum, and C.J. Tabin. 2009. Cell movements at Hensen's node establish left/right asymmetric gene expression in the chick. *Science*. 324:941-944.

Hamada, H. 2020. Molecular and cellular basis of left-right asymmetry in vertebrates. *Proc Jpn Acad Ser B Phys Biol Sci*. 96:273-296.

Hardt, M., and H. Plattner. 2000. Sub-second quenched-flow/X-ray microanalysis shows rapid Ca2+ mobilization from cortical stores paralleled by Ca2+ influx during synchronous exocytosis in *Paramecium* cells. *Eur J Cell Biol*. 79:642-652.

Hartwell, L.H. 1971. Genetic control of the cell division cycle in yeast. IV. Genes controlling bud emergence and cytokinesis. *Exp Cell Res*. 69:265-276.

Hayashi, Y., M. Hayashi, and S. Kobayashi. 2004. Nanos suppresses somatic cell fate in *Drosophila* germ line. *Proc Natl Acad Sci U S A*. 101:10338-10342.

Hergovich, A. 2013. Regulation and functions of mammalian LATS/NDR kinases: looking beyond canonical Hippo signalling. *Cell Biosci*. 3:32.

Hill, K.L., N.L. Catlett, and L.S. Weisman. 1996. Actin and myosin function in directed vacuole movement during cell division in *Saccharomyces cerevisiae*. *J Cell Biol*. 135:1535-1549.

Honts, J.E., and N.E. Williams. 2003. Novel cytoskeletal proteins in the cortex of *Tetrahymena*. *J Eukaryot Microbiol*. 50:9-14.

Ingham, P.W., N.E. Baker, and A. Martinez-Arias. 1988. Regulation of segment polarity genes in the Drosophila blastoderm by fushi tarazu and even skipped. *Nature*. 331:73-75.

Jerka-Dziadosz, M. 1981. Cytoskeleton-related structures in *Tetrahymena thermophila*: microfilaments at the apical and division-furrow rings. *Journal of cell science*. 51:241-253.

Jerka-Dziadosz, M., L.M. Jenkins, E.M. Nelsen, N.E. Williams, R. Jaeckel-Williams, and J. Frankel. 1995. Cellular polarity in ciliates: persistence of global polarity in a

disorganized mutant of *Tetrahymena thermophila* that disrupts cytoskeletal organization. *Dev Biol*. 169:644-661.

Jerka-Dziadosz, M., I. Strzyewska-Jowko, U. Wojsa-Lugowska, W. Krawczynska, and A. Krzywicka. 2001. The dynamics of filamentous structures in the apical band, oral crescent, fission line and the postoral meridional filament in *Tetrahymena thermophila* revealed by monoclonal antibody 12G9. *Protist*. 152:53-67.

Jiang, Y.-Y., S. Kumar, and A.P. Turkewitz. 2024. The secretory pathway in *Tetrahymena* is organized for efficient constitutive secretion at ciliary pockets. *iScience*. 27.

Jiang, Y.Y., W. Maier, R. Baumeister, E. Joachimiak, Z. Ruan, N. Kannan, D. Clarke, P. Louka, M. Guha, J. Frankel, and J. Gaertig. 2019. Two Antagonistic Hippo Signaling Circuits Set the Division Plane at the Medial Position in the Ciliate *Tetrahymena*. *Genetics*. 211:651-663.

Jiang, Y.Y., W. Maier, R. Baumeister, G. Minevich, E. Joachimiak, Z. Ruan, N. Kannan, D. Clarke, J. Frankel, and J. Gaertig. 2017. The Hippo Pathway Maintains the Equatorial Division Plane in the Ciliate *Tetrahymena*. *Genetics*. 206:873-888.

Jiang, Y.Y., W. Maier, U.N. Chukka, M. Choromanski, C. Lee, E. Joachimiak, D. Wloga, W. Yeung, N. Kannan, J. Frankel, and J. Gaertig. 2020. Mutual antagonism between Hippo signaling and cyclin E drives intracellular pattern formation. *J Cell Biol*. 219.

Johnson, D.I., and J.R. Pringle. 1990. Molecular characterization of CDC42, a *Saccharomyces cerevisiae* gene involved in the development of cell polarity. *J Cell Biol*. 111:143-152.

Jordan, S.N., T. Davies, Y. Zhuravlev, J. Dumont, M. Shirasu-Hiza, and J.C. Canman. 2016. Cortical PAR polarity proteins promote robust cytokinesis during asymmetric cell division. *J Cell Biol*. 212:39-49.

Kapoor, S., and S. Kotak. 2019. Centrosome Aurora A regulates RhoGEF ECT-2 localisation and ensures a single PAR-2 polarity axis in *C. elegans* embryos. *Development*. 146.

Kay, A.J., and C.P. Hunter. 2001. CDC-42 regulates PAR protein localization and function to control cellular and embryonic polarity in C. elegans. *Curr Biol*. 11:474-481.

Kirk, K.E., C. Christ, J.M. McGuire, A.G. Paul, M. Vahedi, K.R. Stuart, and E.S. Cole. 2008. Abnormal micronuclear telomeres lead to an unusual cell cycle checkpoint and defects in *Tetrahymena* oral morphogenesis. *Eukaryot Cell*. 7:1712-1723.

Klinkert, K., N. Levernier, P. Gross, C. Gentili, L. von Tobel, M. Pierron, C. Busso, S. Herrman, S.W. Grill, K. Kruse, and P. Gonczy. 2019. Aurora A depletion reveals centrosome-independent polarization mechanism in *Caenorhabditis elegans*. *Elife*. 8.

Kobayashi, S., M. Yamada, M. Asaoka, and T. Kitamura. 1996. Essential role of the posterior morphogen nanos for germline development in *Drosophila*. *Nature*. 380:708-711.

Kozubowski, L., K. Saito, J.M. Johnson, A.S. Howell, T.R. Zyla, and D.J. Lew. 2008. Symmetry-breaking polarization driven by a Cdc42p GEF-PAK complex. *Curr Biol*. 18:1719-1726.

Kraut, R., and M. Levine. 1991. Mutually repressive interactions between the gap genes giant and Krüppel define middle body regions of the *Drosophila* embryo. *Development*. 111:611-621.

Lang, C.F., and E. Munro. 2017. The PAR proteins: from molecular circuits to dynamic self-stabilizing cell polarity. *Development*. 144:3405-3416.

Lange, S., N. Klauke, and H. Plattner. 1995. Subplasmalemmal Ca2+ stores of probable relevance for exocytosis in *Paramecium*. Alveolar sacs share some but not all characteristics with sarcoplasmic reticulum. *Cell Calcium*. 17:335-344.

Lee, C., W. Maier, Y.Y. Jiang, K. Nakano, K.F. Lechtreck, and J. Gaertig. 2024. Global and local functions of the Fused kinase ortholog CdaH in intracellular patterning in *Tetrahymena*. *J Cell Sci*. 137.

Lee, H., J. Kang, S. Ahn, and J. Lee. 2019. The Hippo Pathway Is Essential for Maintenance of Apicobasal Polarity in the Growing Intestine of *Caenorhabditis elegans*. *Genetics*. 213:501-515.

Lepesant, J.A. 1990. [Homeotic genes]. *Reprod Nutr Dev*. Suppl 1:9s-26s.

Manzi, N.I., B.N. de Jesus, Y. Shi, and D.J. Dickinson. 2024. Temporally distinct roles of Aurora A in polarization of the *C. elegans* zygote. *Development*. 151.

Martin, S.G., and R.A. Arkowitz. 2014. Cell polarization in budding and fission yeasts. *FEMS Microbiol Rev*. 38:228-253.

McCoy, J. 1974. New features of the tetrahymenid cortex revealed by protargol staining. *Acta Protozoologica*. 13.

Meitinger, F., and S. Palani. 2016. Actomyosin ring driven cytokinesis in budding yeast. *Semin Cell Dev Biol*. 53:19-27.

Mendes, R.V., G.G. Martins, A.M. Cristovao, and L. Saude. 2014. N-cadherin locks left-right asymmetry by ending the leftward movement of Hensen's node cells. *Dev Cell*. 30:353-360.

Michgehl, U., H. Pavenstadt, and B. Vollenbroker. 2017. Cross talk between the Crumbs complex and Hippo signaling in renal epithelial cells. *Pflugers Arch*. 469:917-926.

Miller, P.J., and D.I. Johnson. 1997. Characterization of the *Saccharomyces cerevisiae cdc42*-1ts allele and new temperature-conditional-lethal *cdc42* alleles. *Yeast*. 13:561-572.

Morata, G. 1993. Homeotic genes of *Drosophila*. *Curr Opin Genet Dev*. 3:606-614.

Morton, D.G., D.C. Shakes, S. Nugent, D. Dichoso, W. Wang, A. Golden, and K.J. Kemphues. 2002. The *Caenorhabditis elegans par-5* gene encodes a 14-3-3 protein required for cellular asymmetry in the early embryo. *Dev Biol*. 241:47-58.

Nanney, D.L., D. Nyberg, S.S. Chen, and E.B. Meyer. 1980. Cytogeometric Constraints in *Tetrahymena* Evolution - Contractile Vacuole Pore Positions in 19 Species of the *Tetrahymena-Pyriformis* Complex. *Am Nat*. 115:705-717.

Novick, P., and D. Botstein. 1985. Phenotypic analysis of temperature-sensitive yeast actin mutants. *Cell*. 40:405-416.

Nusslein-Volhard, C., and E. Wieschaus. 1980. Mutations affecting segment number and polarity in *Drosophila*. *Nature*. 287:795-801.

Pacquelet, A. 2017. Asymmetric Cell Division in the One-Cell *C. elegans* Embryo: Multiple Steps to Generate Cell Size Asymmetry. *Results Probl Cell Differ*. 61:115-140.

Paulin, J.J., and J. Bussey. 1971. Oral regeneration in the ciliate *Stentor coeruleus*: a scanning and transmission electron optical study. *J Protozool*. 18:201-213.

Pelvat, B., and G. Dehaller. 1979. La Regeneration de L'appareil Oral chez *Stentor coeruleus*: Etude au Protargol et Essai de Morphogenese Comparee. *Protistologica*. 15:369-386.

Plattner, H., and N. Klauke. 2001. Calcium in ciliated protozoa: Sources, regulation, and calcium-regulated cell functions. *Int Rev Cytol*. 201:115-208.

Plattner, H., I.M. Sehring, I.K. Mohamed, K. Miranda, W. De Souza, R. Billington, A. Genazzani, and E.M. Ladenburger. 2012. Calcium signaling in closely related protozoan groups (Alveolata): non-parasitic ciliates (*Paramecium*, *Tetrahymena*) vs. parasitic Apicomplexa (*Plasmodium*, *Toxoplasma*). *Cell Calcium*. 51:351-382.

Reich, J.D., L. Hubatsch, R. Illukkumbura, F. Peglion, T. Bland, N. Hirani, and N.W. Goehring. 2019. Regulated Activation of the PAR Polarity Network Ensures a Timely and Specific Response to Spatial Cues. *Curr Biol*. 29:1911-1923 e1915.

Rock, J.M., D. Lim, L. Stach, R.W. Ogrodowicz, J.M. Keck, M.H. Jones, C.C. Wong, J.R. Yates, 3rd, M. Winey, S.J. Smerdon, M.B. Yaffe, and A. Amon. 2013. Activation of the yeast Hippo pathway by phosphorylation-dependent assembly of signaling complexes. *Science*. 340:871-875.

Rose, L., and P. Gonczy. 2014. Polarity establishment, asymmetric division and segregation of fate determinants in early *C. elegans* embryos. *WormBook*:1-43.

Rosenberg, U.B., C. Schröder, A. Preiss, A. Kienlin, S. Côté, I. Riede, and H. Jäckle. 1986. Structural homology of the product of the *Drosophila* Krüppel gene with Xenopus transcription factor IIIA. *Nature*. 319:336-339.

Sadian, Y., C. Gatsogiannis, C. Patasi, O. Hofnagel, R.S. Goody, M. Farkasovsky, and S. Raunser. 2013. The role of Cdc42 and Gic1 in the regulation of septin filament formation and dissociation. *Elife*. 2:e01085.

Sagot, I., S.K. Klee, and D. Pellman. 2002. Yeast formins regulate cell polarity by controlling the assembly of actin cables. *Nat Cell Biol*. 4:42-50.

Schubert, C.M., R. Lin, C.J. de Vries, R.H. Plasterk, and J.R. Priess. 2000. MEX-5 and MEX-6 function to establish soma/germline asymmetry in early C. elegans embryos. *Mol Cell*. 5:671-682.

Schulz, C., and D. Tautz. 1995. Zygotic caudal regulation by hunchback and its role in abdominal segment formation of the Drosophila embryo. *Development*. 121:1023-1028.

Se´galen, M., C.A. Johnston, C.A. Martin, J.G. Dumortier, K.E. Prehoda, N.B. David, C.Q. Doe, and Y. Bellaiche. 2010. The Fz-Dsh planar cell polarity pathway induces oriented cell division via Mud/NuMA in *Drosophila* and zebrafish. *Dev Cell*. 19:740-752.

Simon, V.R., S.L. Karmon, and L.A. Pon. 1997. Mitochondrial inheritance: cell cycle and actin cable dependence of polarized mitochondrial movements in *Saccharomyces cerevisiae*. *Cell Motil Cytoskeleton*. 37:199-210.

Singh, J., and M. Mlodzik. 2012. Planar cell polarity signaling: coordination of cellular orientation across tissues. *Wiley Interdiscip Rev Dev Biol*. 1:479-499.

Slabodnick, M.M., J.G. Ruby, J.G. Dunn, J.L. Feldman, J.L. DeRisi, and W.F. Marshall. 2014. The kinase regulator mob1 acts as a patterning protein for *stentor* morphogenesis. *PLoS Biol*. 12:e1001861.

Snustad, D.P., and M.J. Simmons. 2009. Principles of genetics. John Wiley & Sons, Hoboken, NJ. xix, 823 p. pp.

Stelly, N., S. Halpern, G. Nicolas, P. Fragu, and A. Adoutte. 1995. Direct visualization of a vast cortical calcium compartment in *Paramecium* by secondary ion mass spectrometry (SIMS) microscopy: possible involvement in exocytosis. *J Cell Sci*. 108 (Pt 5):1895-1909.

Stelly, N., J.P. Mauger, M. Claret, and A. Adoutte. 1991. Cortical alveoli of *Paramecium*: a vast submembranous calcium storage compartment. *J Cell Biol*. 113:103-112.

Sulston, J.E., E. Schierenberg, J.G. White, and J.N. Thomson. 1983. The embryonic cell lineage of the nematode *Caenorhabditis elegans*. *Dev Biol*. 100:64-119.

Sung, Y.H., I.J. Baek, Y.H. Kim, Y.S. Gho, S.P. Oh, Y.J. Lee, and H.W. Lee. 2016. PIERCE1 is critical for specification of left-right asymmetry in mice. *Sci Rep*. 6:27932.

Takizawa, P.A., A. Sil, J.R. Swedlow, I. Herskowitz, and R.D. Vale. 1997. Actin-dependent localization of an RNA encoding a cell-fate determinant in yeast. *Nature*. 389:90-93.

Tartar, V. 1956a. Further experiments correlating primordium sites with cytoplasmic pattern in *stentor coeruleus*. *Journal of Experimental Zoology*. 132:269-297.

Tartar, V. 1956b. Grafting Experiments Concerning Primordium Formation in *Stentor Coeruleus*. *Journal of Experimental Zoology*. 131:75-121.

Tartar, V. 1956c. IV. PATTERN AND SUBSTANCE IN *STENTOR*. *In* Cellular Mechanics in Differentiation and Growth. Princeton University Press, Princeton. 73-100.

Tartar, V. 1961. The biology of *Stentor*. Pergammon Press, Oxford, New York,. x, 413 p. pp.

Tartar, V. 1968. Micrurgical experiments on cytokinesis in *Stentor coeruleus*. *J Exp Zool*. 167:21-36.

Tavares, A., J. Goncalves, C. Florindo, A.A. Tavares, and H. Soares. 2012. Mob1: defining cell polarity for proper cell division. *J Cell Sci*. 125:516-527.

Tong, Z., X.D. Gao, A.S. Howell, I. Bose, D.J. Lew, and E. Bi. 2007. Adjacent positioning of cellular structures enabled by a Cdc42 GTPase-activating protein-mediated zone of inhibition. *J Cell Biol*. 179:1375-1384.

Trammell, M.A., N.M. Mahoney, D.A. Agard, and R.D. Vale. 2008. Mob4 plays a role in spindle focusing in Drosophila S2 cells. *J Cell Sci*. 121:1284-1292.

Uhlig, G. 1960. Entwicklungsphysiologische Untersuchungen zur Morphogenese von *Stentor coeruleus* Ehrbg. *Arch. Protistenk.* 105:1-109.

Varelas, X. 2014. The Hippo pathway effectors TAZ and YAP in development, homeostasis and disease. *Development*. 141:1614-1626.

Wang, C., L.K. Dickinson, and R. Lehmann. 1994. Genetics of nanos localization in *Drosophila*. *Dev Dyn*. 199:103-115.

Wang, Y., J. Yan, H. Lee, Q. Lu, and P.N. Adler. 2014. The proteins encoded by the *Drosophila* Planar Polarity Effector genes inturned, fuzzy and fritz interact physically and can re-pattern the accumulation of "upstream" Planar Cell Polarity proteins. *Dev Biol*. 394:156-169.

Williams, N.E. 2004. The epiplasm gene EPC1 influences cell shape and cortical pattern in Tetrahymena thermophila. *J Eukaryot Microbiol*. 51:201-206.

Witte, K., D. Strickland, and M. Glotzer. 2017. Cell cycle entry triggers a switch between two modes of Cdc42 activation during yeast polarization. *Elife*. 6.

Wu, C.F., J.G. Chiou, M. Minakova, B. Woods, D. Tsygankov, T.R. Zyla, N.S. Savage, T.C. Elston, and D.J. Lew. 2015. Role of competition between polarity sites in establishing a unique front. *Elife*. 4.

Wu, Z., and K.L. Guan. 2021. Hippo Signaling in Embryogenesis and Development. *Trends Biochem Sci*. 46:51-63.

Yang, H.C., and L.A. Pon. 2002. Actin cable dynamics in budding yeast. *Proc Natl Acad Sci U S A*. 99:751-756.

Ye, X., N. Nikolaidis, M. Nei, and Z.-C. Lai. 2009. Evolution of the mob Gene Family. *The Open Cell Signaling Journal*. 1.

Yu, F., C.T. Kuo, and Y.N. Jan. 2006. Drosophila neuroblast asymmetric cell division: recent advances and implications for stem cell biology. *Neuron*. 51:13-20.

CHAPTER 2

Global and local functions of the Fused kinase ortholog CdaH in intracellular patterning in *Tetrahymena*

Lee, C., Maier, W., Jiang, Y. Y., Nakano, K., Lechtreck, K. F., & Gaertig, J. (2024). Global and local functions of the Fused kinase ortholog CdaH in intracellular patterning in *Tetrahymena*. Journal of cell science,137(5), jcs261256. https://doi.org/10.1242/jcs.261256

ABSTRACT

Ciliates assemble numerous microtubular structures into complex cortical patterns. During ciliate division, the pattern is duplicated by intracellular segmentation that produces a tandem of daughter cells. In *Tetrahymena thermophila*, the induction and positioning of the division boundary involves two mutually antagonistic factors: posterior CdaA (cyclin E) and anterior CdaI (Hippo kinase). Here, we characterized the related *cdaH-1* allele, which confers a pleiotropic patterning phenotype including an absence of the division boundary and an anterior–posterior mispositioning of the new oral apparatus. CdaH is a Fused or Stk36 kinase ortholog that localizes to multiple sites that correlate with the effects of its loss, including the division boundary and the new oral apparatus. CdaH acts downstream of CdaA to induce the division boundary and drives asymmetric cytokinesis at the tip of the posterior daughter. CdaH both maintains the anterior–posterior position of the new oral apparatus and interacts with CdaI to pattern oral rows within the oral apparatus. Thus, CdaH acts at multiple scales, from induction and positioning of structures on the cell-wide polarity axis to local organelle-level patterning.

Keywords: Cell cortex, Ciliate, Patterning, Polarity

Summary: CdaH, a conserved Fused kinase, acts at multiple stages and scales to generate a pattern of cortical organelles during cell division in the ciliate *Tetrahymena thermophila.*

INTRODUCTION

Ciliates have two permanent cell polarity axes: anterior–posterior and circumferential (left–right) (Fig. 2.1). In *Tetrahymena thermophila*, the oral apparatus (OA) is located near the anterior cell end, whereas the osmoregulatory contractile vacuole pores and the cytoproct (where spent food vacuoles are egested) are located near the posterior cell end, but at

different circumferential positions. As proposed by V. Tartar based on his famous microsurgical studies of *Stentor coeruleus*, ciliates divide by a process that amounts to a developmental segmentation of a single cell (Tartar, 1968). The extensive cortical remodeling that takes place throughout the midbody of the dividing ciliate is remarkably precise and, consequently, in the population, the cortical pattern is nearly invariant, which has enabled isolation of unique intracellular patterning mutants (reviewed in Frankel, 1989,2008). Recently, reverse and forward genetic approaches (Galati et al., 2014) have enabled identification of a number of gene products that contribute to patterning in ciliates (reviewed in Cole and Gaertig, 2022). On the anterior–posterior axis, several highly conserved kinases and kinase regulators control the positions of forming cortical structures, including Elo1 (Lats kinase) (Jiang et al., 2019a), CdaI (Hippo kinase) (Jiang et al., 2017), Mob1 (Slabodnick et al., 2014; Tavares et al., 2012) and CdaA (cyclin E) (Jiang et al., 2020). These proteins appear to form a signaling 'prepattern' that acts by localized inhibition: forming structures are excluded from the cortical areas where these prepatterning factors are enriched.

The generation of the division boundary (DB) at the equator of the ciliate parental cell is a key step that precedes cytokinesis and morphogenesis of new cell ends. In *T. thermophila*, loss-of-function mutations of either the posteriorly enriched CdaA or the anteriorly enriched CdaI cause either a failure or a shift in the position of the DB. CdaA and CdaI engage in a mutual antagonism that induces and positions the DB (Jiang et al., 2017,2020). Here, we investigate a closely related conditional allele, *cdaH-1*, the molecular identity of which has remained unknown since its original description over 40 years ago (Frankel et al., 1980). *cdaH-1* confers a pleiotropic patterning phenotype that includes an absence of the DB and an anterior displacement and partial resorption of the new OA (Frankel, 2008;Frankel et al., 1980). We show that *CDAH* encodes an ortholog of the highly conserved *Drosophila* Fused

(Cole et al.) and human Stk36 kinases. Our observations suggest that CdaH contributes to both global (cell-wide) and local (organelle-level) intracellular patterning.

MATERIALS AND METHODS

Tetrahymena strains

All strains were obtained from the *Tetrahymena* Stock Center (Cornell University, Ithaka, NY, USA). CU428 (TSC_SD00178) was used as the wild type. IA450 (TSC_SD01593) is homozygous for *cdaH-1*, IA104 (TSC_SD01447) is homozygous for *cdaA-1*, and IA237 (TSC_SD01449) is homozygous for *cdaI-1* (Frankel, 2008; Jiang et al., 2017). Double-mutant homozygotes were generated by crosses to create double heterozygotes, and self-crosses using B*VII (TSC_SD00023) to generate micronuclear homozygotes. The micronuclear genotypes of the self-cross progeny were determined using outcrosses to single-mutant homozygotes. Pairs of strains with the desired micronuclear genotypes were crossed to each other to obtain double-mutant homozygote progeny. The genotypes of final double homozygotes were verified by PCR amplification and Sanger DNA sequencing across the base positions of mutant alleles. Strains were cultured in SPP medium (1% proteose–peptone, 0.2% dextrose, 0.1% yeast extract and 0.003% EDTA:ferric sodium salt) supplemented with antibiotics (SPPA medium) (Gaertig et al., 2013;Gorovsky, 1973).

Mapping of *cdaH-1* by comparative next-generation sequencing

We applied the ACCA workflow (Jiang et al., 2017) to map the causal mutation for *cdaH-1*. IA450 was crossed to CU427 [strain homozygous forchx1-1a cycloheximide (cy)-resistant allele in the micronucleus, TSC_SD00715], and the resulting F1s presumed to be double heterozygotes (*cdaH-1/CDAH*; *chx1-1/CHX1*) were allowed to undergo phenotypical assortment to cy sensitivity by multiplication for ~60 generations in a non-selective medium. Subsequently we crossed several F1s in multiple combinations and selected F2 progeny using cy resistance (15 μg/ml). We picked 38 and 31 F2s with a *cdaH-1*and wild-type

phenotype, respectively, and pooled them according to the phenotype. The mutant and wild-type F2 pools were cultured to a mid-log phase in 25 ml of SPPA medium at room temperature, starved for 2 days also at room temperature in 60 mM Tris-HCl, pH 7.5, and total genomic DNA was extracted from each pool using the urea method (Gaertig et al., 1994). Genomic libraries were constructed with the Illumina Truseq primer adapters and sequenced on an Illumina HiSeq X, which generated paired-end reads of 150 bp length at ~90× genome coverage. The sequence reads were deposited at the Sequence Read Archive (SRA) database (Bioproject accession numberPRJNA999728). The Mutation Identification in Model Organism Genomes using Desktop PCs (MiModD) suite of bioinformatics tools (version 0.1.8;https://sourceforge.net/projects/mimodd/) was used on the Galaxy Europe bioinformatics server (https://usegalaxy.eu) to execute the ACCA variant mapping workflow as follows. The sequencing reads of the *cdaH-1* and wild-type F2 pools were aligned to the macronuclear reference genome of the wild-type strain SB210 (GenBank assembly accession GCA_000189635) (Eisen et al., 2006) and a multi-sample variant calling was conducted. Variants were annotated with predicted effect on gene products, and linkage scores were calculated on the basis of contrast between the allelic composition of the wild-type and the mutant pool. The linkage scores were plotted against the micronuclear genome assembly (GenBank assembly accession GCA_000261185.1) (Hamilton et al., 2016) coordinates along the five micronuclear chromosomes. This analysis displayed a peak in the ACCA signal at a location of ~0.05 Mb of chromosome 5, and nearby variants with a predicted effect on a gene product were considered candidate causative variants.

Phylogenetic and structural analyses

The predicted gene model for *CDAH/TTHERM_01345780* was corrected based on the mRNA sequence data available at the *Tetrahymena* Functional Genomics Database (http://tfgd.ihb.ac.cn), which revealed an additional intron near the end of the coding region. A phylogenetic analysis was performed using 497 sequences of human kinase domains

(Modi and Dunbrack, 2019b) and the corresponding amino acid sequences of CdaH/TTHERM_01345780, TTHERM_00756520 and TTHERM_00726480. The following analyses were performed at the NGPhylogeny.fr server (Lemoine et al., 2019;https://ngphylogeny.fr/). A multiple sequence alignment was produced using the Multiple Alignment using Fast Fourier Transform (MAFFT) program (Katoh and Standley, 2013) and curated using trimAl (Capella-Gutiérrez et al., 2009). A neighbor-joining phylogeny was constructed using FastME and the statistical support of branches was tested by bootstrap resampling with 1000 replicates (Lefort et al., 2015). The tree was visualized with iTOL (https://itol.embl.de). A multiple sequence alignment of the entire amino acid sequences of CdaH and other Fused/Stk36 kinases was obtained with Clustal Omega at the European Molecular Biology Laboratory (EMBL)-European Bioinformatics Institute (EBI) (Sievers et al., 2011) and visualized with mView (Brown et al., 1998). Protein domains were detected using the SMART (http://smart.embl-heidelberg.de/) tool and homologs in other species were identified using the Blastp tool at the Cildb database (http://cildb.i2bc.paris-saclay.fr/).

Genome editing in the macronucleus

To rescue the *cdaH-1* phenotype, starved IA450 cells were subjected to biolistic bombardment with a ~1.5-kb fragment of *TTHERM_01345780* amplified from the wild-type genomic DNA (strain CU428) using the primers 5′-GCATTTCTCTAAAATTATTTTTGTATCC-3 and 5′-GTTCTGCAATTCCATTATCATC-3′. The bombarded ($\sim 5\times10^6$) and mock-transformed cells were cultured in SPPA medium at 25°C for 1 day, replicated onto fresh 96-well plates and incubated at 38°C. We searched for wells containing cells that regained the ability to multiply. To further confirm the location of the *cdaH-1* causal mutation, we constructed plasmids carrying a portion of the 5′ UTR ofTTHERM_01345780, followed byneo5,the MTT1 promoter and a portion of the coding sequence of *TTHERM_01345780* that terminated either 63 bp upstream or 568 bp downstream of the suspected *cdaH-1* causal variant site. To

construct the above plasmids, the 5′ UTR region was amplified with the primers 5′-GAATTGGAGCTCAATCTATAAAATCTTGATTTCTCTTT-3′ and 5′-TGCCATCCGCGGTCTAACAATCTAACATTAAAACA-3′and cloned between the SacI and SacII sites of pLF4gOEneo2-4 (Jiang et al., 2019b). The coding region of *TTHERM_01345780* was amplified with the forward primer 5′-ACTTAAAATAATGGCCAAGTCGACGATGGAGAATTATCATATTCTT-3′ and either 5′-AGGGAACAAAAGCTGGGTACCAAAATGTTTGTATTGTTT-3′ (long coding fragment) or 5′-AGGGAACAAAAGCTGGGTACCCAAAACCGAAATCGCATAATTTTACAA-3′ (short coding fragment), and cloned using the KpnI and SalI sites. The targeting fragments of the resulting plasmids (pMTT1_CDAHov_long and pMTT1_CDAHov_short) were separated from their plasmid backbones using KpnI and SacI and introduced into the *cdaH-1* mutants (IA450) by biolistic bombardment. Transformants were selected with 100 µg/ml paromomycin at room temperature. Wells containing transformants were replicated onto fresh SPPA medium with 400 µg/ml paromomycin, incubated overnight at 38°C and scored for cell multiplication.

To express CdaH–GFP, we added a DNA sequence encoding GFP, a 3′ UTR region of BTU1 and a neo5 selectable marker to the 3′ end of *TTHERM_01345780/CDAH* by homologous DNA recombination. The flanking DNA sequences for targeting *CDAH* were amplified using the following primer pairs: forward, 5′-GGGCGAATTGGCCGGCATTATTTCATTCAAAGTTTGTTATTTC-3′, and reverse, 5′-ATCAAGCTTGCCATCCGCGGTTATTGCATGTCCTAATC-3′; forward, 5′-GCTTATCGATACCGTCGACCACAAATTAATTTAAGAATTATGA-3′, and reverse: 5′-AGGGAACAAAAGCTGGGTACGATTATGTCGATTAAACTGAA-3′. The two fragments were subcloned into the plasmid pNeo2_4-GFP (Jiang et al., 2019b). The *CDAH* gene was tagged in the wild-type (CU428), *cdaA-1* (IA104) and *cdaI-1* (IA237) backgrounds. Transformants were selected with 100 µg/ml paromomycin. The copy number of the engineered allele was increased by the phenotypical assortment with increasing concentration of paromomycin. The targeting plasmids for GFP tagging of CDAI and CDAA in the *cdaH-1* background were

described previously (Jiang et al., 2017, 2020).

Microscopic imaging

T. thermophila cells were fixed and immunostained using the quick method that includes simultaneous fixation and/or permeabilization and drying of cells on the cover glass (Gaertig et al., 2013) with small modifications. After placing on the cover glass, 20 µl of cell culture was mixed with an equal volume of 0.25% Triton X-100 and 1% paraformaldehyde in PHEM buffer (60 mM PIPES, 25 mM HEPES, 10 mM EGTA and 2 mM MgSO4, pH 6.9). The cover glass was air dried, washed three times with PBS and incubated with primary antibodies in PBS supplemented with 3% BSA fraction V and 0.01% Tween-20. The primary antibodies were: polyclonal rabbit anti-GFP (Rockland Immunochemicals, 600-401-215; 1:800), monoclonal mouse anti-centrin 20H5 (EMD Millipore, 41624; ~1:200–1:400), and anti-polyglycine polyclonal serum 2302 (Shang et al., 2002) (1:200). The secondary antibodies were conjugated to either Cy3 or FITC (Jackson ImmunoResearch, 115-095-146 and 111-165-003; 1:100–1:300). The nuclei were stained with DAPI (Sigma-Aldrich). The stained cells were embedded in 90% glycerol, 10% PBS supplemented with 100 mg/ml DABCO (Sigma-Aldrich). Confocal images were collected on a Zeiss LSM 710 microscope with a Plan-Apochromat 63×/1.40 oil DIC M27 objective. SR-SIM imaging was conducted on an ELYRA S1 microscope equipped with a 63× NA 1.4 Oil Plan-Apochromat DIC objective. The optical slices were processed using Fiji/ImageJ (z-project tool). To image actin and CdaH–GFP, the CdaH–GFP-expressing cells were fixed with cold methanol (−80°C) for 30 min, washed three times with 1 ml of PBS, followed by a wash with 1 ml of PBS containing 1% BSA (PBSB) for 30 min. The primary and the secondary antibodies used were the anti-*Tetrahymena* Act1 actin rabbit serum (Shiozaki et al., 2013; 1:200 dilution in PBSB) and the goat anti-rabbit IgG H/L antibodies coupled to Alexa Fluor 594 (Thermo Fisher Scientific, R37117; 1:200), respectively. The cells were observed using an Olympus BX51 fluorescence microscope equipped with a 100× lens (NA 1.40) and the images were collected on a

Hamamatsu Photonics ORCA-3CCD camera. For SR-SIM co-imaging of CdaH–GFP and actin, cells were fixed and dried on coverslips as described above, the coverslips washed three times for 5 min in PBS, treated with 1% SDS in PBS for 20 min, and washed three times for 5 min in PBS. The primary antibodies used were anti-Act1 guinea pig serum (Shiozaki et al., 2013; 1:80) and anti-GFP (Rockland Immunochemicals, 600-401-215; 1:800), and the secondary antibodies used were goat-anti-guinea pig IgG-FITC (Sigma-Aldrich, F6261; 1:100) and goat-anti-rabbit IgG-Cy3 (Jackson ImmunoResearch, 111-165-003; 1:200). The anti-actin antibodies were validated based on detection of a single band with the size expected for actin on western blots using total extracts ofT. thermophila.The TIRF microscope set-up has been previously described (Lechtreck, 2016). TIRF imaging was done as previously described (Jiang et al., 2015) except that cells were immobilized by entrapment in a small volume and without NiCl2. To perform FRAP, a 488 nm laser beam was split using a zero-order half-wave plate and a broad band polarized beam splitter. One of the beams was used for TIRF illumination and the other beam was send to the specimen for photobleaching. The bleaching beam was expanded using a 3× beam expander, focused using a 200 mm plano-convex lens and a 35 mm plano-convex lens and recombined with the TIRF beam using a polarized beam splitter (all parts from Thorlabs Inc.). A motorized mirror connected to a joystick (Newfocus) was used to move the bleaching laser to the desired location and the size of the laser spot was controlled manually by moving the 35 mm lens. Samples were prepared for electron microscopy as previously described (Vasudevan et al., 2015).

Statistical analysis

The sample sizes were chosen based on the previous research. To quantify the phenotypic defects, 10–50 dividing cells were scored per genotype. Differences were evaluated by GraphPad PRISM software. An unpaired two-tailed t-test was used and $P<0.05$ was considered to be statistically significant.

RESULTS

The pleiotropic phenotype of *cdaH-1*

In *Tetrahymena*, the anterior–posterior cell polarity is reflected by the different curvatures of cell extremities and asymmetrically placed structures: the anterior OA and the posterior contractile vacuole pores and cytoproct (Fig. 2.1, stage 1). The main elements of the cortical pattern are the basal bodies (BBs), most of which are ciliated. The majority of BBs are aligned in ~20 longitudinal rows, whereas a subset of BBs forms four short oral rows. Cell division is initiated with assembly of the new OA (oral primordium, OP) at the subequatorial position on the ventral side (Fig. 2.1, stage 2). The OP starts as a group of randomly oriented BBs that gradually align into four oral rows: three diagonally oriented membranelles (M1, M2and M3) and the undulating membrane (UM) (Fig. 2.1, stages 2 and 3) (Bakowska et al., 1982a). Subsequently, the DB forms at the cell equator and anteriorly to the OP (Fig. 2.1, stage 4). The DB starts as an array of gaps in all ciliary rows that circumvent the cell (the stage of 'cortical subdivision') (Frankel et al., 1981). The sculpturing of new cell ends occurs concurrently with cytokinesis and, eventually, two complete daughters emerge and split apart (Fig. 2.1, stage 5). The micronucleus divides (by mitosis) at the time of cortical subdivision, whereas the macronucleus divides (by amitosis) concurrently with cytokinesis (Jerka-Dziadosz et al., 2001; Kirk et al., 2008). The overall cortical pattern can be assessed using the 20H5 anti-centrin monoclonal antibody (Salisbury et al., 1988), which marks the BBs. At 22°C, most of the *cdaH-1* homozygotes divided normally (Fig. 2.2A–E). At 39°C, the *cdaH-1* cells assembled an OP (Fig. 2.2F,G), but most mutants failed to develop the cortical subdivision (Fig. 2.2H,I, compare to Fig. 2.2C,D). The OP displaced anteriorly to land in the vicinity of the old OA ('op' in Fig. 2.2I, also Fig. 2.2O). In the displaced OP, the oral rows were partially degraded and mispositioned ('op' in Fig. 2.2I). The micronucleus divided but the macronuclear amitosis failed ('ma' in Fig. 2.2I, compare to Fig. 2.2D). The cell division-blocked *cdaH-1* cells entered the next cell cycle and developed a second-generation OP

('op2' in Fig. 2.2J, also Fig. 2.2P). In a minority of mutants, the cortical subdivision formed and the macronucleus divided, but there was a subsequent arrest in cytokinesis, followed by translocation of the entire cortices of hemi-cells that produced variable cell morphologies (Fig. 2.2L–N, compare to Fig. 2.2K,Q), as already reported for other mutants blocked in cytokinesis (Brown et al., 1999; Williams et al., 2006).

CdaH is a Fused/Stk36 kinase ortholog

cdaH-1 is a recessive allele on the micronuclear chromosome 5 (Frankel, 2008; Frankel et al., 1980). To map *cdaH-1* by next generation sequencing, we outcrossed *cdaH-1* homozygotes (strain IA450) and the resulting F1 heterozygotes were crossed to each other to obtain F2 progeny. We pooled a number of phenotypically mutant and wild-type F2s, sequenced the pooled genomes and used the allelic composition contrast analysis (ACCA) bioinformatics workflow (Jiang et al., 2017) to search for genomic variants that cosegregated with the mutant phenotype. A strong 'variant-to-phenotype' linkage signal was detected near the end of the left arm of chromosome 5 at ~0.05 Mb (Fig. 2.3A). Within this genomic region, two homozygous variants were found that were predicted to affect gene products: G/A at chr5:49333 and C/T at chr5:501775. The latter variant results in a V1176I substitution in TTHERM_00649260, a protein with homology to the mammalian centrosomal protein Ccdc81 (Firat-Karalar et al., 2014). The former variant results in an A168T substitution in TTHERM_01345780, a protein kinase. We attempted to rescue the multiplication arrest of *cdaH-1* mutants by biolistic introduction of wild-type fragments spanning

the variant position in either TTHERM_01345780 or TTHERM_00649260, followed by screening for clones capable of multiplying at the restrictive temperature. Using ~5×106 mutant cells, two rescue clones were obtained with the TTHERM_01345780 but not the TTHERM_ 00649260 fragment (Fig. 2.3B–D). Sequencing of TTHERM_01345780 in the two rescue clones revealed both a variant and a wild-type base, consistent with partial replacement of the 90 gene copies in the macronucleus (Zhou et al., 2022) (Fig. 2.3E). Next,

we edited TTHERM_01345780 in the *cdaH-1* homozygotes by homologous DNA recombination using fragments carrying a portion the 5′ untranslated region (UTR) (with an embedded neo5 marker) and a portion of the adjacent coding region that terminated either 63 bp upstream or 568 bp downstream of codon 168 (see Materials and Methods for details). At the restrictive temperature of 38°C, all tested paromomycin-resistant transformants that integrated the DNA fragment covering codon 168 proliferated (n=95), whereas no rescues were observed in transformants that integrated a fragment that terminated upstream of codon 168 (n=96). We conclude that the causal mutation for *cdaH-1* is the A168T substitution inTTHERM_01345780 and the TTHERM_ 00649260 variant is noncausal but closely linked (in agreement with the estimated rate of meiotic genetic recombination in *T. thermophila*, at ~50 kb/cM;Orias, 1998).The TTHERM_01345780 gene (or *CDAH*, following the gene naming recommendations; Allen et al., 1998) encodes a protein, CdaH, with an N-terminal kinase domain. A Blastp search of the human proteome retrieved Stk36, an ortholog of the ‘segment polarity’ gene product of *Drosophila* melanogaster Fu (Fused, CG6551) (Therond et al., 1993) as the closest match. The amino acid sequence of the kinase domain of CdaH is 64% identical to that of the kinase domain of human Stk36 and 47% identical to that of *D. melanogaster* Fu. In *Dictyostelium discoideum*, TsuA (Tsunami) is a Fused/Stk36 ortholog that is required for cell polarization (Tang et al., 2008) (Fig. 2.3F). Blastp searches using Fu, Stk36 or TsuA sequences against the predicted *T. thermophila* proteome all returned CdaH as a top match. In a phylogenetic analysis that included the amino acid sequences of 497 human kinase domains (Modi and Dunbrack, 2019b), CdaH formed a statistically supported clade with Stk36 (Fig. 2.S1). Alignment of the entire amino acid sequences of CdaH and established Fused/Stk36 orthologs showed strong homology within and weaker homology outside of the N terminal kinase domain (Fig. 2.S2). The *cdaH-1* mutation A168T is within the highly conserved ‘APE’ motif located at the end of the kinase activation loop (Modi and Dunbrack, 2019a). Diverse kinases almost invariably have an alanine at this position. Thus, the *cdaH-1* phenotype is likely a result of

reduced kinase activity of CdaH. Intriguingly, in mammalian Stk36, the amino acid at the homologous position is a serine. It is possible that Stk36 has weak kinase activity or is a pseudokinase, as is the mammalian paralogUlk4 (Khamrui et al., 2020). CdaH also has an armadillo repeats domain (Pfam PF00514) near the C-terminus. In Stk36, there is a related C-terminal HEAT domain (Pfam PF02985), which, similar to the armadillo repeats domain, forms a superhelix (Fig. 2.3F). Overall, CdaH is a compelling ortholog of Fused/Stk36 kinases. In animals, Fused/Stk36 kinases participate in Hedgehogsignaling during embryonic development (reviewed in Maloverjan and Piirsoo, 2012). However, in mammals (Edelbusch et al., 2017; Liu et al., 2016; Nozawa et al., 2013; Wilson et al., 2009) and in the kinetoplastid *Leishmania mexicana* (McCoy et al., 2023), deficiencies in Fused/Stk36 kinases cause structural defects in motile 9+2 cilia, including a failure to assemble central microtubules. *Tetrahymena* assembles numerous motile 9+2 cilia that are used for cell locomotion and feeding. Although the *cdaH-1* mutant phenotype is distinct from the phenotypes reported for ciliary mutants (reviewed in Bayless et al., 2019), we nonetheless examined the *cdaH-1* mutants grown for 3 h at 39°C (a time sufficient to induce cell division arrest) and found no gross defects in the number or length of cilia and in axoneme ultrastructure (Fig. 2.S3).

During cell division, CdaH accumulates at multiple sites, mostly within the posterior hemi-cell

We tagged CdaH with GFP at the C-terminus by editing the *CDAH* locus. No CdaH–GFP signal above the background was present in non-dividing cells (Fig. 2.4A,A′). In early dividers (in which the OP had just started to form), a faint CdaH–GFP signal appeared along the entire length of somatic ciliary rows and in the OP (Fig. 2.4B,B′,compare to Fig. 2.4A,A′). Later in development, CdaH–GFP presented as streaks of dots near the BBs of somatic rows and the dot intensity was higher within the posterior hemi-cell; the anterior margin of strong CdaH–GFP signal corresponded to the future plane of cortical subdivision (Fig. 2.4C,C′; Fig. 2.S4B–B″). At the onset of cortical subdivision, the CdaH–GFP streaks became

polarized in signal intensity (Fig. 2.4D,D′). Live observations using total internal reflection fluorescence (TIRF) microscopy revealed that each streak had multiple dots, the signal intensities of which formed a gradient decreasing toward the posterior cell end (Fig. 2.5A,F–F″; Movie 1). It has been suggested that in ciliates, the anterior–posterior patterning factors are distributed by motors along the cortical longitudinal microtubules (Cole and Gaertig, 2022; Marshall, 2021). However, kymograms did not reveal signals moving between the dots either within the streaks or between the streaks (Fig. 2.S5A–B′). In contrast, after photobleaching, the dot signals recovered to near pre-bleach level within ∼1 min (Fig. 2.S5C,C′), indicating a rapid turnover, likely by exchange with soluble CdaH in the cell body and possibly with involvement of intracytoplasmic microtubules that connect to the BBs (Gaertig et al., 1993). When the cortical subdivision (‘cs’ in Fig. 2.4E–F′) was fully developed and cytokinesis and macronuclear amitosis had started, CdaH formed a ring around the cell equator (Fig. 2.4E–F′). An apparent transition from the streak pattern to the ring pattern was seen by TIRF microscopy (Fig. 2.5B; Fig. 2.S5B,B′). Super-resolution structured illumination microscopy (SR-SIM) revealed that the CdaH–GFP ring was subequatorial and positioned at the posterior edge of the cortical subdivision (Fig. 2.S4C–D″). At the stage when the ring was fully formed, the most anterior BBs of a subset of the posterior half-rows exist as pairs called BB couplets (marked ‘c’ in Fig. 2.4G′,H′) (Jerka-Dziadosz,1981; McCoy, 1974; Numata et al., 1995). Later on, the BB couplets associate laterally to form the new ‘apical crown’ (AC), an incomplete circle of paired BBs that represent the apex of the cell (marked ‘ac’ in Fig. 2C). The CdaH–GFP ring was located immediately anterior to the BB couplets (Fig. 2.4G′,H′). After photobleaching of a portion of the ring in live cells, the signal recovered to 90% of the pre-bleach level within 50 s, indicating a rapid turnover (Fig. 2.5G,G′; Movie 2). During the course of cytokinesis, the CdaH–GFP ring narrowed along with the degree of cell constriction (Fig. 2.4G–H′, Fig. 2.5C,D; Fig. 2.S4D–E″). When the two daughters were about to split apart, a residual CdaH–GFP ring was present at the anterior tip of the posterior daughter (Fig. 2.4I–J′,Fig. 2.5E; Fig. 2.S4E–E″). A distinct CdaH–GFP signal was also

present near the old anterior cell end, as a short ribbon near the ends of somatic rows on the ventral right side, partially overlapping with the AC and connecting to the old OA. We will refer to this CdaH–GFP pool as the anterior suture (AS) (‘as’ in Fig. 2.4E,E′,J,J′;Fig. 2.S4C′,C″,E′,E″). The AS appeared at the same time as the CdaH ring (Fig. 2.4E,E′, compare to Fig. 2.4D,D′). These two CdaH–GFP pools (the AS and the ring) could be related, as both were positioned near the anterior ends of ciliary rows (old and new, respectively). CdaH also localized to the OP and less consistently to the old OA. CdaH–GFP appeared as a uniform signal across the entire OP during the early phase of oral morphogenesis (Fig. 2.4C,C′). When the rows emerged within the OP, a narrow patch of CdaH–GFP formed anteriorly to the new M1 (most anterior) membranelle. We will refer to this pool of CdaH–GFP as the ‘M1 arc’ (M1A) (labeled ‘m1a’ in Fig. 2.4D,D′,F,F′; Fig. 2.S4C′,D′,D″). During early cytokinesis, CdaH–GFP also marked the UM (Fig. 2.4F–G′; Fig. 2.S4D′,D″). Whereas the CdaH population associated with the division plane (streaks and ring) correlates with roles in the cortical subdivision and cytokinesis, the OP-associated CdaH could be involved in OP positioning and morphogenesis (see below).

CdaH colocalizes with the cytokinetic actin ring at the anterior end of the posterior hemi-cell

The timing and position of the subequatorial CdaH–GFP ring coincides with the assembly of the microfilament-rich cytokinetic ring (Jerka-Dziadosz, 1981; Yasuda et al., 1980). We therefore explored the relationship between the two rings by co-imaging CdaH–GFP and actin (Act1). The CdaH–GFP ring started to form shortly before the actin ring appeared at the onset of cytokinesis (Fig. 2.6A–B″) and the two rings strictly colocalized during the course of cell constriction based on fluorescence (Fig. 2.6A–D″) and super-resolution (Fig. 2.6G–G″) imaging. Strikingly, before the scission of daughter cells, both rings co-localized at the anterior tip of the posterior daughter (Fig. 2.6E–E″). Moreover, shortly after cytokinesis, residual actin and CdaH–GFP ring signals were present at the tip of the posterior postdivider (Fig. 2.6F–F″,H–H″). These data indicate that the CdaH ring is associated with or is even a

part of the cytokinetic ring. Additionally, in *Tetrahymena*, the contractile ring appears to form and operate at the tip of the posterior hemi-cell throughout cytokinesis.

Distribution of CdaH within the posterior hemi-cell requires CdaA

The anterior CdaI and posterior CdaA are two mutually antagonistic factors that interact to induce and position the DB. One or both of these proteins might interact with CdaH, based on the overlaps in the loss-of-function phenotypes (Fig. 2.S6) and localizations. We therefore examined how the distribution of CdaH–GFP is affected by expression of the loss-of-function alleles *cdaI-1* or *cdaA-1*. In *cdaI-1* homozygotes, at the permissive temperature of 22°C, as expected, the localization pattern of CdaH–GFP was unaffected (Fig. 2.7A–E,K). At 39°C, the distribution of CdaH–GFP appeared normal except that all pools within the posterior hemi-cell were shifted anteriorly, consistent with the global displacement of the division plane conferred by *cdaI-1* (Fig. 2.7F–J). It therefore appears that the distribution of CdaH is not directly dependent on CdaI. In the *cdaA-1* background, at the permissive temperature of 22°C, pattern of CdaH–GFP was unaffected as expected (Fig. 2.7L–P, see also 7V). At the restrictive temperature of 39°C, the posterior CdaH–GFP signal was greatly diminished (Fig. 2.7Q–U, compare toFig. 2.7L–P, see also 7V). Specifically, both the posterior streaks and the subequatorial ring were not detectable at stages at which they were present at the permissive temperature (Fig. 2.7R–U, compare to Fig. 2.7M–P). Interestingly, the AS and OP (including M1A) signals of CdaH–GFP appeared unaffected (insets in Fig. 2.7T). Thus, the distribution of CdaH–GFP is dependent on CdaA in a subset of locations that are associated with the cortical subdivision and cytokinesis. In a reciprocal experiment, the distribution of CdaA–GFP was unaffected by conditional expression of *cdaH-1* (Fig. 2.S7). These data support the placement of CdaH downstream of CdaA in the context of the formation of the posterior streaks and the subequatorial ring, which correlates with its functions in DB formation and cytokinesis.

CdaH interacts with CdaI to pattern the oral primordium

To further explore interactions between CdaH and either CdaA or CdaI, we examined the

phenotypes of double mutants using loss-of-function alleles: c*cdaH-1*, *cdaA-1* and *cdaI-1*. Conveniently, alleles are highly penetrant at 39°C. The phenotype of most of the *cdaH-1;cdaA-1* double homozygotes at 39°C (3–6 h) was similar to that of *cdaH-1* alone: a frequent failure of the DB formation, an anterior OP displacement and partial degradation of the OP(Fig. 2.8A–E,I,J). Although the double-mutant phenotype did not reveal an interaction, there was no contradiction to the model that CdaH acts downstream of CdaA in the context of the DB formation and cytokinesis, and that CdaH has a CdaA-independent role in OP positioning and stability. Similarly, the phenotype of the *cdaH-1;cdaI-1* at 39°C resembled that of *cdaH-1* alone, with the cortical subdivision failing to develop in most cells and an extreme anterior displacement of the OP (Fig. 2.8F–I). Unexpectedly, the OP degradation conferred by *cdaH-1* alone was partially suppressed in the double *cdaH-1;cdaI-1* mutants. In particular, whereas the UM was usually severely degraded in the *cdaH-1* mutants, it remained intact in the double mutants, both in the first- and second-generation OPs (Fig. 2.8G,H, compare to Fig. 2.8E; also Fig. 2.8J). Thus, CdaI activity might inhibit the CdaH activity that prevents OP degradation. Furthermore, the second-generation OP of the *cdaH-1;cdaI-1* double mutants often had an excessive number of membranelles. As an example, in the double-mutant cell shown in Fig. 2.8H, the second-generation OP(‘op2’) had seven (instead of the normal three) membranelles. Importantly, the allelic *cdaI-2* mutants were reported to have an increased number of membranelles in the OA (Frankel, 2008). Indeed, the *cdaI-1* single mutants used here also had extra membranelles (Fig. 2.8F,J). Although the addition of *cdaH-1* did not increase the average number of membranelles per OA, it increased the penetrance of the extra-membranelle phenotype (Fig. 2.8J,K). All these observations indicate that CdaH not only participates in the global positioning of the OP on the anterior–posterior axis, but also contributes to the local patterning of the OP where it might interact with CdaI.

DISCUSSION

The cortical patterns of ciliates exceed in complexity the most sophisticated intracellular patterns seen in other eukaryotic cells (Frankel, 1989, 2008). Powerful self-organizing mechanisms are likely involved, based on the ability of some ciliates to generate the pattern *de novo* during encystation (Fryd-Versavel et al., 2010; Grimes, 1973a,b) or during regeneration from small cell fragments (Gruber, 1885; Morgan, 1901; Tartar, 1960, 1961). Surprisingly, despite the peculiar features of the ciliate phylum, recent studies in *Tetrahymena* revealed that the positions of forming cortical structures on the anterior–posterior axis are controlled by several conserved kinases and kinase-binding proteins, including orthologs of Hippo signaling components (reviewed in Cole and Gaertig,2022; Soares et al., 2019). These proteins appear to form a prepattern that excludes forming structures from specific cortical regions. The prepatterning activities occur in two phases. Before the stage of cortical subdivision, the posteriorly enriched ‘early Hippo circuit’ (with Elo1) positions the entire division plane including the OP and DB (Jiang et al., 2019a). Subsequently, a mutually antagonistic pair of the anterior ‘late Hippo circuit’ (with CdaI) and the posterior CdaA induce and position the DB (Jiang et al.,2017, 2020; Tavares et al., 2012). In addition, at the time of the DB appearance, CdaI maintains the subequatorial OP position by preventing its anterior displacement (Jiang et al., 2017). Based on the phenotype of the single available allele (*cdaH-1*), CdaH acts during the late stage that involves CdaI and CdaA. CdaH has multiple functions that can be seen as either global or local. The global function of CdaH is in maintaining the position of the OP in reference to the anterior–posterior cell polarity axis. The local functions involve execution of cortical subdivision and cytokinesis and shaping the OP. CdaH presents at multiple locations that correlate with its multiple patterning functions, offering an explanation for the highly pleiotropic phenotype of *cdaH-1*.These observations agree with the relatively long period of temperature sensitivity for *cdaH-1* expression during cell division compared to that of *cdaA-1* that specifically affects

DB formation (Frankel et al., 1980).

The global function of CdaH: positioning the oral primordium on the anterior–posterior axis

cdaH-1 confers a dramatic anterior displacement of the OP that phenocopies *cdaI-1* (Frankel, 2008; Jiang et al., 2017). As documented earlier for *cdaI-1*, in the *cdaH-1* mutants, the initial position of the OP is correct and the structure shifts anteriorly later at the time of the DB formation. Both CdaI–GFP and CdaH–GFP are enriched at the OP, whereas CdaA–GFP is not. Thus, there is a correlation between the role of CdaH in OP positioning and presence within the structure. CdaH and CdaI activities might anchor the OP at the correct anterior–posterior position in response to global positioning cues. It remains to be explored whether CdaH and CdaI interact to execute the OP positioning as they do to pattern the internal organization of the OA (see below).

The local functions of CdaH

Shaping the oral primordium

The morphogenesis of the OP is a remarkably complex process of apparent self-organization that includes proliferation of BBs, formation of BB pairs, alignment of BB pairs into rows, emergence of BB triplets and quartets, and resorption of some and movements of other BBs (Bakowska et al., 1982b). The exact course of these events is row specific and, consequently, each row acquires a unique organization. Both CdaI and CdaH localize to the OP but, within the organelle, they occupy non-identical domains. The M1A pool of CdaH–GFP is of particular interest as, to our knowledge, the first row-specific marker. The *cdaI* alleles increase the number of membranelle rows in the OP (Frankel, 2008; Jiang et al., 2017) and we show here that *cdaH-1* increases the penetrance of this phenotype. In contrast, *cdaH-1* confers broad degeneration of oral rows and this phenotype is suppressed by *cdaI-1*. During the normal course of late OP development, a number of BBs at multiple positions (including the right margins of membranelles and the most posterior region of the

OP) are resorbed (Bakowska et al., 1982b). The programmed BB resorption could be a part of the mechanism that determines the row number and generates the unique organization of specific oral rows. CdaI and CdaH might act within the OA to control the resorption of BBs.

In division boundary formation and cytokinesis

During the course of cell division, the earliest defect conferred by *cdaH-1* is the block in DB formation. We showed previously that the induction and positioning of the DB on the anterior–posterior axis are coupled and involve mutually antagonistic posterior CdaA and anterior CdaI (Jiang et al., 2020). Prior to DB formation, CdaH colocalizes with CdaA to the posterior half-rows in a CdaA-dependent manner. Shortly before the cortical subdivision, CdaH is enriched at several BBs proximal to the cortical gap as a gradient decreasing toward the posterior cell end. The same area contains a posteriorly decreasing gradient of phosphoserine– or phosphothreonine–proline epitopes (Kaczanowska et al., 1999). Thus, CdaH might contribute to generation of the gradient of protein phosphorylation within the subequatorial region that might drive the formation of the DB. We show that following DB formation, CdaH is required for the execution of cytokinesis and that CdaH forms a ring that colocalizes with the actin contractile ring. As in other eukaryotes, in *Tetrahymena*, the contractile ring contains microfilaments, actin and actin-binding proteins (Edamatsu et al., 1992; Gonda and Numata, 2002; Jerka-Dziadosz, 1981; Numata and Gonda, 2001; Numata et al., 2000; Shirayama and Numata, 2003; Watanabe et al.,1998). Although it is assumed that the microfilaments and myosin motors generate the force for cell constriction, this has not yet been firmly established as ciliates lack myosin-2, the principle force producer in animal cytokinesis (Sugita et al., 2011) and, in *Tetrahymena*, cytokinesis is not sensitive to the actin inhibitor latrunculin A (Shimizu et al., 2013). Nevertheless, cytokinesis is blocked by depletion of cleavage furrow-associated actin-4 in Paramecium (Sehring et al., 2007, 2010) and by overexpression of GFP–Act1 in *Tetrahymena* (Hosein et al., 2003). The CdaH ring appears to form shortly before the actin ring, indicating that CdaH promotes contractile ring assembly. Importantly, we found that the contractile ring assembled at the anterior margin of

the posterior hemicell and its apparent remnant was inherited by the posterior daughter. Thus, in *Tetrahymena* and likely in other ciliates as well, the contractile ring is placed asymmetrically. Interestingly, the anterior tip of an interphase *Tetrahymena* cell contains a band of microfilaments (apical band) that is attached to the most anterior BBs (the AC) (Jerka-Dziadosz et al., 1981, 2001). The two microfilament-rich organelles that form at the new anterior cell end (contractile ring and apical band), might be separate structures. Alternatively, the remnant of the contractile ring might be remodeled into the apical band. U Ultrastructural studies are needed to resolve the relationships between CdaH, the contractile ring and the apical band.

Evolution of Fused kinases

The multifunctionality of CdaH is surprising because the genomes of ciliates encode an extraordinarily large number of kinases (1069 in *T. thermophila*) that arose by gene duplications and likely gained lineage-specific functions (Aury et al., 2006; Eisen et al., 2006; Reiffand Marshall, 2017 preprint; Swart et al., 2013). However, there already are well-documented cases of ‘pleiotropic’ kinases in animals, including the Aurora B and Polo kinases, that play multiple roles during cell division (Hadders and Lens, 2022; Zitouni et al., 2014). Given that ciliates are an ‘early-branching’ non-opisthokont lineage of eukaryotes (Burki et al., 2020), our studies shed light on the evolution of the Fused kinases. Fused was discovered as a product of a ‘segment polarity’ gene in *Drosophila* (Busson et al.,1988; Gergen and Wieschaus, 1986; Nusslein-Volhard and Wieschaus, 1980; Perrimon and Mahowald, 1987) and, in animals, Fused kinases function in Hedgehog signaling (reviewed in Maloverjan and Piirsoo, 2012). Ciliate genomes appear to lack homologs of proteins that participate in Hedgehog signaling other than Fused. Although Fused is required for proper Hedgehog signaling during embryogenesis in *Drosophila* (Maloverjan and Piirsoo, 2012), in mammals, the Fused ortholog Stk36 plays a nonessential function in Hedgehog signaling (Maloverjan and Piirsoo,2012), possibly redundant with Ulk3 (Han et al., 2019). Intriguingly, in mice, Stk36 and a closely related kinase, Ulk4, are required for assembly of central

microtubules in the 9+2 cilia (Liu et al., 2016; Nozawa et al., 2013; Wilson et al., 2009). The ciliary role of Fused kinases could be ancestral, based on the recent report that Fused and Ulk4 are required for correct assembly of flagellar axonemes in the kinetoplastid *Leishmania* (McCoy et al.,2023). Although our study did not reveal a ciliary function for CdaH, the genome of *Tetrahymena* encodes orthologs of Ulk4 (TTHERM_00756520 and TTHERM_00726480) that could fulfill the ciliary roles (Fig. 2.S1). If such a division of labor exists, the *Tetrahymena* model could be useful in dissecting the ciliary versus non-ciliary functions of Fused-related kinases. We reveal here a role for Fused in intracellular patterning. In *Dictyostelium*, the Fused ortholog TsuA is required for cell polarization during developmental aggregation, and, intriguingly, TsuA colocalizes with microtubules (Tang et al., 2008). In *Drosophila*, Fused phosphorylates Cos2 kinesin to activate Hedgehog signaling (Nybakken et al., 2002; Raisin et al., 2010; Ruel et al., 2007). In *Arabidopsis thaliana*, the Fused ortholog TIO is required for expansion of the microtubule-rich phragmoplast during cytokinesis and associates with two members of the kinesin12 family (Oh et al., 2012). CdaH is closely associated with the microtubule-rich BBs. As suggested by others (Oh et al., 2012; Tang et al., 2008), the evolutionarily conserved molecular function of Fused kinases could be to phosphorylate microtubule motors and, specifically, kinesins. In addition, studies in *Dictyostelium* and our work implicate Fused kinases in cell polarity-related phenomena: formation of the cell polarity axis (Tang et al., 2008) and positioning and patterning of organelles (this study). It is possible that Fused orthologs have conserved roles in distributing polarity-related molecules along microtubules via regulation of kinesin motors. Such activities could also be behind the role of Fused homologs in the assembly of ciliary axonemes (Liu et al., 2016; McCoy et al.,2023; Nozawa et al., 2013; Wilson et al., 2009). The genome of *Tetrahymena* encodes an unusually large number of kinesins (77) (Wickstead and Gull, 2006) and, therefore, some could participate in intracellular positioning as phosphorylation targets of CdaH. However, our study also points to a close relationship of Fused with actin.

Acknowledgements

We thank Joseph Frankel (University of Iowa) and Maria Jerka-Dziadosz (Nencki Institute of Experimental Biology, Warsaw, Poland) for reading the manuscript and comments; Peter Kner (University of Georgia) and Dorota Wloga (Nencki Institute of Experimental Biology, Warsaw, Poland) for valuable advice; Muthugapatti K. Kandasamy (Biomedical Microscopy Core, University of Georgia) for training and assistance with confocal and super-resolution imaging; and Mary Brown Ard (Georgia Electron Microscopy, University of Georgia) for expert assistance with electron microscopy.

Competing interests

The authors declare no competing or financial interests.

Author contributions

Conceptualization: J.G.; Methodology: C.L., K.F.L.; Software: W.M.; Investigation: C.L., W.M., Y.-Y.J., K.N., K.F.L.; Resources: W.M., K.F.L.; Writing - original draft: J.G.; Writing - review & editing: C.L., W.M., Y.-Y.J., K.N.; Visualization: C.L.; Supervision: J.G.; Project administration: J.G.; Funding acquisition: W.M., K.N., K.F.L., J.G.

Funding

This work was supported by the National Institutes of Health (grants R01GM135444to J.G. and R01GM110413 to K.F.L.), the Grant-in-Aid for Scientific Research from the Ministry of Education, Culture, Sports, Science and Technology (MEXT), Japan (16K07338 to K.N.) and the German Federal Ministry of Education and Research (Bundesministerium für Bildung und Forschung) (grant 031L0101C de.NBI-epi toW.M.). Open access funding provided by the University of Georgia. Deposited in PMC for immediate release.

Data availability

The sequence reads of the *Tetrahymena cdaH-1* mutant have been deposited at the Sequence Read Archive (SRA) database (Bioproject accession numberPRJNA999728).

Peer review history

The peer review history is available online at

https://journals.biologists.com/jcs/lookup/doi/10.1242/jcs.261256.reviewer-comments.pdf

Reference

Allen, S. L., Altschuler, M. I., Bruns, P. J., Cohen, J., Doerder, F. P., Gaertig, J., Gorovsky, M., Orias, E. and Turkewitz, A. (1998). Proposed genetic nomenclature rules for *Tetrahymena thermophila*, *Paramecium primaurelia* and *Paramecium tetraurelia*. Genetics 149, 459-462. doi:10.1093/genetics/149.1.459

Aury, J. M., Jaillon, O., Duret, L., Noel, B., Jubin, C., Porcel, B. M., Segurens, B., Daubin, V., Anthouard, V., Aiach, N. et al. (2006). Global trends of whole genome duplications revealed by the ciliate *Paramecium tetraurelia*. Nature 444,171-178. doi:10.1038/nature05230

Bakowska, J., Frankel, J. and Nelsen, E. M. (1982a). Regulation of the pattern of basal bodies within the oral apparatus of *Tetrahymena thermophila*. J. Embryol.Exp. Morphol. 69, 83-105. doi:10.1242/dev.69.1.83

Bakowska, J., Nelsen, E. M. and Frankel, J. (1982b). Development of the ciliary pattern of the oral apparatus of *Tetrahymena thermophila*. J. Eukaryot. Microbiol.29, 366-382. doi:10.1111/j.1550-7408.1982.tb05416.x

Bayless, B. A., Navarro, F. M. and Winey, M. (2019). Motile cilia: innovation and insight from ciliate model organisms. Front. Cell Dev. Biol. 7, 265. doi:10.3389/fcell.2019.00265

Brown, N. P., Leroy, C. and Sander, C. (1998). MView: a web-compatible database search or multiple alignment viewer. Bioinformatics 14, 380-381. doi:10.1093/bioinformatics/14.4.380

Brown, J. M., Marsala, C., Kosoy, R. and Gaertig, J. (1999). Kinesin-II is preferentially targeted to assembling cilia and is required for ciliogenesis and normal cytokinesis in *Tetrahymena*. Mol. Biol. Cell 10, 3081-3096. doi:10.1091/mbc.10.10.3081

Burki, F., Roger, A. J., Brown, M. W. and Simpson, A. G. B. (2020). The new tree of eukaryotes. Trends Ecol. Evol. 35, 43-55. doi:10.1016/j.tree.2019.08.008

Busson, D., Limbourg-Bouchon, B., Mariol, M.-C., Preat, T. and Lamour-Isnard, C. (1988). Genetic analysis of viable and lethal fused mutants of *Drosophila melanogaster*. Rouxs Arch Dev. Biol. 197, 221-230. doi:10.1007/BF02439429

Capella-Gutiérrez, S., Silla-Martınez, J. M. and Gabaldo´n, T. (2009). trimAl: a tool for automated alignment trimming in large-scale phylogenetic analyses. Bioinformatics 25, 1972-1973. doi:10.1093/bioinformatics/btp348

Cole, E. and Gaertig, J. (2022). Anterior-posterior pattern formation in ciliates.J. Eukaryot. Microbiol. 69, e12890. doi:10.1111/jeu.12890

Edamatsu, M., Hirono, M. and Watanabe, Y. (1992). *Tetrahymena* profilin is localized in the division furrow. J. Biochem. 112, 637-642. doi:10.1093/oxfordjournals.jbchem.a123952

Edelbusch, C., Cindrić, S., Dougherty, G. W., Loges, N. T., Olbrich, H., Rivlin, J.,Wallmeier, J., Pennekamp, P., Amirav, I. and Omran, H. (2017). Mutation ofserine/threonine protein kinase 36 (STK36) causes primary ciliary dyskinesia with a central pair defect. Hum. Mutat. 38, 964-969. doi:10.1002/humu.23261

Eisen, J. A., Coyne, R. S., Wu, M., Wu, D., Thiagarajan, M., Wortman, J. R.,Badger, J. H., Ren, Q., Amedeo, P., Jones, K. M. et al. (2006). Macronuclear genome sequence of the ciliate *Tetrahymena thermophila*, a model eukaryote. PLoS Biol. 4, e286. doi:10.1371/journal.pbio.0040286

Firat-Karalar, E. N., Sante, J., Elliott, S. and Stearns, T. (2014). Proteomic analysis of mammalian sperm cells identifies new components of the centrosome. J. Cell Sci. 127, 4128-4133. doi:10.1242/jcs.157008

Frankel, J. (1989). Pattern Formation: Ciliate Studies and Models. USA: Oxford University Press.

Frankel, J. (2008). What do genic mutations tell us about the structural patterning ofa complex single-celled organism? Eukaryot. Cell 7, 1617-1639. doi:10.1128/EC.00161-08

Frankel, J., Mohler, J. and Frankel, A. K. (1980). Temperature-sensitive periods of mutations affecting cell division in *Tetrahymena thermophila*. J. Cell Sci. 43,59-74. doi:10.1242/jcs.43.1.59

Frankel, J., Nelsen, E. M. and Martel, E. (1981). Development of the ciliature of *Tetrahymena thermophila*. II. Spatial subdivision prior to cytokinesis. Dev. Biol.88, 39-54. doi:10.1016/0012-1606(81)90217-7

Fryd-Versavel, G., Lemullois, M. and Aubusson-Fleury, A. (2010). Maintaining cell polarity through vegetative cell pattern dedifferentiation: cytoskeleton and morphogenesis in the hypotrich ciliate Sterkiella histriomuscorum. Protist 161,222-236. doi:10.1016/j.protis.2009.11.001

Gaertig, J., Thatcher, T. H., Mcgrath, K. E., Callahan, R. C. and Gorovsky, M. A.(1993). Perspectives on tubulin isotype function and evolution based on the observation that *Tetrahymena thermophila* microtubules contain a single alpha- and beta-tubulin. Cell Motil. Cytoskeleton 25, 243-253. doi:10.1002/cm.970250305

Gaertig, J., Thatcher, T. H., Gu, L. and Gorovsky, M. A. (1994). Electroporation-mediated replacement of a positively and negatively selectable beta-tubulin gene in *Tetrahymena thermophila.* Proc. Natl. Acad. Sci. USA 91, 4549-4553. doi:10.1073/pnas.91.10.4549

Gaertig, J., Wloga, D., Vasudevan, K. K., Guha, M. and Dentler, W. (2013). Discovery and functional evaluation of ciliary proteins in *Tetrahymena thermophila.* Methods Enzymol. 525, 265-284. doi:10.1016/B978-0-12-397944-5.00013-4

Galati, D. F., Bonney, S., Kronenberg, Z., Clarissa, C., Yandell, M., Elde, N. C.,Jerka-Dziadosz, M., Giddings, T. H., Frankel, J. and Pearson, C. G. (2014).DisAp-dependent striated fiber elongation is required to organize ciliary arrays. J. Cell Biol. 207, 705-715. doi:10.1083/jcb.201409123

Gergen, J. P. and Wieschaus, E. F. (1986). Localized requirements for gene activity in segmentation of *Drosophila* embryos: analysis of armadillo, fused, giant and unpaired mutations in mosaic embryos. Rouxs Arch. Dev. Biol. 195, 49-62.doi:10.1007/BF00444041

Gonda, K. and Numata, O. (2002). p85 binds to G-actin in a Ca(2+)/calmodulin-dependent manner, thus regulating the initiation of cytokinesis in *Tetrahymena.* Biochem. Biophys. Res. Commun. 292, 1098-1103. doi:10.1006/bbrc.2002.6777

Gorovsky, M. A. (1973). Macro- and micronuclei of *Tetrahymena pyriformis*: a model system for studying the structure and function of eukaryotic nuclei.J. Protozool. 20, 19-25. doi:10.1111/j.1550-7408.1973.tb05995.x

Grimes, G. W. (1973a). Differentiation during encystment and excystment in *Oxytricha fallax*. J. Protozool. 20, 92-104. doi:10.1111/j.1550-7408.1973.tb06009.x

Grimes, G. W. (1973b). Morphological discontinuity of kinetosomes during the lifecycle of *Oxytricha fallax.* J. Cell Biol. 57, 229-232. doi:10.1083/jcb.57.1.229

Gruber, A. (1885). Über künstliche Teilung bei Infusorien. Biol. Zentralbl. 3,580-582.

Hadders, M. A. and Lens, S. M. A. (2022). Changing places: chromosomal passenger complex relocation in early anaphase. Trends Cell Biol. 32, 165-

176.doi:10.1016/j.tcb.2021.09.008

Hamilton, E. P., Kapusta, A., Huvos, P. E., Bidwell, S. L., Zafar, N., Tang, H.,Hadjithomas, M., Krishnakumar, V., Badger, J. H., Caler, E. V. et al. (2016).Structure of the germline genome of *Tetrahymena thermophila* and relationship to the massively rearranged somatic genome. Elife 5, e19090. doi:10.7554/eLife.19090

Han, Y., Wang, B., Cho, Y. S., Zhu, J., Wu, J., Chen, Y. and Jiang, J. (2019). Phosphorylation of Ci/Gli by fused family kinases promotes hedgehog signaling. Dev. Cell 50, 610-626.e4. doi:10.1016/j.devcel.2019.06.008

Hosein, R. E., Williams, S. A., Haye, K. and Gavin, R. H. (2003). Expression of GFP-actin leads to failure of nuclear elongation and cytokinesis in *Tetrahymena thermophila.* J. Eukaryot. Microbiol. 50, 403-408. doi:10.1111/j.1550-7408.2003.tb00261.x

Jerka-Dziadosz, M. (1981). Cytoskeleton-related structures in *Tetrahymena thermophila*: microfilaments at the apical and division-furrow rings. J. Cell Sci.51, 241-253. doi:10.1242/jcs.51.1.241

Jerka-Dziadosz, M., Strzyewska-Jowko, I., Wojsa-Lugowska, U., Krawczynska,W. and Krzywicka, A. (2001). The dynamics of filamentous structures in the apical band, oral crescent, fission line and the postoral meridional filament in *Tetrahymena thermophila* revealed by monoclonal antibody 12G9. Protist 152,53-67. doi:10.1078/1434-4610-00043

Jiang, Y. Y., Lechtreck, K. and Gaertig, J. (2015). Total internal reflection fluorescence microscopy of intraflagellar transport in *Tetrahymena thermophila*. Methods Cell Biol. 127, 445-456. doi:10.1016/bs.mcb.2015.01.001

Jiang, Y. Y., Maier, W., Baumeister, R., Minevich, G., Joachimiak, E., Ruan, Z.,Kannan, N., Clarke, D., Frankel, J. and Gaertig, J. (2017). The hippo pathway maintains the equatorial division plane in the ciliate *Tetrahymena*. Genetics 206,873-888. doi:10.1534/genetics.117.200766

Jiang, Y. Y., Maier, W., Baumeister, R., Joachimiak, E., Ruan, Z., Kannan, N.,Clarke, D., Louka, P., Guha, M., Frankel, J. et al. (2019a). Two antagonistic hippo signaling circuits set the division plane at the medial position in the ciliate *Tetrahymena*. Genetics 211, 651-663. doi:10.1534/genetics.118.301889

Jiang, Y.-Y., Maier, W., Baumeister, R., Minevich, G., Joachimiak, E., Wloga, D.,Ruan, Z., Kannan, N., Bocarro, S., Bahraini, A. et al. (2019b). LF4/MOK and aCDK-related kinase regulate the number and length of cilia in *Tetrahymena*. PLoSGenet. 15, e1008099. doi:10.1371/journal.pgen.1008099

Jiang, Y. Y., Maier, W., Chukka, U. N., Choromanski, M., Lee, C., Joachimiak, E.,Wloga, D., Yeung, W., Kannan, N., Frankel, J. et al. (2020). Mutual antagonism between Hippo signaling and cyclin E drives intracellular pattern formation. J. CellBiol. 219, e202002077. doi:10.1083/jcb.202002077

Kaczanowska, J., Joachimiak, E., Buzanska, L., Krawczynska, W., Wheatley,D. N. and Kaczanowski, A. (1999). Molecular subdivision of the cortex of dividing *Tetrahymena* is coupled with the formation of the fission zone. Dev. Biol. 212,150-164. doi:10.1006/dbio.1999.9362

Katoh, K. and Standley, D. M. (2013). MAFFT multiple sequence alignment software version 7: improvements in performance and usability. Mol. Biol. Evol.30, 772-780. doi:10.1093/molbev/mst010

Khamrui, S., Ung, P. M. U., Secor, C., Schlessinger, A. and Lazarus, M. B.(2020). High-

resolution structure and inhibition of the schizophrenia-linked pseudokinase ULK4. J. Am. Chem. Soc. 142, 33-37. doi:10.1021/jacs.9b10458

Kirk, K. E., Christ, C., McGuire, J. M., Paul, A. G., Vahedi, M., Stuart, K. R. and Cole, E. S. (2008). Abnormal micronuclear telomeres lead to an unusual cell cycle checkpoint and defects in *Tetrahymena* oral morphogenesis. Eukaryot. Cell 7,1712-1723. doi:10.1128/EC.00393-07

Lechtreck, K. F. (2016). Methods for studying movement of molecules within cilia. Methods Mol. Biol. 1454, 83-96. doi:10.1007/978-1-4939-3789-9_6

Lefort, V., Desper, R. and Gascuel, O. (2015). FastME 2.0: a comprehensive, accurate, and fast distance-based phylogeny inference program. Mol. Biol. Evol.32, 2798-2800. doi:10.1093/molbev/msv150

Lemoine, F., Correia, D., Lefort, V., Doppelt-Azeroual, O., Mareuil, F., Cohen-Boulakia, S. and Gascuel, O. (2019). NGPhylogeny.fr: new generation phylogenetic services for non-specialists. Nucleic Acids Res. 47, W260-W265.doi:10.1093/nar/gkz303

Liu, M., Guan, Z., Shen, Q., Lalor, P., Fitzgerald, U., O'brien, T., Dockery, P. and Shen, S. (2016). Ulk4 is essential for ciliogenesis and CSF flow. J. Neurosci. 36,7589-7600. doi:10.1523/JNEUROSCI.0621-16.2016

Maloverjan, A. and Piirsoo, M. (2012). Mammalian homologues of *Drosophila* fused kinase. Vitam. Horm. 88, 91-113. doi:10.1016/B978-0-12-394622-5.00005-5

Marshall, W. F. (2021). Regeneration in *Stentor coeruleus.* Front. Cell Dev. Biol. 9,753625. doi:10.3389/fcell.2021.753625

Mccoy, C. J., Paupelin-Vaucelle, H., Gorilak, P., Beneke, T., Varga, V. and Gluenz, E. (2023). ULK4 and Fused/STK36 interact to mediate assembly of a motile flagellum. Mol. Biol. Cell 34, ar66. doi:10.1091/mbc.E22-06-0222

Mccoy, J. W. (1974). New features of the tetrahyminid cortex revealed by protargol staining. Acta Protozool. 13, 155-159.

Modi, V. and Dunbrack, R. L., Jr. (2019a). Defining a new nomenclature for the structures of active and inactive kinases. Proc. Natl. Acad. Sci. USA 116,6818-6827. doi:10.1073/pnas.1814279116

Modi, V. and Dunbrack, R. L., Jr. (2019b). A structurally-validated multiple sequence alignment of 497 human protein kinase domains. Sci. Rep. 9, 19790.doi:10.1038/s41598-019-56499-4

Morgan, T. H. (1901). Regeneration of Proportionate Structures in Stentor. Biol. Bull.2, 311-328. doi:10.2307/1535709

Nozawa, Y. I., Yao, E., Lin, C., Yang, J. H., Wilson, C. W., Gacayan, R. and Chuang, P. T. (2013). Fused (Stk36) is a ciliary protein required for central pair assembly and motile cilia orientation in the mammalian oviduct. Dev. Dyn. 242,1307-1319. doi:10.1002/dvdy.24024

Numata, O. and Gonda, K. (2001). Determination of division plane and organization of contractile ring in *Tetrahymena*. Cell Struct. Funct. 26, 593-601. doi:10.1247/csf.26.593

Numata, O., Suzuki, H., Ohba, H. and Watanabe, Y. (1995). The mutant gene product of a *Tetrahymena* cell-division-arrest mutant cdaA is localized in the accessory structure of specialized basal body close to the division furrow. Zoolog.Sci. 12, 133-135. doi:10.2108/zsj.12.133

Numata, O., Gonda, K., Watanabe, A. and Kurasawa, Y. (2000). Cytokinesis in *Tetrahymena*: determination of division plane and organization of contractile ring. Microsc. Res. Tech. 49, 127-135. doi:10.1002/(SICI)1097-0029(20000415)49:23.0.CO;2-K

Nusslein-Volhard, C. and Wieschaus, E. (1980). Mutations affecting segment number and polarity in *Drosophila.* Nature 287, 795-801. doi:10.1038/287795a0

Nybakken, K. E., Turck, C. W., Robbins, D. J. and Bishop, J. M. (2002). Hedgehog-stimulated phosphorylation of the kinesin-related protein Costal2 is mediated by the serine/threonine kinase fused. J. Biol. Chem. 277, 24638-24647.doi:10.1074/jbc.M110730200

Oh, S. A., Allen, T., Kim, G. J., Sidorova, A., Borg, M., Park, S. K. and Twell, D.(2012). Arabidopsis Fused kinase and the Kinesin-12 subfamily constitute a signalling module required for phragmoplast expansion. Plant J. 72, 308-319.doi:10.1111/j.1365-313X.2012.05077.x

Orias, E. (1998). Mapping the germ-line and somatic genomes of a ciliated protozoan, *Tetrahymena thermophila*. Genome Res. 8, 91-99. doi:10.1101/gr.8.2.91

Perrimon, N. and Mahowald, A. P. (1987). Multiple functions of segment polarity genes in *Drosophila*. Dev. Biol. 119, 587-600. doi:10.1016/0012-1606(87)90061-3

Raisin, S., Ruel, L., Ranieri, N., Staccini-Lavenant, L. and Therond, P. P. (2010).Dynamic phosphorylation of the kinesin Costal-2 in vivo reveals requirement of fused kinase activity for all levels of hedgehog signalling. Dev. Biol. 344, 119-128.doi:10.1016/j.ydbio.2010.04.021

Reiff, S. B. and Marshall, W. F. (2017). A large kinome in a large cell: *Stentor coeruleus* possesses highly expanded kinase families and novel domain architectures. bioRxiv 168187. doi:10.1101/168187

Ruel, L., Gallet, A., Raisin, S., Truchi, A., Staccini-Lavenant, L., Cervantes, A. and Therond, P. P. (2007). Phosphorylation of the atypical kinesin Costal2 by the kinase Fused induces the partial disassembly of the Smoothened-Fused-Costal2-Cubitus interruptus complex in Hedgehog signalling. Development 134,3677-3689. doi:10.1242/dev.011577

Salisbury, J. L., Baron, A. T. and Sanders, M. A. (1988). The centrin-based cytoskeleton of *Chlamydomonas reinhardtii*: distribution in interphase and mitotic cells. J. Cell Biol. 107, 635-641. doi:10.1083/jcb.107.2.635

Sehring, I. M., Reiner, C., Mansfeld, J., Plattner, H. and Kissmehl, R. (2007). A broad spectrum of actin paralogs in *Paramecium tetraurelia* cells display differential localization and function. J. Cell Sci. 120, 177-190. doi:10.1242/jcs.03313

Sehring, I. M., Reiner, C. and Plattner, H. (2010). The actin subfamily PtAct4, out of many subfamilies, is differentially localized for specific local functions in *Paramecium tetraurelia* cells. Eur. J. Cell Biol. 89, 509-524. doi:10.1016/j.ejcb.2010.02.003

Shang, Y., Li, B. and Gorovsky, M. A. (2002). *Tetrahymena thermophila* contains a conventional gamma-tubulin that is differentially required for the maintenance of different microtubule-organizing centers. J. Cell Biol. 158, 1195-1206. doi:10.1083/jcb.200205101

Shimizu, Y., Kushida, Y., Kiriyama, S., Nakano, K. and Numata, O. (2013). Formation and ingression of division furrow can progress under the inhibitory condition of actin polymerization in ciliate *Tetrahymena pyriformis.* Zoolog. Sci.30, 1044-1049. doi:10.2108/zsj.30.1044

Shirayama, S. and Numata, O. (2003). *Tetrahymena* fimbrin localized in the division furrow

bundles actin filaments in a calcium-independent manner.J. Biochem. 134, 591-598. doi:10.1093/jb/mvg183

Sievers, F., Wilm, A., Dineen, D., Gibson, T. J., Karplus, K., Li, W., Lopez, R., Mcwilliam, H., Remmert, M., Soding, J. et al. (2011). Fast, scalable generation of high-quality protein multiple sequence alignments using Clustal Omega. Mol.Syst. Biol. 7, 539. doi:10.1038/msb.2011.75

Shiozaki, N., Nakano, K., Kushida, Y., Noguchi, T. Q., Uyeda, T. Q., Wloga, D.,Dave, D., Vasudevan, K. K., Gaertig, J. and Numata, O. (2013). ADF/cofilinis not essential but is critically important for actin activities during phagocytosis in *Tetrahymena thermophila.* Eukaryot Cell 12, 1080–1086. doi:10.1128/EC.00074-13

Slabodnick, M. M., Ruby, J. G., Dunn, J. G., Feldman, J. L., Derisi, J. L. and Marshall, W. F. (2014). The kinase regulator mob1 acts as a patterning protein for *stentor* morphogenesis. PLoS Biol. 12, e1001861. doi:10.1371/journal.pbio.1001861

Soares, H., Carmona, B., Nolasco, S. and Viseu Melo, L. (2019). Polarity in ciliate models: from cilia to cell architecture. Front. Cell Dev. Biol. 7, 240. doi:10.3389/fcell.2019.00240

Sugita, M., Iwataki, Y., Nakano, K. and Numata, O. (2011). Unique sequences and predicted functions of myosins in *Tetrahymena thermophila.* Gene 480, 10-20.doi:10.1016/j.gene.2011.02.006

Swart, E. C., Bracht, J. R., Magrini, V., Minx, P., Chen, X., Zhou, Y., Khurana,J. S., Goldman, A. D., Nowacki, M., Schotanus, K. et al. (2013). The *Oxytricha trifallax* macronuclear genome: a complex eukaryotic genome with 16,000 tinychromosomes. PLoS Biol. 11, e1001473. doi:10.1371/journal.pbio.1001473

Tang, L., Franca-Koh, J., Xiong, Y., Chen, M. Y., Long, Y., Bickford, R. M.,Knecht, D. A., Iglesias, P. A. and Devreotes, P. N. (2008). tsunami, the *Dictyostelium* homolog of the Fused kinase, is required for polarization and chemotaxis. Genes Dev. 22, 2278-2290. doi:10.1101/gad.1694508

Tartar, V. (1960). Reconstitution of minced *Stentor coeruleus.* J. Exp. Zool. 144,187-207. doi:10.1002/jez.1401440208

Tartar, V. (1961). The Biology of *Stentor*. Oxford, New York: Pergammon Press.

Tartar, V. (1968). Micrurgical experiments on cytokinesis in *Stentor coeruleus*.J. Exp. Zool. 167, 21-36. doi:10.1002/jez.1401670103

Tavares, A., Goncalves, J., Florindo, C., Tavares, A. A. and Soares, H. (2012).Mob1: defining cell polarity for proper cell division. J. Cell Sci. 125, 516-527.doi:10.1242/jcs.096610

Therond, P., Busson, D., Guillemet, E., Limbourg-Bouchon, B., Preat, T.,Terracol, R., Tricoire, H. and Lamour-Isnard, C. (1993). Molecular organization and expression pattern of the segment polarity gene fused of *Drosophila melanogaster*. Mech. Dev. 44, 65-80. doi:10.1016/0925-4773(93)90017-R

Vasudevan, K. K., Song, K., Alford, L. M., Sale, W. S., Dymek, E. E., Smith, E. F.,Hennessey, T., Joachimiak, E., Urbanska, P., Wloga, D. et al. (2015). FAP206 is a microtubule-docking adapter for ciliary radial spoke 2 and dynein c. Mol. Biol.Cell 26, 696-710. doi:10.1091/mbc.E14-11-1506

Watanabe, A., Kurasawa, Y., Watanabe, Y. and Numata, O. (1998). A new *Tetrahymena* actin-binding protein is localized in the division furrow. J. Biochem.123, 607-613. doi:10.1093/oxfordjournals.jbchem.a021980

Wickstead, B. and Gull, K. (2006). A “holistic” kinesin phylogeny reveals new kinesin families and predicts protein functions. Mol. Biol. Cell 17, 1734-1743.doi:10.1091/mbc.e05-11-1090

Williams, N. E., Tsao, C.-C., Bowen, J., Hehman, G. L., Williams, R. J. and Frankel, J. (2006). The actin gene ACT1 is required for phagocytosis, motility, and cell separation of *Tetrahymena thermophila*. Eukaryot. Cell 5, 555-567. doi:10.1128/EC.5.3.555-567.2006

Wilson, C. W., Nguyen, C. T., Chen, M.-H., Yang, J.-H., Gacayan, R., Huang, J.,Chen, J. N. and Chuang, P. T. (2009). Fused has evolved divergent roles invertebrate Hedgehog signalling and motile ciliogenesis. Nature 459, 98-102.doi:10.1038/nature07883

Yasuda, T., Numata, O., Ohnishi, K. and Watanabe, Y. (1980). A contractile ring and cortical changes found in the dividing *Tetrahymena pyriformis*. Exp. Cell Res.128, 407-417. doi:10.1016/0014-4827(80)90076-2

Zhou, Y., Fu, L., Mochizuki, K., Xiong, J., Miao, W. and Wang, G. (2022). Absolute quantification of chromosome copy numbers in the polyploid macronucleus of *Tetrahymena thermophila* at the single-cell level. J. Eukaryot. Microbiol. 69,e12907. doi:10.1111/jeu.12907

Zitouni, S., Nabais, C., Jana, S. C., Guerrero, A. and Bettencourt-Dias, M.(2014). Polo-like kinases: structural variations lead to multiple functions. Nat. Rev.Mol. Cell Biol. 15, 433-452. doi:10.1038/nrm3819

Figure legends

Fig. 2.1. Anterior-posterior patterning during cell division in *Tetrahymena.* The diagram (modified from fig. 11 in Cole and Gaertig, 2022 with permission from Wiley; ©2022 The Authors. Journal of Eukaryoti Microbiology published by Wiley Periodicals LLC on behalf of International Society of Protistologists) summarizes the course of cell division in *Tetrahymena*, the localizations of CdaH and other pattern regulators and interactions among them. Stages: 1, interphase; 2, early oral primordium (Gao et al.) development; 3, midstage of OP development (shortly before the cortical subdivision); 4, cortical subdivision; and5, cytokinesis and morphogenesis of new cell ends. A/P, anterior–posterior; cvp, contractile vacuole pores; cyp, cytoproct; m1, m2 and m3, membranelles; oa, oral apparatus; op, oral primordium; um, undulating membrane.

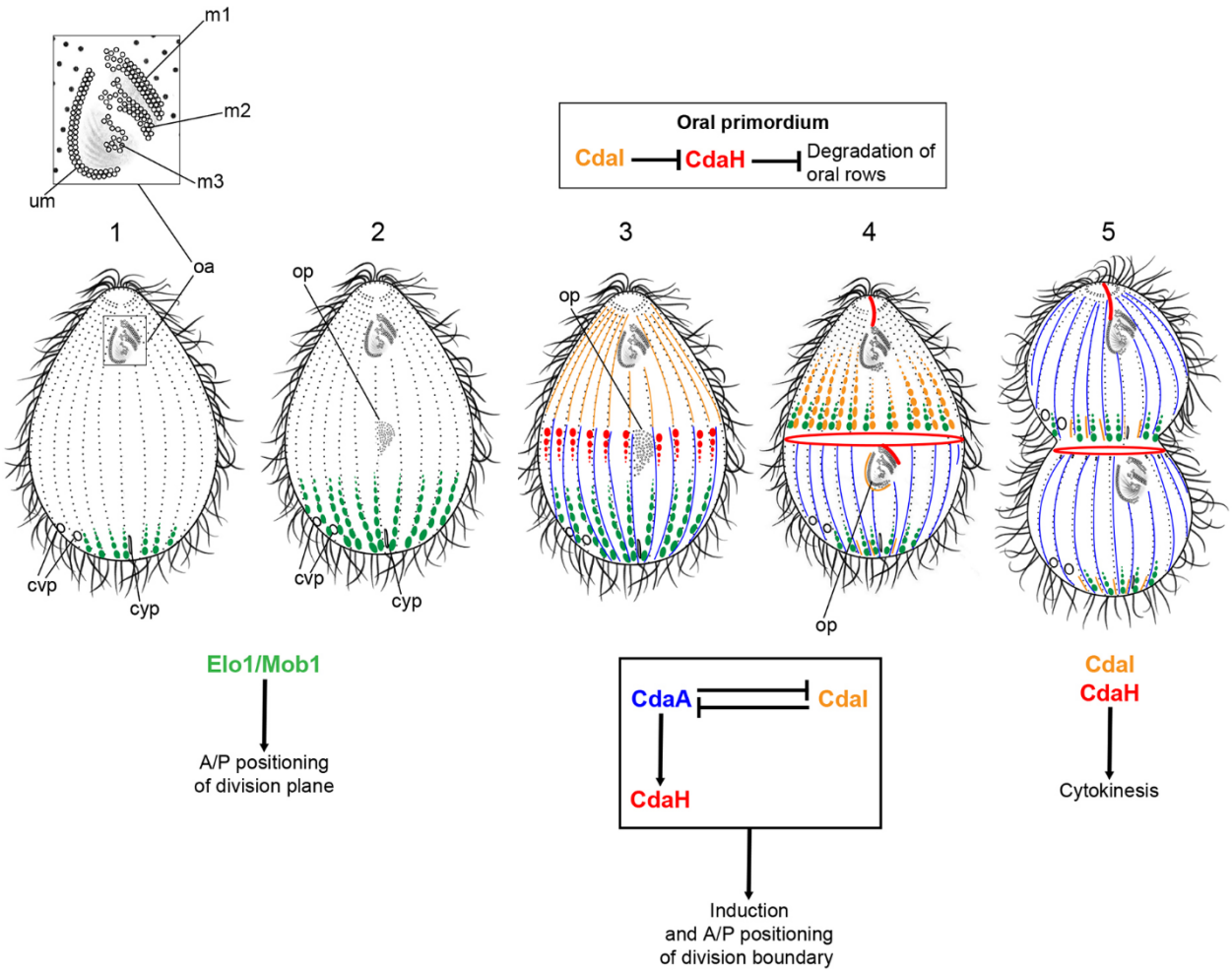
m1
m2
m3
um
1
2
3
4
5
oa
op
cvp
cyp
Oral primordium
Cdal
CdaH
Degradation of oral rows
Elo1/Mob1
A/P positioning of division plane
CdaA
Cdal
CdaH
Induction and A/P positioning of division boundary
Cdal
CdaH
Cytokinesis

Fig. 2.2. *cdaH-1* confers temperature-sensitive defects in patterning during cell division. (A–N) Representative SR-SIM images of *cdaH-1* mutants labeled with the 20H5 anti-centrin antibody (green) and DAPI (blue), grown at either 22°C (A–E,K) or 39°C (F–J,L–N). Cells documented in panels A–J,O,P were exposed to 39°C for 3 h, whereas those shown in panels K–N,Q were exposed to 39°C for 1 h. The images are representative of three (A–J) and two (K–N) independent experiments, respectively. ac, apical crown; cs, cortical subdivision; ma, macronucleus; mi, micronucleus; oa, oral apparatus; op, oral primordium; op1, op2, first and second-generation oral primordium, respectively. Scale bars: 20 μm. (O–Q) Quantitative analyses of phenotypic defects in the *cdaH-1* mutants. (O) The frequencies of cells with an OP abnormally close to the old OA. (P) The average number of OAs (old and new) per cell. The asterisks mark significant differences between the datasets ($P<0.05$ using a two-tailed unpaired t-test). The bars represent mean±s.d. The numbers of cells scored are displayed. (Q) The graph documents the frequency of *cdaH-1* cells blocked either before or after the stage of cortical subdivision (during cytokinesis). The quantitative data shown in panels O–Q were obtained by scoring dividing cells in two independent experiments.

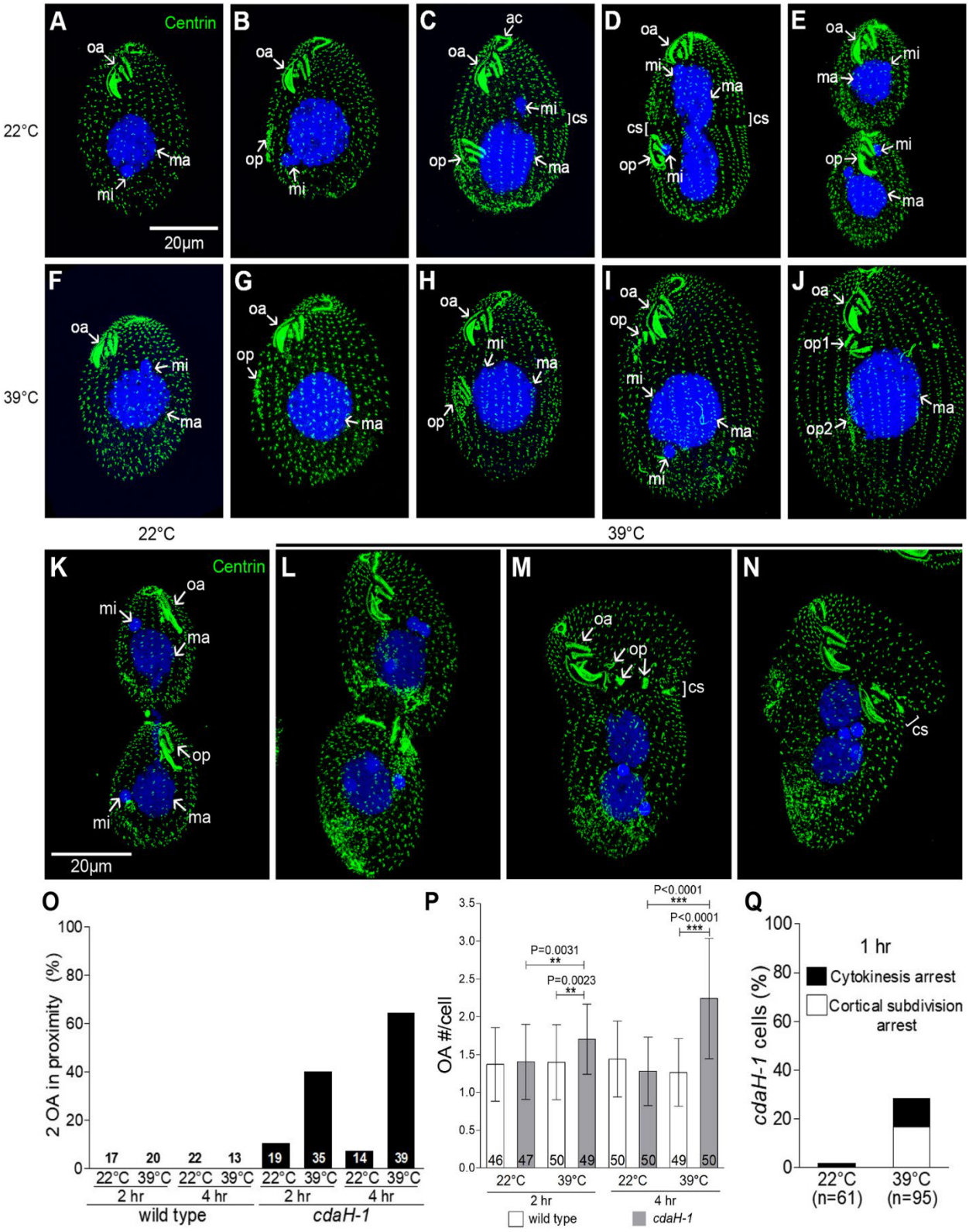
A
Centrin
oa
ma
mi
20μm
B
op
C
ac
]cs
D
cs[
E
F
G
H
I
J
op1
op2
22°C
39°C
K
L
M
N
O
2 OA in proximity (%)
17
20
22
13
19
35
14
39
2 hr
4 hr
wild type
cdaH-1
P
OA #/cell
P=0.0031
P=0.0023
P<0.0001
46
47
50
49
Q
1 hr
Cytokinesis arrest
Cortical subdivision arrest
cdaH-1 cells (%)
22°C (n=61)
39°C (n=95)

Fig. 2.3. Mapping of the *cdaH-1* causal mutation to *TTHERM_01345780.* (A) Mapping of genomic sequence variants linked to *cdaH-1* onto the micronuclear genome by the ACCA method. (B–D) A wild-type *TTHERM_01345780* fragment rescued the *cdaH-1* phenotype by homologous DNA recombination. *cdaH-1* negative control (B) and rescue clone cells (C) maintained at 38°C and fluorescently labeled using anti-centrin (green) and DAPI (blue). Note a dividing cell with a proper fission line in the rescue population (arrow). The images are representative of three experiments. Scale bar: 40 μm.(D) Culture growth curves of *cdaH-1* cells (IA450) and two *cdaH-1+TTHERM_01345780* rescue clones. The cultures were initially grown at 25°C and transferred to 38°C at the time indicted by the arrow. The data points and error bars are the mean±s.d. from three independent experiments. (E) DNA sequencing chromatograms of an amplified region of *TTHERM_01345780* containing the *cdaH-1*-linked variant (arrows). The top panel is the original sequence in the *cdaH-1* mutant (IA450), whereas the two bottom panels show the same sequence in the two independent rescue clones. (F) Domain organization of CdaH and Fused (Cole et al.)/Stk36 orthologs.

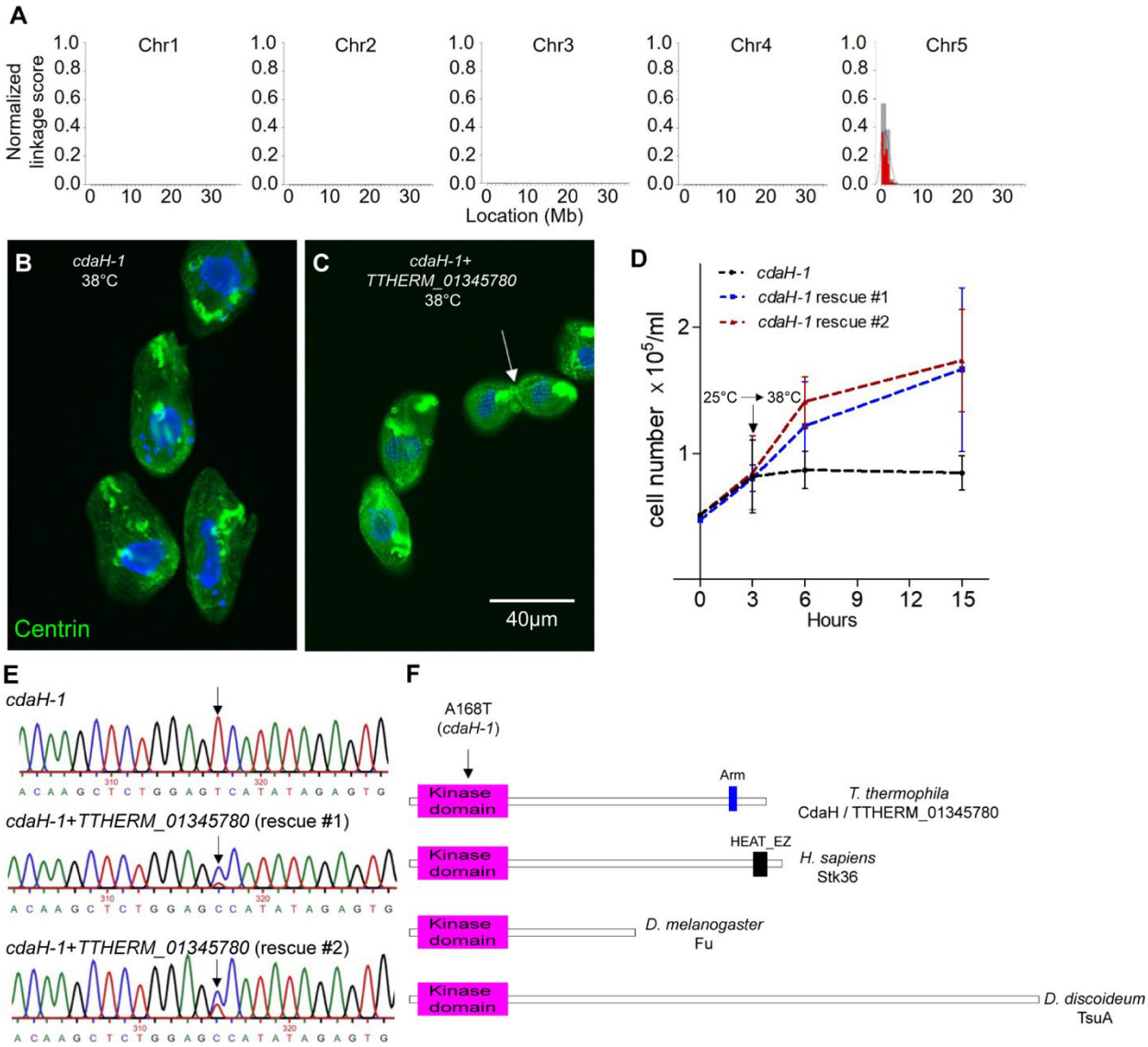
A
Chr1
Chr2
Chr3
Chr4
Chr5
Normalized linkage score
Location (Mb)
B
cdaH-1
38°C
Centrin
C
cdaH-1+
TTHERM_01345780
38°C
40µm
D
cdaH-1
cdaH-1 rescue #1
cdaH-1 rescue #2
25°C → 38°C
cell number x 10^5/ml
Hours
E
cdaH-1
cdaH-1+TTHERM_01345780 (rescue #1)
cdaH-1+TTHERM_01345780 (rescue #2)
F
A168T
(cdaH-1)
Kinase domain
Arm
T. thermophila
CdaH / TTHERM_01345780
HEAT_EZ
H. sapiens
Stk36
D. melanogaster
Fu
D. discoideum
TsuA

Fig. 2.4. CdaH–GFP accumulates at multiple locations during cell division. Confocal images of cells expressing CdaH–GFP, arranged according to the cell cycle stage. The cells were labeled by anti-GFP (magenta) and anti-centrin (green) antibodies and DAPI (blue). (A,A′) Interphase. Note that antibodies frequently bind to the OA, especially its posterior region, resulting in background fluorescence (Jiang et al., 2017). (B–C′) Early OP development. (D,D′) Onset of cortical subdivision. The OP is in an advanced stage, and all rows are visible. (E–H′) Cytokinesis and formation of new cell ends. (I–J′) Scission. The images are representative of five independent immunofluorescence experiments. as, anterior suture; c, BB couplet; cs, cortical subdivision; m1a, M1 arc; op, oral primordium; um, undulating membrane. Scale bar: 20 μm.

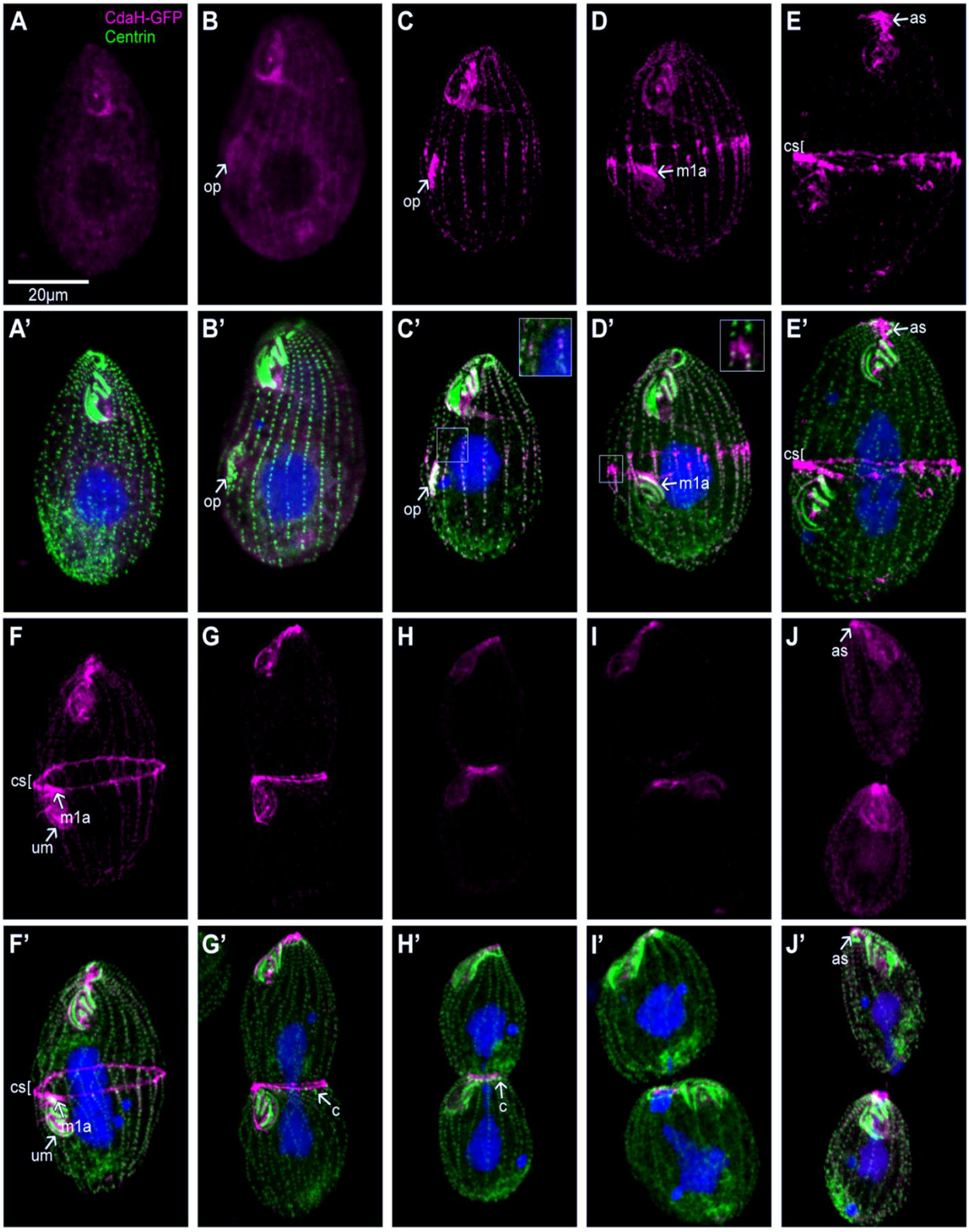
A
CdaH-GFP
Centrin
20µm
B
op
C
op
D
m1a
E
as
cs[
A'
B'
op
C'
op
D'
m1a
E'
as
cs[
F
cs[
m1a
um
G
H
I
J
as
F'
cs[
m1a
um
G'
c
H'
c
I'
J'
as

Fig. 2.5. TIRF imaging of CdaH–GFP. Live cells expressing CdaH–GFP were imaged after partial immobilization. Red arrows mark the anterior–posterior cell axis. (A–E) Still images of the peri-equatorial region shortly before or at the onset of cortical subdivision (A), and during early (B,C) and late (D,E) stages of cytokinesis. (F–F″) Within the posterior streaks, CdaH–GFP forms a concentration gradient decreasing toward the posterior cell end. F and F′ show the same image. F″ is a signal intensity plot along a single streak marked in F′ with a yellow line. In F′,F″, red arrowheads orient the density plot. (G,G′) Fluorescence recovery after photobleaching (FRAP) experiments reveal that CdaH–GFP within the ring turns over. Following bleaching with a focused laser beam, the signal intensities were analyzed using kymograms. The quantitative analysis of the signal intensity during FRAP is shown in G′. The data are representative of observations done on three cells in the ring stage (in two independent experiments). A, anterior cell end; P, posterior cell end. Scale bars: 10 μm (A–E, kymogram in G); 5 μm (F–F″); 20 μm (G, still images).

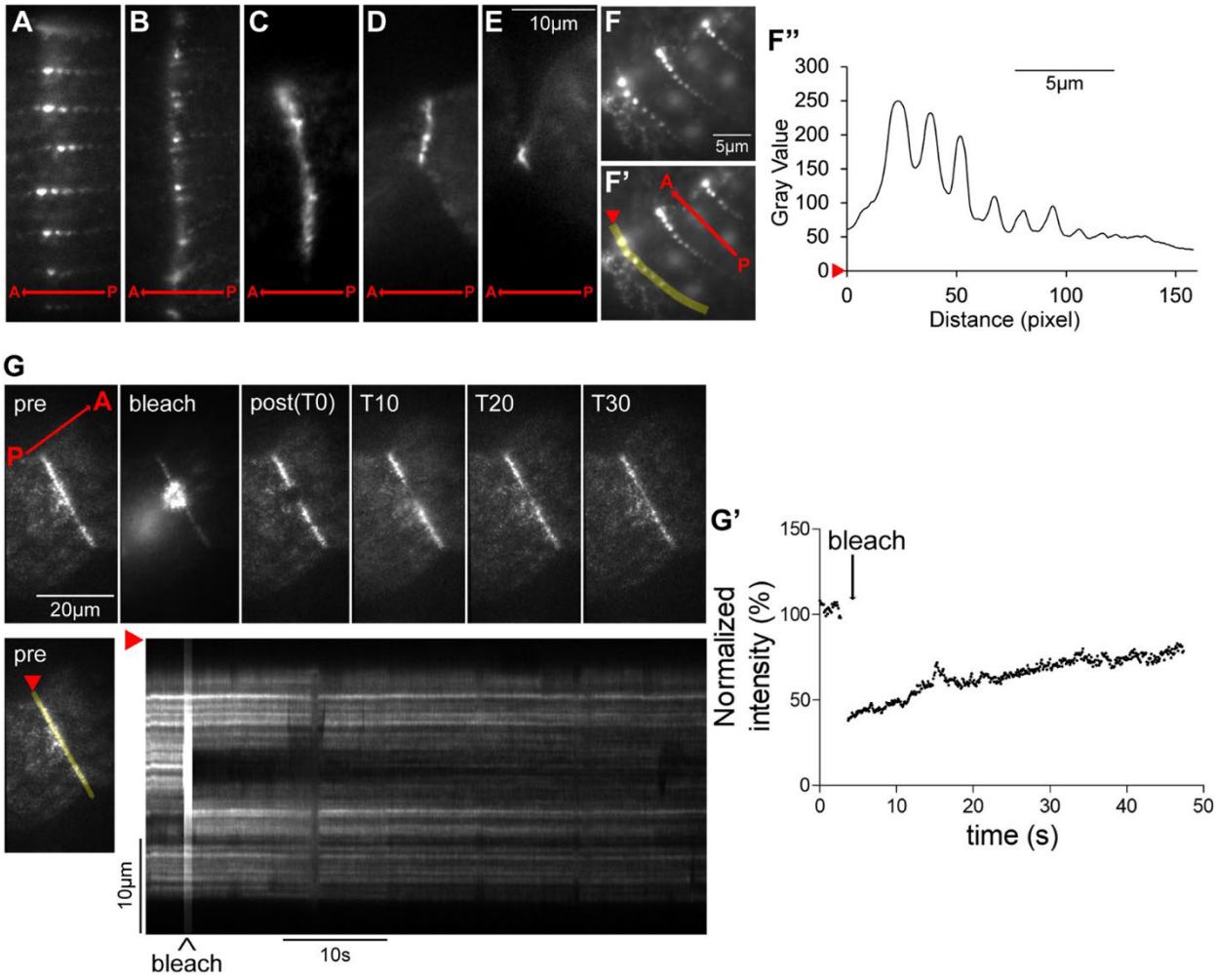
A
B
C
D
E
10μm
F
5μm
F'
A
P
F"
300
250
200
150
100
50
0
5μm
Gray Value
0
50
100
150
Distance (pixel)
G
pre
A
P
bleach
post(T0)
T10
T20
T30
20μm
pre
10μm
bleach
10s
G'
150
100
50
0
bleach
Normalized intensity (%)
0
10
20
30
40
50
time (s)

Fig. 2.6. CdaH–GFP colocalizes with actin at the anterior margin of the posterior daughter cell. (A–F″) The CdaH–GFP-expressing cells were fixed with cold methanol and labeled with polyclonal anti-Act1 actin antibodies (green) and CdaH–GFP was imaged directly (magenta).(A–A″) Cortical subdivision prior to cytokinesis.(B–E″) Stages of cytokinesis. (F–F″) An early posterior post-divider. The images shown in panels A–F″ are representative of four independent experiments. (G–H″) SR-SIM images of cells fixed with paraformaldehyde in alate stage of cytokinesis around at the time of scission (G–G″) and of a posterior post-divider shortly after scission (H–H″) labeled with anti-GFP (magenta), anti-Act1 (green) and DAPI(blue). Note that, using this fixation method, the direct GFP signal of CdaH–GFP was not visible in the green channel. The images shown in panels G–H″ are representative of two independent experiments. Scale bars: 10 μm (A–F″); 20 μm (G–H″).

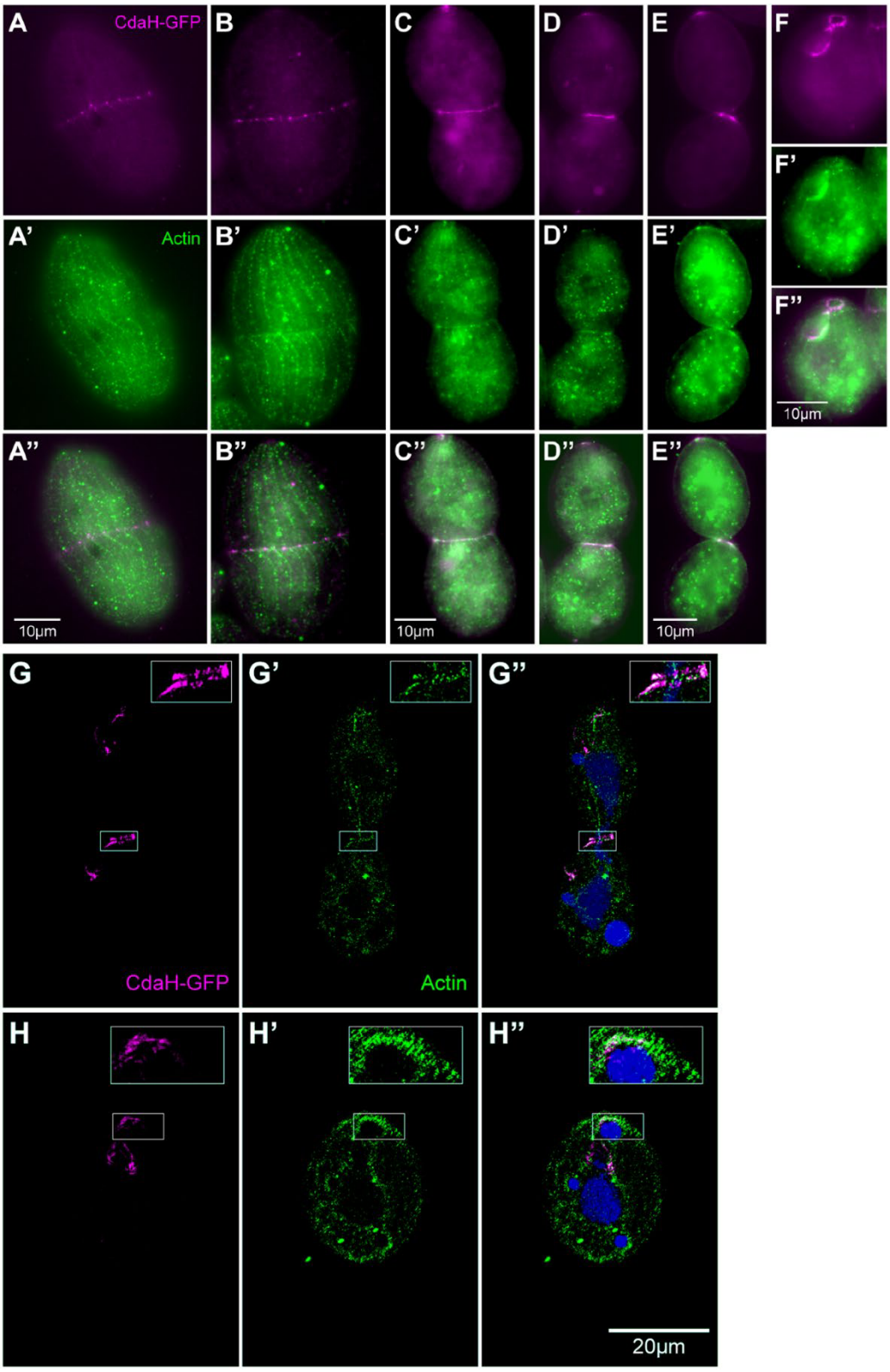
A
CdaH-GFP
B
C
D
E
F
F'
A'
Actin
B'
C'
D'
E'
F''
10μm
A''
B''
C''
D''
E''
10μm
10μm
10μm
G
G'
G''
CdaH-GFP
Actin
H
H'
H''
20μm

Fig. 2.7. CdaA, but not CdaI, is required for proper distribution of CdaH. (A–J) Confocal images of *cdaI-1* cells expressing CdaH–GFP, labeled with anti-GFP (magenta), anti-centrin (green) and DAPI (blue). Prior to staining, cells were incubated at either 22°C (A–E) or 39°C (F–J) for 2 h. (K) The graph shows the percentage of dividing cells with a (stage-appropriate) pattern of CdaH–GFP. (L–U) Confocal images of *cdaA-1* cells expressing CdaH–GFP, labeled with anti-GFP (magenta), anti-centrin (green) and DAPI (blue), incubated at either 22°C (L–P) or 39°C (Q–U) for 2 h. (V) The graph shows the percentage of dividing cells with CdaH–GFP in the form of either posterior streaks or a subequatorial ring (sub-pools associated with the cortical subdivision and cytokinesis). The images shown are representative of three independent experiments. Scale bars: 20 μm.

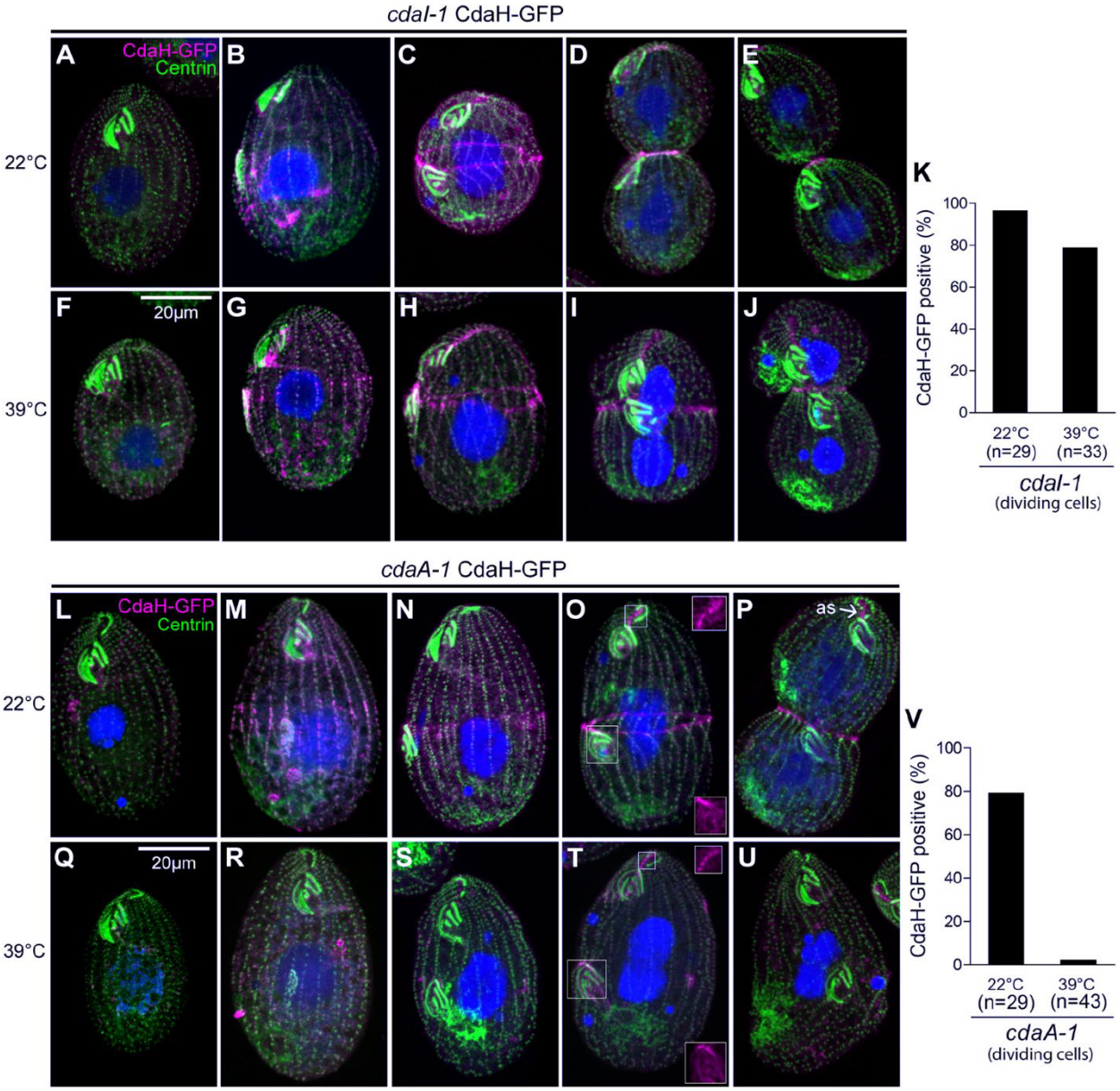
cdaI-1 CdaH-GFP
CdaH-GFP
Centrin
22°C
39°C
20µm
K
CdaH-GFP positive (%)
100
80
60
40
20
0
22°C (n=29)
39°C (n=33)
cdaI-1
(dividing cells)
cdaA-1 CdaH-GFP
as
V
22°C (n=29)
39°C (n=43)
cdaA-1
(dividing cells)

Fig. 2.8. CdaH interacts with CdaI to shape the developing oral primordium. (A–H) Representative confocal images of single- and double-mutant cells with the indicated genotypes, labeled with the anti-centrin antibody (green) and DAPI (blue) after incubation for 3–6 h at 39°C. (I–K) The graphs quantify the following phenotypes in the dividing cells at 39°C: the frequency of cells with a displaced OP (I), the frequency of cells with an OP that was either partially degraded or had extra membranelle rows in the OP (J), and the number of membranelles per OP (K). The bars indicate mean±s.d. The numbers of cells scored are displayed on bars. Phenotype scoring was done on dividing cells in two independent experiments. ns, not significant (two-tailed unpaired t-test).

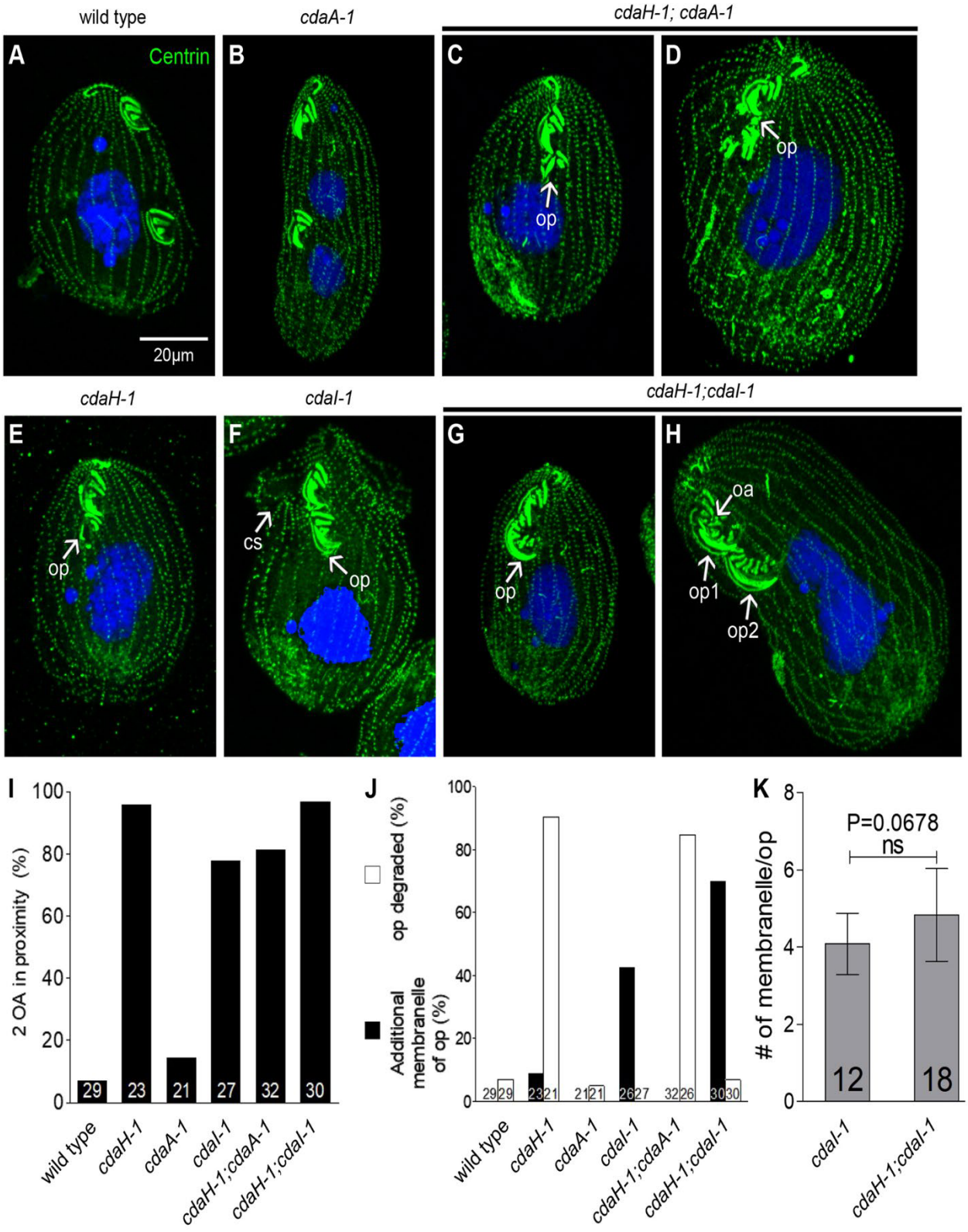
wild type
cdaA-1
cdaH-1; cdaA-1
A
Centrin
B
C
D
op
op
20µm
cdaH-1
cdaI-1
cdaH-1;cdaI-1
E
F
G
H
op
cs
op
op
oa
op1
op2
I
2 OA in proximity (%)
100
80
60
40
20
0
29
23
21
27
32
30
wild type
cdaH-1
cdaA-1
cdaI-1
cdaH-1;cdaA-1
cdaH-1;cdaI-1
J
op degraded (%)
Additional membranelle of op (%)
100
80
60
40
20
0
29 29
23 21
21 21
26 27
32 26
30 30
wild type
cdaH-1
cdaA-1
cdaI-1
cdaH-1;cdaA-1
cdaH-1;cdaI-1
K
# of membranelle/op
8
6
4
2
0
P=0.0678
ns
12
18
cdaI-1
cdaH-1;cdaI-1

Fig. 2.S1. CdaH as an STK36 ortholog. A neighbor-joining phylogenetic analysis was performed using 497 sequences of human kinase domains (Modi and Dunbrack, 2019b) and kinase domain sequences of *Tetrahymena*: CdaH/ TTHERM_01345780, TTHERM_00756520 and TTHERM_00726480. The numbers represent statistical support for branches based on 1000 bootstrap resamples. The tree is rooted to the human PLK7. The three *Tetrahymena* sequences are labeled in red.

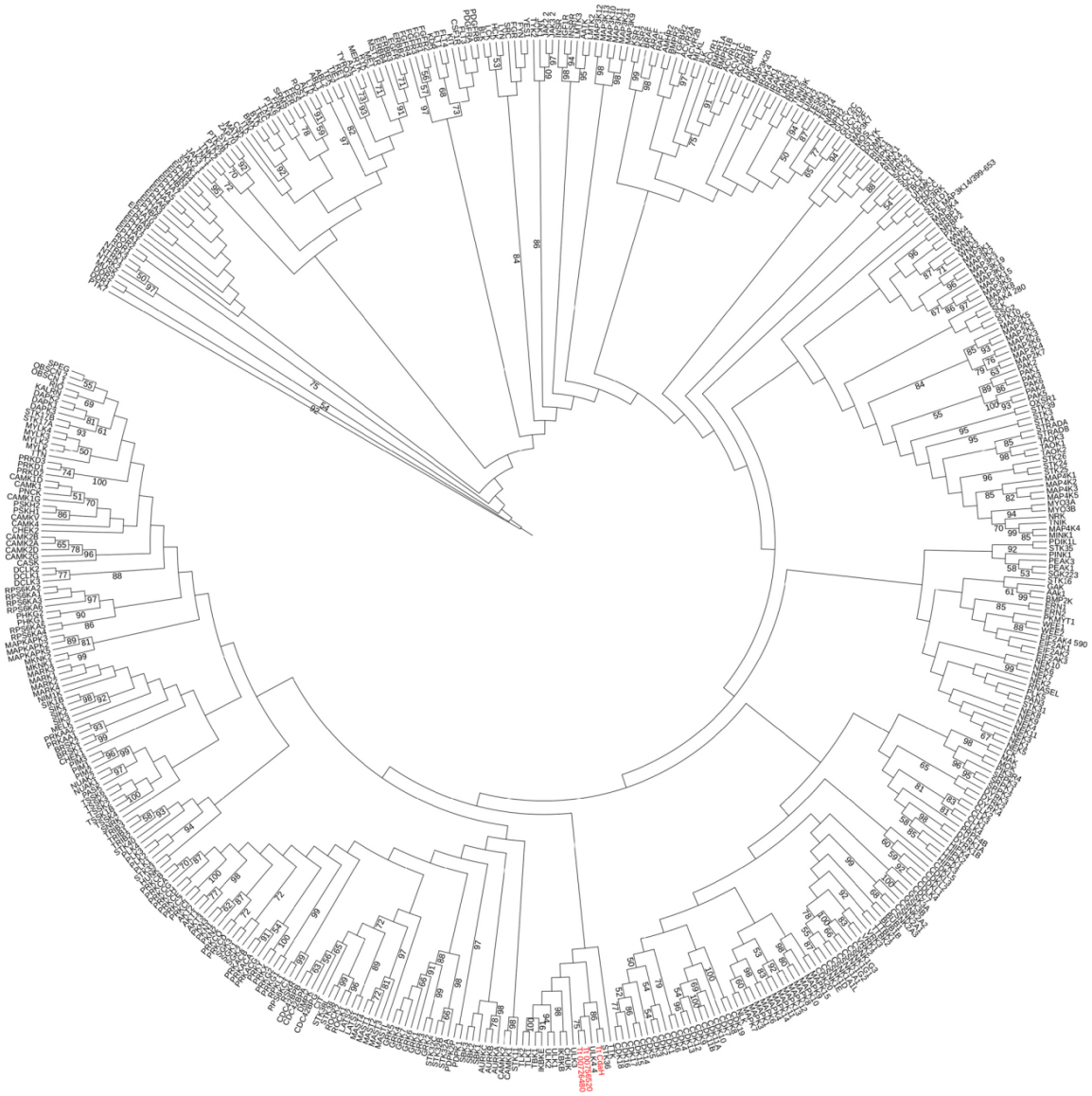

Fig. 2.S2. A multiple amino acid sequence alignment of CdaH and Fused/Stk36 orthologs. A multiple sequence alignment of CdaH, human Stk36, Fu of *D. melanogaster* and TsuA of *D. discoideum*. Note strong homology within the N-terminal kinase domain and a weaker homology outside of the kinase domains.

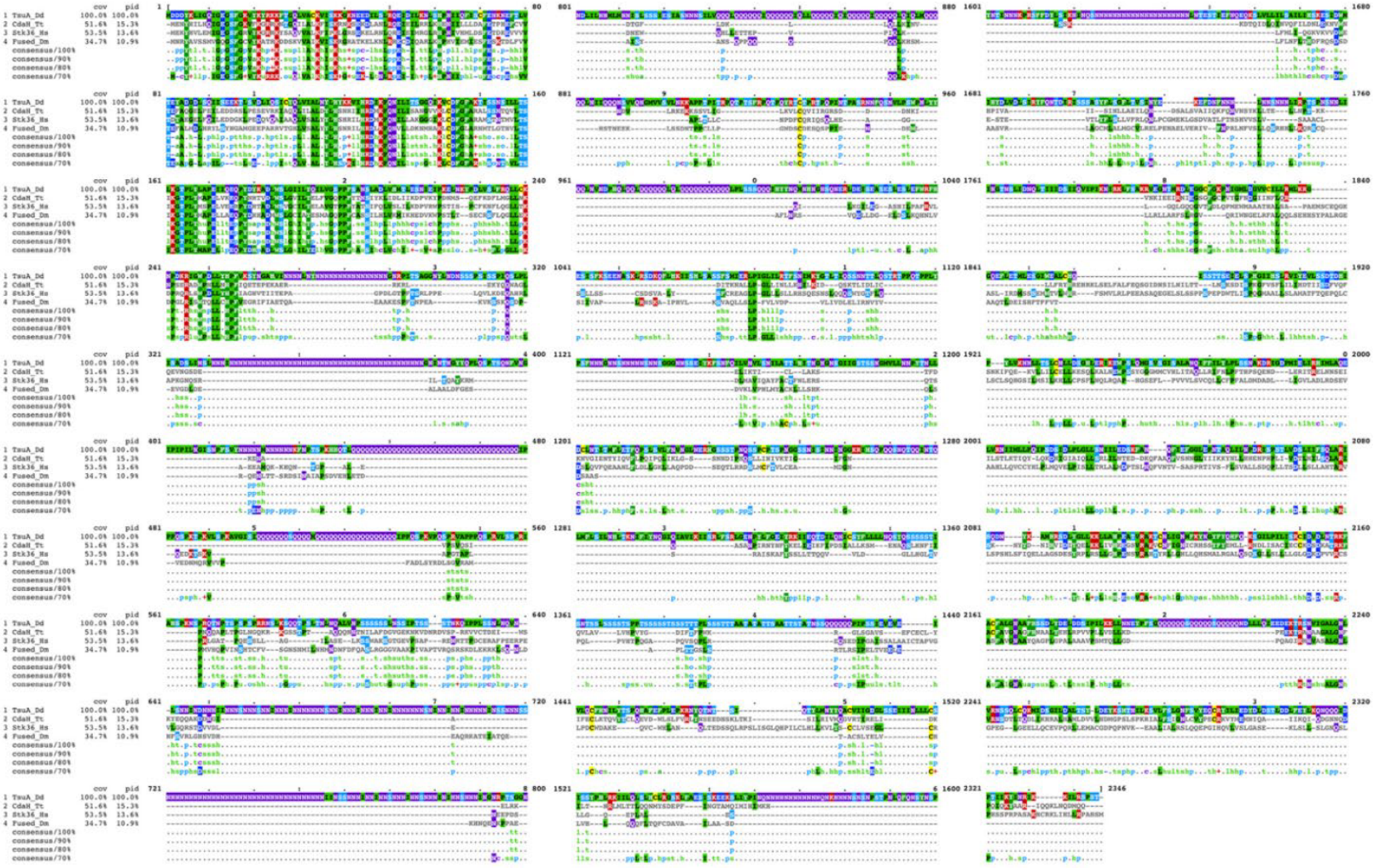

Fig. 2.S3. *cdaH-1* mutants assemble structurally normal 9+2 cilia. (A-F) Confocal images of the wild-type and *cdaH-1* mutant cells labeled by the anti-polyG tubulin antibodies (magenta), the anti-centrin antibody (green) and DAPI (blue). (G,H) Transmission electron micrographs of sections of the wild-type and the *cdaH-1* mutant cell with cross-sections of oral cilia. The images are representative. For the mutant, we analyzed a total 83 cross-sections of axonemes on multiple sections representing multiple cells.

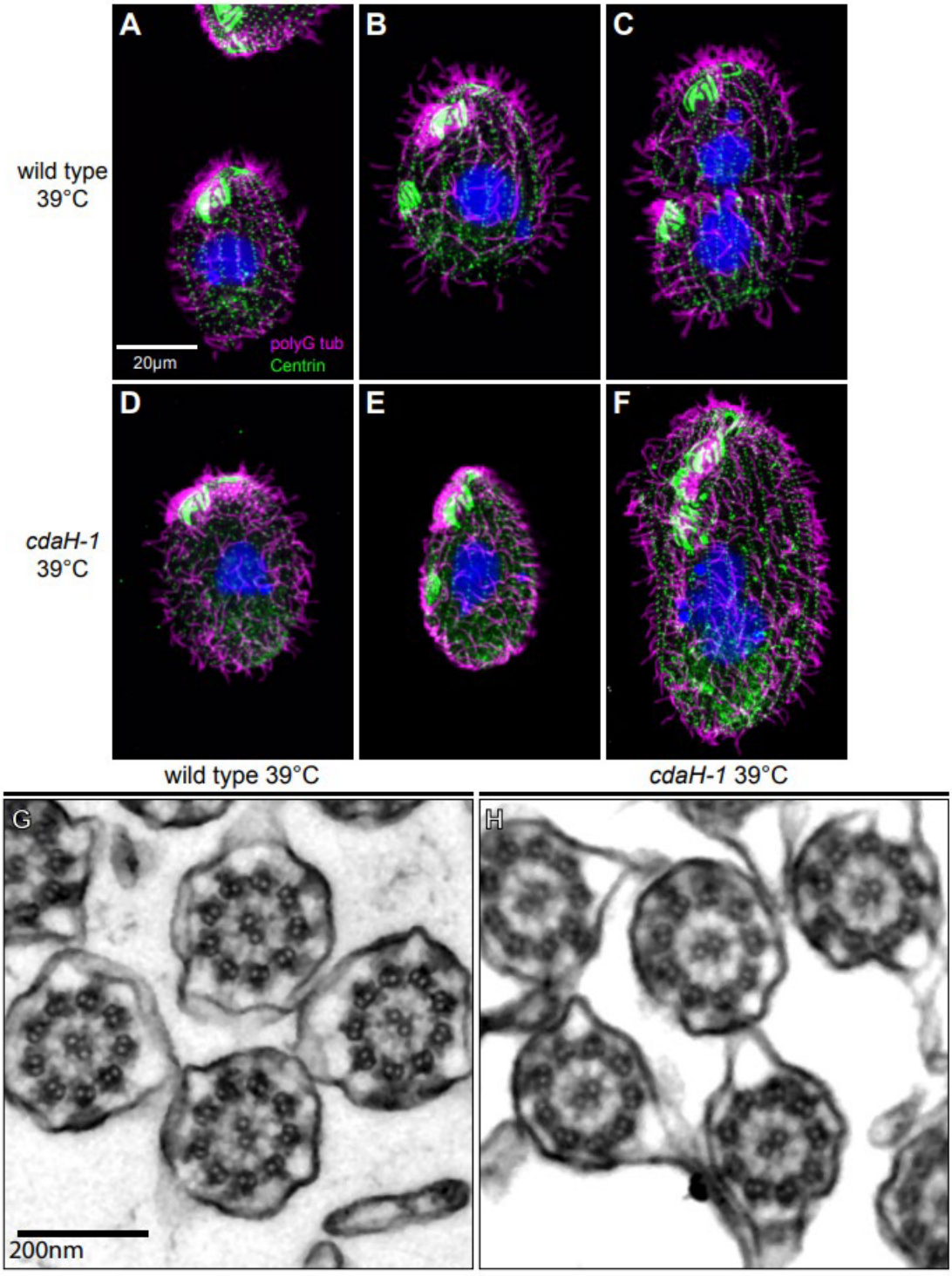
wild type
39°C
A
B
C
20µm
polyG tub
Centrin
cdaH-1
39°C
D
E
F
wild type 39°C
cdaH-1 39°C
G
H
200nm

Fig. 2.S4. SR-SIM imaging of CdaH-GFP. (A-E’’). The CdaH-GFP expressing cells were labeled by immunofluorescence using the anti-GFP antibodies (magenta), the anti-centrin antibody (green) and DAPI (blue). (A-A’’) Interphase. (B-B”) Early OP development. (C-C”) Cortical subdivision. (D-E”) Cytokinesis. Abbreviations: as, anterior suture; m1a, M1 arc; um, undulating membrane. The imaging of CdaH-GFP was conducted 5 times and representative images are displayed.

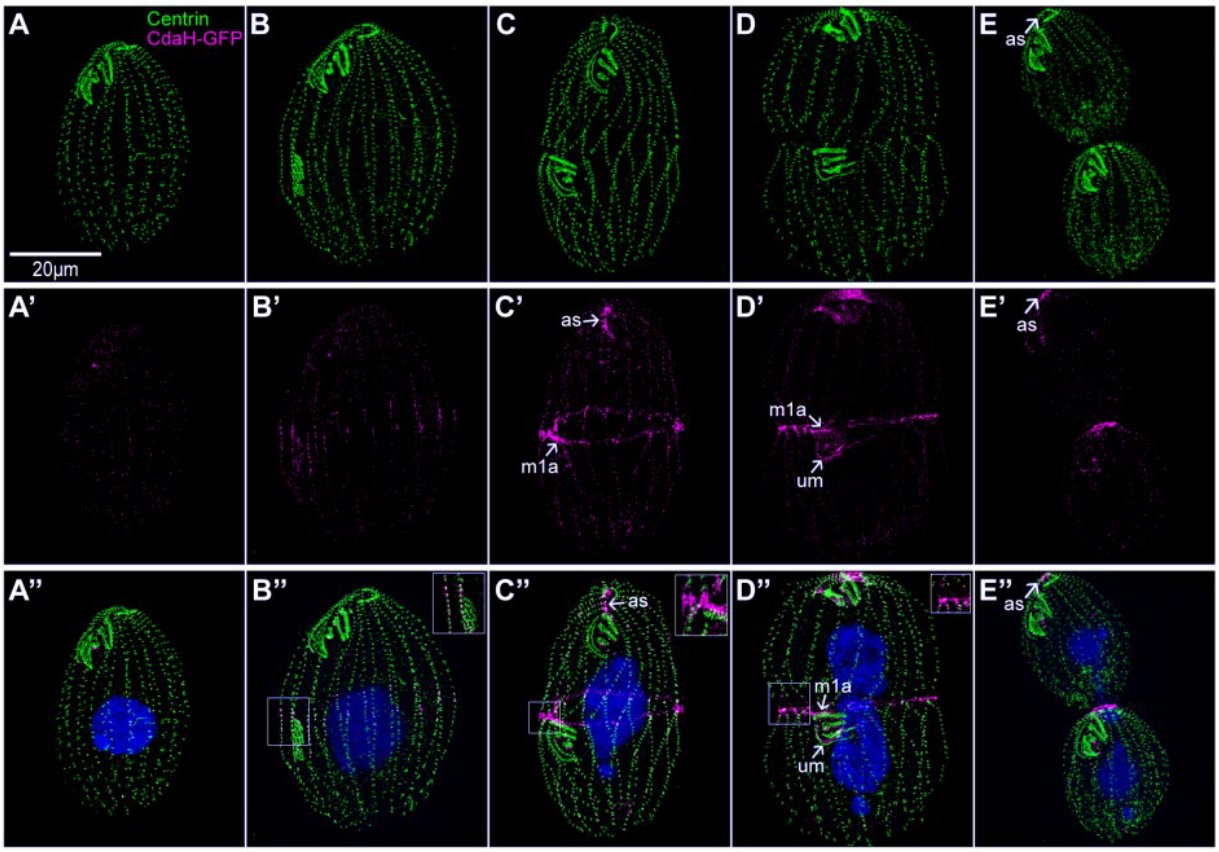
A
Centrin
CdaH-GFP
20μm
B
C
D
E
as
A'
B'
C'
as
m1a
D'
m1a
um
E'
as
A''
B''
C''
as
D''
m1a
um
E''
as

Fig. 2.S5. TIRF imaging of CdaH-GFP. (A-B'). Kymograms reveal that the dot signals are stationary and there is no detectable movement of CdaH-GFP between the dots, both along the same streak and between the streaks. The yellow lines mark the areas analyzed in the kymograms. The red arrowheads orient the kymograms. (C-C') FRAP experiment reveals that CdaH-GFP within the streak turns over rapidly. Following bleaching with a focused laser beam the signal intensities were analyzed using kymograms. Individual frame for the image showing bleach, and 10 frame average for the rest of the images. The quantitative analysis of the signal intensity in the course of FRAP is shown in C'. The data are representative of observations done on 5 cells in the posterior streaks stage. The live imaging experiments were conducted twice and representative images are shown.

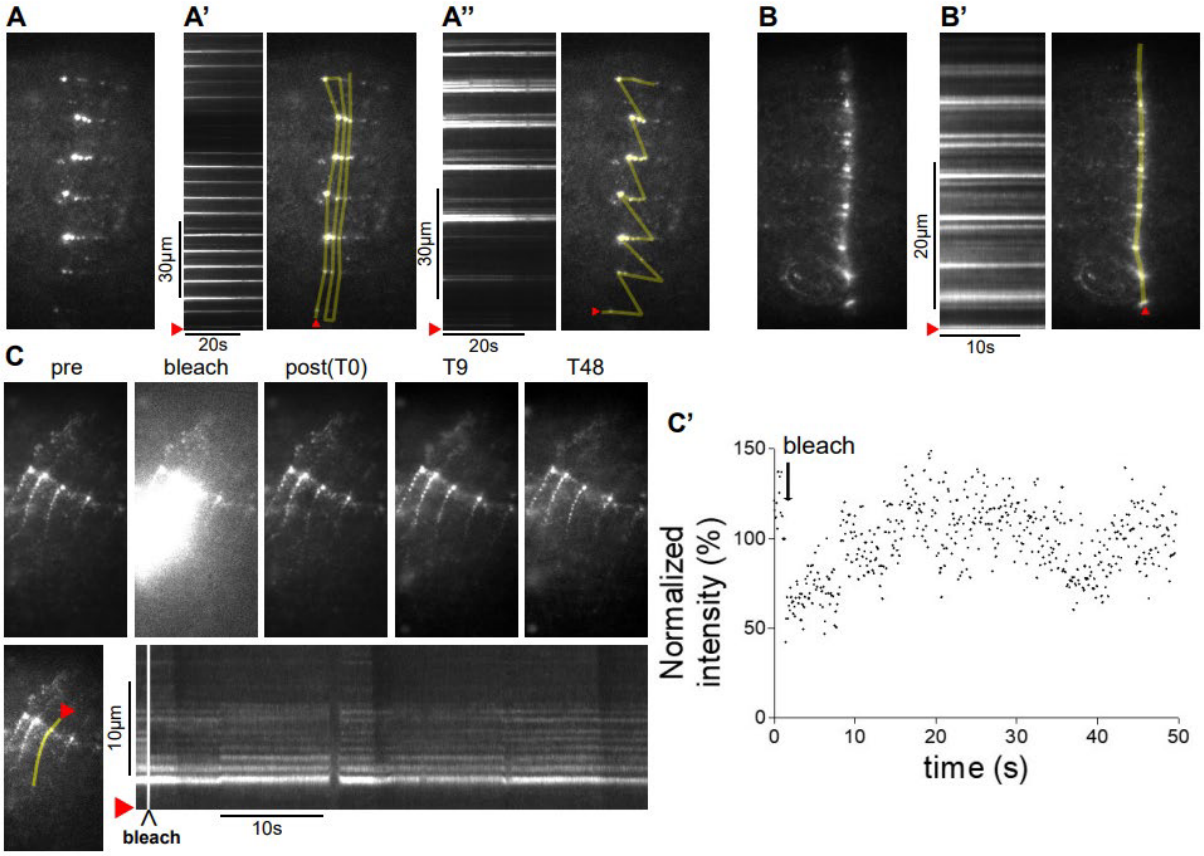
A
A'
A''
B
B'
30µm
20s
30µm
20s
20µm
10s
C
pre
bleach
post(T0)
T9
T48
10µm
bleach
10s
C'
bleach
Normalized intensity (%)
150
100
50
0
0
10
20
30
40
50
time (s)

Fig. 2.S6. A comparison of the phenotypes of single and double mutants used in this study. The following cortical structures are shown in black: oral apparatus (triangle), division boundary (horizontal bar), and contractile vacuole pore (circle). Using the same shapes, the new structures that form during cell division are shown in red. The blue arrows show the direction of displacement of the OP. The dashed line depicts OP undergoing degradation.

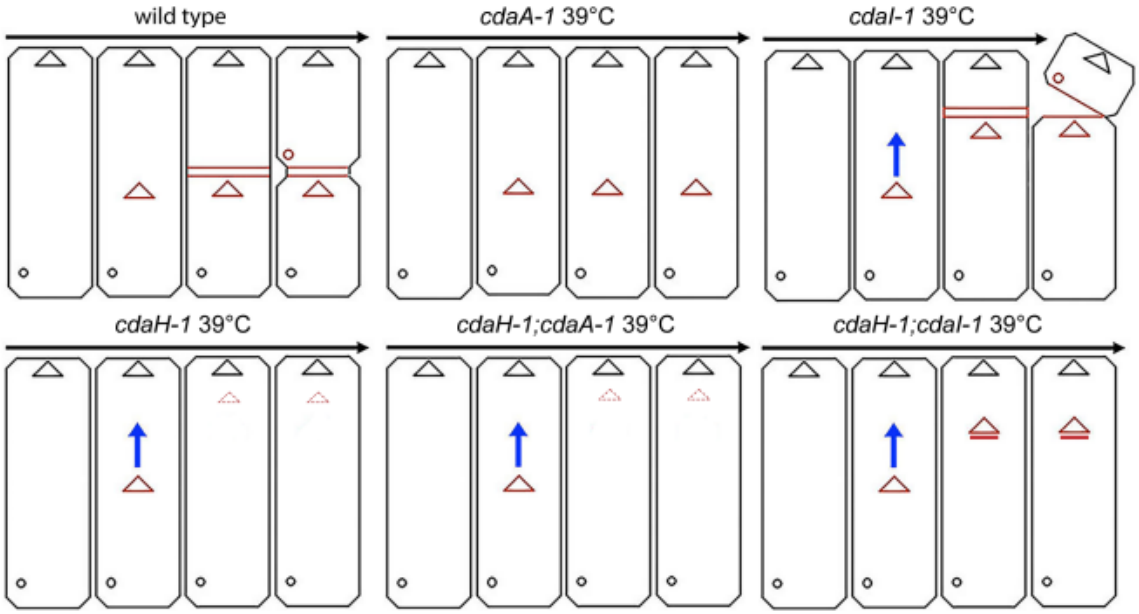
wild type
cdaA-1 39°C
cdaI-1 39°C
cdaH-1 39°C
cdaH-1;cdaA-1 39°C
cdaH-1;cdaI-1 39°C

Fig. 2.S7. *cdaH-1* expression does not affect the cortical distribution of CdaA. Confocal images of *cdaH-1* cells expressing CdaA-GFP. The cells were labeled by the anti-GFP antibodies (magenta), anti-centrin (green) antibody and DAPI (blue). Before staining, the cells were incubated at either 22°C (A-E) or 39°C (F-J) for 2 hr. (K) The graph shows the fractions of (stage appropriate) CdaA-GFP-positive dividing cells in the *cdaH-1* mutants. The representative images are derived from 3 independent experiments.

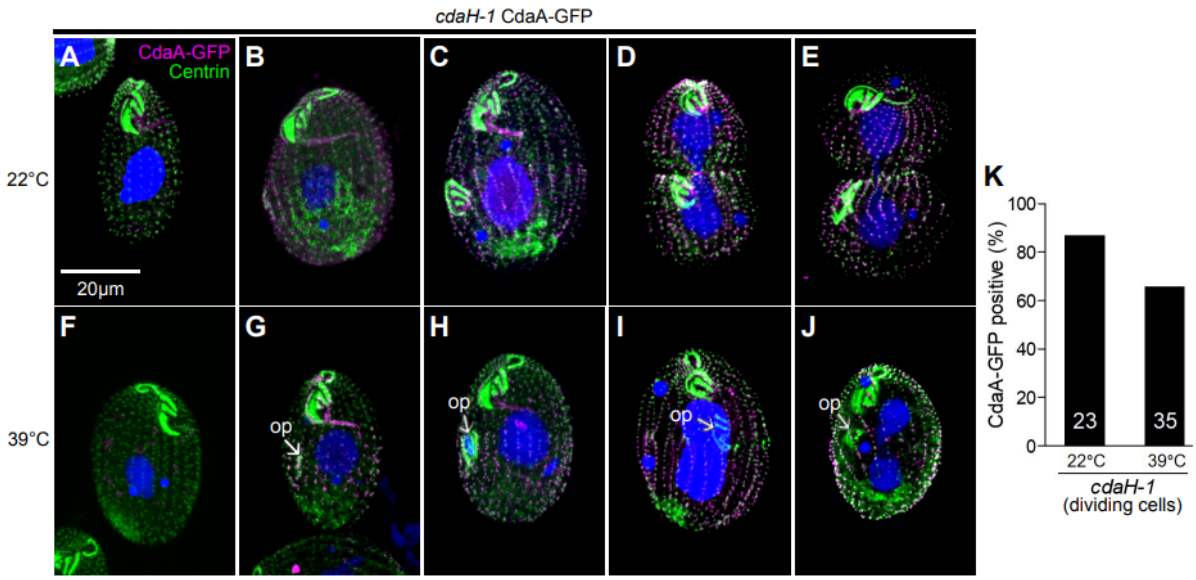
cdaH-1 CdaA-GFP
A
CdaA-GFP
Centrin
B
C
D
E
22°C
20µm
F
G
H
I
J
39°C
op
op
op
op
K
CdaA-GFP positive (%)
100
80
60
40
20
0
23
35
22°C
39°C
cdaH-1
(dividing cells)

Movies

Movie 2.1. http://movie.biologists.com/video/10.1242/jcs.261256/video-1

Movie 2.2. http://movie.biologists.com/video/10.1242/jcs.261256/video-2

CHAPTER 3

Left-right cortical interactions drive intracellular pattern formation in the ciliate *Tetrahymena*

Left-right cortical interactions drive intracellular pattern formation in the ciliate *Tetrahymena*
Chinkyu Lee, Ewa Joachimiak, Wolfgang Maier, Yu-Yang Jiang, Karl F. Lechtreck, Eric S. Cole, Jacek Gaertig
bioRxiv 2024.12.18.629246; doi: https://doi.org/10.1101/2024.12.18.629246

To be submitted to PLOS Genetics

SUMMARY
In ciliates, cortical organelles are positioned at precise locations along two polarity axes: anterior-posterior and circumferential (lateral). We explored the poorly understood mechanism of circumferential patterning, which generates left-right asymmetry. The model ciliate *Tetrahymena* has a single anteriorly-located oral apparatus. During cell division, a single new oral apparatus forms near the equator of the parental cell and along the longitude of the parental organelle. Cells homozygous for *hypoangular 1* (*hpo1*) alleles, assemble multiple oral apparatuses positioned either to the left or right flanking the normal oral longitude. We identified *HPO1* as a gene encoding an ARMC9-like protein. Hpo1 colocalizes with ciliary basal bodies, forming a bilateral concentration gradient with the high point on the cell's right side and a sharp drop-off that marks the longitude at which oral development initiates on the ventral side. Hpo1 acts to exclude oral development from the cell's right side. Hpo1 interacts with the Beige-Beach domain protein Bcd1, a cell's left side-enriched factor, whose loss also confers formation of multiple oral apparatuses. A loss of both Hpo1 and Bcd1 is lethal and profoundly disrupts both positioning and organization of the forming oral apparatus (including its internal left-right polarity). We conclude that in ciliates, the circumferential/chiral patterning involves gradient-forming factors that are concentrated on either the cell's right or left side and that the two sides of the cortex interact to create boundary effects that induce, position and shape developing cortical organelles.

Introduction

Eukaryotic cells typically have a prominent anterior-posterior (also called front-to-rear or apical-basal) polarity. In addition, some cell types, including cells that move while adhering to a substrate or single-cell metazoan embryos, also have a distinguishable dorsal-ventral polarity axis. Moreover, some cells display chiral asymmetries in reference to the anterior-posterior axis. Ciliated protists have features that are favorable for exploring how multiple

polarities and chiral asymmetries are generated in the cell. In the genetic model ciliate *Tetrahymena thermophila* cortical organelles occupy specific positions along the anterior-posterior axis and around the cell circumference (Fig. 3.1A-1). All cortical structures are duplicated during a type of binary fission called “tandem duplication”, in the course of which a single parental cell is subdivided into two daughter cells arranged head-to-tail (Fig. 3.1A). The anterior daughter cell assembles new posterior organelles while the posterior daughter cell assembles new anterior organelles. A new oral apparatus (oral primordium) forms on the ventral surface near the future anterior end of the posterior daughter cell (Fig. 3.1A-2). Remarkably, the primordium almost always assembles in association with basal bodies of a single specific ciliary row (row 0, Fig. 3.1B). The anterior-posterior position of the oral primordium is regulated by a set of conserved cortical proteins, (including components of the Hippo signaling pathway) that appear to act by marking cortical domains where organelle assembly is disallowed (reviewed by Cole and Gaertig (2022)). The principles of lateral positioning (around the circumferential axis) are less understood but could be exceptionally revealing as the responsible mechanism must generate precise coordinates in the absence of structural landmarks available for the anterior-posterior positioning (such as cell ends). Furthermore, studies in ciliates may provide insights into mechanisms that generate chiral asymmetries. In multicellular models, mutations in cytoskeletal proteins (including myosin, α-tubulin and β-tubulin) can invert the left-right positioning of body organs ((Hatori et al., 2014; Hozumi et al., 2006; Ishida et al., 2007; Speder et al., 2006), reviewed in (Inaki et al., 2016)). Intriguingly in ciliates, alterations of left-right organelle positioning can be caused by mutations in non-cytoskeletal proteins (including a protein associated with vesicle trafficking and a kinase (Cole et al., 2023; Cole, 2024)) or by trauma that alters the cortical organization in a way that is epigenetically heritable across multiple cell generations (Nelsen and Frankel, 1989; Nelsen et al., 1989).

Tetrahymena thermophila is a fast growing ciliate that is widely used as a genetic model with both reverse (Yao and Yao, 1991) and forward (Galati et al., 2014) genetics strategies. A library of unique *Tetrahymena* mutants with defects in cortical patterning has been developed and extensively characterized by Joseph Frankel and colleagues (University of Iowa) (Frankel, 1989; Frankel, 2008). The mutants of interest here are those in which the principal defect is in the positioning of organelles around the circumferential axis. The *hpo1* and *bcd1* alleles (Cole et al., 1987; Cole et al., 2023; Frankel et al., 1993) exhibit multiple oral primordia assembled at incorrect circumferential locations. Recently, Cole and colleagues identified the *BCD1* gene product as a Beige-BEACH domain protein orthologous to the mammalian NBEA and Rugose of *D. melanogaster*. Bcd1 is enriched on the cell's left side and appears to act by regulating the balance between delivery and retrieval of organelle assembly components through endocytosis and exocytosis, to control the size of cortical domains competent for organelle formation (Cole et al., 2023). Here, we used comparative next generation sequencing (NGS) to identify *HPO1* as a gene encoding a protein similar to ARMC9, a highly conserved ciliary distal tip protein. Remarkably, Hpo1 is enriched on the *Tetrahymena* cell's right side where it forms a bilateral concentration gradient that diminishes both dorsally and ventrally. Oral development occurs at positions at which Hpo1 levels drop abruptly. Our data suggest that Hpo1 functions as a bidirectional repressor excluding oral morphogenesis from the cell's right lateral side. We also reveal that together, the right-side-biased Hpo1 and the left-side-biased Bcd1 are required for cell viability and that mutants lacking both proteins display diverse and severe patterning defects including local defects in the organization of cortical structures. We propose that in a ciliate, circumferential patterning involves multiple cortical subdomains formed by bilateral gradients of pattern regulators that interact with each other and act by generating cortical boundaries that define sites of organelle assembly.

Results

Hpo1 is an ARMC9-like protein, TTHERM_001276421

Tetrahymena cells have two permanent polarity axes: anterior-posterior (AP) and circumferential (C). AP polarity is reflected by an asymmetric placement of major cortical organelles: the oral apparatus (OA) near the anterior cell end, the contractile vacuole pores (CVPs) and the cytoproct near the posterior cell end (Fig. 3.1A-1). C axis polarity is revealed by asymmetric lateral positions of cortical organelles. While the cytoproct is located at the same longitude as the OA, the CVPs are located on the cell's right lateral side (Fig. 3.1A-1). During cell division new organelles form at the same cell longitudes as the preexisting organelles. The new OA (oral primordium or OP) assembles initially as a group of ciliary basal bodies (BBs) forming at a subequatorial AP position in the middle of the cell's ventral side, precisely on the left side of row 0 (Fig. 3.1A-2). BBs proliferate and form four oral ciliary rows (UM on the right and M1, M2 and M3 on the left) (Fig. 3.1A-4, 1B). In an advanced stage of oral development, a fission zone bisects all somatic ciliary rows anteriorly to the OP (Fig. 3.1A-3-5). The new CVPs and the new cytoproct form at the posterior ends of the anterior half-rows (Fig. 3.1A-5). The cell completes nuclear divisions and undergoes cytokinesis (Fig. 3.1A-5).

We adopted the longitudinal row numbering scheme after Cole and colleagues (Cole et al., 1987). The right postoral (stomatogenic) row is designated as row 0 (Fig. 3.1B). The remaining rows are numbered as +1 or higher when moving to the cell's right side or -1 or lower when moving to the cell's left side (Fig. 3.1B). *hpo1* (*hypoangular 1*) alleles disturb the positioning of oral development along the C axis (Frankel et al., 1993). While in the wild type a single OP forms near the left side of row 0, in the *hpo1* mutants, multiple OPs form near several adjacent ventral rows located to either the left (rows -1, -2…) or right (rows +1, +2…)

of the stomatogenic row 0 (Fig. 3.2B,E compare to Fig. 3.2A,D; Fig. 3.2H). One complication is that in some *hpo1* mutant cells the oral apparatus is wider than normal, which is correlated with the presence of 3 post-oral rows. In such cases we designated the middle postoral row as 0 (Frankel et al., 1993). As described by Frankel and colleagues (Frankel et al., 1993), in the *hpo1-3* mutants, the extra OPs form more frequently to the right of row 0 (Fig. 3.2B,E,H). However, when multiple OPs were present, they were located near adjacent rows, typically including row 0 or a row in the proximity of row 0. Thus, in the *hpo1* mutants, the OP positions are not random. The *hpo1* phenotype can be described as an inability to focus to OP position to a single ventral row. Also as described (Frankel et al., 1993), the severity of the *hpo1* allele phenotypes increases at 38^{o}C as compared to the standard temperature 30^{o}C (Fig. 3.2H). As oral development progresses, adjacent OPs frequently fuse into one oral field and consequently most mutant cells have a single, mature OA (OA in Fig. 3.2B,E). Intriguingly, the *hpo1* alleles also reduce the number of CVPs per cell: while most wild-type cells have two CVPs (near two adjacent rows on the right side, usually +4 and +5), *hpo1* mutant cells often have only one CVP (Frankel et al., 1993), (Fig. 3.S1B compare to Fig. 3.S1A; Fig. 3.S1H).

We used comparative NGS to map genomic variants that co-segregate with each of the four available *hpo1* alleles (*hpo1-1*, *hpo1-2*, *hpo1-3* and *hpo1-4*). Linkage peaks were consistently detected on the micronuclear chr3 around ~5 Mb (see the data obtained for *hpo1-3* in Fig. 3.3A), in agreement with the previous assignment of *hpo1-1* to chr3 using complementation tests in crosses between mutant homozygotes and nullisomic strains lacking specific micronuclear chromosomes (Frankel et al., 1993). Within the linkage peak region, we located two homozygous variants: chr3:5363773 G/A in *hpo1-1* and *hpo1-4* and chr3:5364108 T/C in *hpo1-2* and *hpo1-3* genomes, respectively. Both variants are located within the same protein-coding gene, *TTHERM_001276421*. BlastP searches identified

TTHERM_001276421 homologs in diverse ciliate species including another oligohymenophoran *Paramecium tetraurelia* (GSPATG00001303001 and 6 paralogs), and more evolutionarily-distant ciliates: the hypotrich *Oxytricha fallax* (g7224, g191167 and g3871) and the heterotrich *Stentor coeruleus* (SteCoe_23425, SteCoe_24205). While BlastP searches failed to identify proteins with significant homology outside of the ciliate phylum, the domain organization of TTHERM_001276421 resembles that of the conserved ciliary tip protein ARMC9, whose mutations cause Joubert syndrome (Latour et al., 2020; Louka et al., 2018; Van De Weghe et al., 2017). Both ARMC9 and TTHERM_001276421 have the same set of protein domains arranged in the same order (Fig. 3.3B,B'). The N-terminal one-third of TTHERM_001276421 is classified by Interpro as the ARMC9 domain (IPRO040369), within which there is a LisH domain (IPR006594), and two coiled-coil regions (Fig. 3.3B,B'). The C-terminal region contains an ARM-like domain (IPRO11989) (Fig. 3.3B,B'). Thus, it appears that TTHERM_001276421 is a ciliate lineage-specific ARMC9-like protein. The chr3:5363773 G/A variant (*hpo1-1*, *hpo1-4*) results in the S236N amino acid substitution, while the chr3:5364108 T/C variant (*hpo1-2*, *hpo1-3*) results in the F318S substitution, both within the ARM-like domain. In agreement with our findings, homozygotes for *hpo1-2* and *hpo1-3* were reported to have a similar temperature-sensitive phenotype, less severe than that of the *hpo1-1* and *hpo1-4* homozygotes ((Frankel et al., 1993), and information deposited at the *Tetrahymena* Stock Center (https://tetrahymena.vet.cornell.edu/display.php?stockid=SD01466).

To test whether *TTHERM_001276421* is the locus of *hpo1* alleles, we used homologous DNA recombination to edit *TTHERM_001276421* to encode the *hpo1-2(3)* linked F318S variant with a C-terminal 3xHA tag. Homozygotes expressing TTHERM_001276421-F318S-3xHA had the phenotype similar to the one observed in the original *hpo1-3* mutants: multiple early-stage OPs forming near adjacent ventral rows (Fig. 3.3D,D' compare to Fig. 3.3C,C') or

a single compound primordium (resulting from fusion of adjacent primordia) at a later cell division stage (Fig. 3.3E,E'). While the wild-type TTHERM_001276421-3xHA protein was enriched near anterior BBs along a subset of ciliary rows on the cell's right side (Fig. 3.3C,C') (see below for a detailed analysis of the localization pattern), the F318S variant was either not-detectable above the background (Fig. 3.3D-D') or greatly diminished but still biased to the cell's right side (Fig. 3.3E-E' compare to 3C,C'). Thus, F318S may reduce the targeting of TTHERM_001276421 protein to the cell cortex or decrease its stability. Next, we created a germ-line based strain with a deletion of *TTHERM_001276421*. The *TTHERM_001276421*-KO homozygotes showed a phenotype similar to the original *hpo1* mutants with a subtle difference: the *knockout* cells had a higher number of OPs per cell as compared to the *hpo1-3* homozygotes (Fig. 3.2C,F,G). Furthermore, while in the *hpo1-3* homozygotes the OPs were predominantly shifted to the cell's right side, in the *TTHERM_001276421*-KO cells the OPs were more frequently shifted to the cell's left side at both 30 and 38^{o}C (Fig. 3.2C,F compare to 2B,E, Fig. 3.2H). A leftward shift was reported to occur in the *hpo1-2* homozygotes grown at 39^{o}C for 24 hr (Frankel et al., 1993). Thus, the direction of the shift in the stomatogenic row position appears to depend on the degree of loss of function of Hpo1 and the original *hpo1* alleles are likely hypomorphs. Overall the phenotypes conferred by the engineered alleles are remarkably similar to the phenotypes observed in the original *hpo1* mutants (Frankel et al., 1993) and therefore we concluded that *TTHERM_001276421* is the sought *HPO1* gene.

Hpo1 forms a circumferential cortical gradient with a high point on the cell's right side

During interphase, Hpo1-3xHA was enriched near the most anterior BBs of ~6 somatic ciliary rows on the cell's right side (Fig. 3.4A-A'''). Along these rows, the levels of Hpo1-3xHA were high within the first most anterior 8-10 BBs and decreased along row length (Fig. 3.4A-A'''). In addition, Hpo1 marked the BBs of the UM row in the OA (um in Fig. 3.4A'). On the

ventral side, there was an abrupt drop in the Hpo1 level between row +1 and row 0 (Fig. 3.4A-A'). This seems important because the OP starts to form in the immediate proximity of BBs of row 0 (likely by nucleation from somatic BBs of row 0 serving as templates (Allen, 1969)). In the early divider with a young OP, the Hpo1-3xHA pattern was unchanged, with a drop-off between rows +1 and 0 and the presence in UM (Fig. 3.4B-B'''). In dividers with a prominent fission line, the pattern of Hpo1-3xHA was duplicated along the AP axis (Fig. 3.4C-C'''). Namely, Hpo1-3xHA appeared along the anterior BBs of a subset of posterior ciliary half-rows on the right side of the cell, mirroring the positions of the pre-existing Hpo1-3xHA in the anterior hemi-cell (Fig. 3.4C-C'''). Thus, the C pattern of Hpo1 is faithfully propagated during the cell cycle. Observations of live cells expressing GFP-Hpo1 revealed a pattern of Hpo1 distribution consistent with the data obtained in fixed cells (Fig. 3.S2B,C). In addition to the localization at BBs, Hpo1 weakly localized at positions consistent with the microtubule bundles associated with the BBs (transverse and longitudinal microtubule bundles, Figure S2A,B,C). We did not detect displacements of GFP-Hpo1 foci.

A close inspection of the levels of Hpo1-3xHA around the cell's circumference revealed a second drop-off on the cell's dorsal side (Fig. 3.4A"-A"', B"-B"', C"-C"'). In the cells stained for fenestrin, a marker of CVPs (Cole et al., 2008; Nelsen et al., 1994), the drop-off was apparent between the second and third row past the CVP row counting clockwise (Fig. 3.5C'). To map the position of the dorsal Hpo1 drop-off more accurately, we imaged the cell's apical region in cell fragments that offered a "polar" view of the circumference (Fig. 3.4D-E). The centrin signal was nearly uniform around the cell circumference (Fig. 3.4D-E). The Hpo1-3xHA signal was highest at row +4 and decreased to almost the background level in two steps: between row +5/+6 and +7/+8. (Fig. 3.4D,D''',D'''',E).

Overexpression of Hpo1-3xHA using the cadmium-dependent promoter *MTT1*(Shang et al., 2002) resulted in strong accumulation in the cell body. However, the right-side- and anterior-biased localization of Hpo1 was still visible and cortical positioning was not disturbed (Fig. 3.S3). Likely, the biased localization of Hpo1 requires its binding to another spatially-biased cortical factor, and Hpo1, while required, is not rate-limiting for precise positioning of organelle development.

The dorsal Hpo1 drop-off marks the position where an extra oral apparatus assembles in the *janus* mutant

In the *janus* mutants (*janA*, *janB* and *janC* allelic groups), ventral structures are abnormally duplicated on the dorsal cell surface (Frankel and Jenkins, 1979; Frankel and Nelsen, 1986; Frankel and Nelsen, 1987; Jerka-Dziadosz and Frankel, 1979). The dorsal (secondary) OA is underdeveloped and often inverted in its left-right internal polarity (sOA in Fig. 3.5B; Fig. 3.S4A). The *janus* phenotype was interpreted as a global mirror-image pattern duplication (Frankel and Nelsen, 1986; Frankel and Nelsen, 1987; Jerka-Dziadosz and Frankel, 1979). In the *janC-4* homozygotes the distribution of Hpo1-3xHA was similar to that in the wild type, including an enrichment of Hpo1 on the cell's right side (Fig. 3.5A-B' compare to Fig. 3.4). The average number of rows with high Hpo1-3xHA (rows between the two drop-off positions) was elevated from 7 in the wild type to 8 in the *janC-4* homozygotes (Fig. 3.5E), but *janC-4* cells had more total rows per cell and therefore the ratio of Hpo1-enriched rows to the total cell circumference was unchanged (Fig. 3.5F). The expression of the sOA in *janus* mutants is partially penetrant (Frankel and Jenkins, 1979; Frankel and Nelsen, 1987; Jerka-Dziadosz and Frankel, 1979). Both *janC-4* mutant cells with and without a sOA had a similar number of Hpo1-enriched rows (Fig. 3.5B,B' compare to 5A,A'). Strikingly, in cells with a fully expressed *Janus* phenotype, the sOA was located at the position of the dorsal discontinuity

of Hpo1 (next to row +7 in Fig. 3.5B,B'; Fig. 3.S4). Thus, in the *janus* background, Hpo1 is a bilateral marker for oral development in the *janus* background.

The *janus* mutants also have an increased number of CVPs that often are arranged as two sets separated by 1-2 rows lacking these organelles (Frankel and Nelsen, 1986; Frankel and Nelsen, 1987). Thus, there is a correlation between the widening of the Hpo1-enriched domain and the increased number of CVPs in the *janC-4* homozygotes. The mid-point of the CVP domain was located along or close to the row with the peak level of Hpo1 in both the wild type (Fig. 3.5C') and *janC-4* cells (Fig. 3.5D').

To summarize, OA development occurs at positions where Hpo1 levels suddenly drop off while CVPs form at the peak level of the Hpo1 circumferential gradient.

Hpo1 acts bidirectionally to restrict circumferential positions competent for oral development

Based on its circumferential distribution pattern in the *janC-1* homozygotes, Hpo1 may act bidirectionally to exclude OPs from the region of its enrichment on the cell's right lateral side. To test this idea, we analyzed double mutant homozygotes, *janC-1;hpo1-3.* The double mutants presented a highly penetrant phenotype, two mature OAs were located side by side near the anterior cell end, sometimes separated by a gap of one or more ciliary rows (Fig. 3.6D compare to 6A-C). While such cells were rare in the single *janC-1* or *hpo1-3* mutants, the frequency reached 70% in the double mutants (Fig. 3.6I,J). When such twin OAs were physically adjacent to one another with no intervening gaps, they often appeared to integrate into a single, compound organelle (Fig. 3.6E). It appears that under Hpo1 deficiency, the two OAs exhibit "cortical slippage" (caused by ongoing shifts in the positions of both OPs) that eventually result in a collision of the formerly separate OPs within the *janC* cortex (a situation

predicted by (Frankel, 2008)) (Fig. 3.6K). Curiously, the direction of cortical slippage appears reversed for the two oral domains: OP slippage appears to occur to the cell right of the primary oral meridian, and to the cell left of the secondary meridian (Fig. 3.6K). Given its high frequency, the “twin OA” configuration appears relatively stable and is likely propagated during division. Occasionally we observed dividing cells seemingly in the course of “cortical slippage” where the distance between the OAs decreased within one generation; the dividing cells in Fig. 3.6F-H have two old OAs still separated by a gap, and multiple immediately adjacent OPs. Overall, these data suggest that Hpo1 acts to separate the regions competent for oral development, one of which (dorsal) is typically repressed in the wild type through action of the *Janus* gene products. These data correlate the bilateral gradient pattern of Hpo1 (described above) with its bilateral (OP excluding) activity.

Hpo1 interacts with Bcd1, a left side-enriched OP positioning factor

Bcd1 is a conserved Beige-BEACH domain protein (Cole et al., 2023) whose loss of function in *Tetrahymena* confers a phenotype superficially similar to that of *hpo1*: multiple adjacent oral primordia (Cole et al., 1987). However, while the *hpo1* alleles reduce the number of CVPs (Fig. 3.S1B,C,H), *bcd1* alleles increase the number of CVPs per cell (Cole et al., 1987; Cole et al., 2023) and (Fig. 3.S1F,H). Also, while Hpo1 is enriched on the cells’ right side, Bcd1 is enriched on the cell’s left side where it appears also to form a bidirectional circumferential gradient when viewed toward the apical cell end (See Fig. 3.5H in (Cole et al., 2023), and Fig. 3.S5A-B”’). The AP distribution of Bcd1 protein resembles that of Hpo1, high near the most anterior row segments and fading away toward the posterior row ends ((Cole et al., 2023) and Fig. 3.S5A-B”’).

The similarity of *hpo1* and *bcd1* OP phenotypes and the enrichment of Hpo1 and Bcd1 proteins on opposite sides of the stomatogenic ciliary row suggest that the two proteins act

collectively to restrict the OP formation from spreading to either the cell's right (Hpo1) or cell's left (Bcd1) of this prominent cortical landmark. To look for potential interactions between Hpo1 and Bcd1, we first examined whether a deficiency of Bcd1 (*bcd1-2*) affects the pattern of Hpo1-3xHA. In the *bcd1-2* homozygotes, the average number of Hpo1-enriched rows (rows between the discontinuities) was increased to 9 (Fig. 3.S6F) but the total number of rows per cell also increased and therefore the Hpo1-enriched domain was proportionally unchanged (Fig. 3.S6G). As in the wildtype, Hpo1 signal showed a dramatic drop-off in concentration both ventrally (near the primary oral meridian) and dorsally (Fig. 3.7B-B" compare to 7A-A"; Fig. 3.7C,E). However, the *bcd1-2* background consistently altered the AP distribution of Hpo1-3xHA. In wild type cells, the anterior-posterior Hpo1-3xHA gradient is steep, dropping to half signal intensity within ~10 BBs of the anterior cell end. In *bcd1-2* homozygotes, the AP gradient of Hpo1-3xHA remained high, only dropping to 75% signal intensity (Fig. 3.7B-B" compare to 7A-A"; Fig. 3.7D). This gradient-altering effect was observed both on the cell's ventral and dorsal side (Fig. 3.S6).

Next, we focused on whether the C distribution of Hpo1 is affected by *bcd1-2*. In wild-type cells, the ventral Hpo1 drop-off occurs between row +1 (contrast row) and row 0. In the dividing *bcd1-2* cells in which the OP fields were shifted laterally, the contrast row position was consistently shifted to the row on the right side of the right-most OP. For example, in the dividing cell shown in Fig. 3.8B-B', there are two early OPs at positions 0 and +1 and the contrast row is located to the right of the OP pair at row +2. While we have not observed clear cases of a shifted contrast row in interphase cells, there were instances of apparent ambiguity in position of the contrast row. In the cell shown in Fig. 3.8A-A', within the anterior 1/3 of the cell the contrast row is +1. However, in the posterior 2/3 of the cell the contrast row is +2. This cell has 3 postoral rows, a feature common to both *bcd1* and *hpo1* mutants that correlates with the increased OA width. However, another interphase *bcd1-2* cell shows

the same “ambiguous contrast row” phenotype in the presence of two postoral rows (Fig. 3.8D-D’). Taken together, these data reveal that the Bcd1 deficiency modifies both the AP and C pattern of Hpo1. These observations suggest that there is a cross-talk between Hpo1 and Bcd1, possibly as a boundary interaction between the right and left ventral cortical region.

No obvious effect of expression of *hpo1-3* on the distribution of Bcd1-GFP was observed but the signal of Bcd1-GFP was weak even in the wild-type background making the evaluation difficult (Fig. 3.S5C-D”’ compare to Fig. 3.S5A-B”’).

We next asked whether there is a functional interaction between Hpo1 and Bcd1 by analyzing the phenotypes of double mutants homozygous for *bcd1-2* and *hpo1-KO*. Surprisingly, the *bcd1-2;hpo1-KO* homozygotes were not viable. To test further for synthetic lethality, we attempted to rescue the progeny of mating (double mutant) heterokaryons by biolistic introduction of a transgene mediating expression of Hpo1-3xHA in an unrelated locus. A total of about 5 x 10^6 mating heterokaryon cells were either subjected to biolistic bombardment with a Hpo1-3xHA transgene or mock-transformed without plasmid DNA and selected with paromomycin (conferred by the *neo* gene embedded in the disrupted *HPO1* gene). Eighteen drug-resistant clones were isolated from the population bombarded with the Hpo1-3xHA plasmid and one clone was isolated from the mock-transformed population. Six clones from the plasmid bombarded cells were analyzed by immunofluorescence and all were positive for Hpo1-HA (Fig. 3.S7B-C’). The single clone selected in the mock-transformed population was negative for Hpo1-HA as expected (Fig. 3.S7A,A’). A PCR amplification detected a wild-type Hpo1 sequence corresponding to the portion that was deleted in the *hpo1*-KO allele in the “escapee” clone (Fig. 3.S7D,D’). Likely, in this single clone there was a transfer of the wild-type *HPO1* gene from the parental macronucleus to

the newly developing macronucleus that rescued the lethality. These observations confirm that the loss of function of Bcd1 and Hpo1 is lethal and 100% penetrant (n=5 x 10^6). Next, we evaluated how the cortical pattern changes during the transition from the wild-type to double mutant phenotype in the mass-selected progeny of mating heterokaryons. To this end, heterokaryons expressing complementary mating types were allowed to mate, refed and selected with paromomycin to kill the non-mating (phenotypically wild-type) parental cells. After 24 hr of drug selection, the double mutant progeny cells looked nearly normal except for the frequent OAs with abnormally wide oral M rows (white arrows in Fig. 3.9A). After 30-46 hr, dividing cells frequently had severely posteriorly displaced primordia (yellow arrows in Fig. 3.9B,E,F,G). In the cells with a posteriorly shifted OP, the division boundary position was variable, either also shifted to the posterior (Fig. 3.9F) or equatorial (Fig. 3.9E) or shifted anteriorly (Fig. 3.9G). Cells with a posteriorly shifted OP and an anteriorly shifted division plane may produce a posterior daughter cell with mature OA near the posterior cell end (Fig. 3.9H). At ~46 hr the cells were uniformly arrested in cell proliferation and had an abnormally elongated and curved morphology with OAs that had curved (pink arrows in Fig. 3.9C,I) or fragmented M rows (green arrows Fig. 3.9C). The somatic ciliary rows appeared excessively long, and sometimes twisted (Fig. 3.9D,H,I). SR-SIM imaging revealed additional patterning defects including OAs that lacked the UM (Fig. 3.9G,I) and OAs with M rows arranged with orthogonal orientations (small arrows in Fig. 3.9J,K). In addition, there were defects in the organization of the buccal cavity including a missing or fragmented ribbed wall of microtubules (Fig. 3.9G,I,J,K). The *bcd1-2*;*hpo1*-KO heterokaryon progeny did not grow on the specialized culture medium (MEPP) that supports proliferation of mutants lacking a functional oral apparatus (Orias and Rasmussen, 1976). Thus, the lethality is not solely caused by a lack of a functional oral apparatus. We conclude either Hpo1 or Bcd1 are required for survival and both contribute to patterning functions that extend beyond

positioning of the OP, including shaping the internal organization of the OA and controlling the longitudinal expansion of the somatic ciliary rows.

Discussion

Ciliates are well suited for studies on intracellular pattern formation but remain relatively unexplored. In *Tetrahymena*, mutations in several loci selectively affect organelle positioning along either the AP or C axes (reviewed in (Cole and Gaertig, 2022; Frankel, 2008)), suggesting that pathways operating on each of the two orthogonal polarity axes have a degree of independence. Several highly conserved kinases and kinase-binding proteins, including components of Hippo signaling, mediate organelle positioning along the AP axis (Jiang et al., 2019; Jiang et al., 2017; Jiang et al., 2020; Lee et al., 2024; Slabodnick et al., 2014; Tavares et al., 2012). The emerging view is that on the AP axis, organelle locations are determined by proteins that mark cortical domains within which new structures are not permitted to form (reviewed in (Cole and Gaertig, 2022)). These inhibitory cortical factors are either permanent (Elo1/Lats (Jiang et al., 2019)) or appear shortly before the structures form (CdaI/Mst (Jiang et al., 2017), CdaA/cyclin E (Jiang et al., 2020)). Here we made an advance toward understanding the far less explored mechanism of patterning around the cell circumference in *Tetrahymena*, by identifying the *HPO1* gene. The *hpo1* alleles disturb circumferential patterning by permitting oral development outside of the standard row 0. Over generations, the ongoing shifts in the positions of oral meridians (cortical slippage) may even produce mutant cells that have CVPs on the left cell's side, and therefore have an inverted overall "handedness" (Frankel et al., 1993).

Hpo1 is a ciliate phylum-specific BB-associated ARMC9-like protein. In *Tetrahymena* and mammalian cells ARMC9 localizes to BBs and the tips of cilia (Breslow et al., 2018; Louka et al., 2018; Van De Weghe et al., 2017). Mutations in ARMC9 cause Joubert syndrome, a

neuro-developmental ciliopathy (Latour et al., 2020; Van De Weghe et al., 2017). Likely, Hpo1 evolved by neofunctionalization of the ancestral ARMC9, following a gene duplication that occurred before the emergence of diverse ciliate subclasses. We recently identified another conserved ciliary protein, a Fused/Stk36 kinase CdaH, as a key regulator of positioning on the AP axis (Lee et al., 2024). Ciliates belong to the protist clade of Alveolata that also includes dinoflagellates and apicomplexans. Among the alveolate protists, only ciliates assemble multi-ciliated arrays. Thus, in the course of emergence of ciliates from an ancestral biciliated alveolate (Cavalier-Smith and Chao, 2004; Janouskovec et al., 2013; Orias, 1976), multiple ciliary proteins could have gained functions in the formation and patterning of ciliary rows.

Hpo1 forms concentration gradients along both cell polarity axes. Remarkably, on the circumferential axis, Hpo1 forms a bilateral concentration gradient with the high point on the cell's lateral right side and sharp drop-offs along the longitudes permissible of oral development. The pattern of Hpo1 appears invariable during the cell cycle. Hpo1 is reminiscent of Elo1, a Lats kinase that marks the posterior cell region and acts to prevent the OP from forming too close to the posterior cell end (Jiang et al., 2019). Thus, the positioning on both orthogonal polarity axes involves gradient-forming proteins that may function as pre-existing markers that define positions at which organelles assemble.

Important early insights into the mechanism of circumferential patterning were obtained using the giant ciliate *Stentor coeruleus*. *Stentor* species have formidable healing and regenerative capabilities. Fragments of *Stentor* lacking most of the cortex can regenerate a complete pattern and recover the ability to grow and divide, which argues that pre-existing cortical organelles are not an essential source of positional information for forming structures (Gruber, 1885; Morgan, 1901; Tartar, 1961). Importantly, in *Stentor*, the circumferential

surface differentiation is apparent along the entire cell length. Unlike in *Tetrahymena*, in *Stentor*, the width of the inter-row spaces (called stripes) gradually changes around the cell circumference. The narrowest stripes are located on the right side of the ventral surface and the stripe width gradually increases clockwise until the widest stripes meet the narrowest stripes within the ventral region named the “locus of stripe contrast” (LSC) (Tartar, 1956b; Uhlig, 1960). OP develops at the LSC, within the narrow stripe zone and close to the margin of the wide stripe zone (Paulin and Bussey, 1971; Pelvat and Dehaller, 1979; Uhlig, 1960). Remarkably, supernumerary OPs can be induced by cortical grafts that juxtapose a narrower stripe cortex with a wider stripe cortex, even if the boundaries of the graft would normally be far from the sites of cortical development (Tartar, 1956a). Thus, oral development occurs at locations that are characterized by a “structural contrast”. In *Tetrahymena*, Hpo1 forms a “molecular contrast” as the sharp level discontinuity between row +1 and the stomatogenic row 0. Topologically, the Hpo1-enriched region in *Tetrahymena* corresponds to the narrow stripe region in *Stentor*. Taken together, our observations and the grafting studies in *Stentor* suggest that the ventral “contrast region” contains both activating and inhibitory influences that control oral development. We speculate that the right lateral region, where Hpo1 is concentrated, is also a source of an unknown “oral activator” that is inhibited by Hpo1 (green gradient in Fig. 3.1C). Hpo1 and the oral activator gradients may overlap for most of the length except at the positions where the Hpo1 levels drop, thus creating conditions permissible for oral development (Fig. 3.1C). Consequently, (in cells having a normal Janus activity, see below) the OP can form at row 0.

By analogy to the emerging principle of positioning on the AP axis (where pattern regulators mark cortical domains where organelle assembly is inhibited), the primary activity of Hpo1 could be an exclusion of oral development from the cell’s right lateral side. Indeed in all original *hpo1* mutants (expressing alleles that are likely hypomorphs) , the extra primordia

form more frequently to the right of row 0 ((Frankel et al., 1993) and this study). Unexpectedly however, in cells with a knockout of *HPO1,* there was an increase in the frequency of extra primordia to the left of row 0. The *hpo1-2* mutants also occasionally form primordia on the left side and that the frequency of left-shifted OPs increases at 39^{o}C ((Frankel et al., 1993) and this study). We speculate that in addition to the exclusionary activity to the right of row zero, Hpo1 stimulates the exclusionary activity to the left of row 0, which requires Bcd1. Both Hpo1 and Bcd1 mutants assemble extra oral primordia on either side of row 0 ((Cole et al., 1987; Frankel et al., 1993) and this study). It is tempting to speculate that Bcd1 and Hpo1 have OP excluding activity in the areas of their enrichment (Hpo1 on the right and Bc1 on the left) and enhance each other's exclusionary activity as a boundary effect across row 0 (Fig. 3.1C).

We show that Hpo1 is organized as a bilateral gradient with drop-offs on the dorsal and ventral side. Both drop-off positions mark sites for oral development in the *janC* homozygotes. *janA* and *janB* alleles confer the same *janus* phenotype as the *janC* alleles used here (Cole et al., 1988; Frankel et al., 1984; Frankel et al., 1987). The JanA gene product was recently identified as a Polo kinase that localizes to the left-to-dorsal circumferential region, with a large overlap with Bcd1 and a partial overlap with Hpo1 on the dorsal side (Cole, 2024) (see Fig. 3.1C). Cole and colleagues propose that JanA represses the expression of ventral features on the dorsal side by interfering with a right-side enriched oral activator (Cole, 2024). We show here that in the double mutant expressing *janC-1*, a loss of Hpo1 reduces the distance between the primary and the secondary OAs. This observation suggests that Hpo1 has bilateral activity, excluding oral development from both dorsal and ventral margins of its gradient. Hpo1 suppression of dorsal oral development is masked by the over-arching Janus suppression activity. The Janus gene products may either act to modify the parameters of the Hpo1 gradient (e.g. by reducing its steepness at

the dorsal drop-off position) or suppress downstream components required for expression of oral structures. While in cells having wild-type Janus gene products, the right-sided influence of Hpo1 on the OP position is not relevant, on the dorsal side Hpo1 may engage in other positional activities, including its potential dorsal interaction with Bcd1 that may control the number of CVPs (see below).

Intriguingly, all gene products studied here in addition to their effects on oral development, also affect the number of CVPs. While all alleles used here either null or hypomorphs, *hpo1* alleles decrease while the *jan* and *bcd1* alleles increase the number of CVPs, respectively. While during cell division, the OP forms before the CVPs, it is unlikely that either the number or positions of OPs affect the number of CVPs based on the phenotypes of *hpo1* and *bcd1* mutants that affect oral development in a similar way but have opposite effects on the number of CVPs. We observed that CVPs are located at the posterior ends of rows whose anterior ends are at or near the high point of the Hpo1 circumferential gradient. Furthermore, we show that a loss of either JanC or Bcd1 expands the Hpo1-enriched domain. Both Bcd1 (Cole et al., 2023) and JanA are located in the left dorsal region (Cole, 2024) and partly overlap with Hpo1 and could act on the CVP rows indirectly by regulating the parameters of the Hpo1 gradient.

Unexpectedly, by combining null alleles *hpo1*-KO and *bcd1-2,* we uncovered that either the right-side-enriched Hpo1 or left-side-enriched Bcd1 are required for *Tetrahymena* survival. The double mutants lacking both Hpo1 and Bcd1 arrest in the cell cycle with a grossly misshaped cortical pattern. One of the prevailing phenotypes in the double mutants are frequent posterior shifts in the OP position. This phenotype was earlier seen in the *hpo1-2* mutants exposed to a higher temperature for a prolonged period (Frankel et al., 1993) and occasionally in the *bcd1-2* mutants (see Fig. 3.4A in (Cole et al., 1987)). Frankel and

colleagues suggested that Hpo1 may be a shared component of pathways that operate on the C and AP axes (Frankel et al., 1993). We note however that all C patterning factors studied to date (Bcd1, JanA and Hpo1) in addition to the circumferential distribution bias, also show a graded distribution along the AP axis ((Cole et al., 2023; Cole, 2024), and this paper). Thus, there could be a deeper relationship between the C and AP positioning pathways.

To our knowledge, we are the first to document essential interactions between the right and left side-enriched pattern regulators. These observations bring to mind some fascinating cortical graft experiments performed on *Stentors* by Vance Tartar and Gotram Uhlig. When grafting created cortical boundaries with a relatively weak stripe contrast (e.g. obtained by juxtaposition of the left and right cortex after removal of most of either the dorsal or ventral surface), oral development was delayed and preceded by a period of remodeling along the heal lines that involved branching of a subset of wider stripes that generated narrowest stripes and consequently created a stronger structural contrast (Tartar, 1956a; Uhlig, 1960) (reviewed in (Frankel, 1989)). Thus, it appears that left and right cortex interact to generate cues that remodel the cortex on both sides of the oral meridian. Double mutants lacking both Bcd1 and Hpo1, show defects not only in the positioning but also in the internal organization (including the left-right polarity of oral structures). Our observations suggest that Bcd1 and Hpo1 are parts of the left-right cross-talk that positions and shapes the ventral features including the oral apparatus.

To summarize, our observations suggest a multi-domain model for circumferential pattern formation in ciliates (Fig. 3.1C). Multiple cortical domains are formed by bilateral gradients of patterning factors including Hpo1, Bcd1 and Janus gene products. Adjacent or overlapping

domains interact to regulate each other's distribution and to create boundary effects that generate positional information for forming organelles.

Materials and methods

Strains and culture

All strains used were obtained from the *Tetrahymena* Stock Center (Cornell University, Ithaca NY, currently housed at Washington University, St Louis, MO USA; https://sites.wustl.edu/tetrahymena/). Cultures were grown in the SPPA medium (1% Proteose-peptone, 0.2% dextrose, 0.1% yeast extract and 0.003% EDTA:ferric sodium salt) supplemented with antibiotics (SPPA) (Gaertig et al., 2013; Gorovsky, 1973). CU428 *mpr1-1/mpr1-1* (*MPR1; VII*)(TSC_SD00178) and B2086 *mat1-2/mat1-2* (*mat1-2; II*) (TSC_SD00709) were used as wild type controls. CU427 *chx1-1/chx1-1* (*CHX1; VI*) (TSC_SD00715) was used for outcrosses to map the *hpo1* alleles. B*VII (TSC_SD00023) was used for self-crosses The following mutant strains were used: IA393 *hpo1-1/hpo1-1; eja1-1/eja1-1* (*hpo1-1, eja1-1; II*) (TSC_SD01463), IA418 *hpo1-2/hpo1-2* (*hpo1-2, VI*) (TSC_SD_01465), IA443 *hpo1-3/hpo1-3* (*hpo1-3; II*) (TSC_SD01455), , IA480 *hpo1-4/hpo1-4* (*hpo1-4, II*) (TSC_SD01466), IA359 *janC-1/janC-1 (janC-1, IV)* (TSC_SD00637), IA479 *janC-4/janC-4* (*janC-4; VII*) (TSC_SD01520), IA342 *bcd1-1/bcd1-1*, *eja1-1/eja1-1* (*bcd1-1, eja1-1*; II) (TSC_SD00635), IA378 *bcd1-2/bcd1-2* (*bcd1-2*, V) (TSC_SD00641), IA437 *janC-1/janC-1*, *hpo1-2/hpo1-2* (*janC-1, hpo1-2(3); IV*) (TSC_SD01576) and IA441 *bcd1-1/bcd1-1*, *hpo1-2/hpo1-2* (*bcd1-1, hpo1-2; IV*). In addition the following strains were made by editing the micronucleus by DNA homologous recombination (see below) and using crosses: UG20 *hpo1-F318S-3xHA-neo4/ hpo1-F318S-3xHA-neo4* (*hpo1-F318S-3xHA-neo4*), UG21 *hpo1::neo2/hpo1::neo2* (*hpo1::neo2*), and heterokaryon strains UG22 *bcd1-2/bcd1-2 hpo1::neo2/hpo1::neo2* (*BCD1, HPO1, pm-s*), UG23 *bcd1-2/bcd1-2 hpo1::neo2/hpo1::neo2* (*BCD1, HPO1, pm-s,* mates with UG22). To obtain progeny cells with the terminally lethal

macronuclear genotype *hpo1::neo2*, *bcd1-2* in the macronucleus, UG22 and UG23 heterokaryon strains were starved and allowed to mate for 24 hr at 30^{o}C, the cell population was incubated in SPPA medium for 6 hr followed by selection with paromomycin 100 mg/ml in SPPA to kill the parental cells.

Mapping of hpo1 alleles and protein structure analysis

We applied ACCA method (Jiang et al., 2017) to map the casual mutation for *hpo1-3* as described below (the same strategy was used to map the remaining three h*po1* alleles using appropriate homozygous strains). Strain IA443 was crossed to CU427 (homozygous for a cycloheximide (cy)-resistant allele *chx1-1* in micronucleus, TSC_SD00715). The heterozygous F1 progeny (*hpo1-3*/*HPO1*; *chx1-1/CHX1*) was assorted in SPPA to cycloheximide (cy) sensitivity. An assorted cy-sensitive F1 was mated to B*VII to produce F2 homozygotes using uniparental cytogamy (Cole and Bruns, 1992). F2 clones were selected with 15 μg/ml cy and the cortical phenotype was evaluated by immunofluorescence. Twenty-three phenotypically wild-type or mutant F2 clones were pooled, cultured in 25ml of SPPA overnight, and subjected to starvation in 60 mM Tris-HCl (pH 7.5) for 2 days at 30°C. Total genomic DNA was extracted from the starved pools and used for generating genomic libraries using Illumina Truseq primer adapters. The libraries were sequence on Illumina HiSeq X to obtain paired-end 150 bp reads at 90x coverage. MiModD in the ACCA workflow was used to identify variants linked to the hpo1 phenotype as described in detail in (Jiang et al., 2017; Jiang et al., 2020). A 3D model of the Hpo1 structure was obtained from the AlphaFold protein structure Database (https://alphafold.com/). Protein domains were identified by InterPro (https://www.ebi.ac.uk/interpro/).

Gene editing in T. thermophila

To construct a plasmid for a genomic knockout of *TTHERM_001276421/HPO1*, fragments were amplified from the genomic DNA of the wild-type strain CU428 and subcloned on the sides of the *neo4* selectable marker using primer pairs: 5'-AATTCCGCGGCGAACTTC TGAGTCATCATTG-3', 5'-AATTCTGCAGCTTAAAGGCGTCTACCATTTTATTC-3' and 5'-ATTCCCGGGTCAAGTATTCAACTCCTCTAAGTG-3', 5'-AATTGGGCCCGAATACTCTGCTCGTGATGTCGA-3'. The resulting plasmid pcand2-KO-neo4 targeted for deletion a portion of the coding region composed of 1383 bp starting at codon 250 and including 371 bp of the 3' UTR. Another targeting plasmid, pIA443-3HA was constructed to introduce the F318S substitution (*hpo1-3*) into the wild type background and simultaneously add a 3xHA epitope tag sequence at the 3' end of the coding region. To this end, fragments were amplified using the total genomic DNA from strain IA443 (homozygous for *hpo1-3*) using primers pairs: 5'-AATTCTCGAGGAACTGTATTAGGAGTGATTTCAC-3', 5'-TTAACTGCAGCATAAAATATCCAATTAATTTCAAATATCCACAAATATTATC-3' and 5'-AATTGGATCCTTAACTAACTTCATCCTAGAAGCATTC-3', 5'-AAATACGCGTTTAGTTCAACACTTAGAGGAGTAGAATAC-3' and used to replace gene targeting parts of the plasmid pIFT54-3HA-native-neo4 (Hazime et al., 2021). The targeting fragments of the above plasmids were released using restriction enzymes cleaving near the ends of flanking homologous sequences and the digested DNA was used for biolistic bombardment of mating CU428 and B2086 cells at an early stage of conjugation optimal for targeting in the micronucleus, followed by standard crosses to make mutant heterokaryons and homokaryons (Dave et al., 2009).

To prepare a strain for live imaging of Hpo1, the coding region of *TTHERM_001276421/HPO1* was cloned into the plasmid pGFP_PLK2-BTU1ov, downstream of the *MTT1* promoter and the GFP sequence. The primer pairs used to amplify the Hpo1 fragment were 5'-CTATACAAACGCGTGATGTAAAACTTACCTGATTGC-3', and

5’-GTTCGCTTACGGATCCTCATTAACTAACTTCATCCTAGAAGC-3’. The transgene was placed between UTR sequences of *BTU1* for targeting to this locus by homologous DNA recombination. The plasmid was digested by BamHI and MluI, biolistically introduced into the CU428 strain and transformants were selected with 100 mg/ml paromomycin.

To overexpress Hpo1-HA, a plasmid was made (pMTT1_Hpo1_HA) with the following sequence elements cloned between the UTR sequences of the *BTU1* gene: *Bsr* selectable marker, *MTT1* promoter, coding region of HPO1 amplified with primers: 5'-TAAAATAATGGCCAAGTCGACAATGTAAAACTTACCTGATTGCG-3' and 5'-AACATCATAAGGATAAGCACCGGATCCTTAACTAACTTCATCCTAGAAGCATTC-3', HA epitope tag sequence. The targeting portion of the plasmid was released with SacI and BamHI, introduced biolistically into the *BTU1* locus (of CU428 strain) and transformants were selected with 60 mg/ml blastidicin S. To induce overproduction, the transgene-carrying cells were exposed to 2.5 mg/ml cadmium chloride for 6 hr.

Microscopic imaging

T. thermophila cells were fixed by and prepared for immunofluorescence as described (Gaertig et al., 2013; Jiang et al., 2020). The primary antibodies used were: anti-GFP (Rockland Immunochemicals, #600-401-215; 1:800 dilution), monoclonal anti-HA 16B12 (Covance; 1:300), and monoclonal anti-centrin 20H5 (EMD Millipore; 1:200-300;(Salisbury et al., 1988)). The secondary antibodies were conjugated to either Cy3 or FITC (Jackson ImmunoResearch, 115-095-146 and 111-165-003; 1:100–1:300). The nuclei were stained with DAPI (Sigma-Aldrich). The labeled cells were mounted in 90% glycerol, 10% PBS supplemented with 100 mg/ml DABCO (Sigma-Aldrich). To image the apical surface of cells, cell fragments were obtained as follows: 1.5 ml of cell culture was concentrated at 2,800 rpm/3 min, and washed with 1 ml of the nuclear isolation medium A (0.1M sucrose, 4% gum

arabic, 0.0015M $MgCl_2$, 0.01% spermidine-HCl, pH 6.75) (Gorovsky, 1970). The cells were concentrated by centrifugation to 150 µl and combined with 160 ml of 1% paraformaldehyde/0.25% Triton X-100 followed by addition of 1.92 ml of octyl alcohol. The mixture was vortexed for 10-60 seconds and 20 ml of the sample was air-dried at the room temperature on a cover glass. Next, immunofluorescence was conducted as described above. The microscope images were collected on a Zeiss LSM 710 confocal microscope with a Plan-Apochromat 63×/1.40 oil DIC M27 objective and on an ELYRA S1 SR-SIM microscope equipped with a 63× NA 1.4 Oil Plan-Apochromat DIC. TIRF microscopy was executed as previously described (Jiang et al., 2015) except that partial immobilization of cells was achieved by entrapment in a small volume of culture medium.

Statistical analysis

Using the GraphPad PRISM software, we executed two-tailed unpaired t-tests to evaluate differences. $P<0.05$ was deemed statistically significant.

References

Allen, R.D. 1969. The morphogenesis of basal bodies and accessory structures of the cortex of the ciliated protozoan *Tetrahymena pyriformis*. *J Cell Biol*. 40:716-733.

Breslow, D.K., S. Hoogendoorn, A.R. Kopp, D.W. Morgens, B.K. Vu, M.C. Kennedy, K. Han, A. Li, G.T. Hess, M.C. Bassik, J.K. Chen, and M.V. Nachury. 2018. A CRISPR-based screen for Hedgehog signaling provides insights into ciliary function and ciliopathies. *Nat Genet*. 50:460-471.

Cavalier-Smith, T., and E.E. Chao. 2004. Protalveolate phylogeny and systematics and the origins of Sporozoa and dinoflagellates (phylum Myzozoa nom. nov.). *Eur J Protistol*. 40:185-212.

Cole, E., and J. Gaertig. 2022. Anterior-posterior pattern formation in ciliates. *J Eukaryot Microbiol*:e12890.

Cole, E.S., P.C. Anderson, R.B. Fulton, M.E. Majerus, M.G. Rooney, J.M. Savage, D. Chalker, J. Honts, M.E. Welch, A.L. Wentland, E. Zweifel, and D.J. Beussman. 2008. A proteomics approach to cloning fenestrin from the nuclear exchange junction of *tetrahymena*. *J Eukaryot Microbiol*. 55:245-256.

Cole, E.S., and P.J. Bruns. 1992. Uniparental cytogamy: a novel method for bringing micronuclear mutations of *Tetrahymena* into homozygous macronuclear expression with precocious sexual maturity. *Genetics*. 132:1017-1031.

Cole, E.S., J. Frankel, and L.M. Jenkins. 1987. *bcd*: A mutation affecting the width of organelle domains in the cortex of *Tetrahymena thermophila*. *Rouxs Arch Dev Biol*. 196:421-433.

Cole, E.S., J. Frankel, and L.M. Jenkins. 1988. Interactions between j*anus* and *bcd* cortical pattern mutants in *Tetrahymena thermophila* : An investigation of intracellular patterning mechanisms using double-mutant analysis. *Rouxs Arch Dev Biol*. 197:476-489.

Cole, E.S., W. Maier, E. Joachimiak, Y.Y. Jiang, C. Lee, E. Collet, C. Chmelik, D.P. Romero, D. Chalker, N.K. Alli, T.M. Ruedlin, C. Ozzello, and J. Gaertig. 2023. The *Tetrahymena bcd1* mutant implicates endosome trafficking in ciliate, cortical pattern formation. *Mol Biol Cell*. 34:ar82.

Cole, E.S., Maier, W., Huynh, H.V., Reister, B., Sowunmi, D.O., Chukka, U.N., Lee, C., Parra, M., and Gaertig,J. 2024. Janus A : a polo kinase whose loss creates a dorsal/ventral intracellular homeosis in the ciliate, *Tetrahymena*.

Dave, D., D. Wloga, and J. Gaertig. 2009. Manipulating ciliary protein-encoding genes in *Tetrahymena thermophila*. *Methods Cell Biol*. 93:1-20.

Frankel, J. 1989. Pattern formation : ciliate studies and models. Oxford University Press, New York. xvii, 314 pages : illustrations pp.

Frankel, J. 2008. What do genic mutations tell us about the structural patterning of a complex single-celled organism? *Eukaryot Cell*. 7:1617-1639.

Frankel, J., and L.M. Jenkins. 1979. A mutant of *Tetrahymena thermophila* with a partial mirror-image duplication of cell surface pattern. II. Nature of genic control. *J Embryol Exp Morphol*. 49:203-227.

Frankel, J., L.M. Jenkins, and J. Bakowska. 1984. Selective mirror-image reversal of ciliary patterns in *Tetrahymena thermophila* homozygous for a *janus* mutation. *Wilehm Roux Arch Dev Biol*. 194:107-120.

Frankel, J., L.M. Jenkins, E.M. Nelsen, and C.A. Stoltzman. 1993. Hypoangular: a gene potentially involved in specifying positional information in a ciliate, *Tetrahymena thermophila*. *Dev Biol*. 160:333-354.

Frankel, J., E. Nelsen, and L. Jenkins. 1987. Intracellular pattern reversal in *Tetrahymena thermophila*: *janus* mutants and their geometrical phenocopies. *In* Symp. Soc. Dev. Biol. Vol. 45. 219-244.

Frankel, J., and E.M. Nelsen. 1986. How the mirror-image pattern specified by a *janus* mutation of *Tetrahymena thermophila* comes to expression. *Dev Genet*. 6:213-238.

Frankel, J., and E.M. Nelsen. 1987. Positional reorganization in compound *janus* cells of *Tetrahymena thermophila*. *Development*. 99:51-68.

Gaertig, J., D. Wloga, K.K. Vasudevan, M. Guha, and W. Dentler. 2013. Discovery and functional evaluation of ciliary proteins in *Tetrahymena thermophila*. *Methods Enzymol*. 525:265-284.

Galati, D.F., S. Bonney, Z. Kronenberg, C. Clarissa, M. Yandell, N.C. Elde, M. Jerka-Dziadosz, T.H. Giddings, J. Frankel, and C.G. Pearson. 2014. DisAp-dependent striated fiber elongation is required to organize ciliary arrays. *J Cell Biol*. 207:705-715.

Gorovsky, M.A. 1970. Studies on nuclear structure and function in *Tetrahymena pyriformis*. 3. Comparison of the histones of macro- and micronuclei by quantitative polyacrylamide gel electrophoresis. *J Cell Biol*. 47:631-636.

Gorovsky, M.A. 1973. Macro- and micronuclei of *Tetrahymena pyriformis*: a model system for studying the structure and function of eukaryotic nuclei. *J Protozool*. 20:19-25.

Gruber, A. 1885. Ueber kiinstliche Teilung bei Infusorien. *Biologisches Zentralblatt*. 3:580-582.

Hatori, R., T. Ando, T. Sasamura, N. Nakazawa, M. Nakamura, K. Taniguchi, S. Hozumi, J. Kikuta, M. Ishii, and K. Matsuno. 2014. Left-right asymmetry is formed in individual cells by intrinsic cell chirality. *Mech Dev*. 133:146-162.

Hazime, K.S., Z. Zhou, E. Joachimiak, N.A. Bulgakova, D. Wloga, and J.J. Malicki. 2021. STORM imaging reveals the spatial arrangement of transition zone components and IFT particles at the ciliary base in *Tetrahymena*. *Sci Rep*. 11:7899.

Hozumi, S., R. Maeda, K. Taniguchi, M. Kanai, S. Shirakabe, T. Sasamura, P. Speder, S. Noselli, T. Aigaki, R. Murakami, and K. Matsuno. 2006. An unconventional myosin in *Drosophila* reverses the default handedness in visceral organs. *Nature*. 440:798-802.

Inaki, M., J. Liu, and K. Matsuno. 2016. Cell chirality: its origin and roles in left-right asymmetric development. *Philos Trans R Soc Lond B Biol Sci*. 371.

Ishida, T., Y. Kaneko, M. Iwano, and T. Hashimoto. 2007. Helical microtubule arrays in a collection of twisting tubulin mutants of *Arabidopsis thaliana*. *Proc Natl Acad Sci U S A*. 104:8544-8549.

Janouskovec, J., D.V. Tikhonenkov, K.V. Mikhailov, T.G. Simdyanov, V.V. Aleoshin, A.P. Mylnikov, and P.J. Keeling. 2013. Colponemids Represent Multiple Ancient Alveolate Lineages. *Current Biology*. 23:2546-2552.

Jerka-Dziadosz, M., and J. Frankel. 1979. A mutant of *Tetrahymena thermophila* with a partial mirror-image duplication of cell surface pattern. I. Analysis of the phenotype. *J Embryol Exp Morphol*. 49:167-202.

Jiang, Y.Y., K. Lechtreck, and J. Gaertig. 2015. Total internal reflection fluorescence microscopy of intraflagellar transport in *Tetrahymena thermophila*. *Methods Cell Biol*. 127:445-456.

Jiang, Y.Y., W. Maier, R. Baumeister, E. Joachimiak, Z. Ruan, N. Kannan, D. Clarke, P. Louka, M. Guha, J. Frankel, and J. Gaertig. 2019. Two Antagonistic Hippo Signaling Circuits Set the Division Plane at the Medial Position in the Ciliate *Tetrahymena*. *Genetics*. 211:651-663.

Jiang, Y.Y., W. Maier, R. Baumeister, G. Minevich, E. Joachimiak, Z. Ruan, N. Kannan, D. Clarke, J. Frankel, and J. Gaertig. 2017. The Hippo Pathway Maintains the Equatorial Division Plane in the Ciliate *Tetrahymena*. *Genetics*. 206:873-888.

Jiang, Y.Y., W. Maier, U.N. Chukka, M. Choromanski, C. Lee, E. Joachimiak, D. Wloga, W. Yeung, N. Kannan, J. Frankel, and J. Gaertig. 2020. Mutual antagonism between Hippo signaling and cyclin E drives intracellular pattern formation. *J Cell Biol*. 219.

Latour, B.L., J.C. Van De Weghe, T.D. Rusterholz, S.J. Letteboer, A. Gomez, R. Shaheen, M. Gesemann, A. Karamzade, M. Asadollahi, M. Barroso-Gil, M. Chitre, M.E. Grout, J. van Reeuwijk, S.E. van Beersum, C.V. Miller, J.C. Dempsey, H. Morsy, G. University of Washington Center for Mendelian, M.J. Bamshad, C. Genomics England Research, D.A. Nickerson, S.C. Neuhauss, K. Boldt, M. Ueffing, M. Keramatipour, J.A. Sayer, F.S. Alkuraya, R. Bachmann-Gagescu, R. Roepman, and D. Doherty. 2020. Dysfunction of the ciliary ARMC9/TOGARAM1 protein module causes Joubert syndrome. *J Clin Invest*. 130:4423-4439.

Lee, C., W. Maier, Y.Y. Jiang, K. Nakano, K.F. Lechtreck, and J. Gaertig. 2024. Global and local functions of the Fused kinase ortholog CdaH in intracellular patterning in *Tetrahymena*. *J Cell Sci*. 137.

Louka, P., K.K. Vasudevan, M. Guha, E. Joachimiak, D. Wloga, R.F. Tomasi, C.N. Baroud, P. Dupuis-Williams, D.F. Galati, C.G. Pearson, L.M. Rice, J.J. Moresco, J.R. Yates, 3rd, Y.Y. Jiang, K. Lechtreck, W. Dentler, and J. Gaertig. 2018. Proteins that control the geometry of microtubules at the ends of cilia. *J Cell Biol*. 217:4298-4313.

Morgan, T.H. 1901. Regeneration of proportionate structures in *stentor*, Boston.

Nelsen, E.M., and J. Frankel. 1989. Maintenance and regulation of cellular handedness in *Tetrahymena*. *Development*. 105:457-471.

Nelsen, E.M., J. Frankel, and N.E. Williams. 1989. Oral assembly in left-handed *Tetrahymena thermophila*. *J Protozool*. 36:582-596.

Nelsen, E.M., N.E. Williams, H. Yi, J. Knaak, and J. Frankel. 1994. "Fenestrin" and conjugation in *Tetrahymena thermophila*. *J Eukaryot Microbiol*. 41:483-495.

Orias, E. 1976. Derivation of Ciliate Architecture from a Simple Flagellate - Evolutionary Model. *T Am Microsc Soc*. 95:415-429.

Orias, E., and L. Rasmussen. 1976. Dual capacity for nutrient uptake in *Tetrahymena*. IV. Growth without food vacuoles and its implications. *Exp Cell Res*. 102:127-137.

Paulin, J.J., and J. Bussey. 1971. Oral regeneration in the ciliate *Stentor coeruleus*: a scanning and transmission electron optical study. *J Protozool*. 18:201-213.

Pelvat, B., and G. Dehaller. 1979. La Regeneration de L'appareil Oral chez *Stentor coeruleus*: Etude au Protargol et Essai de Morphogenese Comparee. *Protistologica*. 15:369-386.

Salisbury, J.L., A.T. Baron, and M.A. Sanders. 1988. The centrin-based cytoskeleton of *Chlamydomonas reinhardtii*: distribution in interphase and mitotic cells. *J Cell Biol*. 107:635-641.

Shang, Y., X. Song, J. Bowen, R. Corstanje, Y. Gao, J. Gaertig, and M.A. Gorovsky. 2002. A robust inducible-repressible promoter greatly facilitates gene knockouts, conditional expression, and overexpression of homologous and heterologous genes in *Tetrahymena thermophila*. *Proc Natl Acad Sci U S A*. 99:3734-3739.

Slabodnick, M.M., J.G. Ruby, J.G. Dunn, J.L. Feldman, J.L. DeRisi, and W.F. Marshall. 2014. The kinase regulator mob1 acts as a patterning protein for *stentor* morphogenesis. *PLoS Biol*. 12:e1001861.

Speder, P., G. Adam, and S. Noselli. 2006. Type ID unconventional myosin controls left-right asymmetry in *Drosophila*. *Nature*. 440:803-807.

Tartar, V. 1956a. Grafting Experiments Concerning Primordium Formation in *Stentor Coeruleus*. *Journal of Experimental Zoology*. 131:75-121.

Tartar, V. 1956b. IV. PATTERN AND SUBSTANCE IN *STENTOR*. *In* Cellular Mechanics in Differentiation and Growth. Princeton University Press, Princeton. 73-100.

Tartar, V. 1961. The biology of *Stentor*. Pergammon Press, Oxford, New York,. x, 413 p. pp.

Tavares, A., J. Goncalves, C. Florindo, A.A. Tavares, and H. Soares. 2012. Mob1: defining cell polarity for proper cell division. *J Cell Sci*. 125:516-527.

Thazhath, R., M. Jerka-Dziadosz, J. Duan, D. Wloga, M.A. Gorovsky, J. Frankel, and J. Gaertig. 2004. Cell context-specific effects of the β-tubulin glycylation domain on assembly and size of microtubular organelles. *Mol Biol Cell*. 15:4136-4147.

Uhlig, G. 1960. Entwicklungsphysiologische Untersuchungen zur Morphogenese von *Stentor coeruleus* Ehrbg. *Arch. Protistenk.* 105:1-109.

Van De Weghe, J.C., T.D.S. Rusterholz, B. Latour, M.E. Grout, K.A. Aldinger, R. Shaheen, J.C. Dempsey, S. Maddirevula, Y.H. Cheng, I.G. Phelps, M. Gesemann, H. Goel, O.S. Birk, T. Alanzi, R. Rawashdeh, A.O. Khan, G. University of Washington Center for Mendelian, M.J. Bamshad, D.A. Nickerson, S.C.F. Neuhauss, W.B. Dobyns, F.S. Alkuraya, R. Roepman, R. Bachmann-Gagescu, and D. Doherty. 2017. Mutations in ARMC9, which Encodes a Basal Body Protein, Cause Joubert Syndrome in Humans and Ciliopathy Phenotypes in Zebrafish. *Am J Hum Genet*. 101:23-36.

Yao, M.C., and C.H. Yao. 1991. Transformation of *Tetrahymena* to cycloheximide resistance with a ribosomal protein gene through sequence replacement. *Proc Natl Acad Sci U S A*. 88:9493-9497.

Figure Legends

Figure 3.1. Circumferential positioning In *Tetrahymena*. (A) Cell cycle stages of *T. thermophila* with emphasis on cortical development. Note that during cell division, new organelles form at same longitudes (same ciliary rows) as old organelles. (B) A detailed view of a stage 2 cell presents the row numbering method. (C) A multi-domain model for circumferential positioning in a ciliate. Abbreviations: oa, oral apparatus; op, oral primordium; cvp, contractile vacuole pore; ncvp, new contractile vacuole pore; m1,m2,m3 oral M (membranelle) rows; um, oral undulating membrane row. Note that the model of mutual enhancement between Hpo1 and Bcd1 is proposed to explain bidirectional shift of OP in *hpo1-3* and *bcd1-1* single mutant.

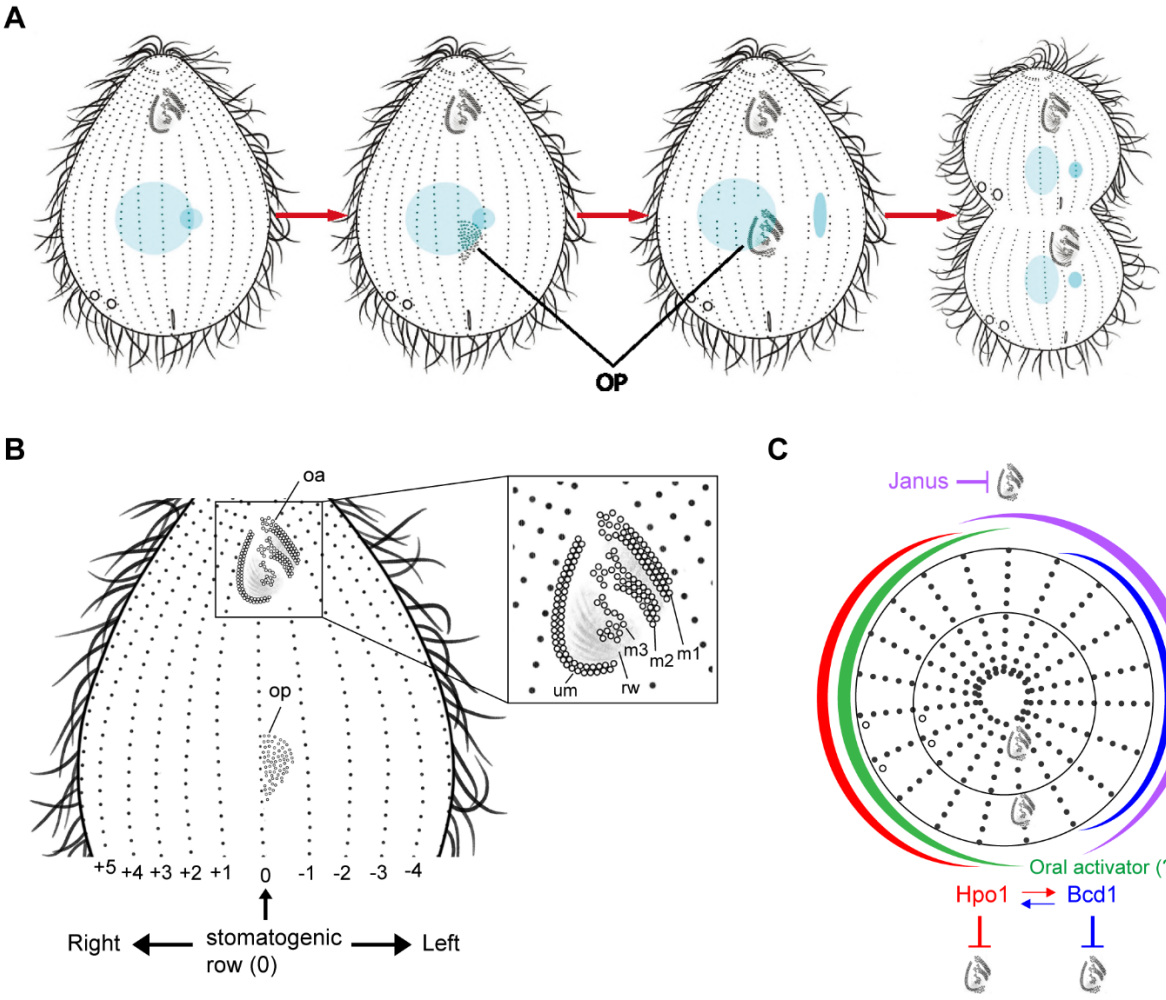
A
OP
B
oa
op
m3
m2
m1
um
rw
+5 +4 +3 +2 +1 0 -1 -2 -3 -4
Right
stomatogenic row (0)
Left
C
Janus
Oral activator (?)
Hpo1
Bcd1

Figure 3.2. *hpo1* alleles disturb the patterning on the circumferential axis by conferring an excessive number of oral primordia and their lateral displacement. (A-F) SR-SIM images of cells labeled with the 20H5 anti-centrin antibody (red) and DAPI (blue). The cells were cultured overnight at either 30°C (A-C) or 38°C (D-F). (G,H) The graphs document an increase in the number of oral primordia (G) and their lateral displacement (H) conferred by the *hpo1* alleles. Abbreviations: oa, oral apparatus; rw, ribbed wall of microtubules. The numbers mark the C positions of ventral rows with OPs.

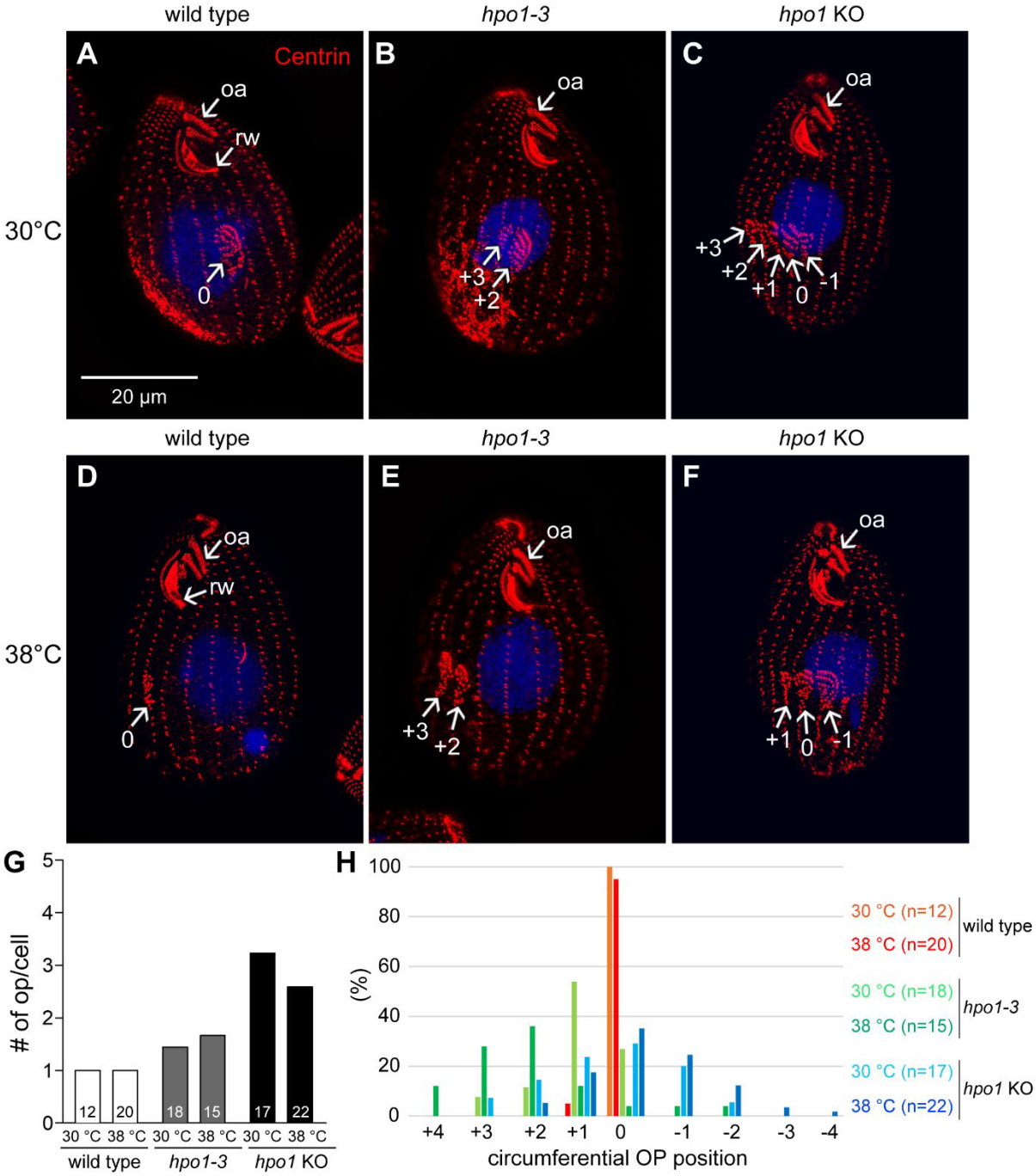
wild type
hpo1-3
hpo1 KO
A
Centrin
B
C
30°C
oa
rw
0
+3
+2
+1
-1
20 µm
D
E
F
38°C
G
# of op/cell
12
20
18
15
17
22
30 °C
38 °C
wild type
hpo1-3
hpo1 KO
H
(%)
circumferential OP position
30 °C (n=12)
38 °C (n=20)
30 °C (n=18)
38 °C (n=15)
30 °C (n=17)
38 °C (n=22)

Figure 3.3. *hpo1* alleles map to *TTHERM_001276421* gene encoding an ARMC9-like protein. (A) Mapping of *hpo1-3* by the ACCA method. A linkage peak is present around 5 mB on the micronuclear chromosome 3. (B) The 3D protein structure of predicted TTHERM_001276421 protein generated by AlphaFold2. (B') The domain organization of TTHERM_001276421 based on InterPro. The positions of two substitutions found in strains homozygous for the four *hpo1* alleles are marked. (C-E') SR-SIM images show the cortical localization of either TTHERM_001276421-3xHA, a C-terminally tagged wild type protein (C,C') or TTHERM_001276421-3xHA with the *hpo1-3*-linked substitution F318S (D-E'). The edited strain used was a homozygote expressing only the variant TTHERM_001276421-F318S protein. Note that expression of the F318S variant of TTHERM_001276421 phenocopies the cortical organization (multiple OPs) of *hpo1-3*. After growth at 38°C for 3 hours, the cells were labeled with the anti-HA antibody (red), 20H5 anti-centrin antibody (green), and DAPI (blue).

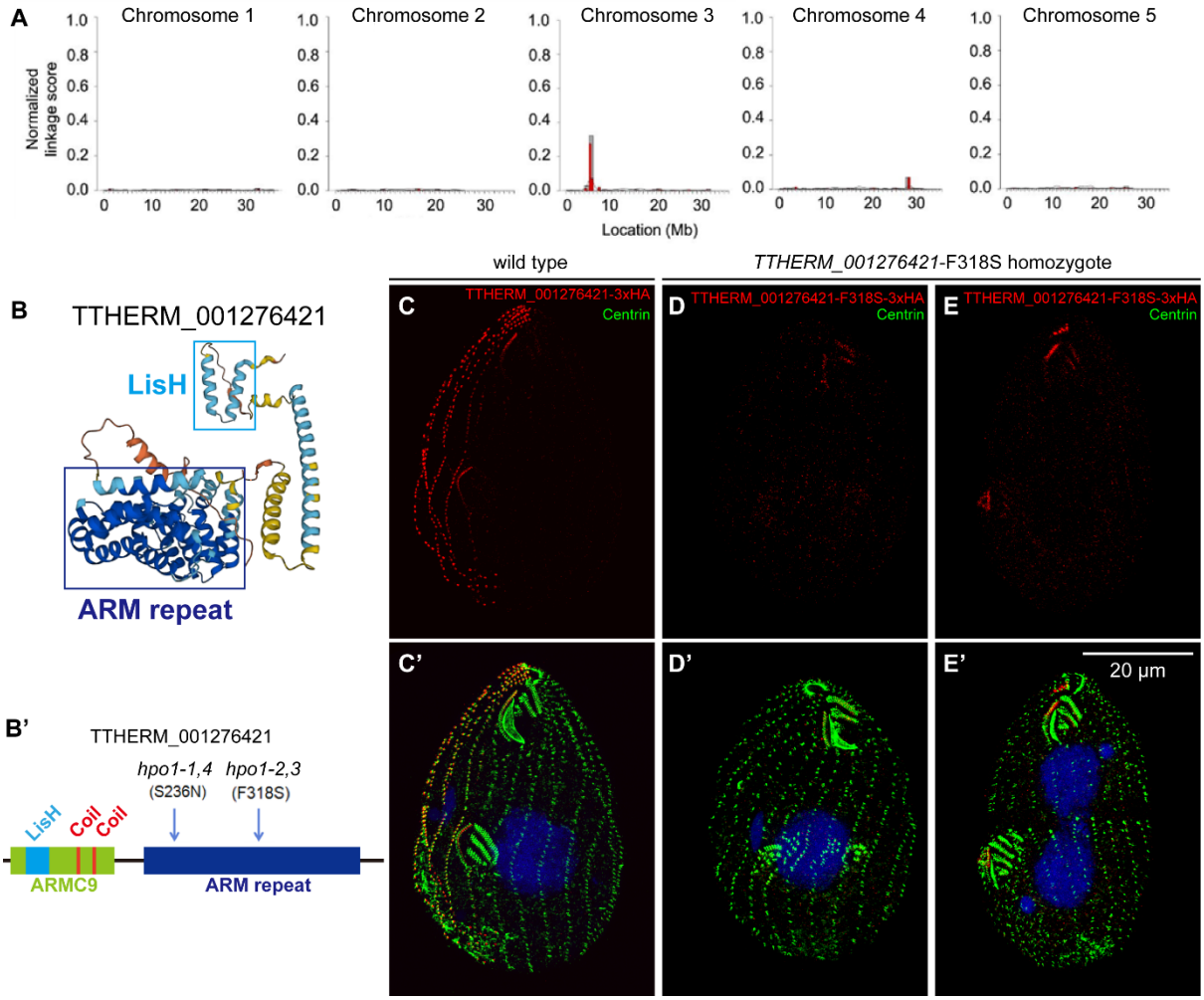
A
Chromosome 1
Chromosome 2
Chromosome 3
Chromosome 4
Chromosome 5
Normalized linkage score
Location (Mb)
B
TTHERM_001276421
LisH
ARM repeat
B'
TTHERM_001276421
hpo1-1,4 (S236N)
hpo1-2,3 (F318S)
LisH
Coil
Coil
ARMC9
ARM repeat
wild type
TTHERM_001276421-F318S homozygote
C
D
E
TTHERM_001276421-3xHA
TTHERM_001276421-F318S-3xHA
Centrin
C'
D'
E'
20 µm

Figure 3.4. Hpo1 forms a bidirectional gradient with a high point on the cell's right lateral side. (A-C’’’) SR-SIM images showing two sides of cells expressing Hpo1-3xHA during the cell cycle. Cells were labeled with the anti-HA (red) and 20H5 anti-centrin (green) antibodies, and DAPI (blue). (D-D’’’’) Confocal images of an apical fragment of a cell expressing Hpo1-3xHA. The cell was labeled with anti-HA (red) and 20H5 anti-centrin (green) antibodies, and DAPI (blue). Single channel gray scale images for centrin (D’,D’’) and Hpo1-3xHA (D’’’,D’’’’) were generated using the confocal image shown in D. (E) The intensity plots document the gray values measured across the region marked by the yellow lines shown in panels D’’ and D’’’’. The orange arrows indicate where the measurements were started, and the purple arrows indicate the position of the dorsal discontinuity. Abbreviations: um, undulating membrane row within the OA; op, oral primordium. The numbers mark ventral row positions.

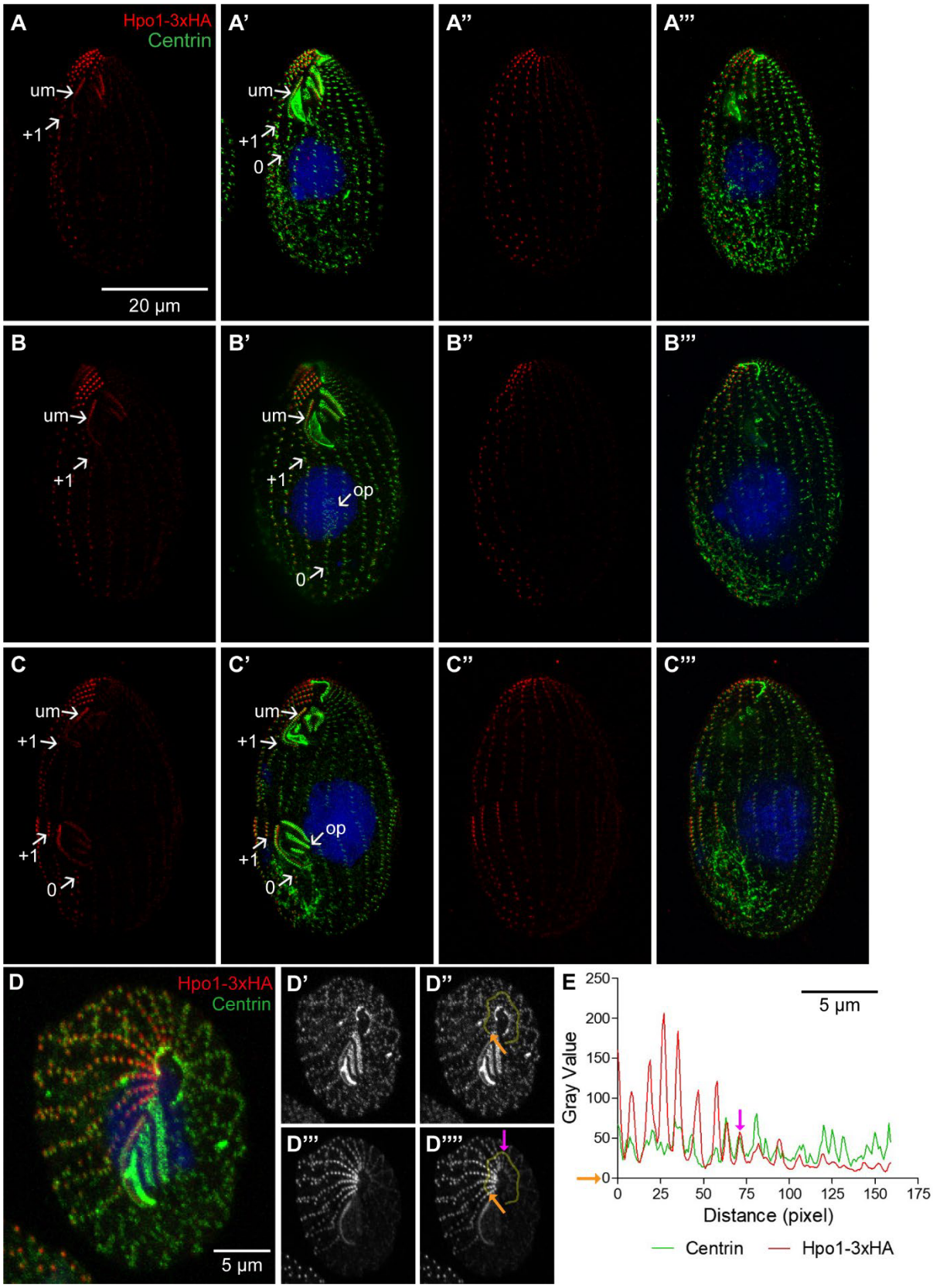
A
Hpo1-3xHA
Centrin
um
+1
20 μm
A'
A''
A'''
B
B'
B''
B'''
op
0
C
C'
C''
C'''
D
D'
D''
D'''
D''''
5 μm
E
Gray Value
Distance (pixel)
Centrin
Hpo1-3xHA

Figure 3.5. The dorsal discontinuity in the Hpo1 gradient marks a cryptic position for oral development expressed in the *Janus* mutant. (A-B') Pairs of confocal images showing two sides of *janC-4 homozygote* cells that have either a single OA (A'A') or two OAs (B-B'). Cells were labeled with the anti-HA (red) and 20H5 anti-centrin (green) antibodies, and DAPI (blue). (C-D') SR-SIM image pairs of cells that are either wild-type (C,C') or *janC-4* homozygotes (D,D') and express Hpo1-3xHA. The cells were decorated with the anti-HA (red), anti-fenestrin (green) antibodies, and DAPI (blue). (E,F) Graphs reveal an increase in the number of rows with enriched Hpo1-3xHA in the *janC-4* background as compared to the wild type (E) but the fraction of the circumference occupied by high Hpo1-3xHA remains unchanged when the increase in the total number of rows is taken into account (F). ns: not significant, Stars indicate statistically significant (*: $P < 0.05$, **: $P < 0.01$, and ***: $P < 0.001$). Abbreviations: pOA, primary oral apparatus; sOA, secondary (dorsal and usually defective) oral apparatus; CVP, contractile vacuole pore.

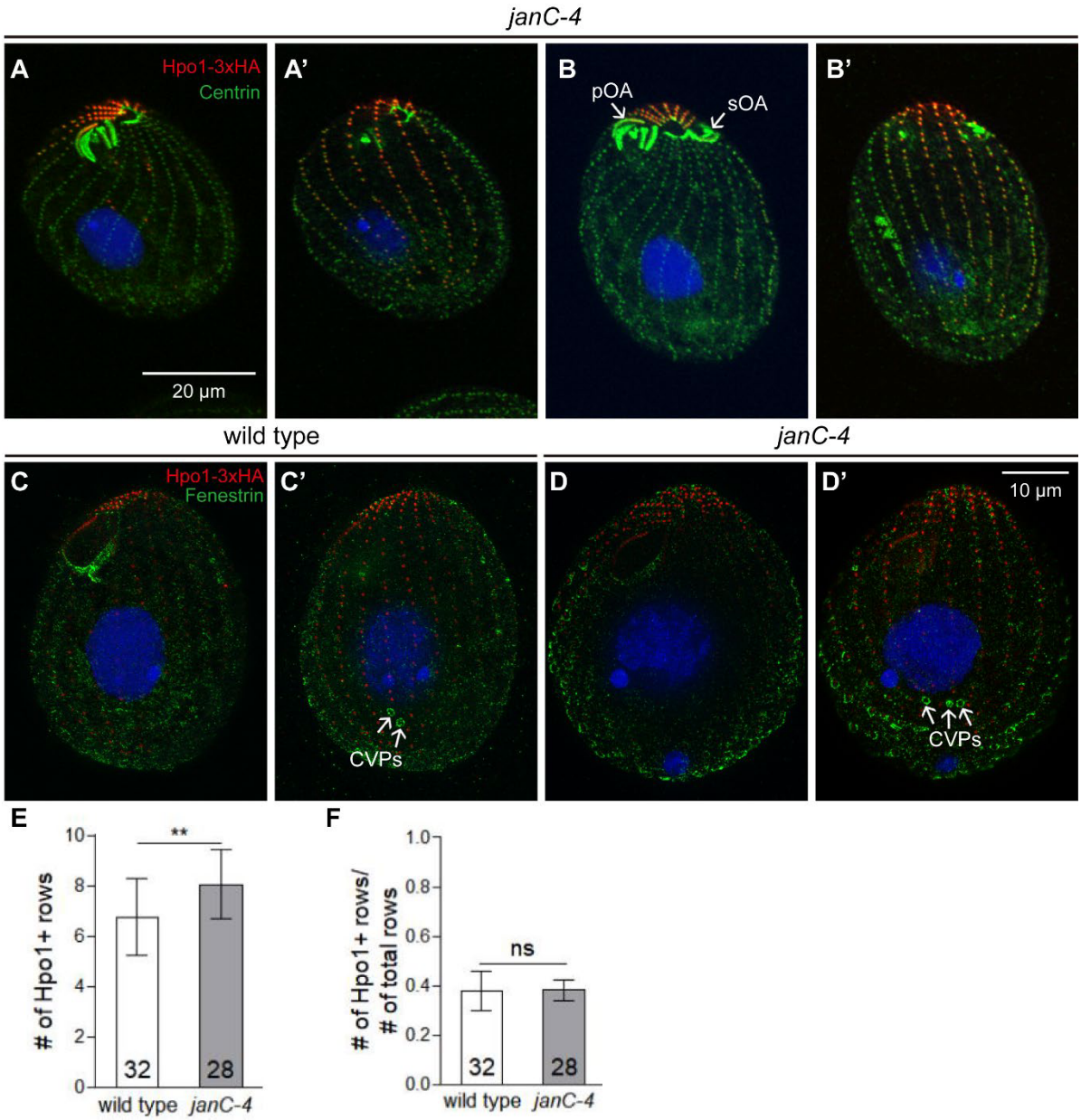
janC-4
A
Hpo1-3xHA
Centrin
A'
B
pOA
sOA
B'
20 µm
wild type
janC-4
C
Hpo1-3xHA
Fenestrin
C'
CVPs
D
D'
10 µm
CVPs
E
# of Hpo1+ rows
**
32
28
wild type
janC-4
F
# of Hpo1+ rows/
# of total rows
ns
32
28
wild type
janC-4

Figure 3.6. Hpo1 acts bidirectionally to separate the two oral apparatuses in the *janus* mutant. Confocal (A-D) and SR-SIM (E-H) images cells with indicated genotypes labeled with the 20H5 anti-centrin antibody (red), and DAPI (blue). Cell shown in all panels except H were incubated for 4 hours at 38°C to enhance the *hpo1-3* phenotype. (I,J) The graphs quantify the frequencies of cells two mature OAs (I), and two OAs in close proximity (J). The bars represent the means ± SD. Two-tailed unpaired t-test was executed for statistical analysis. ns: not significant. Stars indicate statistically significant (*: $P < 0.05$, **: $P < 0.01$, and ***: $P < 0.001$). (K) The drawing summarizes the outcome of the genetic interaction between *janC-1* and *hpo1-3*. The yellow ovals are OPs. The green arrows shows the proposed predominant direction of shifts in the OP positions. Abbreviations: pOA primary OA; sOA secondary OA; op, oral primordium.

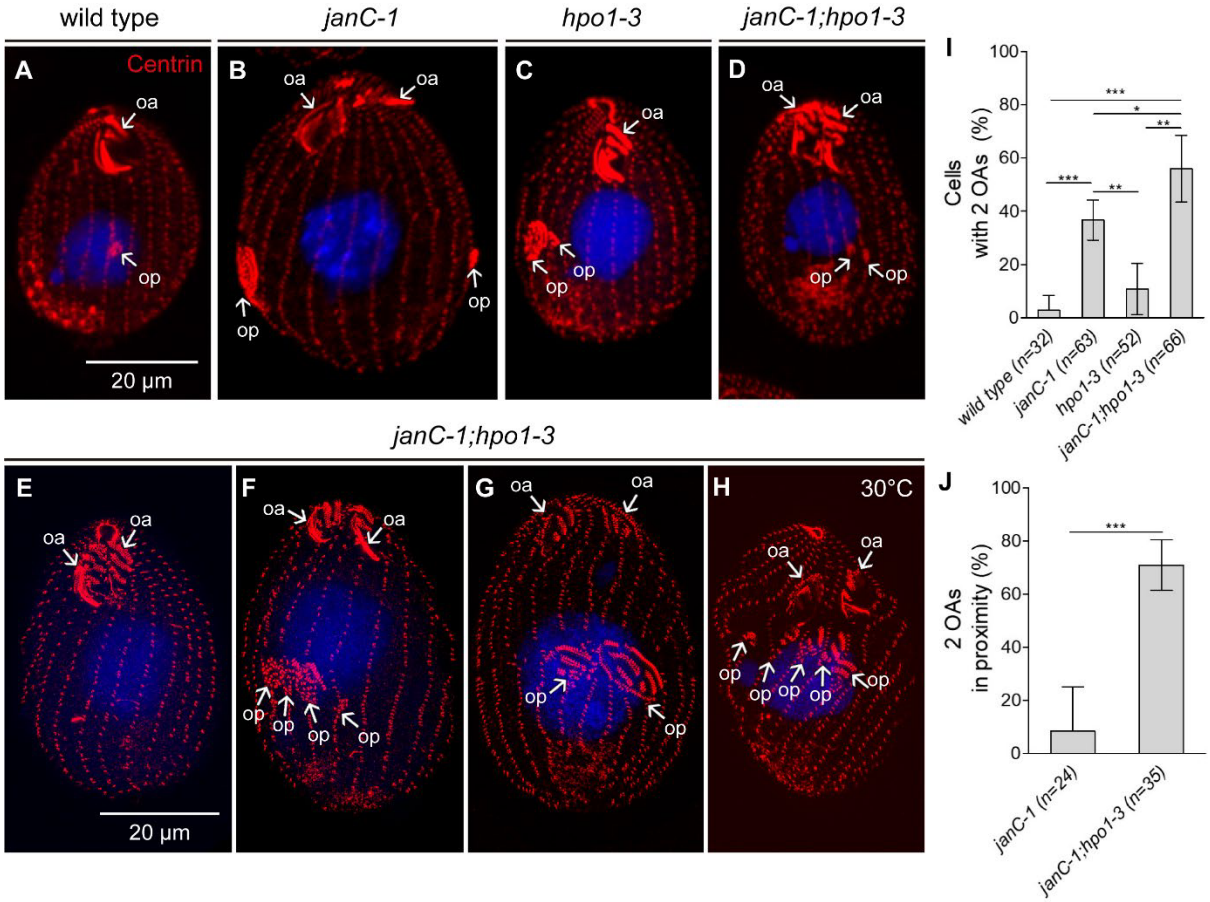
wild type
janC-1
hpo1-3
janC-1;hpo1-3
A
Centrin
oa
op
20 µm
B
C
D
janC-1;hpo1-3
E
F
G
H
30°C
I
Cells with 2 OAs (%)
wild type (n=32)
janC-1 (n=63)
hpo1-3 (n=52)
janC-1;hpo1-3 (n=66)
J
2 OAs in proximity (%)
janC-1 (n=24)
janC-1;hpo1-3 (n=35)

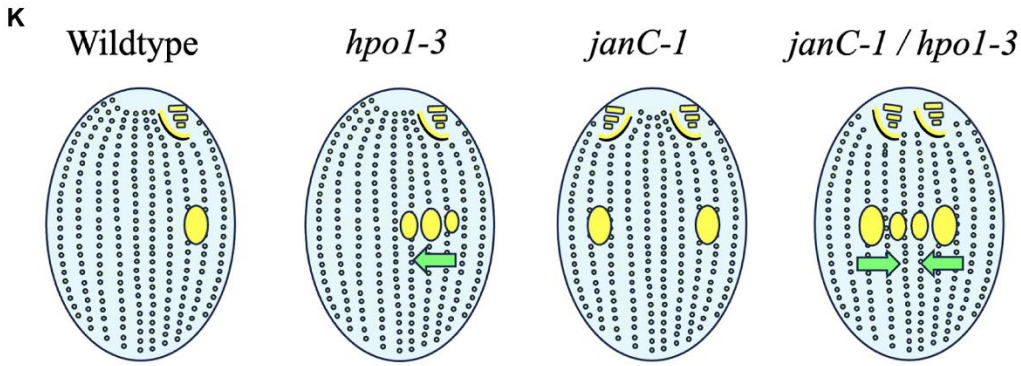
K
Wildtype
hpo1-3
janC-1
janC-1 / hpo1-3

Figure 3.7. A Bcd1 deficiency changes the A/P distribution of Hpo1. (A-B'') SR-SIM images of Hpo1-3xHA-expressing cells that are either otherwise wild-type (A-A'') or *bcd1-2* homozygotes (B-B''). The cells were labeled with the anti-HA (red), 20H5 anti-centrin (green) antibodies, and DAPI (blue). The grey scale images are the single channel signals of Hpo1-3xHA. The yellow lines (A'' and B'') cover the region whose gray values were measured along the A/P axis, and the light blue arrow indicates the initial point of measurement. The corresponding A/P grey value intensity plots for Hpo1-3xHA in the two genetic backgrounds are shown in the graph in panel D. (C-C'') An SR-SIM image of the cell's apical region from a cell expressing Hpo1-3xHA (red) in the *bcd1-2* background, also stained with anti-centrin (green) antibody. The single channel grey scale images for centrin (C') and Hpo1-3xHA (C'') were used for measurements of the circumferential signal intensities. The measured regions are marked by the yellow lines and the orange arrows orient the measurements. The resulting signal intensity plots are shown in the graph in panel E.

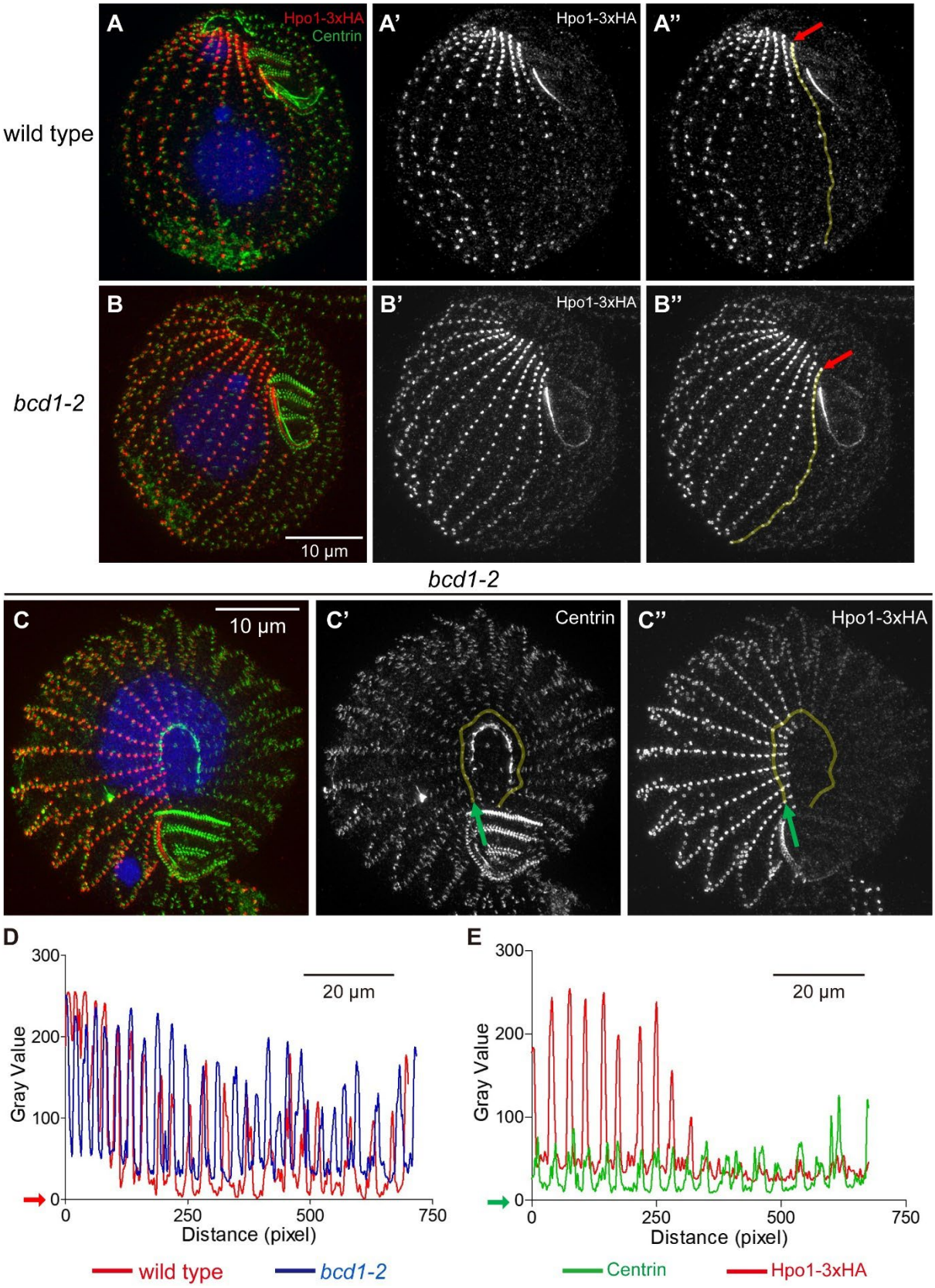
wild type
bcd1-2
A
Hpo1-3xHA
Centrin
A'
Hpo1-3xHA
A''
B
B'
Hpo1-3xHA
B''
10 μm
bcd1-2
C
10 μm
C'
Centrin
C''
Hpo1-3xHA
D
300
200
100
0
Gray Value
20 μm
0
250
500
750
Distance (pixel)
wild type
bcd1-2
E
300
200
100
0
Gray Value
20 μm
0
250
500
750
Distance (pixel)
Centrin
Hpo1-3xHA

Figure 3.8. Bcd1 influences the circumferential pattern of Hpo1-3xHA. Confocal (A-C') and SR-SIM (D-E'') images of cells expressing Hpo1-3xHA that are homozygous for *bcd1-2*. After overnight incubation at 30°C, the cells were labeled with the anti-HA (red), 20H5 anti-centrin (green) antibodies, and DAPI (blue). The numbers mark the ventral row positions.

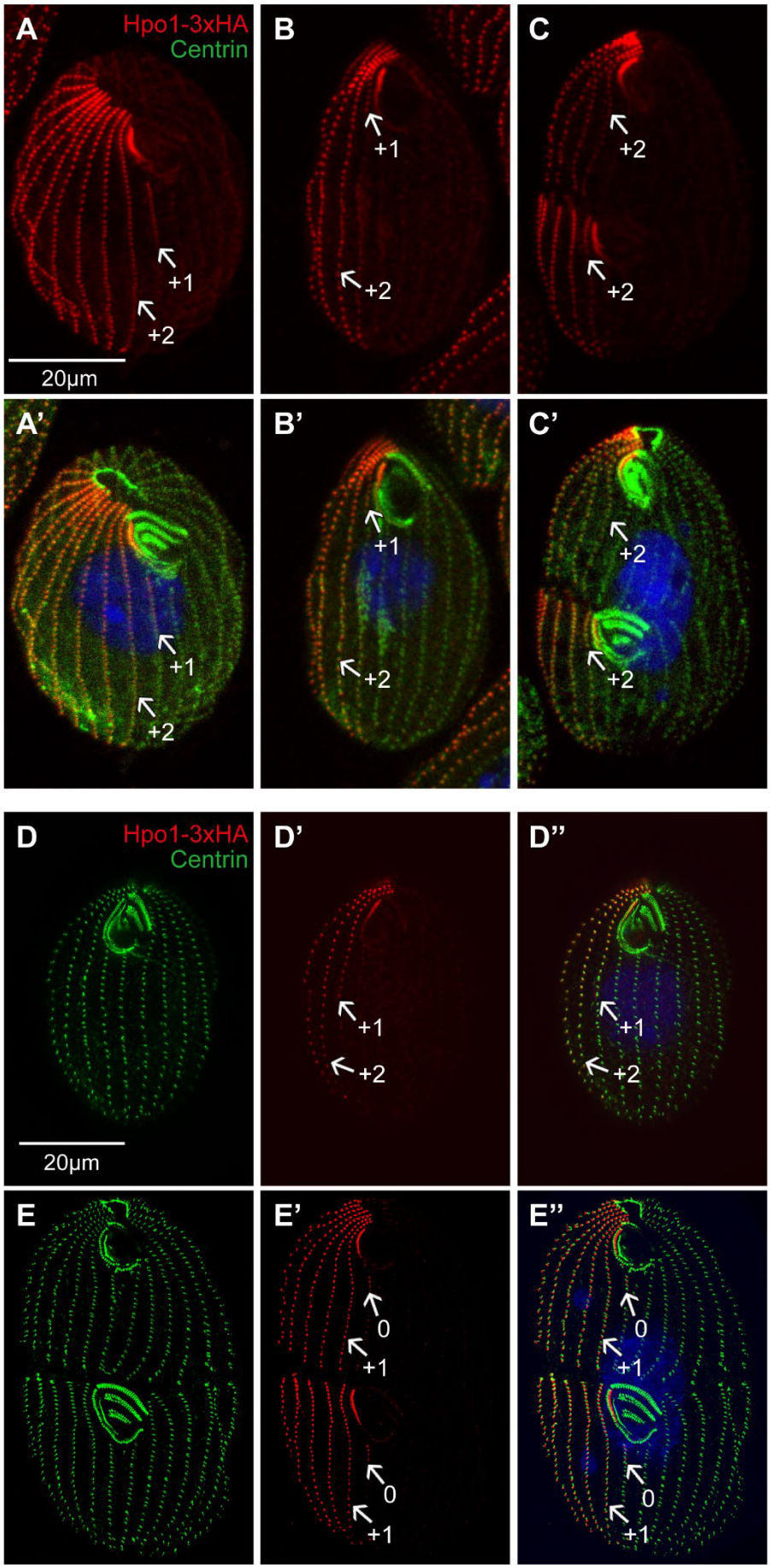
A
Hpo1-3xHA
Centrin
+1
+2
20µm
B
+1
+2
C
+2
+2
A'
+1
+2
B'
+1
+2
C'
+2
+2
D
Hpo1-3xHA
Centrin
20µm
D'
+1
+2
D''
+1
+2
E
E'
0
+1
0
+1
E''
0
+1
0
+1

Figure 3.9. A loss of both the left-side enriched Bcd1 and the right-side enriched Hpo1 severely disturbs cortical patterning. Confocal (A-C) and SR-SIM (D-K) images of *bcd1-2*;*hpo1*-KO double homozygotes obtained as progeny of mating heterokaryons. The times shown in panels A-C refer to the period after refeeding of the mating heterokaryons (after 18 hr of mating at 30^{o}C). Cells were labeled with the 20H5 anti-centrin antibody (red), and DAPI (blue). Abbreviations: m, M oral row; um, UM oral row; rw, ribbed wall of microtubules; ac, apical crown; cs, cortical subdivision. The stars show the gaps in the longitudinal rows that indicate the position of the “cortical subdivision” (a set of gaps in rows at the division plane). Arrows of multiple colors indicate types of cortical defects: white, OAs with long oral rows; yellow, OP displaced posteriorly; green, OA with disorganized rows; pink, OA with circular rows.

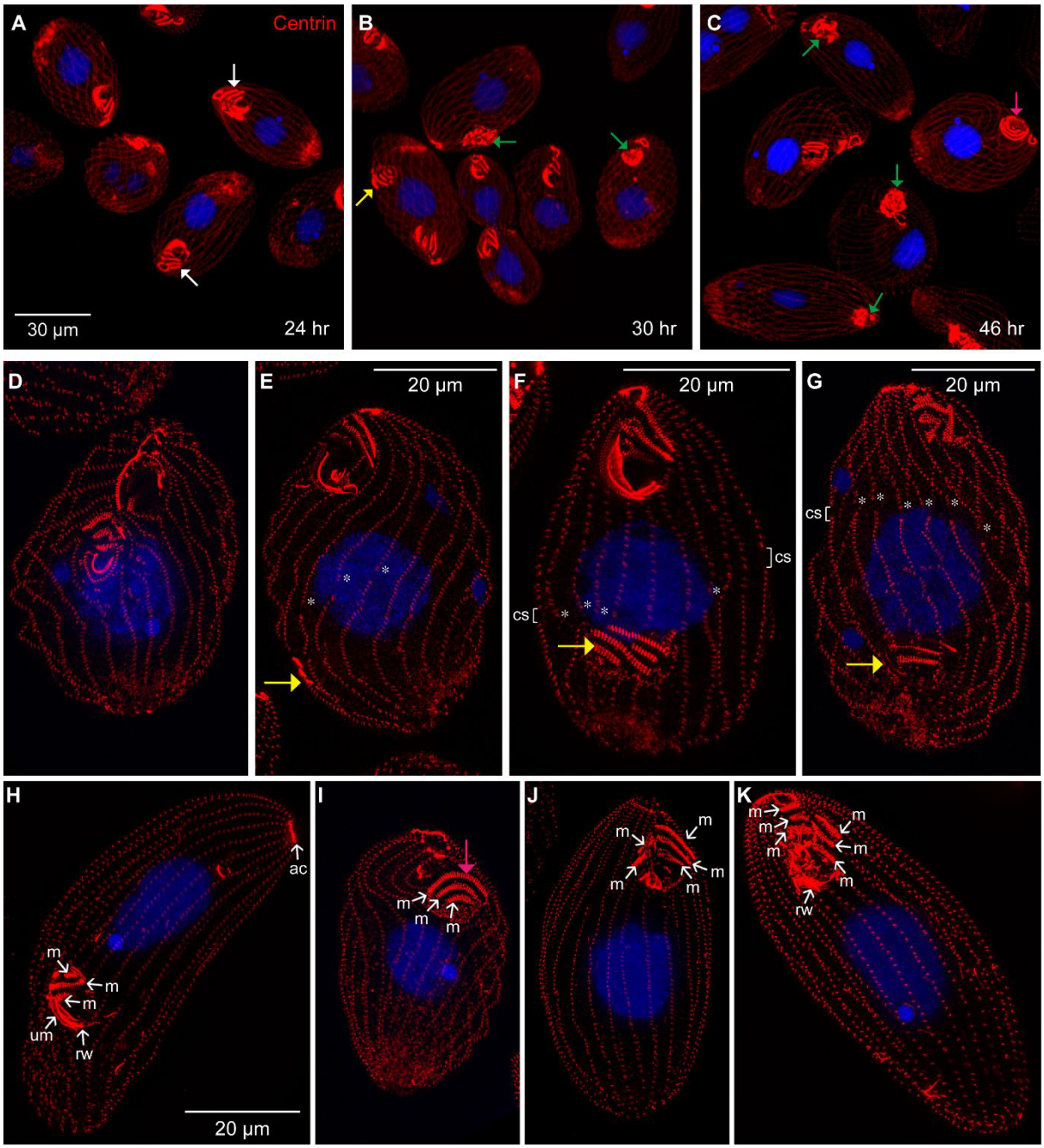
A
Centrin
30 µm
24 hr
B
30 hr
C
46 hr
D
E
20 µm
F
20 µm
cs
G
20 µm
cs
H
ac
m
um
rw
20 µm
I
m
J
m
K
m
rw

Figure 3.S1. Quantification of the number of CVPs per cell. All genotypes are homozygous as indicated in the figure panels. (A-G) Confocal images of wild type (A), single mutants (B-D,F), and double mutants (E,G). The cells were labeled with the anti-fenestrin antibody (red), and DAPI (blue) after incubation for 4 hours at 38°C. Panels are representative of each genotype. The white arrows point to the CVPs. (H) The graph quantifies the number of CVPs per cell. The bars represent the means ± SD. The number of cells scored is displayed in each of the bar. A two-tailed unpaired t-test was executed for statistical analysis. ns: not significant. Stars indicate statistically significant (*: $P < 0.05$, **: $P < 0.01$, and ***: $P < 0.001$). Abbreviations: pOA, primary OA; sOA, secondary OA (in *janC-1* background).

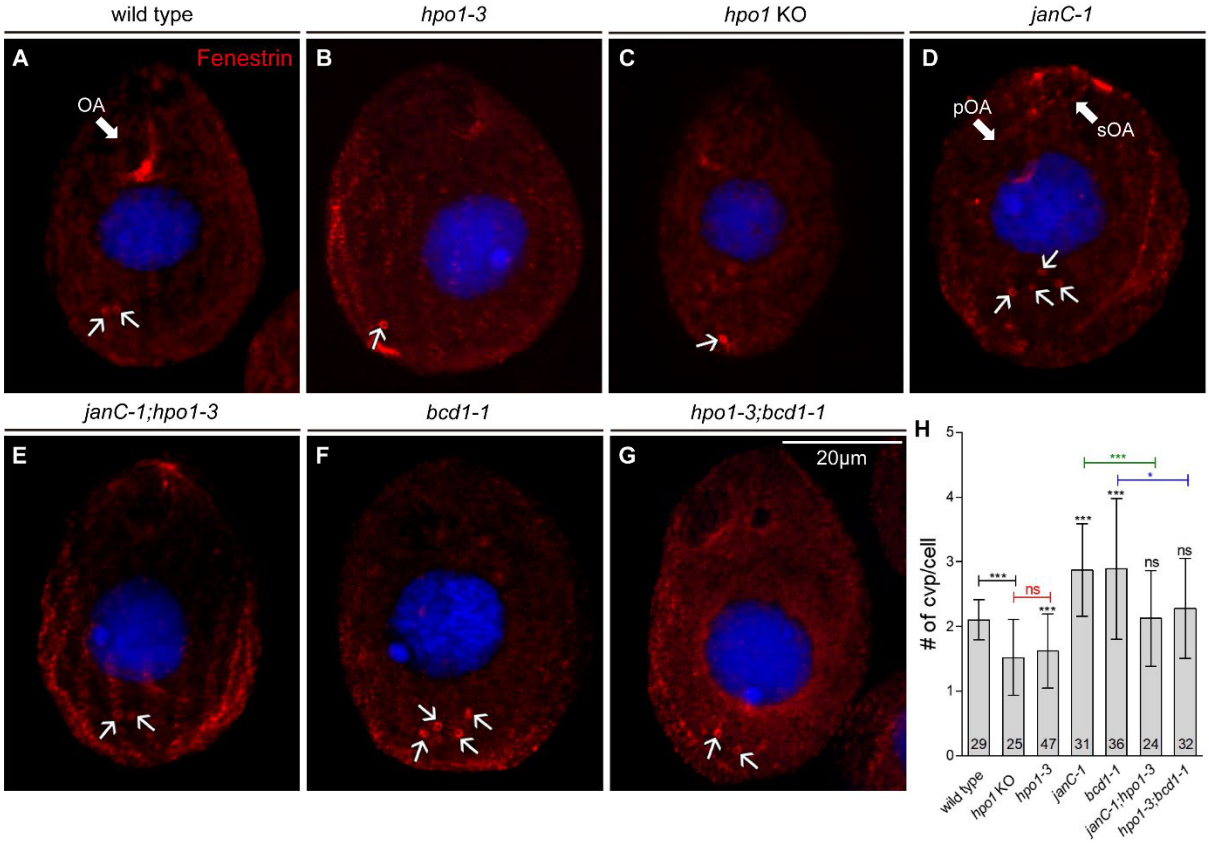
wild type
hpo1-3
hpo1 KO
janC-1
A
Fenestrin
OA
B
C
D
pOA
sOA
janC-1;hpo1-3
bcd1-1
hpo1-3;bcd1-1
E
F
G
20µm
H
# of cvp/cell
0
1
2
3
4
5
29
25
47
31
36
24
32
***
ns
***
***
***
*
ns
ns
wild type
hpo1 KO
hpo1-3
janC-1
bcd1-1
janC-1;hpo1-3
hpo1-3;bcd1-1

Figure 3.S2. *In vivo* Hpo1 marks basal bodies and adjacent microtubule bundles (A) Illustration of *T. thermophila* with the magnified inset describing a portion of cell cortex (from (Thazhath et al., 2004)). (B,C) Still images of live cells expressing GFP-Hpo1 that localizes at positions consistent with the basal bodies and microtubule bundles (indicated by arrows). Abbreviations: tm, transverse microtubule; lm, longitudinal microtubule; pc, postciliary microtubule; bb, basal body, kd, kinetodesmal fiber (nonmicrotubular), m, membranelle; um, undulating membrane; oa, oral apparatus; mic, micronucleus; mac, macronucleus; cvp(s), contractile vacuole pore(s).

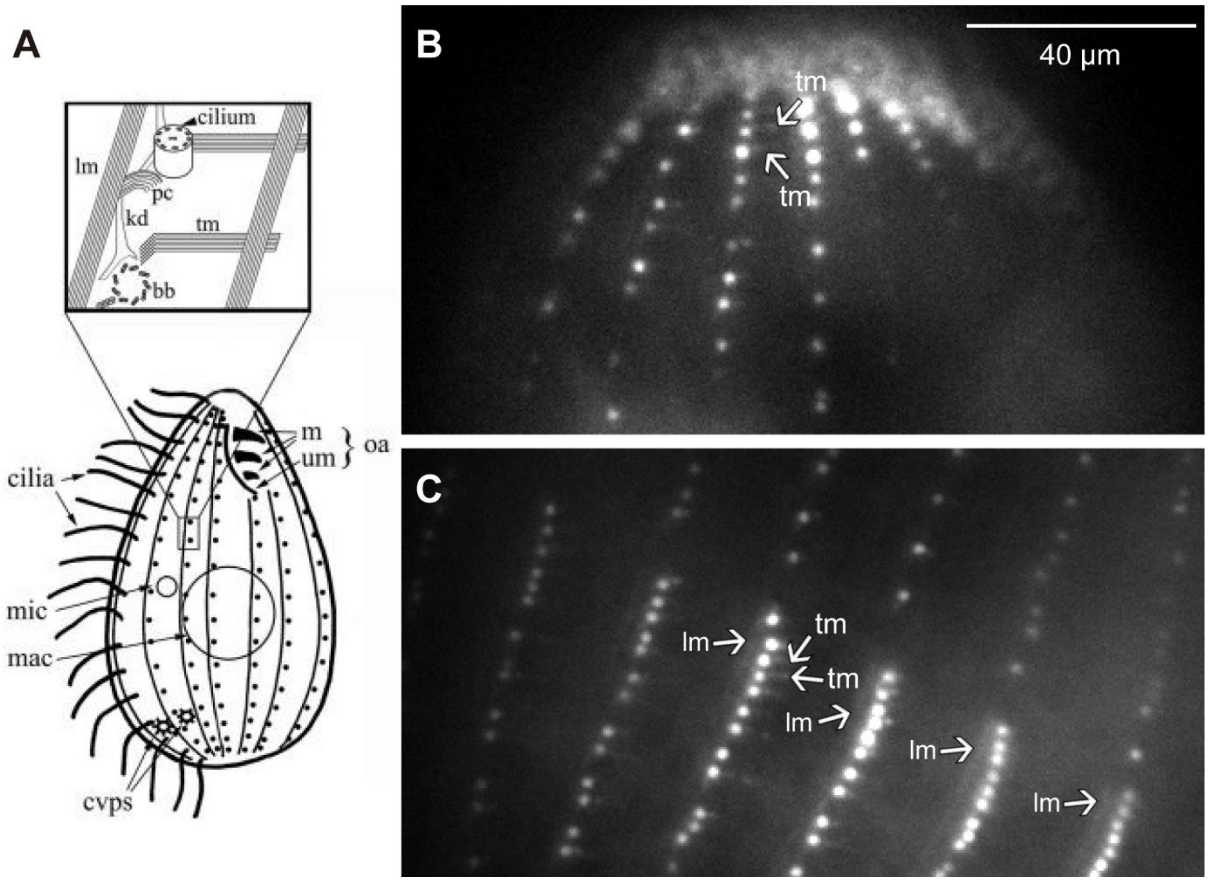
A
cilium
lm
pc
kd
tm
bb
m
um
oa
cilia
mic
mac
cvps
B
40 µm
tm
tm
C
lm
tm
tm
lm
lm
lm

Figure 3.S3. Overexpression of Hpo1 does not affect the cortical organelle pattern. Cells carrying a transgene expressing Hpo1-HA under the *MTT1* promoter were grown either without (A-D') or with addition of 2.5 mg/ml cadmium chloride for 6 hr (E-H'), fixed and labeled with the anti-HA (red) and either anti-centrin (A'-C'; E'-G') or anti-fenestrin (D',H') (green) antibodies and DAPI (blue). Note an accumulation of Hpo1-HA in the cell body of overproducing cells. Despite overproduction, the right-side and anterior gradients of Hpo1 are still apparent and the positions and number of OPs (E-G' compare to A-C') and the number of CVPs (H,H' compare to D,D') are unaffected.

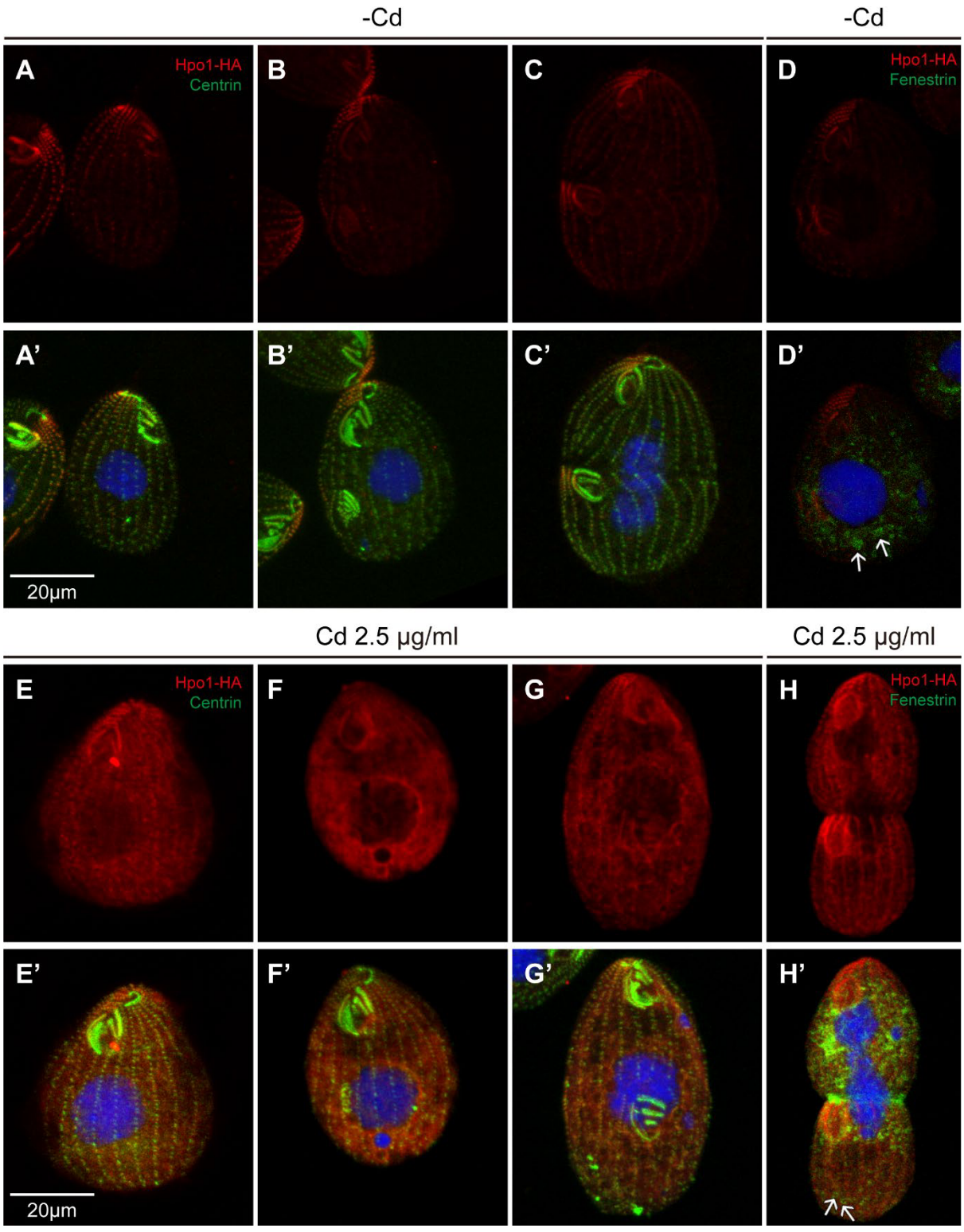
-Cd
-Cd
A
Hpo1-HA
Centrin
B
C
D
Hpo1-HA
Fenestrin
A'
B'
C'
D'
20µm
Cd 2.5 µg/ml
Cd 2.5 µg/ml
E
Hpo1-HA
Centrin
F
G
H
Hpo1-HA
Fenestrin
E'
F'
G'
H'
20µm

Figure 3.S4. Quantification of the circumferential distribution of Hpo1-3xHA in the *janC-4* homozygote. (A-A’’’’) An SR-SIM image of Hpo1-3xHA and centrin in an apical cell fragment of the *janC-4* homozygote. (A) The cell fragment was labeled with anti-HA (red), 20H5 anti-centrin antibody (green), and DAPI (blue) after overnight incubation at 30°C. Duplicates of single channel grey scale images for centrin (A’,A’’) and Hpo1-3-HA (A’’’,A’’’’) are shown. The yellow lines mark the area used for measurements of signal intensity. The pink arrows show the start locations for signal intensity measurements. The orange and cyan arrow indicates initial and end point of gap, respectively. (B) The graph shows that signal intensity plots for Hpo1-3xHA (red line) and centrin (green line).

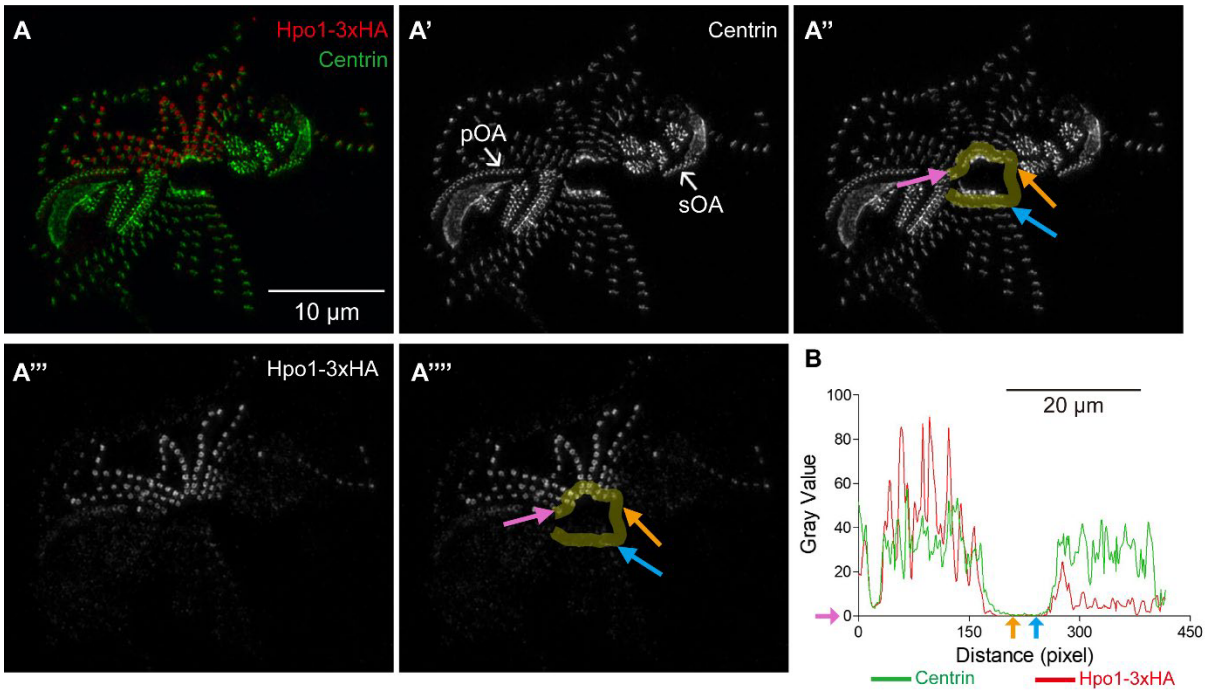
A
Hpo1-3xHA
Centrin
10 μm
A'
Centrin
pOA
sOA
A''
A'''
Hpo1-3xHA
A''''
B
20 μm
Gray Value
100
80
60
40
20
0
0
150
300
450
Distance (pixel)
Centrin
Hpo1-3xHA

Figure 3.S5. Localization of Bcd1-GFP in *hpo1-3 homozygotes*. (A-D’’’) Pairs of SR-SIM images showing two sides of the same cells that express Bcd1-GFP and are either otherwise wild-type (A-B’’’) or *hpo1-3* (C-D’’’). The cells were labeled with the anti-GFP antibodies (red), 20H5 anti-centrin antibody (green), and DAPI (blue) after a period of growth for 4 hours at 39°C.

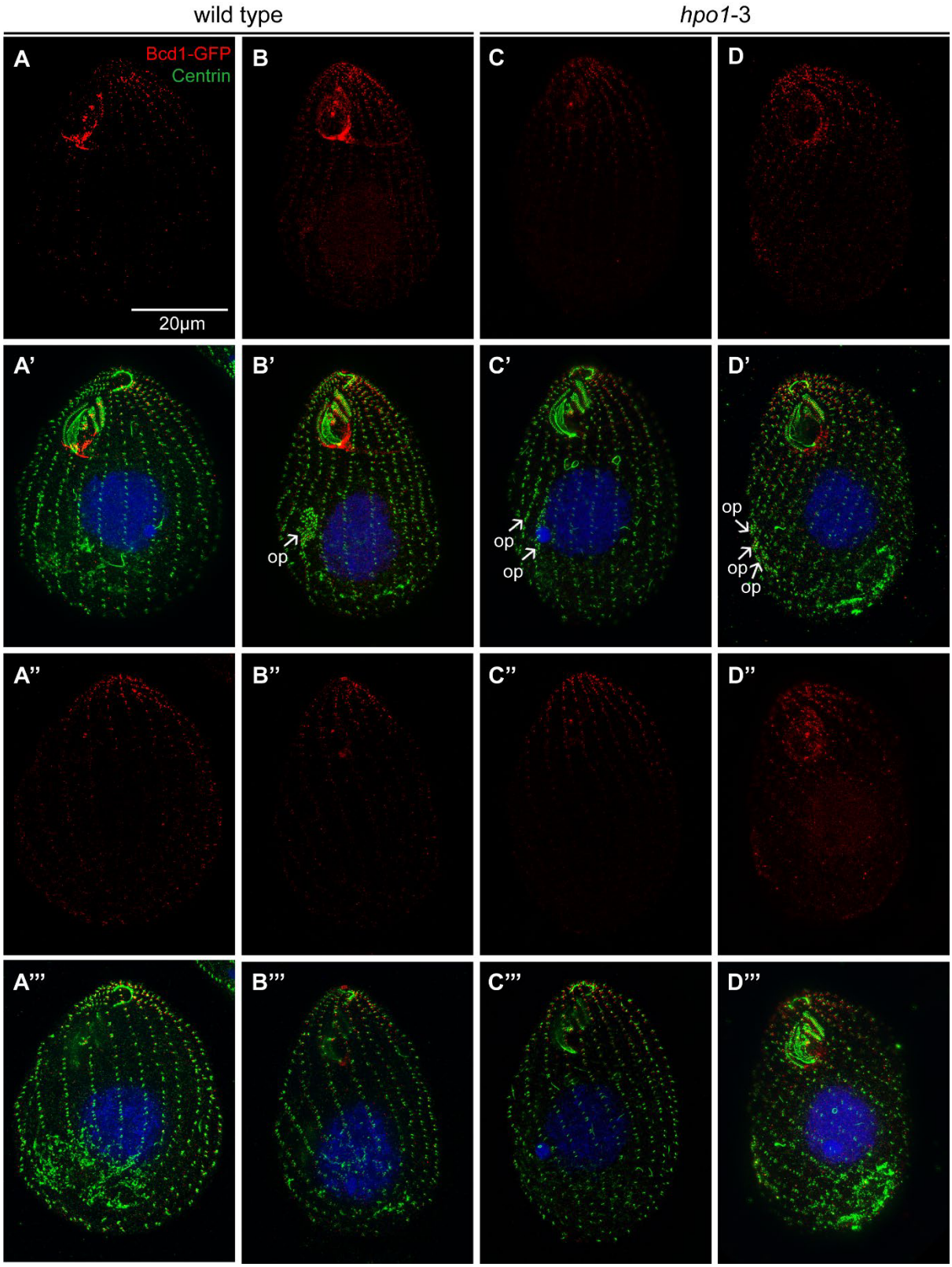
wild type
hpo1-3
A
Bcd1-GFP
Centrin
20µm
B
C
D
A'
B'
op
C'
op
op
D'
op
op
op
A''
B''
C''
D''
A'''
B'''
C'''
D'''

Figure 3.S6. Comparison of Hpo1-3xHA distributions between the wild type and *bcd1-2* homozygotes. (A-E’’’) Confocal images of Hpo1-3xHA expressed in wild type (A-B’’’) or *bcd1-2* homozygotes (C-E’’’). The same images for *bcd1-2* background were also used for the Figure 8. After overnight incubation at 30°C, the cells were labeled with anti-HA antibodies (red), 20H5 anti-centrin antibody (green), and DAPI (blue). (F,G) Graphs quantify the number of rows enriched in Hpo1-3xHA (F), and the ratio of Hpo1 enriched rows to the total number of rows per cell (G). ns: not significant. Stars indicate statistically significant (*: $P < 0.05$, **: $P < 0.01$, and ***: $P < 0.001$).

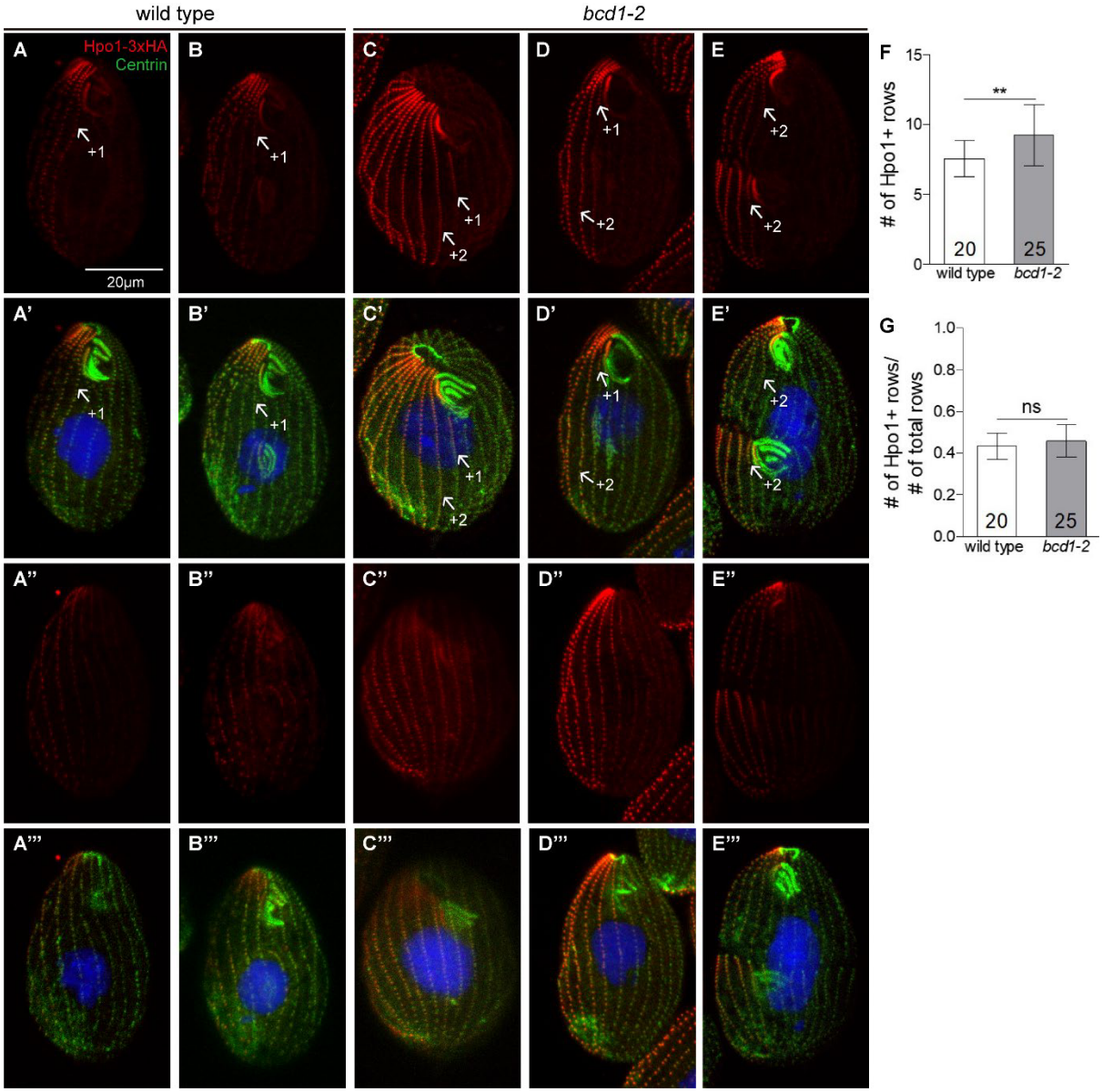
wild type
bcd1-2
A
Hpo1-3xHA
Centrin
B
C
D
E
+1
+2
20µm
A'
B'
C'
D'
E'
A''
B''
C''
D''
E''
A'''
B'''
C'''
D'''
E'''
F
# of Hpo1+ rows
**
20
25
wild type
bcd1-2
G
# of Hpo1+ rows/
# of total rows
ns

Figure 3.S7. The lethality caused by the loss of function of both Bcd1 and Hpo1 can be rescued by a transgene encoding Hpo1-3xHA. (A-C') SR-SIM images clones selected from the population of mating heterokaryons homozygous in the micronucleus for *bcd1-2* and *hpo1*-KO alleles that were either subjected to a mock biolistic bombardment (without transgene DNA) (A,A') or biolistically transformed with a transgene encoding MTT1-Hpo1-3xHA (B-C'). The cells were labeled with anti-HA (red), 20H5 anti-centrin antibody (green), and DAPI (blue) after overnight incubation at 30°C. (D,D') The diagram shows the positions of PCR primers designed for amplification of the portion of *HPO1* gene sequence deleted in the *hpo1-KO* allele (D) and the gel image showing the PCR products amplified from the genomic DNA isolated either from the escapee clone or from rescued clone (D').

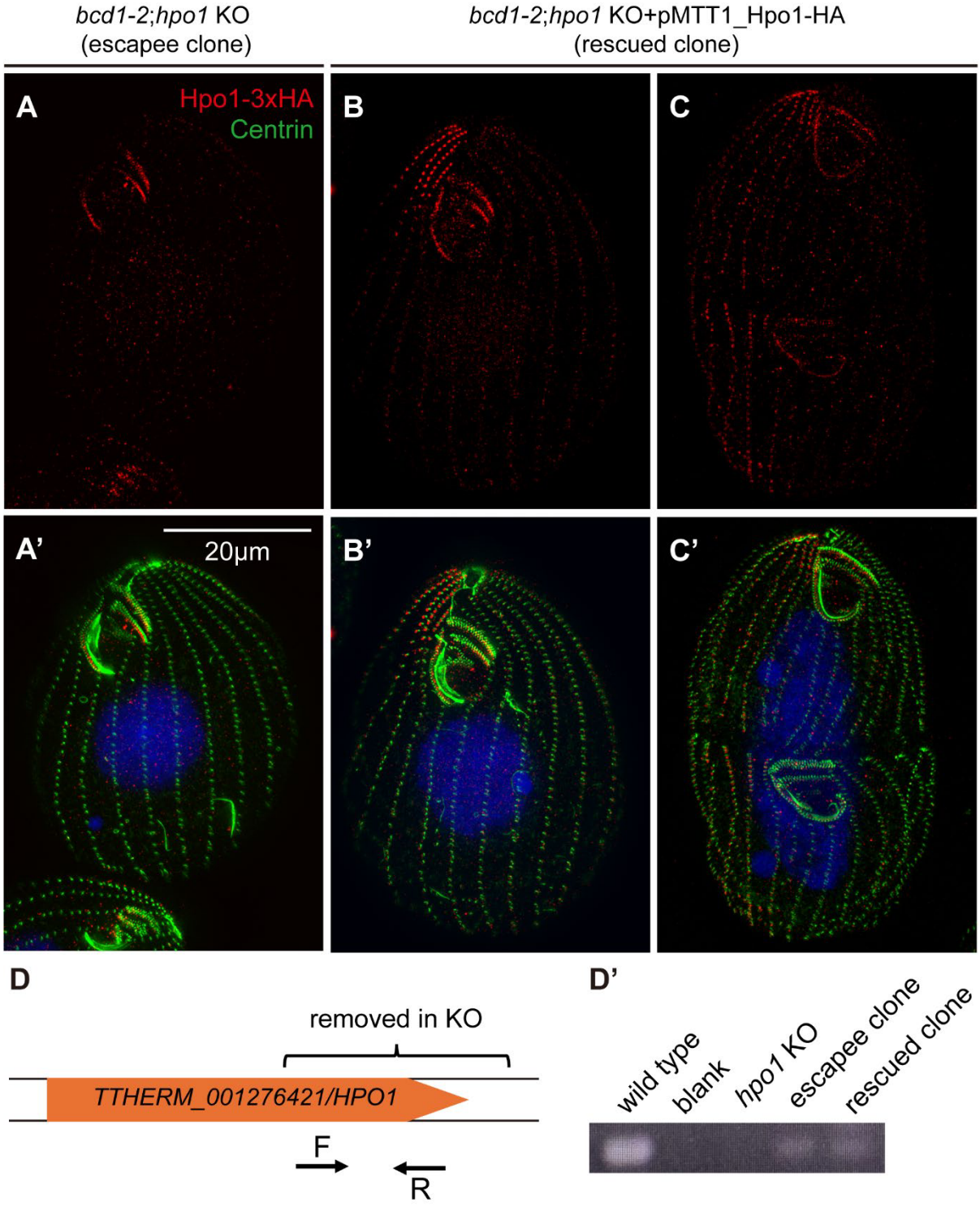
bcd1-2;hpo1 KO
(escapee clone)
bcd1-2;hpo1 KO+pMTT1_Hpo1-HA
(rescued clone)
A
Hpo1-3xHA
Centrin
B
C
A'
20μm
B'
C'
D
removed in KO
TTHERM_001276421/HPO1
F
R
D'
wild type
blank
hpo1 KO
escapee clone
rescued clone

Acknowledgements

This work was supported by the National Institutes of Health (grant R01GM135444 to J.G., R01GM110413 to K.F.L.), National Science Foundation (grant 1947608 to E.C.) and the German Federal Ministry of Education and Research (Bundesministerium für Bildung und Forschung) (grant 031L0101C de.NBI-epi to W.M.). The SR-SIM imaging was done at the Biomedical Microscopy Core, University of Georgia.

Author contributions

Jacek Gaertig conceived the project. Wolfgang Maier and Ewa Joachimiak mapped the allele by the bioinformatics approach. Ewa Joachimiak and Jacek Gaertig constructed plasmid or strain. Chinkyu Lee executed the rest of the experiments. Karl Lechtreck assisted TIRF microscopy and provided the images of live cells. Chinkyu Lee wrote the original draft of manuscript. Jacek Gaertig reviewed and developed the manuscript by proofreading and adding ideas and logics. Chinkyu Lee also predominantly organized the results into the figures whose structures and orders were mainly determined by Jacek Gaertig. Yu-Yang Jiang provided feedback for the manuscript. Eric Cole provided the illustration for the figure, proposing the principle of defects displayed in the *janC-1;hpo1-3* double mutant. The NIH-originated funding for this research was acquired by Jacek Gaertig who led this project.

CHAPTER4

CONCLUSIONS

Principles underlying cell polarity still remain largely unknown. Being impressed by strikingly invariable placement of organelles at each of specific cortical domain of *T. thermophila*, I began my doctorate research with strong desire to dissect molecular mechanisms underlying such precise intracellular pattern formation. I was able to take advantage of availability of cortical mutants thanks to pioneering work of Joseph Frankel and his students (University of Iowa, USA) who isolated and characterized the *Tetrahymena* mutant strains on the basis of patterning defects affecting cell polarity or shape of organelle (reviewed in (Frankel, 1989; Frankel, 2008)). In recent years, Wolfgang Maier (University of Freiburg, Germany) in collaboration with our laboratory developed bioinformatics approaches enabling mapping mutation in the *Tetrahymena* genome and we have mapped several causal mutations to genes that encode factors implicated in intracellular pattern formation. By this method previously described (Jiang et al., 2017; Jiang et al., 2020), multiple pattern regulator gene products have been recently implicated in placement of organelle along anterior-posterior (A/P) axis , most of which are conserved kinases or kinase-binding proteins, (Jiang et al., 2019; Jiang et al., 2017; Jiang et al., 2020; Lee et al., 2024; Slabodnick et al., 2014; Tavares et al., 2012). Following these groundbreaking studies, I began to delve into exploring the *cdaH-1* allele as my first doctoral project (Lee et al., 2024). *cdaH-1* confers a rather complex and puzzling phenotype with most (but not all) defects specific positioning on the A/P axis: an anterior shift of the OA followed by its instability, a failure to develop the DB and an arrest in cytokinesis (Frankel et al., 1980; Lee et al., 2024). Recent studies have determined that the DB induction and positioning involves mutually-antagonistic factors: anterior CdaI (Mst/Hippo kinase) (Jiang et al., 2017) and posterior CdaA (cyclin E) (Jiang et al., 2020), whose mutations produce partially overlapping

phenotypes with *cdaH-1*. For example, *cdaA-1* confers a failure to develop the DB (Frankel, 2008; Frankel et al., 1980; Jiang et al., 2020), while *cdaI-1* confers an anterior shift of the OA (Jiang et al., 2019; Jiang et al., 2017) (reviewed in (Frankel, 2008)). We therefore hypothesized that CdaH interacts with CdaA or CdaI (or both) and could be a participant or even outcome of the mutual antagonism between CdaI and CdaA. My initial contribution to this project was an identification of the *CDAH* gene among the two candidate genes proposed based on a pair of closely-linked variants co-segregated with *cdaH-1* using Maier's

bioinformatics pipeline: G/A at chr5:49333 and C/T at chr5:501775. The former variant causes amino acid replacement (A168T) in TTHERM_01345780 whereas the latter variant causes V1176I substitution in TTHERM_00649260. I amplified the wild-type fragments containing each of the variant region and then introduced each fragment into the *cdaH-1* mutant. Testing at the restrictive temperature 38°C (note that *cdaH-1* is a temperature-sensitive allele), we observed a rescue of capability of cell division in the *cdaH-1* cells transformed by the *TTHERM_01345780* fragment, but not in the *cdaH-1* cells transformed by *TTHERM_00649260* fragment. Thus, we identified *CDAH* gene as *TTHERM_01345780* that encodes an ortholog of one of the most highly conserved kinases: *H. Sapiens* Stk36 and *D. melanogaster* Fused Fu (Lee et al., 2024). Our BlastP analysis for Stk36, Fu, and TsuA (Fused/Stk36 ortholog in *Dictyostelium*) (Tang et al., 2008) against *T. thermophila* proteome all placed CdaH as a top match. In *Drosophila*, Fused is required for proper establishment of segment polarity during embryonic development and for development of wings and legs during the larval stage (Maloverjan and Piirsoo, 2012). However, in the kinetoplastid *L. Mexicana* (McCoy et al., 2023) and in mammals (Edelbusch et al., 2017; Liu et al., 2016; Nozawa et al., 2013; Wilson et al., 2009), Fused/Stk36 is essential for normal structure of motile 9+2 cilia. Specifically, in cells lacking Fused/Stk36, cilia lack the central microtubules (become 9+0) (Liu et al., 2016; McCoy et al., 2023; Nozawa et al., 2013; Wilson et al., 2009).We tested if CdaH is essential for ciliary phenotypes in *T. thermophila* by electron microscopy with assistance of Mary Ard (GEM, University of Georgia). We found no obvious ciliary defects in the *cdaH-1 Tetrahymena* mutant and thus we suggest that CdaH is involved in pattern formation and execution of cell division and not in cilia biogenesis in *T. thermophila*. This conclusion is limited as we have only characterized a single allele, *cdaH-1*, and we do not know whether this is a null. However, the pattern of localization of CdaH (see below) and in particular its apparent absence from cilia, suggests that CdaH does not have a ciliary role. Given that in diverse eukaryotic lineages, Fused/Stk36 orthologs have been implicated in ciliary functions (Liu et al., 2016; McCoy et al., 2023; Nozawa et al., 2013;

Wilson et al., 2009) and that motile 9+2 cilia were present in the ancestral eukaryotes(McCoy et al., 2023) , it is possible that the ciliary role of Fused is also ancestral and that the pattern formation role of CdaH has emerged in the phylum of ciliates. However, it is intriguing that in *Drosophila*, Fu is required for “segment polarity” (Busson et al., 1988; Gergen and Wieschaus, 1986; Nusslein-Volhard and Wieschaus, 1980; Perrimon, 1994; Perrimon and Mahowald, 1987), a function that probably is likely non-ciliary as embryonic cells of *Drosophila* lack cilia (Kuzhandaivel et al., 2014). Segment polarity involves signaling between cells generated by Wnt and Hedgehog pathways (Colosimo and Tolwinski, 2006; Swarup and Verheyen, 2012) (reviewed in (Perrimon, 1994)). Wnt signaling is a key part of the Planar cell Polarity (PCP). It is intriguing to note that a dividing *Tetrahymena* cell can be seen as a special example of PCP as at the end of cell division the two daughter cells assume the same orientation. Even if this is a pure coincidence, we should be open to a possibility that both roles of Fused: in cilia and in cell signaling related to cell and embryonic polarity are both ancient. Furthermore, a ciliary role of Fused in *Tetrahymena* may be fulfilled by several paralogs of CdaH (Lee et al., 2024) .

After identifying *CDAH* gene, we aimed at observing cortical localization of CdaH by tagging GFP to CdaH. In the wild-type cells expressing CdaH-GFP along the course of cell division, CdaH-GFP forms “streaks” in posterior cell half during early division stage and eventually forms a subequatorial ring across the division boundary that colocalize with the actin contractile (cytokinetic) ring; interestingly the actin/CdaH ring remained exclusively at the tip of the posterior daughter cell, indicating that in *Tetrahymena*, cytokinesis is entirely asymmetric (the division machinery forms in the posterior daughter and “cuts out” the anterior daughter. (Lee et al., 2024). We also recognized CdaH-GFP localization at cell tip and in the oral apparatus (Lee et al., 2024) and thus we suggested that CdaH is involved in multiple functions at multiple locations. Next, to see CdaH-GFP cortical pattern *in vivo*, we asked for TIRF microscopy by Karl Lechtreck (University of Georgia, USA). The TIRF

imaging with the protocol described previously (Jiang et al., 2015) revealed that the localization pattern of CdaH is overall consistent with what was observed in the fixed cells. Our additional goal of the TIRF imaging was to reveal how CdaH is loaded onto cortex. One possibility was that CdaH is distributed by motor proteins walking along microtubules, referring to the published suggestions that in ciliates, factors that contribute to pattern formation along anterior-posterior axis are distributed by motor proteins working along longitudinal microtubule bundles in cortex ((Cole and Gaertig, 2022; Marshall, 2021)). However, the kymogram analyses failed to reveal CdaH movements within or between CdaH streak(s), suggesting that CdaH cortical distribution is not dependent on cortical microtubule networks and thus CdaH is placed in cortex by another mechanism (Lee et al., 2024). On the other hand, FRAP experiments revealed that CdaH pools (streaks and the ring) are dynamic indicating a rapid exchange, possibly with soluble CdaH from the cell body. Being especially interested in CdaH-GFP ring observed during a time when cell forms cortical subdivision and subsequently undergoes cytokinesis, we tested if CdaH and the main cytokinetic ring component actin (Act1) are co-localized. To label Act1, we fixed the cells with 1% paraformaldehyde and then treated 1% SDS (See the ‘MATERIALS and METHODS’ section of the Chapter 2.) to unfold Act1 as the anti-Act1 polyclonal antibodies were generated against the linear sequence of Act1 and these antibodies do not work well in detection of the folded Act1. Our data consistently show that Act1 and CdaH-GFP ring are-colocalized during cytokinesis stage and that a residue of both rings remained in posterior daughter cell even after completion of cytokinesis (Lee et al., 2024). Dr. Nakano’s images additionally show that CdaH-GFP ring appears earlier than assembly of actin ring and this indicates that CdaH may be required for assembly of Act1 ring. The fate of residues of Act1 and CdaH-GFP ring in posterior daughter cell needs to be further explored by ultrastructural analysis. One speculation we propose is that CdaH-GFP remnant may be required for remodeling of Act1 into the apical crown, a structure located at the anterior tip of interphase and dividing *Tetrahymena*. The CdaH ring is reminiscent of the septin ring in budding yeast (Bi and Park,

2012; Sadian et al., 2013) in regard to localization and ring-shape assembly. Therefore, I suggest CdaH may also recruit the cytokinetic ring by distinctive mechanism, given its absence of a GTP-binding domain. Next, as referred above, given similarities of defects displayed in the mutants, I tested if CdaH interacts with CdaI (Mst/Hippo kinase) or CdaA (cyclin E) (Frankel, 2008; Jiang et al., 2017; Jiang et al., 2020). By immunofluorescence and subsequent microscopy we tested if CdaH distribution is affected by *cdaA-1* or *cdaI-1* allele and also if CdaA or CdaI distribution is affected by *cdaH-1* allele. We found out that CdaH-GFP posterior streaks (observed during early division phase) and ring (observed during subdivision and cytokinesis followed) were absent at restrictive temperature 39°C in the temperature-sensitive *cdaA-1* background, whereas in another temperature sensitive *cdaI-1* background, there was no critical effect of CdaH-distribution except for its anterior shift that was expected as this is the phenotype conferred by *cdaI-1* alone (Lee et al., 2024). Both CdaA and CdaH are required for the formation of division boundary (Frankel, 2008; Jiang et al., 2020; Lee et al., 2024), and likely CdaH acts downstream of CdaA in proper induction of division boundary and cytokinesis, whereas the distribution of CdaH is not directly dependent on functionality of CdaI. To further explore how CdaH interacts with CdaA or CdaI, I investigated phenotypes of *cdaH-1;cdaA-1* and *cdaH-1;cdaI-1* double mutants. My confocal microscope images show that phenotype displayed in the *cdaH-1;cdaA-1* double mutant is similar to that of *cdaH-1* single mutant : a lack of DB formation and degradation of OP shifted anteriorly (Lee et al., 2024). This doesn't indicate any gene interaction, but at least this result is consistent with our important findings that CdaH acts downstream of CdaA in formation of DB and CdaH is not dependent on CdaA in global (positioning) and local patterning (stability) of op, given redundancy of CdaA in placement of op along A/P axis. In the *cdaH-1;cdaI-1* double mutant, we detected absence of severe op degradation displayed in *cdaH-1* single mutant and this may suggest that CdaI inhibits CdaH activity required for prevention of op degradation (Lee et al., 2024). We also observed excess of oral rows in op (phenotype also shown in *cdaI-1* but with relatively lower frequency) displayed in the *cdaH-*

1;cdaI-1 double mutant. Interestingly, in the double mutant *cdaH-1* didn't enhance excess of membranelle/op but at least increased penetrance of the additional-membranelle defect. This finding indicates that CdaH and CdaI interact in regulation of op sizing (Lee et al., 2024). To summarize, my studies on CdaH reveal its multiple roles correlated with multiple locations. CdaH role in the DB formation is likely downstream of the posterior CdaA. Its role in the OP positioning is likely separate and executed by the OP-restricted pool. CdaH also interacts with CdaI in shaping the oral apparatus. The pleiotropic phenotype of *cdaH-1* is consistent with its proposed multiple roles. As CdaH is a kinase, one could imagine how the same kinase can be targeted to multiple locations by diverse binding partners and have multiple activities by phosphorylating multiple protein substrates. Given its multifunctionality, further dissection of CdaH roles could be challenging. On the other hand, CdaH appears to be closer to the effector end of the pattern formation pathways and therefore its further characterization could be seen as low priority if someone aims at discovering the actual "pattern formation" mechanism.

However, there is more of complication in understanding pattern formation of *T. thermophila* due to necessity of investigating organelle placement along circumferential (left-right) axis. If we take into account only the longitudinal ciliary rows, *Tetrahymena* cells display almost a perfect radial symmetry without a clear distinction between the ventral and dorsal surfaces (the cell is shape more or less like a barrel). However, the major organelles, such as the OA, CVPs and CYP have asymmetric positions around the cell. Namely, CYP is positioned at the same longitude as the OA and CVPs are located several rows to the right of the OA/CYP longitude. This pattern is transmitted faithfully during cell division. However, the pattern is not absolutely invariable. Nanney found that while most of the time the OP forms near the same postoral row (right), occasionally the OP forms along the row shifted to either cell's left or less frequently right side (Nanney, 1967). This phenomenon was named "cortical slippage". Interestingly, in these cases the

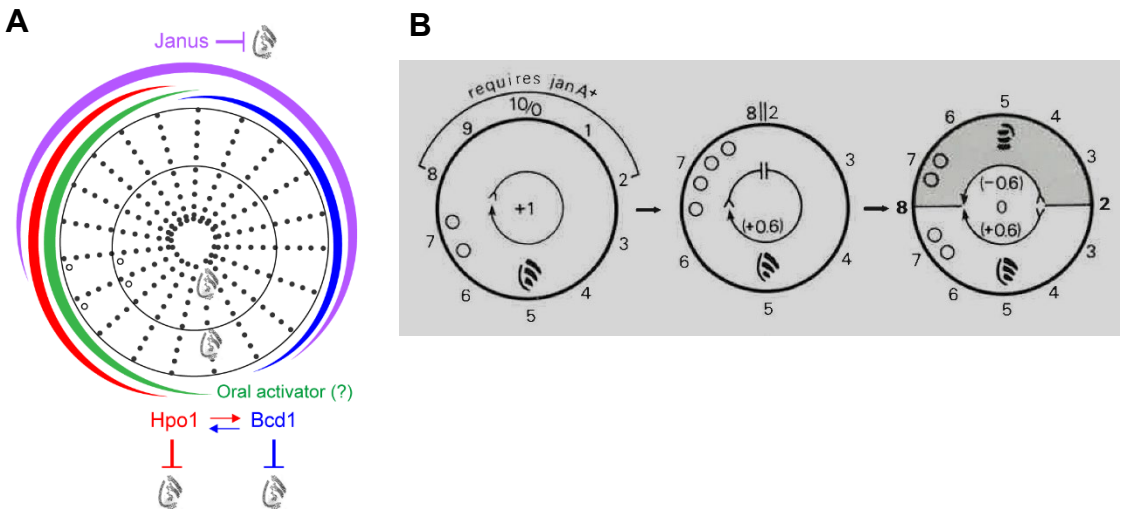

Figure 4.1. The Cylindrical model. (A) The illustration of top view of *T. thermophila* and patterning factors (Fig. 1 of the Chapter 3). (B) The cylindrical model (the picture borrowed from (Frankel, 1989)) that defines position of organelle based on the position values ranging from 0 to 10 (OA assigned to 5, and CVP assigned to 7). Note the process of loss of the values and subsequent intercalation under the effect of *janA* allele.

positions of CVPs and CYP were also shifted in agreement with the position of the OP arguing that there is a “global” positioning system that maintains relative placements of organelles.

Frankel’s work on the *janus* mutant led to a model for circumferential positioning called the cylindrical coordinate model (CCM) (Fig. 4.1B). CCM was inspired by the “polar coordinate model” developed for principle of distal regeneration of appendages of insects and vertebrates (French et al., 1976). CCM postulates that there is a circumferential positioning system that produces unique “values” to longitudes. *Tetrahymena* cell would be organized like a clock face with 0 to 10 values. OA can be arbitrary assigned to value 5, CVPs to value 7 (the first depiction of Fig. 4.1B). Somewhere on the cell’s left side value 10 would be next to value 0 (Frankel and Nelsen, 1987). In the *janus* mutant there is a second OA that forms on the dorsal side and what appears to be a duplication of the CVP domain. The dorsal second OA is often in a reverse orientation (Figure 5,S4 of the Chapter 3). Frankel proposed that *janus* mutant lost the ability to express the dorsal CCM values (from 8 to 2) (the middle

depiction of Fig. 4.1B). Next Frankel postulated that the positioning system does not tolerate sharp boundaries, the *janus* case 8 would be next to 2. The cell fills in the missing values with a reversed ventral domain (8-2 is replaced by 8-7-6-5-4-3-2) to minimize the contrast between adjacent values (the last depiction of Fig. 4.1B) (Frankel and Nelsen, 1987). Note that CCM is entirely a theoretical framework that attempts to explain cortical variations. Frankel himself all but abandoned CCM when characterizing the *hypoangular 1* (*hpo1*) mutant whose complexities seriously challenged CCM (Frankel et al., 1993). For example, it appears that *hpo1* has lost the ability for expressing some right-ventral longitudes which results in the CVPs positioned closer to the OP during division. However, this happens without any attempt on the cell side to fill-in the missing region by “reversed intercalation”. While our data do not disapprove CCM entirely, we reexamined *hpo1-1*, mapped the mutated gene, localized the gene product and studied its interactions, which led us to propose an alternative model for circumferential positioning based on “bilateral gradients” (see below).

I launched on studying *hpo1* alleles conferring patterning defects along cell the circumference as my second doctoral research project. We could confirm that *hpo1-3* mutant and *hpo1* knockout strains both display excess of oral primordia often shifted to either the left or right from correct position 0 (Fig.1 of the Chapter 3), with additional observation that the degree of such abnormalities appeared higher in the KO strain (Fig. 2 of the Chapter 3). By application of comparative next-generation sequencing (Galati et al.), Wolfgang Maier mapped both *hpo1-1* and *hpo1-3* alleles to the *TTHERM_001276421* gene that encodes a ciliary tip- and BB-enriched protein ARMC9, whose loss of functionality in humans triggers Joubert syndrome, one of the diseases derived from defective cilia (Latour et al., 2020; Louka et al., 2018; Van De Weghe et al., 2017). Hpo1 orthologs appear limited to diverse ciliate lineages. Likely, Hpo1 emerged by gene duplication of the ancestral ARMC9 during the emergence of ciliates. Both *hpo1-1* (S236N) and *hpo1-3* (F318S) affect Armadillo repeat domain of TTHERM_001276421 protein (Fig. 3 of the Chapter 3) and with this information,

Ewa Joachimiak (Nencki Institute of Experimental Biology of Polish Academy of Sciences, Poland) by homologous DNA recombination generated a homozygote strain expressing *hpo1-3* version of Hpo1 with an HA tag. I labeled this strain with antibodies and the cell appears to phenocopy the *hpo1-3* mutant strain, showing extra OPs and their deviations from normal position. So we were clearly convinced that *TTHERM_001276421* is *HPO1* gene. To see the pattern of Hpo1, I stained the wild type background strains expressing Hpo1-3xHA protein. Throughout the entire cell cycle, we could observe accumulation of Hpo1-3xHA on right side (cell's perspective) of cell cortex in a form of a circumferential bilateral gradient whose the highest point on the right lateral side of cell (midregion of the gradient ranging from ventral to dorsal side) (Fig. 4 of the Chapter 3). It is likely important that the Hpo1 gradient is not uniform and displays sharp drop-off on the ventral side between row +1 and 0. The OA normally forms on the left side of row 0. So we hypothesized that the Hpo1 +1/0 discontinuity may be important for determining the site permissible for oral development. Interestingly, we detected a second drop-off of Hpo1 levels on the dorsal side at the location where an extra OA forms in the *janC-1* background (Fig. 5,S4 of the Chapter 3). We concluded from these observations that the dorsal discontinuity in the Hpo1 gradient acts as a marker for development of a cryptic oral apparatus and that the Janus gene product suppresses that Hpo1 discontinuity site's ability to support oral development on the dorsal side (Fig. 1,5 of the Chapter 3). From analyzing phenotypes of double mutant *janC-1;hpo1-3*, separation of two oral apparatuses (OAs) conferred by *janC-1* was significantly diminished by expression of *hpo1-3* (Fig. 6 of Chapter 3). We proposed that Hpo1 contributes to placement of oral apparatus by exclusion of the Hpo1 enriched zone along the cell circumference. Namely, we propose that in *T. thermophila*, OA is placed at the contrast positions formed by bidirectional gradient of Hpo1. Hpo1 could be acting as an inhibitor of oral development and consequently the OA can form only at the drop-off positions (and the dorsal position is normally suppressed by Janus activity). These observations led us to revisit the interesting discoveries about oral development made in *Stentor*. Importantly, in

Stentor, the circumferential pattern is profoundly asymmetric. Namely, the width of the gap (called stripe) between the ciliary rows gradually increases in a clockwise direction along cell circumference. The narrowest stripe (on the right) meet the widest stripe (on the left) on the ventral surface. During cell division the OP develops at that position named the “locus of stripe contrast (LSC)”, the domain where the narrowest and the widest stripes border each other (Tartar, 1956b; Uhlig, 1960). Thus, we conclude that *Stentor* and *T. thermophila* use “structural contrast” and “molecular contrast”, respectively in determining site for oral development. That oral development in *Stentor* is induced by the “structural contrast” was confirmed in microsurgery experiments in which a portion of the wide stripe cortex was excised transplanted into the narrow stripe region of another *Stentor*. This led to the generation of two new zones of contrast at the margins between the transplant and the recipient cortex. Remarkably, the operated *Stentors* developed an OP at the original position and two extra OPs at positions of margins corresponding to the two new contrast zones (Tartar, 1956b). We postulated that Hpo1 is a component that generates the circumferential contrast needed for oral development. Hpo1 appears to act as an inhibitor for oral development by exclusion from its occupying domain. We speculated that the Hpo1 domain (cell’s right side) is also a source of currently unknown “oral activator”. The activator gradient could extend beyond the Hpo1 inhibitor gradient at the Hpo1 discontinuity position, permitting oral development on cortical domain free of Hpo1 influence (Fig. 1 of the Chapter 3). Thus, our model that oral development is governed by communication between a currently unknown OP activator, Hpo1 as an inhibitor, and Janus as a dorsal suppressor.

The nearly invariable positioning of only one oral apparatus may be possibly discussed in an analogous perspective with the bud emergence in *S. cerevisiae*, whose singularity is regulated by competition between Cdc42 patches and subsequent selection of one Cdc42-enriched site for bud growth governed by the cues generated by the scar from the previous

budding site(Witte et al., 2017; Wu et al., 2015) (reviewed in (Chiou et al., 2017)). Interestingly, Hpo1 (and also Bcd1, see later) could also be seen as factors needed for singularity of oral development. Both *hpo1* and *bcd1* alleles induce multiple adjacent OPs. One can propose that in analogy to the bud formation mechanism in yeast, in ciliates there is competition among multiple adjacent sites on the ventral side of the cortex but eventually only one site “wins” and is selected for placement of oral primordium. The Hpo1/unknown activator system could be important in fine tuning the position of OP and maintaining its singularity (Fig. 1 of the Chapter 3). Importantly, while both *hpo1* and *bcd1* alleles (see below) cause shifts and multiplicity in OP development, the positions of OPs still cluster around the same region close to row 0. Again these observations position Hpo1 as a local rather than global positioning factor. Thus “OP site focusing” function is likely executed as an interaction with the right-side enriched Bcd1 (see below).

Another cortical organelle system that is subject to circumferential positioning is the contractile vacuole pore(s) (CVP(s)), structures that are required for osmoregulation. In most cells two CVPs are located (Fig. S1 of the Chapter 3) near posterior ends of two adjacent rows to the right of the oral apparatus. We observed that the CVP region overlaps with the high point of Hpo1 in *T. thermophila* (Fig. 5 of the Chapter 3). Intriguingly, *hpo1* mutants have fewer CVPs (Fig. S1 of the Chapter 3). We know that the positions of OA, CYP and CVPs are coordinated (Nanney, 1967). Somehow, in the *hpo1* mutants this coordination fails resulting in variation between the positions of oral structures and CVPs (in the *hpo1* original mutants the CVP domain is closer to the oral domain, hence the name of the mutant “*hypoangular*” referring to the decreased angle between the positions of these organelles when viewed from the cell’s apical end as a polar projection). It is however puzzling that *hpo1* mutations decrease the number of CVPs. *bcd1* mutants also have an increased number of OPs but also have more CVPs. Possibly, Hpo1 induces CVPs at the high level of its expression and induces OPs at a low level of its expression (likely indirectly), see above).

Hpo1 circumferential gradient is used in determining location for cortical organelles in a manner that pattern formation of each organelle is assigned to different parts of the circumferential gradient. This is reminiscent of the link between molecular gradients and patterning in other organisms (Gao et al., 2011; Hersch et al., 2015; Kiekebusch and Thanbichler, 2014; Thanbichler and Shapiro, 2006). Likely, principle of molecular gradients driving pattern formation is conserved in diverse evolutionary lineages, including *T. thermophila* and we suggest that Hpo1 may serve as morphogen (defined as molecule emanated from a specific set of cells and distributed in a concentration-gradient that specifies the fate of each cell (reviewed in (Mehlen et al., 2005)) at the single cell level, given bidirectional gradient of Hpo1 that appears to overlap with CVP and contrast against OA. Overproduction of Hpo1-HA under the *MTT1* promoter by treatment of cadmium chloride doesn't appear to affect cortical cortical pattern (Fig. S3 of the Chapter 3), indicating that Hpo1 is not a rate-limiting factor, interacting with binding partner or an activator.

The final part of this project was an analysis of a genetic interaction between *hpo1* and *bcd1* alleles. Bcd1 is a highly conserved Beige-Beach domain protein orthologous to the human NBEA, implicated in vesicle trafficking including exocytosis and endocytosis (Cole et al., 2023). In *Tetrahymena*, Bcd1 is enriched as a gradient on the cell's left side, which is opposite to the pattern of Hpo1. Furthermore, *bcd1* loss of function alleles produce an OP phenotype that is remarkably similar to that of *hpo1* alleles: multiple adjacent OPs shifted to either left or right of row 0 (Fig. S5 of the Chapter 3). These observations suggested that there could be an interaction across row 0 between right-enriched Hpo1 and left-enriched Bcd1 that focuses OP to row 0. We analyzed the pattern of Hpo1-3xHA gradient in the *bcd1-2* background. Our microscope images show that expression of *bcd1-2* allele in a subtle way altered the pattern of Hpo1 on both the A/P (characterized by correct steepness) and C axis (characterized by a more clear definition of Hpo1-based contrast row on ventral side) of Hpo1 3xHA are dependent on functionality of Bcd1 (Fig. 7,8,S6 of the Chapter 3). Bcd1 acts

to maintain proper C polarity but uniquely by regulating membrane trafficking that prevents excessive cortical loading of organelle components (Cole et al., 1987; Cole et al., 2023). We subsequently analyzed phenotypes of the double mutant *bcd1-2;hpo1 KO* generated by genetic crosses between heterokaryons. Surprisingly the progeny of double mutant heterokaryons was not viable. I subsequently analyzed the double mutant progeny of heterokaryons before their ultimate death. My SR-SIM microscopy revealed diverse patterning defects including significant displacements of oral primordium toward the posterior cell end, an abnormal shape of entire cell and defects in the internal organization of the oral apparatus (Fig. 9 of the Chapter 3). Surprisingly, among the most predominant defects in the double mutant is the posterior migration of op. Posteriorly biased op was also occasionally found in the single mutants expressing either *hpo1* (Frankel et al., 1993) or *bcd1* alleles (Cole et al., 1987). This indicates that molecular mechanisms driving either A/P or C patterning are not completely separated. While the C patterning is more sensitive to the loss of either Hpo1 or Bcd1, the A/P patterning is strongly affected when both factors are lost. Possibly, the distributions of A/P factors such as CdaI (Jiang et al., 2017), Elo1 (Jiang et al., 2019), and CdaA (Jiang et al., 2020) are modified in the double mutant *bcd1-2;hpo1* KO. In particular, we were surprised to find out that this double mutant phenotype is lethal. Introduction of a wild type Hpo1 into the double mutant successfully rescued the lethality (Fig. S7 of the Chapter 3). We conclude from all of these phenotypes of *bcd1-2*;*hpo1* KO that either Hpo1 and Bcd1 is required for *Tetrahymena* cell survival. We speculate that there is an essential left-right cross-talk between Hpo1 and Bcd1 that mediates the placement and shaping of cortical features including oral apparatus. The idea of a left-right cross-talk reminded us of the grafting experiment executed by Vance Tartar and Gotram Uhlig that showed remodeling of cortex for induction of relatively lower stripe (ciliary row) contrast of *Stentor* and subsequently OP development delayed until the cortex undergoes remodeling by branching of a subset of wider stripes that generated contrast strong enough for oral induction (Tartar, 1956a; Uhlig, 1960). This provides clear evidence that left and right cortex

interact for cortical development. I also see a possibility of left-right interaction at local scale from observation of defects such as symmetrical alignment of oral rows or excessively long membranelle forming circular shape of oral apparatus in the *bcd1-2*;*hpo1* KO strain (Fig. 9 of the Chapter 3). Likely, given undulating membrane (um) decorated by antibody targeting Hpo1-3xHA (Fig. 3,4 of the Chapter 3), and left adjacent site decorated by antibody targeting Bcd1-GFP (Fig. S5 of the Chapter 3), Hpo1 and Bcd1 may possibly interact for correct shaping of oral apparatus. Unlike the double mutant, *hpo1-3* single mutant displays almost intact oral rows. Bcd1 appears to accumulate near oral rows (Fig. S5 of the Chapter 3), and such local Bcd1 may display accessory role in assembly of oral rows. But overall, link between C factors and internal polarity of oral apparatus still remains to be explored. From examination on the phenotypes of double mutants expressing *hpo1-3* and either *bcd1-2* or *janC-1*, we didn't see clear indication of gene interaction driving pattern formation of CVP (Fig. S1 of the Chapter 3).

Another discovery we made in relation to the interaction between Hpo1 and Bcd1 was mutual enhancement of Hpo1 and Bcd1. We initially anticipated that given lateral misplacement of OPs in the *hpo1-3* and *bcd1-1* single mutants, we anticipated that Hpo1 (enriched on the right side) and Bcd1 (enriched on the left side) would unidirectionally exclude OP from its domain. However, we observed that OPs were either misplaced in either left or right direction in both of the single mutants. This may indicate that Hpo1 and Bcd1 mutually enhance its exclusion activity against OPs. Namely, loss of Hpo1 may also affect Bcd1 to some extent, permitting shift of OP not only in Hpo1-free direction but also in Bcd1 direction and vice versa. Although we see the sign of mutual enhancement, it is reminiscent of mutual inhibition between CdaA and CdaI whose balanced activity is required for patterning along the A/P axis (Jiang et al., 2020). We conclude that Mutual interaction (either inhibition or enhancement) is extensively employed in patterning of organelles along the polarity axes.

One important unanswered question is how the cell generates the polarized distribution of Hpo1. The TIRF microscopy done in collaboration with Karl Lechtreck (University of Georgia) showed weak presence of Hpo1 along the microtubule networks associated with BBs including transverse microtubules TMs (Fig. S2 of the Chapter 3). The TM localization is of interest because these microtubules align with the axis of circumferential polarity. While the TMs of adjacent rows are short and do not overlap, one could imagine that motors distribute Hpo1 along the TMs with breaks for diffusion between the adjacent rows (not unlike motors move cargo along the short microtubules in the axon between the cell body and the synaptic terminal). This implies that motor proteins moving along the microtubules may transport Hpo1 as the cargo and given gradient of Hpo1, such transfer may be regulated differentially depending on the cortical domain. Involvement of the cytoskeleton in generation of polarized distributions has been observed in diverse species. For example, in *S. cerevisiae* actin cable acts as a track for vesicles essential for polarized budding (Adams and Pringle, 1984; Novick and Botstein, 1985). I speculate that during evolution, strategies for generation of polarized distributions has been diversified.

In short, for my doctorate research, I have characterized functions of gene products required for pattern formation of organelles along A/P or C polarity axes. I summarize my doctorate studies with key findings or conclusions as below:

1) CdaH, identified as Fused kinase in *T. thermophila*, acts downstream of CdaA (cyclin E) in inducing division boundary and interacts with CdaI (Mst/Hippo kinase) to regulate overall size of oral primordium. Thus from the perspective of CdaH, an interacting partner for global scale patterning is CdaA whereas interacting partner for local scale patterning is CdaI.

2) CdaH forms ring-shape assembly around division boundary and accumulates exclusively on posterior daughter cell after completion of cytokinesis. This indicates that remnant of CdaH may send cues for establishment of A/P axis for new daughter cell. CdaH ring may serve its role similar to that of Septin ring of *S. cerevisiae.*
3) CdaH was found redundant in assembly of cilia, indicating distinctive roles of Fused kinase depending on the species.

4) Hpo1 is an Armc9-like protein that contributes to placement of oral apparatus by communication with currently unknown activator, taking inhibitory role along cell circumference.
5) Janus acts as a dorsal suppressor for oral development, so inhibitory impact Hpo1 has on oral development is masked on dorsal side.
6) Either Hpo1 and Bcd1 is required for viability of *T. thermophila* (synthetic lethality in *bcd1-2;hpo1* KO double mutant), and Hpo1 and Bcd1 are involved in left-right cross-talk that leads to cortical development, as reflected in abnormal cell morphologies.
7) There may be some extent of shared mechanism or component required for both A/P and C pattern formation (e.g. Hpo1 is C factor whose mutation also causes posterior migration of op.).
8) Pattern formation of CVP still remains largely elusive, but discovery that CVP domain and high point of Hpo1 domain within its bidirectional gradient overlaps indicate that enrichment of Hpo1 acts as a marker (morphogenic effect at single cell level) for placement of CVP.

References

Adams, A.E., and J.R. Pringle. 1984. Relationship of actin and tubulin distribution to bud growth in wild-type and morphogenetic-mutant *Saccharomyces cerevisiae*. *J Cell Biol*. 98:934-945.

Bi, E., and H.O. Park. 2012. Cell polarization and cytokinesis in budding yeast. *Genetics*. 191:347-387.

Busson, D., B. Limbourg-Bouchon, M.C. Mariol, T. Preat, and C. Lamour-Isnard. 1988. Genetic analysis of viable and lethalfused mutants of *Drosophila melanogaster*. *Rouxs Arch Dev Biol*. 197:221-230.

Chiou, J.G., M.K. Balasubramanian, and D.J. Lew. 2017. Cell Polarity in Yeast. *Annu Rev Cell Dev Biol*. 33:77-101.

Cole, E., and J. Gaertig. 2022. Anterior-posterior pattern formation in ciliates. *J Eukaryot Microbiol*. 69:e12890.

Cole, E.S., J. Frankel, and L.M. Jenkins. 1987. *bcd*: A mutation affecting the width of organelle domains in the cortex of *Tetrahymena thermophila*. *Rouxs Arch Dev Biol*. 196:421-433.

Cole, E.S., W. Maier, E. Joachimiak, Y.Y. Jiang, C. Lee, E. Collet, C. Chmelik, D.P. Romero, D. Chalker, N.K. Alli, T.M. Ruedlin, C. Ozzello, and J. Gaertig. 2023. The *Tetrahymena bcd1* mutant implicates endosome trafficking in ciliate, cortical pattern formation. *Mol Biol Cell*. 34:ar82.

Colosimo, P.F., and N.S. Tolwinski. 2006. Wnt, Hedgehog and junctional Armadillo/beta-catenin establish planar polarity in the *Drosophila* embryo. *PLoS One*. 1:e9.

Edelbusch, C., S. Cindric, G.W. Dougherty, N.T. Loges, H. Olbrich, J. Rivlin, J. Wallmeier, P. Pennekamp, I. Amirav, and H. Omran. 2017. Mutation of serine/threonine protein kinase 36 (STK36) causes primary ciliary dyskinesia with a central pair defect. *Hum Mutat*. 38:964-969.

Frankel, J. 1989. Pattern formation : ciliate studies and models. Oxford University Press, New York. xvii, 314 pages : illustrations pp.

Frankel, J. 2008. What do genic mutations tell us about the structural patterning of a complex single-celled organism? *Eukaryot Cell*. 7:1617-1639.

Frankel, J., L.M. Jenkins, E.M. Nelsen, and C.A. Stoltzman. 1993. Hypoangular: a gene potentially involved in specifying positional information in a ciliate, *Tetrahymena thermophila*. *Dev Biol*. 160:333-354.

Frankel, J., J. Mohler, and A.K. Frankel. 1980. Temperature-sensitive periods of mutations affecting cell division in Tetrahymena thermophila. *J Cell Sci*. 43:59-74.

Frankel, J., and E.M. Nelsen. 1987. Positional reorganization in compound *janus* cells of *Tetrahymena thermophila*. *Development*. 99:51-68.

French, V., P.J. Bryant, and S.V. Bryant. 1976. Pattern regulation in epimorphic fields. *Science*. 193:969-981.

Galati, D.F., S. Bonney, Z. Kronenberg, C. Clarissa, M. Yandell, N.C. Elde, M. Jerka-Dziadosz, T.H. Giddings, J. Frankel, and C.G. Pearson. 2014. DisAp-dependent striated fiber elongation is required to organize ciliary arrays. *J Cell Biol*. 207:705-715.

Gao, B., H. Song, K. Bishop, G. Elliot, L. Garrett, M.A. English, P. Andre, J. Robinson, R. Sood, Y. Minami, A.N. Economides, and Y. Yang. 2011. Wnt signaling gradients establish planar cell polarity by inducing Vangl2 phosphorylation through Ror2. *Dev Cell*. 20:163-176.

Gergen, J.P., and E.F. Wieschaus. 1986. Localized requirements for gene activity in segmentation of *Drosophila* embryos: analysis of armadillo, fused, giant and unpaired mutations in mosaic embryos. *Rouxs Arch Dev Biol*. 195:49-62.

Hersch, M., O. Hachet, S. Dalessi, P. Ullal, P. Bhatia, S. Bergmann, and S.G. Martin. 2015. Pom1 gradient buffering through intermolecular auto-phosphorylation. *Mol Syst Biol*. 11:818.

Jiang, Y.Y., K. Lechtreck, and J. Gaertig. 2015. Total internal reflection fluorescence microscopy of intraflagellar transport in *Tetrahymena thermophila*. *Methods Cell Biol*. 127:445-456.

Jiang, Y.Y., W. Maier, R. Baumeister, E. Joachimiak, Z. Ruan, N. Kannan, D. Clarke, P. Louka, M. Guha, J. Frankel, and J. Gaertig. 2019. Two Antagonistic Hippo Signaling Circuits Set the Division Plane at the Medial Position in the Ciliate *Tetrahymena*. *Genetics*. 211:651-663.

Jiang, Y.Y., W. Maier, R. Baumeister, G. Minevich, E. Joachimiak, Z. Ruan, N. Kannan, D. Clarke, J. Frankel, and J. Gaertig. 2017. The Hippo Pathway Maintains the Equatorial Division Plane in the Ciliate *Tetrahymena*. *Genetics*. 206:873-888.

Jiang, Y.Y., W. Maier, U.N. Chukka, M. Choromanski, C. Lee, E. Joachimiak, D. Wloga, W. Yeung, N. Kannan, J. Frankel, and J. Gaertig. 2020. Mutual antagonism between Hippo signaling and cyclin E drives intracellular pattern formation. *J Cell Biol*. 219.

Kiekebusch, D., and M. Thanbichler. 2014. Spatiotemporal organization of microbial cells by protein concentration gradients. *Trends Microbiol*. 22:65-73.

Kuzhandaivel, A., S.W. Schultz, L. Alkhori, and M. Alenius. 2014. Cilia-mediated hedgehog signaling in *Drosophila*. *Cell Rep*. 7:672-680.

Latour, B.L., J.C. Van De Weghe, T.D. Rusterholz, S.J. Letteboer, A. Gomez, R. Shaheen, M. Gesemann, A. Karamzade, M. Asadollahi, M. Barroso-Gil, M. Chitre, M.E. Grout, J. van Reeuwijk, S.E. van Beersum, C.V. Miller, J.C. Dempsey, H. Morsy, G. University of Washington Center for Mendelian, M.J. Bamshad, C. Genomics England Research, D.A. Nickerson, S.C. Neuhauss, K. Boldt, M. Ueffing, M. Keramatipour, J.A. Sayer, F.S. Alkuraya, R. Bachmann-Gagescu, R. Roepman, and D. Doherty. 2020. Dysfunction of the ciliary ARMC9/TOGARAM1 protein module causes Joubert syndrome. *J Clin Invest*. 130:4423-4439.

Lee, C., W. Maier, Y.Y. Jiang, K. Nakano, K.F. Lechtreck, and J. Gaertig. 2024. Global and local functions of the Fused kinase ortholog CdaH in intracellular patterning in *Tetrahymena*. *J Cell Sci*. 137.

Liu, M., Z. Guan, Q. Shen, P. Lalor, U. Fitzgerald, T. O'Brien, P. Dockery, and S. Shen. 2016. Ulk4 Is Essential for Ciliogenesis and CSF Flow. *J Neurosci*. 36:7589-7600.

Louka, P., K.K. Vasudevan, M. Guha, E. Joachimiak, D. Wloga, R.F. Tomasi, C.N. Baroud, P. Dupuis-Williams, D.F. Galati, C.G. Pearson, L.M. Rice, J.J. Moresco, J.R. Yates, 3rd, Y.Y. Jiang, K. Lechtreck, W. Dentler, and J. Gaertig. 2018. Proteins that control the geometry of microtubules at the ends of cilia. *J Cell Biol*. 217:4298-4313.

Maloverjan, A., and M. Piirsoo. 2012. Mammalian homologues of *Drosophila* fused kinase. *Vitam Horm*. 88:91-113.

Marshall, W.F. 2021. Regeneration in *Stentor coeruleus*. *Front Cell Dev Biol*. 9:753625.

McCoy, C.J., H. Paupelin-Vaucelle, P. Gorilak, T. Beneke, V. Varga, and E. Gluenz. 2023. ULK4 and Fused/STK36 interact to mediate assembly of a motile flagellum. *Mol Biol Cell*. 34:ar66.

Mehlen, P., F. Mille, and C. Thibert. 2005. Morphogens and cell survival during development. *J Neurobiol*. 64:357-366.

Nanney, D.L. 1967. Cortical Slippage in Tetrahymena. *Journal of Experimental Zoology*. 166:163-+.

Novick, P., and D. Botstein. 1985. Phenotypic analysis of temperature-sensitive yeast actin mutants. *Cell*. 40:405-416.

Nozawa, Y.I., E. Yao, C. Lin, J.H. Yang, C.W. Wilson, R. Gacayan, and P.T. Chuang. 2013. Fused (Stk36) is a ciliary protein required for central pair assembly and motile cilia orientation in the mammalian oviduct. *Dev Dyn*. 242:1307-1319.

Nusslein-Volhard, C., and E. Wieschaus. 1980. Mutations affecting segment number and polarity in *Drosophila*. *Nature*. 287:795-801.

Perrimon, N. 1994. Signalling pathways initiated by receptor protein tyrosine kinases in *Drosophila*. *Curr Opin Cell Biol*. 6:260-266.

Perrimon, N., and A.P. Mahowald. 1987. Multiple functions of segment polarity genes in *Drosophila*. *Dev Biol*. 119:587-600.

Sadian, Y., C. Gatsogiannis, C. Patasi, O. Hofnagel, R.S. Goody, M. Farkasovsky, and S. Raunser. 2013. The role of Cdc42 and Gic1 in the regulation of septin filament formation and dissociation. *Elife*. 2:e01085.

Slabodnick, M.M., J.G. Ruby, J.G. Dunn, J.L. Feldman, J.L. DeRisi, and W.F. Marshall. 2014. The kinase regulator mob1 acts as a patterning protein for *stentor* morphogenesis. *PLoS Biol*. 12:e1001861.

Swarup, S., and E.M. Verheyen. 2012. Wnt/Wingless signaling in *Drosophila*. *Cold Spring Harb Perspect Biol*. 4.

Tang, L., J. Franca-Koh, Y. Xiong, M.Y. Chen, Y. Long, R.M. Bickford, D.A. Knecht, P.A. Iglesias, and P.N. Devreotes. 2008. tsunami, the Dictyostelium homolog of the Fused kinase, is required for polarization and chemotaxis. *Genes Dev*. 22:2278-2290.

Tartar, V. 1956a. Grafting experiments concerning primordium formation in *Stentor coeruleus*. *Journal of Experimental Zoology*. 131:75-121.

Tartar, V. 1956b. IV. PATTERN AND SUBSTANCE IN *STENTOR*. *In* Cellular Mechanics in Differentiation and Growth. Princeton University Press, Princeton. 73-100.

Tavares, A., J. Goncalves, C. Florindo, A.A. Tavares, and H. Soares. 2012. Mob1: defining cell polarity for proper cell division. *J Cell Sci*. 125:516-527.

Thanbichler, M., and L. Shapiro. 2006. MipZ, a spatial regulator coordinating chromosome segregation with cell division in *Caulobacter*. *Cell*. 126:147-162.

Uhlig, G. 1960. Entwicklungsphysiologische Untersuchungen zur Morphogenese von *Stentor coeruleus* Ehrbg. *Arch. Protistenk.* 105:1-109.

Van De Weghe, J.C., T.D.S. Rusterholz, B. Latour, M.E. Grout, K.A. Aldinger, R. Shaheen, J.C. Dempsey, S. Maddirevula, Y.H. Cheng, I.G. Phelps, M. Gesemann, H. Goel, O.S. Birk, T. Alanzi, R. Rawashdeh, A.O. Khan, G. University of Washington Center for Mendelian, M.J. Bamshad, D.A. Nickerson, S.C.F. Neuhauss, W.B. Dobyns, F.S. Alkuraya, R. Roepman, R. Bachmann-Gagescu, and D. Doherty. 2017. Mutations in ARMC9, which Encodes a Basal Body Protein, Cause Joubert Syndrome in Humans and Ciliopathy Phenotypes in Zebrafish. *Am J Hum Genet*. 101:23-36.

Wilson, C.W., C.T. Nguyen, M.H. Chen, J.H. Yang, R. Gacayan, J. Huang, J.N. Chen, and P.T. Chuang. 2009. Fused has evolved divergent roles in vertebrate Hedgehog signalling and motile ciliogenesis. *Nature*. 459:98-102.

Witte, K., D. Strickland, and M. Glotzer. 2017. Cell cycle entry triggers a switch between two modes of Cdc42 activation during yeast polarization. *Elife*. 6.

Wu, C.F., J.G. Chiou, M. Minakova, B. Woods, D. Tsygankov, T.R. Zyla, N.S. Savage, T.C. Elston, and D.J. Lew. 2015. Role of competition between polarity sites in establishing a unique front. *Elife*. 4.